Tropical Water Quality Hub

National **Environmental Science** Programme

What's really damaging the Reef?

Tracing the origin and fate of the ecologically detrimental sediment and associated bioavailable nutrients

Stephen Lewis, Zoe Bainbridge, Thomas Stevens, Alex Garzon-Garcia, Chengrong Chen, Mohammad Bahadori, Joanne Burton, Mehran Rezaei Rashti, Cassandra James, Scott Smithers and Jon Olley

JAMES COOK UNIVERSITY
AUSTRALIA

What's really damaging the Reef?

Tracing the origin and fate of the ecologically detrimental sediment and associated bioavailable nutrients

Stephen Lewis[1], Zoe Bainbridge[1], Thomas Stevens[1], Alex Garzon-Garcia[2],
Chengrong Chen[3], Mohammad Bahadori[3], Joanne Burton[2], Mehran Rezaei Rashti[3],
Cassandra James[1], Scott Smithers[1,4] and Jon Olley[3]

[1] Catchment to Reef Research Group, TropWATER, James Cook University, Townsville
[2] Queensland Department of Environment and Science, Brisbane
[3] Australian Rivers Institute Griffith University, Brisbane
[4] Environmental Science and Management, College of Science and Engineering,
James Cook University, Townsville

Cover photographs: (front) Aerial photograph of the Burdekin River in full flood at Inkerman Bridge, in February 2019. Image: Matt Curnock, CSIRO; (back) In situ instrument and SediSampler® sediment trap set up, with project team member Tom Stevens diving to change over array. Image: Cassandra Thompson, JCU.

This report is available for download from the NESP Tropical Water Quality Hub website:
http://www.nesptropical.edu.au

CONTENTS

LIST OF TABLES

LIST OF FIGURES

ACRONYMS

CDOM .... Coloured dissolved organic matter
EoR .... End-of-river
GBR .... Great Barrier Reef
GSA .... Grain Size Analysis
GOF .... Goodness of Fit
DIN................ Dissolved inorganic nitrogen
DOC .... Dissolved organic carbon
DON .... Dissolved organic nitrogen
LAT............... Lowest Astronomical Tide
LOI................ Loss on Ignition
MMP.............. Marine Monitoring Program
NESP .... National Environmental Science Program
NO$_x$-N .... Nitrogen oxides
NTU............... Nephelometric Turbidity Units
NTUe............. Nephelometric Turbidity Units (equivalent) – these readings have been calibrated to two grey colour standards to correct for voltage offsets between instruments
OSL............... Optimally Stimulated Luminescence
PAR .... Photosynthetic Active Radiation
PIN................ Particulate inorganic nitrogen
PN .... Particulate nitrogen
POC .... Particulate organic carbon
PON .... Particulate organic nitrogen
PO$_4$$^{-2}$-P .... Phosphate
PPT .... Parts per Thousand (salinity unit equivalent to PSU)
PSU............... Practical Salinity Units
RO water ...... Reverse Osmosis Water
SPM .... Suspended particulate matter
SSC .... Suspended sediment concentration
TN .... Total nitrogen
TOC .... Total organic carbon
TSS .... Total suspended solids
TWQ.............. Tropical Water Quality

DATA STORAGE AND AVAILABILITY

All data generated by this project have been stored in the eAtlas (website run by AIMS) as a requirement for all of the National Environmental Science Program Tropical Water Quality Hub projects. We also plan to make all relevant data available in the supplement sections of future papers.

ACKNOWLEDGEMENTS

MEMORIAL DEDICATION

In memorial to our two dear friends, colleagues, mentors. Their passion for our field of research will be greatly missed.

Phil Moody has greatly inspired our work linking the biogeochemistry of soils at source with sediments in catchments and marine sediment plumes. His immense knowledge and pioneering work in soil biogeochemistry has expanded through this project to broader realms.

Jon Brodie was a colossal figure in water quality, who helped shape water quality research and monitoring across the Great Barrier Reef catchment to reef continuum. His *science for management* approach greatly influenced policy, and helped lead to the development of the Reef Water Quality Protection Plan.

EXECUTIVE SUMMARY

The influence of anthropogenic sediment and associated particulate nutrients delivered to the Great Barrier Reef (GBR) lagoon has been contested over the past few decades. Indeed, six key systematic questions arise to help inform this debate which include:

1. What is the influence of the newly-delivered sediment (i.e. from flood plumes) on turbidity regimes at coral reef and seagrass locations of the inshore GBR?

2. What is the contribution of the anthropogenic component of this sediment on turbidity regimes?

3. What are the characteristics of the suspended particulate matter (and associated particulate nutrients) that influence light and turbidity regimes and how do these change over the estuarine mixing gradient of flood plumes?

4. How does the particulate organic component of the suspended particulate matter and associated microbial community composition change from the catchment to reef?

5. How bioavailable is the suspended particulate matter along the estuarine mixing gradient

6. Where does the sediment (and associated particulate nutrients) that influence light and turbidity regimes in the GBR come from in the Burdekin catchment so that management efforts can be prioritised?

Our NESP project was designed to address these questions and provide new insights on the sources, transport, fate and impacts of suspended particulate matter across the catchment to reef continuum. Indeed, several novel sampling techniques and processing innovations were first applied within this project to help achieve these outcomes. This final project report is divided into eight separate stand-alone research chapters which collectively address these six key questions. Here we provide brief summaries of the key findings from each chapter and then collectively apply them to address our key research questions.

Chapter 1: A flume and field study on the role of spacing and tilt on suspended particulate matter collection in sediment traps deployed at coral reefs: a case study from the Great Barrier Reef, Australia

This chapter examined the ability of SediSampler® sediment traps to quantify spatial and temporal variation in sediment exposure at inshore sites in the GBR. Specifically, replicated laboratory flume and field studies were carried out to examine trap measurement accumulation rates and precision under different spacing and tilt conditions. The resulting data show that the sediment traps deployed three diameter widths apart (as applied at our instrumented sites), and with trap tilt angles < 5° provided reproducible measurements of sediment accumulation rates normalised in the form of $mg.cm^{-2}.day^{-1}$. The importance of consistent deployment depths in the water column was also highlighted, with increased accumulation rates for traps deployed closer to the substrate. Overall, the data show that when key protocols related to trap design and deployment are followed, sediment traps not only provide a robust measure of the spatial and temporal variability in sediment exposure at marine sites but also capture the composition of the sediment for characterisation and tracing purposes.

Chapter 2: Methods to best measure sediment grain size across the catchment to reef continuum

This study examined new methods to standardise grain size measurement across the freshwater, estuarine and marine environments as well as to provide insights on the physical and compositional changes of suspended particulate matter (SPM) as it is transported across the catchment to marine continuum. Various treatment methods were explored to examine their influence on grain size distribution using the Malvern Mastersizer 3000 instrument including salt removal (for estuarine and marine samples), H_2O_2 treatment to remove organic matter, HCl treatment to remove carbonates and sieving to remove coarse diatoms. The data highlight the importance of removing organic matter for the end-of-river (EoR) and estuarine samples and both organics and carbonate in the marine sediment trap samples to provide the closest approximation of primary particle size. For marine sediment trap data, this method allows for the addition of newly delivered sediments to be better quantified through the normalisation to mineral-only accumulation rates. Collectively, microscopy and grain size analyses reveal the transformation of SPM across the catchment to marine continuum whereby the mineral particles become finer (< 20 μm), more organic rich, contain diatoms and other plankton and form larger sediment floc aggregates as they move further offshore in flood plumes. The capability of the novel SediPump® high-volume filtration system to faithfully collect representative samples of flood plume SPM where low concentrations (i.e. < 10 mg.L^{-1}) traditionally prevented sampling and characterisation has also been validated. This new protocol for grain size analysis provides a way forward to collect valuable and previously inaccessible data to inform catchment and marine modelling exercises. Burdekin and Tully EoR, estuarine and flood plume sediment characterisation data collected in this chapter will be valuable input parameters for components of the eReefs model that are currently not well constrained, and could also support future modifications to the "fluff/dust"-layer.

Chapter 3: Examining turbidity regimes on the inner Great Barrier Reef: quantifying the influence of newly delivered riverine sediments

This contribution established seven instrumented logger and SediSampler® sediment trap sites at key coral reef and seagrass locations on the inshore central GBR. Sites were strategically located to examine the spatial and temporal variability in turbidity and light regimes in response to the delivery of newly delivered terrigenous sediment and associated particulate nutrients in flood plumes. The loggers provided continuous 10 min readings of turbidity/suspended sediment, PAR/light, wave pressure (RMS) and current while the sediment traps provided replicated measures of accumulation rates and compositional change over each deployment. Collectively our time-series data demonstrate the influence of newly delivered terrigenous sediment (and particulate nutrients) in flood plumes at all sites where the highest sediment concentration coincided directly with the flood event and/or the highest accumulation rates (and highest total nutrient concentrations) in the sediment traps. However, key differences were evident at the sites that reflected the length of influence of the newly delivered fine sediment as well as local scale conditions. Three key mechanisms of impact were identified which include:

1. Increased suppression of light in shallow turbid water environments both during the flood plume and the months afterwards;

2. Pulsed delivery and deposition of flood plume sediment and associated nutrients to inshore coral reef sites which favour an increase in macroalgae cover and corresponding decrease in live coral cover and;

3. Development of chronic persistent turbidity (and reduced photic depth) for long periods as a result of wave and current disturbance (resuspension) of the sediment bed or new sediment delivery.

Chapter 4: Characterising the sediment that causes 'persistent turbidity' through the Whitsunday Island Group

This chapter collected suspended particulate matter and benthic sediment grab samples from the inner and outer sections of the Whitsunday Island Group to characterise and trace the material thought to be the cause of persistent turbidity issues in the region. We applied novel sediment collection methods (SediPump®), our developed grain size methods, clay mineralogy and geochemistry to show that a combination of fine (< 20 µm) mineral sediment of similar composition and diatoms and organic materials were causing persistent turbidity in the region. Indeed, our data demonstrate relatively small changes in water column suspended particulate matter/turbidity concentration (i.e. an increase by ~ 1 mg.L^{-1} or ~ 1 NTU) can reduce the water clarity by over half (i.e. visibility from 9 m to 4 m). Importantly, our tracing data reveal that the suspended particulate matter and benthic sediment compositions were well mixed throughout the Whitsunday region and were derived from a similar source (with the possible exception of the suspended particulate matter sample from Blue Pearl Bay). We provide possible causes for the origin of the suspended particulate matter, further research direction to determine this cause/source and recommendations for the subsequent management response once the cause is identified.

Chapter 5: The dissipation of suspended particulate matter in river flood plumes and implications for marine ecosystems: case studies from the Great Barrier Reef

This study examined the dispersion of flood plume suspended particulate matter through the water column along transects sampled during Burdekin and Tully River plume events. We also compared light/PAR profile data of the water column during the plume and ambient conditions to demonstrate and quantify the change in euphotic depth between the two sampling periods. Our sampling program was fortunate to collect samples from these river plumes that impinged on the mid shelf of the GBR and hence we provide a case study to consider the influence of newly delivered sediment on the mid shelf of the GBR. We conducted remote sensing analysis of satellite imagery over a 17-year period (2003 to 2019) to examine the frequency of floods reaching the mid shelf and the exposure (frequency and duration) of flood plumes in this zone and provide first order approximations of terrigenous sediment volumes potentially transported to these more distal sections of the GBR during large flow events. We find that during large flow events a previously unrecognised mass of terrigenous sediments can be delivered to the mid shelf which also has the capacity to at least temporarily suppress light conditions to deeper (> 5 m) sections of the water column for days to weeks. Based on our preliminary findings, we provide recommendations on how to better examine and quantify the influence of suspended particulate matter and associated nutrients on the mid shelf.

Chapter 6: The shift in the chemical composition of particulate organic matter and microbial community from catchment to reef

This work explored the shift in the chemical composition and bioavailability of particulate organic matter from the catchment to marine environments using isotopic ($\delta^{15}N$, $\delta^{13}C$) and ^{13}C nuclear magnetic resonance (^{13}C-NMR) spectroscopy approaches. The change in the microbial community and composition was also examined using DNA sequencing to provide insights on the origin and fate of sediments and associated organic matter during their transportation from soil to freshwater and eventually into the GBR lagoon. The ^{13}C NMR data show that soil samples from different land uses were more enriched in labile (i.e. bioavailable) fractions (e.g., carbohydrates), while marine sediments were more enriched in the recalcitrant organic carbon fractions (e.g., aliphatic compounds). The ^{13}C NMR signatures of freshwater plume samples from three rivers (the Johnstone, Tully and Burdekin) were quite similar to soil samples, indicating their terrestrial origin. The isotopic signatures ($\delta^{13}C$ and $\delta^{15}N$) displayed considerable variability from the catchment soils to the marine sediment traps which also demonstrate the transformation of organics across the catchment to marine continuum. The microbial community composition changed considerably along the sediment transportation pathway from soil to freshwater and marine environment. Proteobacteria, Actinobacteria and Acidobacteria were predominant groups of bacteria in soil and freshwater plume sediments while Protobacteria and Bacteroidetes were dominantly associated with the estuarine flood plume and trap sediments. The change in the microbial community composition was due to the shift in environmental factors (e.g., pH and salinity) and chemical composition of organic matter from soil to freshwater and marine environment. The results of this study provide a better understanding on the origin and fate of terrestrially derived organic matter in the GBR lagoon which is critical for developing targeted management actions to improve water quality in the GBR.

Chapter 7: The bioavailability of nitrogen associated with sediment in riverine plumes entering coastal environments of the Great Barrier Reef

This study quantified the amount of dissolved inorganic nitrogen (DIN) that could potentially become bioavailable (i.e. released) from the particulate nitrogen pool via ammonium desorption and microbial processing in estuarine flood plumes. A series of water samples were taken from end of river sites as well as at different positions in three riverine sediment plumes from the Burdekin River and one plume from the Tully River. Adsorbed ammonium extraction methods were used to quantify the conversion from particulate inorganic nitrogen to DIN while controlled incubation experiments were undertaken to quantify the conversion of particulate (and dissolved) organic nitrogen to DIN by microbial communities. The estimated potential DIN load generated from the particulate nitrogen in the three Burdekin River plumes was equivalent to approximately 9 to 30% of the corresponding end-of-catchment DIN load in 4 to 5 days of plume travel time. However, the generation of DIN from particulate nitrogen in the Tully River plume was negligible. Of the generated DIN load in the Burdekin plume, ammonium desorption was an important process in the early estuarine mixing reaches of the plume (< 10 PSU salinity) and accounted for between 25% and 100% of the total generated load. The remaining contribution was provided by microbial mineralisation of the organic nitrogen component with this mineralisation of DIN increasing linearly towards the end of the incubation experiments (7 days). This result indicates that the sediment and associated particulate nitrogen have the potential to continue to produce DIN once deposited on the marine floor and/or resuspended. Multivariate analysis indicates that the source of the organic

matter in the plumes and the availability of DIN relative to the available organic matter for mineralisation are important determinants of mineralisation/immobilisation in marine sediment plumes.

Chapter 8: Geochemistry and provenance of sediment plume samples collected from the Burdekin region of the Great Barrier Reef Lagoon, Australia

This chapter examined the geochemistry, radionuclide and clay mineral composition of the terrigenous sediment component of Burdekin plume suspended particulate matter for source tracing across the catchment to marine continuum. The geochemical tracing reveal that distinct sources can be identified across the Burdekin River plumes measured in 2017, 2018 and 2019 as well as clearly delineate the major sub-catchment sources throughout the Burdekin catchment. In the Bowen River dominated event in 2017, a clear Bowen River source was identified in the plume, and likewise in the 2018 Upper Burdekin/Cape River dominated event, a source from these tributaries were identified. The 2019 flood plume mixed source from the Bowen and Upper Burdekin tributaries requires further examination, although it appears that the flood plume samples reveal a predominant upper Burdekin River source. The samples collected from the Burdekin flood plumes in 2019 show a marked increase in the proportion of the expandable clay (i.e. smectite-type) fraction that preferentially travels further in the marine environment. The radiogenic tracing (^{137}Cs and ^{210}Pb$_{ex}$) of end of river and flood plume sediment (<10 µm) show that the mineral sediments were almost exclusively eroded from sub-surface (>15 cm depth) erosion sources. Additional tracing in the Bowen sub-catchment reveals a mixture of soil source contributions with a high proportion contributed by chromosol sub-soils while the highest contributors to the bioavailable nutrients were surface dermosols in 2017 and surface vertosols and subsurface chromosols in both 2017 and 2019 events. Overall, this contribution provides an additional line of evidence to support the existing sediment budget work in the Burdekin catchment and highlights that the sediment sources can be traced across the catchment to reef. Indeed, the work also provides new insights on the preferential transport of sediment fractions in the flood plume that contribute the sediment that has the potential to cause most impact in the GBR. Our data not only provide new insights on the preferential movement of suspended particulate matter in the marine environment but also provide improved source identification of the key terrigenous sediments delivered from the Burdekin catchment for management prioritisation.

Addressing the key research questions

1. What is the influence of the newly delivered sediment (i.e. from flood plumes) on turbidity regimes at coral reef and seagrass locations of the inshore GBR?

Our logger data reveal a clear influence of the newly delivered sediment from flood plumes on both the initial suspended particulate matter (SPM) concentration and exposure (and the resultant light) during the plume event and, at some sites, in the resuspension events over the few months following the flood event (Chapter 3). The particulate nutrients in association with the SPM also likely favour the proliferation of macroalgae growth at coral reef sites. We have defined three main pathways for impact from the newly delivered terrigenous sediment and associated particulate nutrients in the GBR which are summarized in the Chapter 3 summary above and covered in Chapter 3 of this report. Our data highlight that SPM concentrations in the water column that have previously been considered 'low' (1 to 5 mg.L^{-1}) as well as relatively small changes in SPM (~ 1 mg.L^{-1}) can produce substantial changes in water clarity and

benthic light in the marine environment (Chapters 2, 4 and 5). Our new findings provide an improved way forward for monitoring and characterising SPM in the marine environment (Chapters 1, 2 and 3) as well as an improved foundation to model the impacts of terrigenous sediment in the GBR.

2.   What is the contribution of the anthropogenic component of this sediment on turbidity regimes?

While it is difficult to distinguish between what could be considered 'natural' and 'anthropogenic' sediment in the marine environment, our preliminary first-order calculations suggest that a considerable proportion of the SPM (i.e. an 'average' in the order of 2 mg.L^{-1}) transported in flood plume could be considered anthropogenic (Chapter 4). Indeed, as demonstrated in Chapters 4 and 5 a change of this magnitude could have significant consequences for water clarity and benthic light in the GBR. In addition, modelling using empirical data in an associated NESP project linking Burdekin sediment loads with seagrass meadow area and condition in Cleveland Bay provide additional evidence that reductions in sediment loads in the Burdekin likely translate to improved ecological outcomes. Hence this provides a link between 'extra sediment' and seagrass health.

3.   What are the characteristics of the suspended particulate matter (and associated particulate nutrients) that influence light and turbidity regimes and do these change over the estuarine mixing gradient of flood plumes?

Our key findings indicate that organic-rich sediment with a primary particle size of < 20 μm travels furthest in the flood plume (Chapter 2). Preferential plume transport of finer clay particles (smectite-type) was also found within some sampled plume events (Chapter 8). In addition, large floc aggregates of mineral sediment, organic matter and diatoms/plankton (Chapter 2) and likely fused together by bacteria-produced mucus (Chapter 6) which produce DIN (Chapter 7), and form in the outer sections of the flood plume. These large floc aggregates are only found in our sediment traps that coincide with the river flooding periods (Chapter 3). These results provide a more thorough characterisation of the processes occurring along the estuarine mixing gradient and identify the key terrigenous sediment fractions that travel furthest and have the potential to cause most impact in the GBR.

4.   How does the particulate organic matter and associated microbial community composition change from the catchment to reef?

Tracing analysis on the organic matter across the catchment to marine continuum show that the organics transform to more recalcitrant forms (i.e. not bioavailable) as it moves further offshore (Chapter 6). In addition, the microbial community composition changes as the SPM moves into the marine waters where they become more enriched in bacteria forms (Chapter 6). These results provide further insights on the processes transforming the organic matter across the estuarine mixing zone.

5.   What is the contribution of particulate nutrients to the bioavailable nutrient pool along the estuarine mixing gradient?

Our data show that throughout the estuarine mixing zone dissolved inorganic nitrogen can be produced via either ammonium desorption (early plume stages < 10 PSU salinity zone) or microbial processing of the particulate nitrogen transported in the plume (Chapter 7, Fig.

ES.1). These bioavailable nutrients can represent a considerable fraction on top of the DIN load delivered by the end of the river and hence the 'bioavailability' of catchment sediments should also be considered in catchment remediation measures to account for the considerable additional 'nutrient saving' (Chapter 7). These results also highlight the ability for DIN to be released from the suspended particulate matter over longer periods following its initial deposition and provides a nutrient source to favour macroalgae growth at inshore coral reefs sites in the months following large river discharge events.
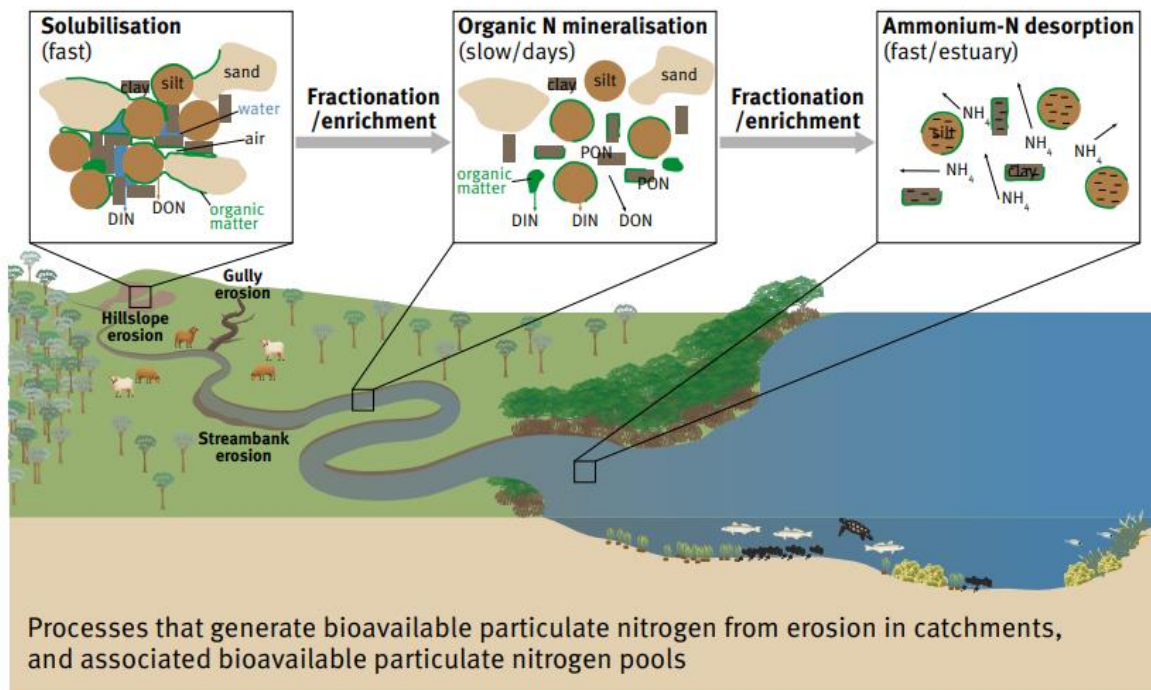
Figure ES.1. Conceptual diagram of the key processes that release dissolved inorganic nitrogen from particulate nitrogen in the river flood plume (Source: J.Burton and S.Lewis).

6. Where does the sediment that most influences light and turbidity regimes in the GBR come from in the catchment so that management efforts can be prioritised?

Our extensive sediment budget, physical (particle size and clay mineralogy) and geochemical dataset reveal two clear sediment source contributions from the Burdekin River catchment: the Upper Burdekin and the Bowen sub-catchments (Chapter 8). Additional fallout radionuclide tracing analysis on a sub-set of EoR and Plume sediment samples confirmed this fine sediment to be predominately sourced to sub-soils within these sub-catchments. Finer-scale tracing indicates that chromosol subsoils make a sizable contribution to the Bowen source and additional geochemical tracing measures are currently refining tributary sources within both the upper Burdekin and Bowen sub-catchments. These data better inform targeted management prioritisation of tributaries in the Burdekin catchment to achieve the most effective reductions of the terrigenous sediment most likely to cause most impact in the GBR.
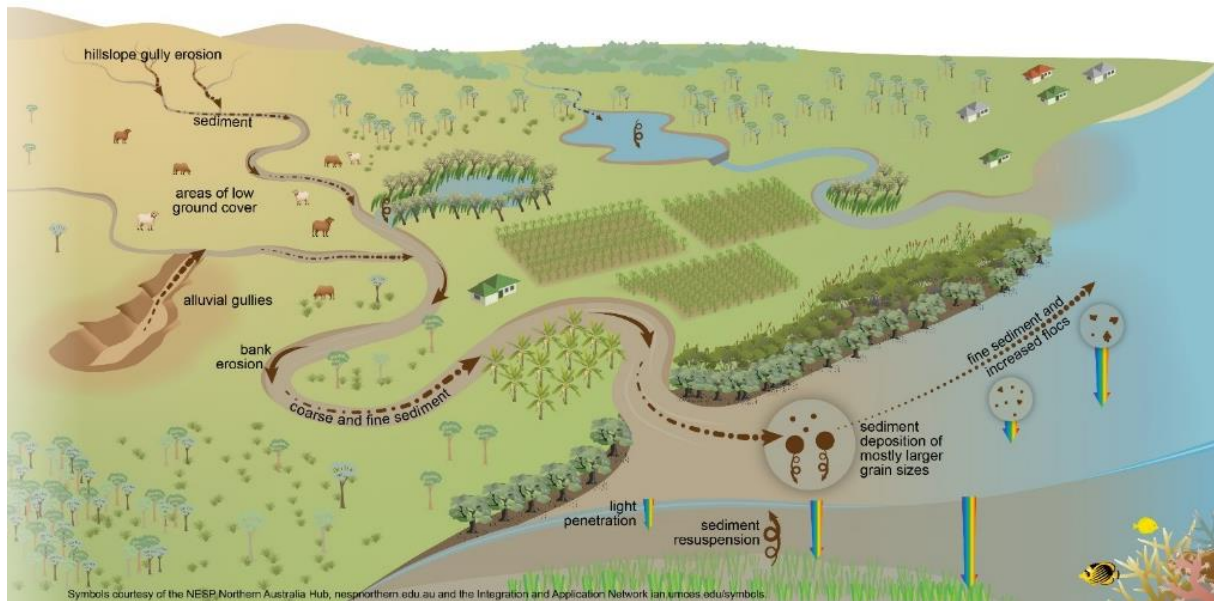
Figure ES.2. Conceptual understanding of sediment sources and transport across the catchment to marine continuum (image developed by Kate Hodge for NESP TWQ Hub Sediment Synthesis Project).

A further synthesis of these chapters can also be found in the NESP Tropical Water Quality Hub Sediment Synthesis case study entitled "Much more than just Sediments: the importance of sediment composition for GBR ecosystems" by Lewis and Bainbridge (2021).

CHAPTER 1

A flume and field study on the role of spacing and tilt on suspended particulate matter collection in sediment traps deployed at coral reefs: a case study from the Great Barrier Reef, Australia

Thomas C. Stevens[1,2*], Stephen E. Lewis[1], Zoe T. Bainbridge[1], Andreas Dietzel[3], Cassandra S. James[1], Scott Smithers[1,4]

[1]Catchment to Reef Research Group, TropWATER, James Cook University
[2]Integral Aqua Pty Ltd
[3]Coral Reef Centre of Excellence, James Cook University
[4]Environmental Science & Management, College of Science & Engineering, James Cook University

Abstract

Sediment traps provide important insights on suspended particulate matter (SPM) exposure, accumulation rates and composition when certain design and deployment protocols are followed. However, aspects of their deployment such as the influence of spacing when using multiple traps and the degree of trap tilt on the amount of SPM collected have received limited attention under both controlled flume and field situations. This study applied 60 mm diameter sediment traps (aspect ratio ≈ 9.4) spaced at 0.7 diameter (D), 3D and 9D widths apart over three replicated flume studies at short intervals (max ~ 8 days). The same traps were deployed at 3D (n = 4) and 9D (n = 8) spacings during four separate ~ 3 month field deployments at two inshore coral reef locations in the central Great Barrier Reef, Australia. The 60 mm traps were also deployed at different tilts (0°, 5°, 10°, 20° and 25°) under flume conditions and at one field location (9D spacing), each replicated three times while a similar setup was also applied using 83 mm D traps (aspect ratio ≈ 6.4). The trap spacing sets displayed excellent reproducibility (Relative Standard Deviation < 10%) in SPM collection rates across the field trials. Furthermore, our results show measured concentrations did not vary significantly between the different spacing patterns in both flume and field studies, but changes in collection at two field deployments varied with trap elevation in the water column. The influence of trap tilting on SPM collection rates was variable, although the data suggest that collection rates potentially increase with tilts > 5°. Cylindrical sediment traps with aspect ratios > 6 and deployed at a similar height above the seabed with tilts < 5° reliably record spatial and temporal SPM exposure regimes at coral reef locations.

1.1 Introduction

The influx of suspended particulate matter (SPM) and associated nutrients into aqueous systems can result in negative ecological effects which may include direct burial, algal blooms, loss of light for photosynthesis and oxygen deficiency (Søndergaard et al. 2003; Donohue and Garcia Molinos, 2009; Erftemeijer et al. 2012; Bartley et al. 2014; Risk, 2014; Bainbridge et al. 2018). Indeed, in marine settings, terrigenous sediment delivered via riverine flood plumes or resuspended from the seafloor can greatly affect the health of the corals and seagrass and the overall condition of the marine ecosystem. Furthermore, the composition of the SPM is an important consideration with the organic (i.e. darker) and finer sediment particles more damaging in terms of coral and seagrass health as well as on light regimes (Weber et al. 2012; Erftemeijer et al., 2012; Storlazzi et al. 2015; Brodersen et al. 2017; Bainbridge et al., 2018). Accurate spatial and temporal measurements of sediment exposure is hence important to understand and quantify the level of SPM exposure at marine sites. However, the monitoring requirements in terms of instrumentation, cost and logistics to achieve such comprehensive resolution and characterisation is often prohibitive for such analysis.

Sediment traps have been widely utilised to assess spatial and temporal variability of the resuspension, exposure and composition of suspended particulate matter (SPM) and associated nutrients across the deep ocean (> 40 m depth), lakes, coral reefs and estuaries (e.g. Bloesch and Burns, 1980; Reynolds et al. 1980; Bothner et al. 2006; Buesseler et al. 2007). Despite many key field and laboratory experiments that have sought to better understand trap design and function to provide 'trap best practice' (e.g. Hargrave and Burns, 1979; Lau, 1979; Gardner, 1980a, 1980b; Gardner et al. 1983, 1985, 1997; Butman, 1986; Butman et al. 1986; Baker et al. 1988; Hawley, 1988; White, 1990; Gust et al. 1996; Jurg, 1996; Bale, 1998; Nodder and Alexander, 1999; Storlazzi et al. 2011), there has been little progress towards a standardised approach for trap design and deployment methods across monitoring programs. Establishing design and deployment protocols for traps to capture suspended load are particularly challenging as predicting the collection efficiency of the sediment trap is highly complex and reliant on many different factors such as variations in hydrodynamics (i.e. horizontal fluid velocity), trap design (i.e. geometry, height, diameter and extensions such as baffles), method of deployment, and the nature of the particles in suspension (Butman, 1986; Storlazzi et al. 2011). Indeed, the selection of the most optimal sediment trap for monitoring programs is also dependent on the main objective of the study and hence a thorough understanding of the trap function (i.e. what the trap is recording in the environment such as vertical and horizontal sediment flux and sediment accumulation/exposure) is required to interpret the resulting trap dataset.

In coral reef studies, sediment traps have been used as a monitoring tool since the 1970s to assess coral health and growth morphology in response to (1) inshore-offshore terrigenous sediment exposure gradients; (2) sediment composition and sources; (3) temporal sediment dynamics and; (4) the influence of bottom resuspension. Such studies have been carried out across the Caribbean (e.g. Dodge et al. 1974; Rogers, 1983; Nugues and Roberts, 2003; Mallela et al. 2004; Smith et al. 2008; Hernandez et al. 2009; Sherman et al. 2014, 2016; Otano-Cruz et al. 2017), Costa Rica (Cortes and Risk, 1985), Hawaii (Storlazzi et al. 2004, 2009, 2011; Bothner et al. 2006; Draut et al. 2009; Takesue et al. 2009; Takesue and Storlazzi, 2019), French Polynesia (Gowan et al. 2014) and the Great Barrier Reef (Marshall and Orr, 1931; Mapstone et al. 1992; Wolanski et al. 2005, 2008; Furnas et al. 2011; Latrille et al.

2019). Several of these studies have applied the trap collection rate (expressed as mg.cm^{-2}.d^{-1}) as a measure of 'sedimentation', a key parameter to assess the health of coral reefs. Indeed the sedimentation rate threshold of 10 mg.cm^{-2}.d^{-1} highlighted in the classic work of Rogers (1990) is still applied in coral reef assessments and this rate was partly derived from field studies applying sediment traps. Based on a literature review on sediment trap design and function coupled with new observations from coral reefs in Hawaii and Guam Storlazzi et al. (2011) concluded traps do not record sedimentation. Although this may be problematic, they argue if deployment standards are developed and applied, sediment traps can provide useful information about the relative magnitude of sediment dynamics including measures of horizontal and vertical sediment flux and relative exposure at coral reef locations (Storlazzi et al. 2011).

Importantly, Storlazzi et al.'s (2011) review provided the first recommendations for sediment trap deployment protocols for application in coral reef settings. These recommendations include the use of cylindrical traps (based on the findings of Gardner, 1980a, 1980b; Butman, 1986 and references therein) with an internal diameter of > 50 mm (Bloesch and Burns, 1980; Blomqvist and Kofoed, 1981; Jurg, 1996) and a trap aspect ratio (trap height: internal diameter) of > 5:1 or preferably > 7:1 (based on findings of Hargrave and Burns, 1979; Lau, 1979; White, 1990; Gust et al. 1996; Jurg, 1996; Gardner et al. 1997). The mouths of the trap should also be deployed vertically at the highest point in the uninterrupted flow above the mooring and reef structure (Gardner, 1980a, 1980b; Butman, 1986; Butman et al. 1986; Gust et al. 1996). Storlazzi et al. (2011) also recommended when using multiple traps they should always be of the same design, deployed at the same depth above the seafloor and be spaced at least 10 diameter (D) widths apart. However, the two studies cited to support the 10D spacing recommendation both suggested a 3D spacing was sufficient to achieve reproducible trap collection rates (Gardner 1980a; Nodder and Alexander, 1999). Further, the original publications recommending a minimum 3D spacing where multiple traps are deployed in cross-stream profiles (Nodder and Alexander, 1999) and a 10D spacing for traps when they are deployed in downstream profiles (Butman, 1984 in U.S. GOFS Report 10, 1989) present no data to support these protocols. The recommendations on trap spacing are thus not fully validated and warrant further examination.

Another aspect of trap deployment that has received scant attention is the influence of tilt on trap collection rates (Gardner, 1985; Chiswell and Nodder, 2015). Indeed, the relatively strong flow conditions observed in coral reef locations (e.g. Storlazzi et al. 2011) may cause traps to tilt off their vertical plane which in turn may influence collection rates. Published opinion on the influence of tilt is contradictory, with Gardner (1985) presenting data to support a 2.5 to 3.0 fold increase in collection rates with traps tilted at 40-45° (traps at 75° collected < 70% less material) while Chiswell and Nodder (2015) showed that traps with tilts between 5 and 20° collected 30 to 50% less material compared to traps with < 4° tilt. It is possible that this discrepancy is related to the type of trap used, as Gardner (1985) used cylindrical traps and Chiswell and Nodder (2015) used a conical trap array. In any case, the role of tilt on sediment trap efficiency is not clear in the literature.

This contribution seeks to examine the influence of spacing and tilt on the collection rate of multiple sediment traps under both laboratory (flume) and field conditions. A series of laboratory (flume) and field experiments were conducted using multiple sediment traps of identical design to examine variability in collection rates across 0.7D (flume only), 3D and 9D

spacing and under variable tilts. Results are presented from replicated flume experiments as well as four ~ 3 monthly field deployments across two coral reef settings in the inshore GBR covering both wet and dry seasons to examine accumulation rates under different spacing. We also show results from replicated flume studies and four ~ 3 monthly field deployments at one coral reef location to examine the influence of tilt. Finally, we consider the role of sediment traps deployed in shallow marine environments as a monitoring tool for sediment dynamics on coral reefs. This experimental work provide new insights on the application and deployment of sediment traps and highlight their veracity at quantifying the spatial and temporal variability in sediment exposure (and associated light regime) in marine settings.

1.2 Methods and experimental design

1.2.1 Sediment traps

The main sediment trap used in this study is the SediSampler[®] 55 (Integral Aqua Pty Ltd) patented cylindrical trap head (Stevens, 2013) with an internal diameter of 52 mm, and 300 mm length, containing 30 mm deep baffles in the upper section (Figure 1.1A). The trap head is designed to screw onto a variety of sample bottles, with a 1 L polypropylene bottle used for this study. The sample bottle added an additional 185 mm to the effective trap length (i.e. aspect ratio ≈ 9.4). In addition, the patented trap heads are entirely coated with antifoul in order to maintain trap surface conditions, collection efficiencies and reduce blockages for long (e.g. 3 months) deployments. The SediSampler[®] 75 patented trap (Stevens, 2013) was used in additional flume and field studies to assess SPM collection rates with a greater surface area. The setup of this trap is identical to the SediSampler[®] 55 except that the internal diameter of the trap is 75 mm (i.e. aspect ratio ≈ 6.4, including bottle) and the baffle depth is 63 mm (Figure 1.1B).

1.2.2 Field study area

Field studies were carried out at two inshore coral reefs in the central Great Barrier Reef, Australia including: (1) Geoffrey Bay, Magnetic Island (19.16° S, 146.86° E) and; (2) Havannah Island (18.84° S, 146.54° E), located approximately 50 km north. These site locations form part of a long-term research project using sediment traps to examine spatial and temporal variability in sediment dynamics and composition in the inshore Great Barrier Reef (refer to Chapter 3). The Geoffrey Bay site is at 5 m mean depth on the eastern side of Magnetic Island, located in the turbid north-facing Cleveland Bay (Larcombe et al. 1995). This site is exposed to prevailing south-easterly winds and swell and is occasionally influenced by flood plumes from the Burdekin and Ross Rivers in the wet season months (November to April). The Havannah Reef site is at 10 m mean depth and located on a relatively sheltered reef slope where turbidity levels tend to be much lower than at Geoffrey Bay. This site is also occasionally influenced by river flood plumes from the Burdekin River (see Lough et al. 2015) and possibly other local coastal streams.

1.2.3 Trap collection mass measurements: Total suspended solids versus total dried mass method

The mass retained by the sediment traps in the 1 L bottles was measured by two methods in particular to determine if the modified total suspended solids (TSS) method provided a robust measure of accumulation mass: (1) The first method was the suspended sediment

concentration (SSC; total dry weight) method where the 1 L sample was transferred to a clean 2 L container and the salts were removed through settling (i.e. to achieve conductivity < 200 µS.cm^{-1}), decanting and adding RO water (ensuring no loss of material). The samples were then transferred to smaller pre-weighed containers (~200 ml) and dried in a 60° C oven. The mass of the dried material was then weighed to the nearest 0.03 g. (2) The second method was the TSS method (Method 2540D; APHA, 2005) in which a well-mixed 30ml aliquot from the 1 L bottle was taken, and from this 30 ml aliquot a 1 to 2 ml subsample was pipetted for analysis. The analysis comprised vacuum filtering known volumes of sample onto pre-weighed Whatman GF/C filter papers (nominal pore size 1.2 µm) which were dried overnight in a 103–105°C oven and reweighed to provide a concentration in g.L^{-1}. Because of the high mass of sediment caught in the 1 L bottles (generally > 20 g), only small sample volumes (i.e. 1 to 2 ml) could be filtered for the TSS method which was modified where the sample was pipetted into a filtering manifold which was prefilled with 250 ml of RO water. To assess the TSS method as a representative measure of sediment mass when sample volumes are low (1 to 2 ml), we ran both TSS and total dry weight methods on several samples. Although the SSC method would clearly be the preferred approach as it more directly measures the total mass of sediment retained, our need to conduct a suite of complementary analyses such as particle size and nutrient contents on these small mass suspended sediment samples prevented this approach on most samples. We plotted the TSS versus the corresponding SSC data and conducted a non-parametric Kendall-Theil regression analysis to determine the correlation significance and the slope of the data.

Based on our measurements, we present a 'total measurement uncertainty' for our data points; this uncertainty represents a combination of the standard deviation of replicated samples as well as the measurement uncertainty of the weighing scales. The total mass (mg) retained in each sediment trap was normalised to the trap cross-sectional area (21.52 cm^2) and divided by the period of deployment (days) to report trap collection rates in mg.cm^{-2}.d^{-1}.

1.2.4 Flume experiments: spacing

Given the difficulty of environmental control in field experiments, we undertook three separate flume spacing experiments to test three different trap spacing arrays including at 0.7D, 3D and 9D for the SediSampler® 55 traps in a ~ 2700 L circular flume (Fast-Set Pool 8ft Clark Rubber Pty Ltd) (Figure 1.1C). Three replicate traps were used for each treatment, with transitional head and tail traps at the same spacing as the adjacent treatment, not included in analysis (i.e. open circles in Figure 1.1C). The sediment traps were carefully positioned the same perpendicular distance (300 mm) from the edge of the flume to the centre of the trap opening at the same height above the flume bottom. Trap tilts were all < 2° with mouths situated between 60-70 mm below the water surface. This variability in water surface height was accountable to a small gradient of the floor surface and evaporation of flume water over the experimental campaigns. The flume was filled with saline water (30 PSU) and dosed with sediment collected from sediment traps that had been deployed in Cleveland Bay, Townsville. The water was continuously circulated and well-mixed in the flume using a submersible pump system which drew water from the center of the flume bottom and discharged in a clockwise direction from 6 evenly spaced outlet nozzles located at the circumference (Figure 1.1C). Sediment deposited on the flume bottom was re-suspended every 8 to 12 hrs using a small push broom with a rapid pumping motion around the circumference of the flume. The turbidity would reach ~ 30 NTU (~ 50 mg.L^{-1}) after resuspension and drop to ~ 15 NTU (~ 25 mg.L^{-1})

after 8 to 12 hrs. The mean flow speed at the mid-point between the 9D spaced traps varied between 4.5 ± 1.6 cm.s^{-1}. This setup was repeated three times to examine replicability in the spacing data with experiments lasting 7 to 8 days (Supplementary material). The sequence of the trap treatments and their position in the flume relative to the nozzle outlets were randomised between experiments to limit possible hydrodynamic effects from 'group spacing' and non-uniform flow streams from the flume nozzle outlets.
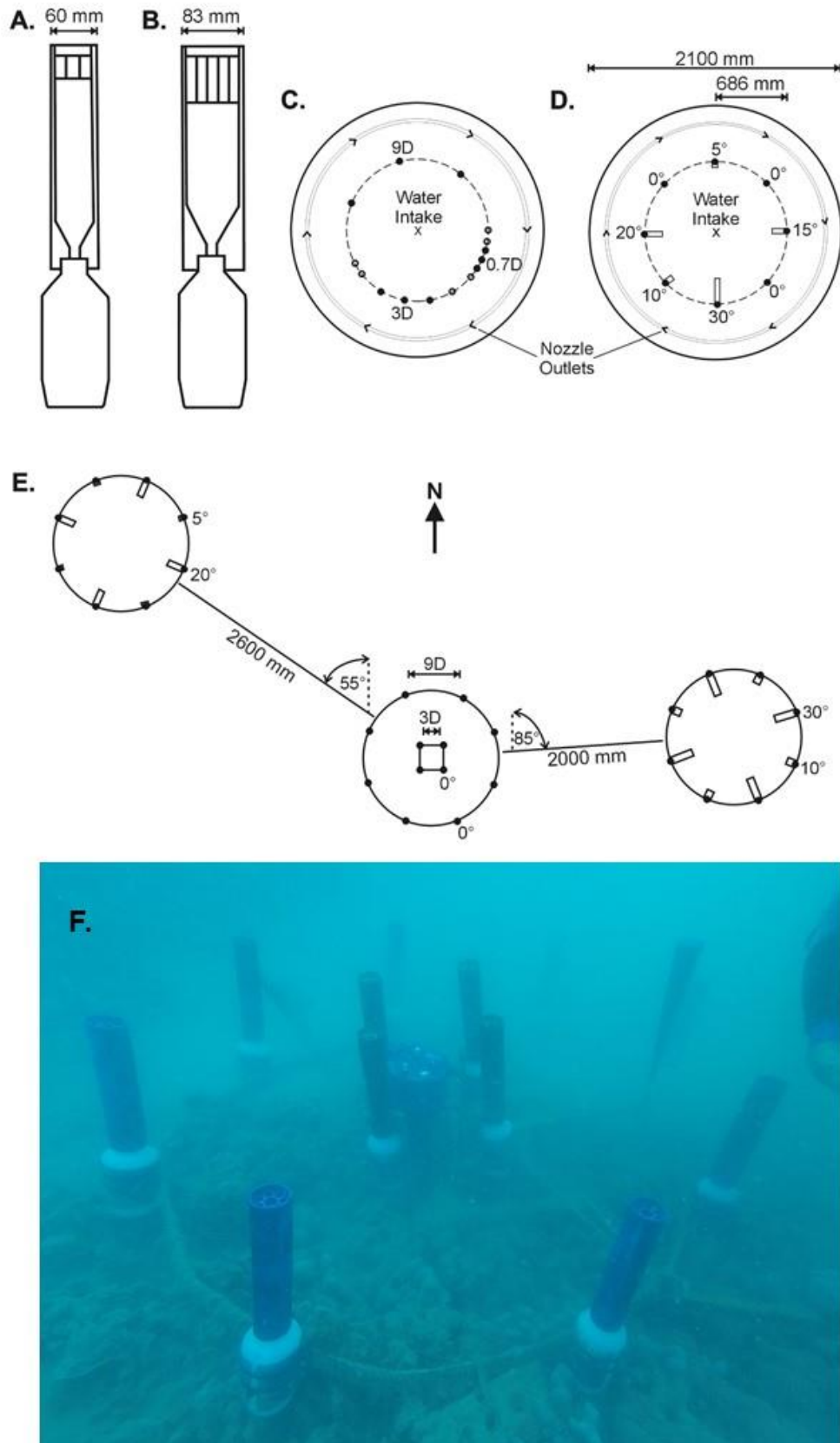
Figure 1.1. Sediment trap, flume and field designs including SediSampler® 55 (A) SediSampler® 75 (B) diameter openings, flume spacing (C), flume tilt (D), field tilt at the Geoffrey Bay coral reef site (E) and field spacing example from the Havannah Island coral reef site (F).

1.2.5 Field experiments: spacing

The setup at both the Geoffrey Bay and Havannah Island sites included an array of 8 evenly spaced SediSampler® 55 sediment traps positioned 540 mm (9 diameter widths: 9D) apart from adjacent traps surrounding an inner frame with traps spaced 3D apart (Figure 1.1F). This outer frame of 9D spaced traps was positioned around the inner frame so that the distance between the 9D and 3D spacing traps was also 540 mm (i.e. 9D width). These traps were paired and positioned parallel to the corresponding frame traps (Figure 1.1F). The 9D array of instruments were positioned so trap mouths were approximately 50 cm off the seafloor and at the same height in the water column while the inner 3D spaced traps were approximately 65 cm off the seafloor. Four separate deployments were carried out at both sites at approximately 3-monthly intervals between December 2017 and March/April 2019 (Supplementary material). These deployment periods cover the wet (December to April) and dry (May to November) seasons in the Great Barrier Reef and two of the deployments coincided with large flooding events in March 2018 and February 2019. Several sediment resuspension events also occurred throughout these deployment periods. The sediment traps were recovered at the end of each deployment period by Scuba Divers where the trap heads were inspected for blockages and the bottles were capped and stored on ice. The samples were stored in a 4° C cold-room prior to analysis via either the dry weight (SSC) or TSS methods (section 1.2.3).

1.2.6 Flume experiments: tilt

Three tilt experiments were undertaken for both the SediSampler® 55 and SediSampler® 75 traps in the circular flume. These deployments ranged from 2 to 31 days (Supplementary material). Eight traps were spaced evenly with the center of each trap orifice positioned 300 mm from the edge of the flume and at the same depth (60 ± 10 mm) from the surface (Figure 1.1D). All trap tilts were orientated outwards, perpendicular to the radial clockwise flow direction. The eight trap tilts per experiment using the SediSampler® 55 and 75 traps were prescribed to be 0° (✕ 3), 5°, 10°, 15°, 20° and 25°. The tilts for all traps were measured at the end of the experiment where the measured tilts could be different to the prescribed tilt due to positioning of the mounting device, floor slope and accuracy of measurement (Supplementary material). The collection rate factors were standardised by dividing each trap's collected mass by the mass from the ~ 0° trap following Gardner (1985).

1.2.7 Field experiments: tilt

Tilt experiments were conducted at the Geoffrey Bay site using the SediSampler® 55s over three separate deployments as well as one tilt experiment using the SediSampler® 75s. The experiments were conducted with two additional frames, similar to the outer 9D spacing frame which were installed more than 2 m apart (Figure 1.1E). Each frame had 8 traps with prescribed alternating treatments of 5° and 20° or 10° and 30° tilts (Figure 1.1E). The central spacing frame represented the 0° tilt treatment (n = 8). Frames were fabricated such that the centres of the trap head orifice were all at the same water column level. The measured trap tilts on retrieval varied from the prescribed treatments due to challenges associated with reef slope, reef topography and movement associated with environmental conditions. The traps with observed blockages causing lost material and with measured tilts > 35° were excluded from the final analysis.

1.2.8 Particle size measurements

Particle size analysis (PSA) was carried out to examine variability across the 3D and 9D spacing arrays with a particular focus on explaining the differences in trap collection at the Geoffrey Bay site. PSA was also undertaken to investigate processes of trap accumulation with changes in tilt. Samples were analysed on a Malvern Mastersizer 3000 at James Cook University using the 'untreated' protocols outlined in Bainbridge et al. (Chapter 2).

1.3 Results

1.3.1 Trap collection mass measurements: TSS versus total dried mass method

A significant correlation was established between the SSC and TSS methods for the measurement of total particulate material trapped ($p < 0.0001$) (Figure 1.2). Three outlier points were excluded where the TSS method greatly underestimated the amount trapped which was likely related to coarser particles in these samples that coincided with deployments where considerable resuspension was recorded (discussed in section 1.4.1). Measurement concentration ranges for the SSC method were 5.1 to 81 g.L^{-1} and 5.2 to 79 g.L^{-1} for the TSS method. The trend line on the plot shows strong agreement between the two methods where the TSS method slightly underestimates sediment mass for the lower concentrations (< 10 g.L^{-1}) and slightly overestimates mass for the higher concentrations (> 35 g.L^{-1}) (Figure 1.2). Importantly, the strong correlation between the two methods confirms that the TSS method produces reliable measurements of the total suspended particulate matter captured in the sediment traps despite the small sample aliquots. We are thus confident that both the SSC and TSS methods can be applied to examine the total mass accumulated in the sediment traps and have used these measurements to examine the influence of spacing and tilt on trap accumulation. Based on these results, we included an additional uncertainty on the TSS data in the spacing and tilt experiments to account for the slight underestimation of trap mass between the SSC and TSS methods.
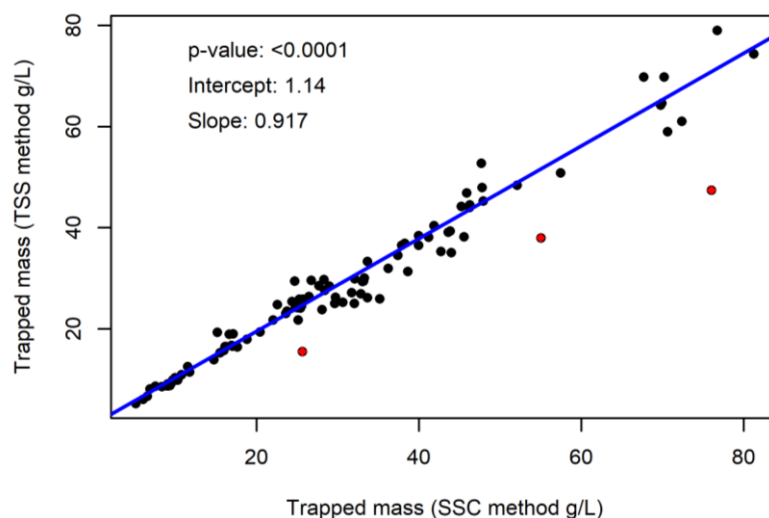
Figure 1.2. Plot comparing the sediment trap collection masses between the TSS and SSC methods (units g.L^{-1}). Outlier points not included in trend line are displayed as red circles.

1.3.2 Reproducibility of multiple trap samples

The reproducibility of the multiple trap arrays in the flume analysis were mostly within 10% and hence displayed reasonable control for comparisons in spacing and tilt to be determined. Similarly, the reproducibility on the multiple trap arrays deployed at the field sites were typically around 10%, although on occasion reached as high as 20% for some deployments in Geoffrey Bay (Figure 1.3). Those deployments coincided with either periods of relatively higher energy (i.e. resuspension) events or the arrays that were deployed closer to the substrate.

1.3.3 Flume experiments: spacing

The flume spacing experiments showed there was no significant differences (Kruskal-Wallis Test) in the collection rates between the 0.7D, 3D and 9D spacings across the three replicated trials (Figure 1.3A). In the first experiment the 0.7D, 3D and 9D spacings had means ± standard errors of 2.48 ± 0.07, 2.54 ± 0.07 and 2.58 ± 0.02 mg.cm^{-2}.d^{-1}, respectively. The second and third experiment had more variability in terms of the means and standard errors which likely reflects the uncertainty of the collection mass measurements (i.e. lower masses collected). In any case, the data for the second experiment also show no significant differences between the 0.7D, 3D and 9D (1.35 ± 0.32, 1.11 ± 0.04 and 1.26 ± 0.23 mg.cm^{-2}.d^{-1}, respectively) and the third experiment showed higher collection rate with the 0.7D spacing and no significant difference with the 3D and 9D traps (1.81 ± 0.06, 1.39 ± 0.23 and 1.15 ± 0.22 mg.cm^{-2}.d^{-1}, respectively).
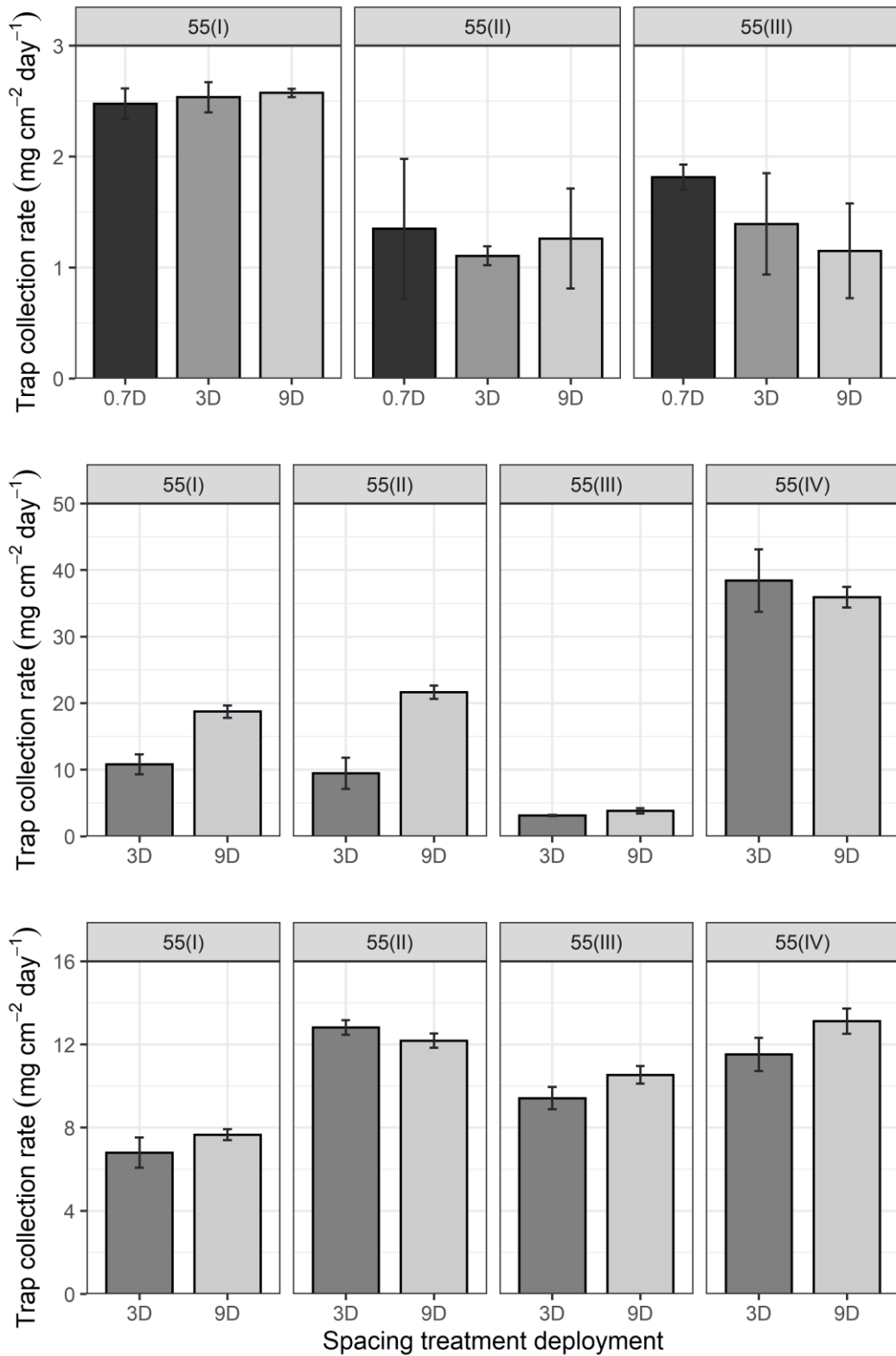
Figure 1.3. Spacing experiments for 0.7 diameter (0.7D), 3D and 9D for the flume (A) and 3D and 9D for the Geoffrey Bay (B) and Havannah Island (C) field deployments I to IV. The error bars relate to 95% confidence intervals.

1.3.4 Field experiments: spacing

The results from the Geoffrey Bay spacing deployments show good reproducibility in the collection rates across both the replicate 3D and 9D spacings with the relative standard deviations (RSD) all within 15% with one exception of the 3D spacing in trial 2 (25%) (Figure 1.3B). Significant differences (Kruskal-Wallis Test) occurred between the 3D and 9D spacings across deployments I (mean ± standard error (SE) = 10.8 ± 0.77 versus 18.7 ± 0.48 mg.cm^{-2}.d^{-1}, respectively; p < 0.01), II (9.45 ± 1.19 versus 21.6 ± 0.50 mg.cm^{-2}.d^{-1}, respectively; p < 0.01) and III (3.12 ± 0.05 versus 3.81 ± 0.20 mg.cm^{-2}.d^{-1}, respectively; p < 0.05). However, no significant differences were found at this same location between the 3D and 9D spacings for deployment IV (38.4 ± 2.39 versus 35.9 ± 0.79 mg.cm^{-2}.d^{-1}, respectively; p = 0.39) (Figure 1.3B).

The trap collection rates during the Havannah spacing study show excellent reproducibility across both the 3D and 9D deployments where all collection rates were within 10% (Figure 1.3C). Furthermore there were no significant differences measured between the 3D and 9D spacings across deployments I (6.79 ± 0.37 versus 7.66 ± 0.14 mg.cm^{-2}.d^{-1}, respectively; p = 0.06) and II (12.8 ± 0.18 versus 12.2 ± 0.17 mg.cm^{-2}.d^{-1}, respectively; p = 0.09). Significant differences were calculated between the 3D and 9D spacings for deployments III (9.42 ± 0.27 versus 10.5 ± 0.21 mg.cm^{-2}.d^{-1}, respectively; p < 0.05) and IV (11.5 ± 0.41 versus 13.1 ± 0.31 mg.cm^{-2}.d^{-1}, respectively; p < 0.05) (Figure 1.3C).

When other sources of error are taken into consideration such as the conversion from TSS to SSC (e.g. Figure 1.2) and the instrumental measurement error as well as the heterogeneity in field conditions, it is arguable that in the majority of cases the differences between 3D and 9D spacings are marginal. The exceptions would be the first two deployments at Geoffrey Bay when both the data (Fig 3B) and the analysis clearly show lower trap collection rates in the 3D compared with the 9D.

1.3.5 Flume experiments: tilt

The results from the flume experiments designed to examine the influence of tilt on SPM accumulation showed that the uncertainties on the trap accumulation amounts for individual samples were much higher for some of the experiments (e.g. Figure 1.4A, 4B, 4D and 4E). These higher uncertainties generally reflect the shorter length (i.e. < 4 days) of those experiments and the resultant lower mass trapped (and hence the higher measurement uncertainty in the accumulation rates). There were also a fairly wide spread of datapoints across different tilts for the experiments (i.e. outside of the prescribed tilt design), which is likely a response to the tilt changing through the course of the experiments. In that regard, the dataset highlight the difficulty in conducting controlled flume experiments for trap tilt and provide insights on the length of time needed to capture adequate material for reporting. In any case, when the sediment collection rates were standardised to the mean value calculated from 0° tilt samples and plotted against their respective tilts, an upward trend in collection rates with increasing trap tilts was apparent in all experiments (Figure 1.4). Indeed, for the experiments where the uncertainty in the collection rates for the individual samples were low, the data show a ~ 20% increase in collection mass for traps tilted at > 5°. Interestingly, there was greater collection mass in the larger 75 mm D traps where a two-fold increase in

accumulation was observed with tilts at 15° in the 75 mm D traps (Figure 1.4F) compared to 25° in the 55 mm D traps (Figure 1.4C).
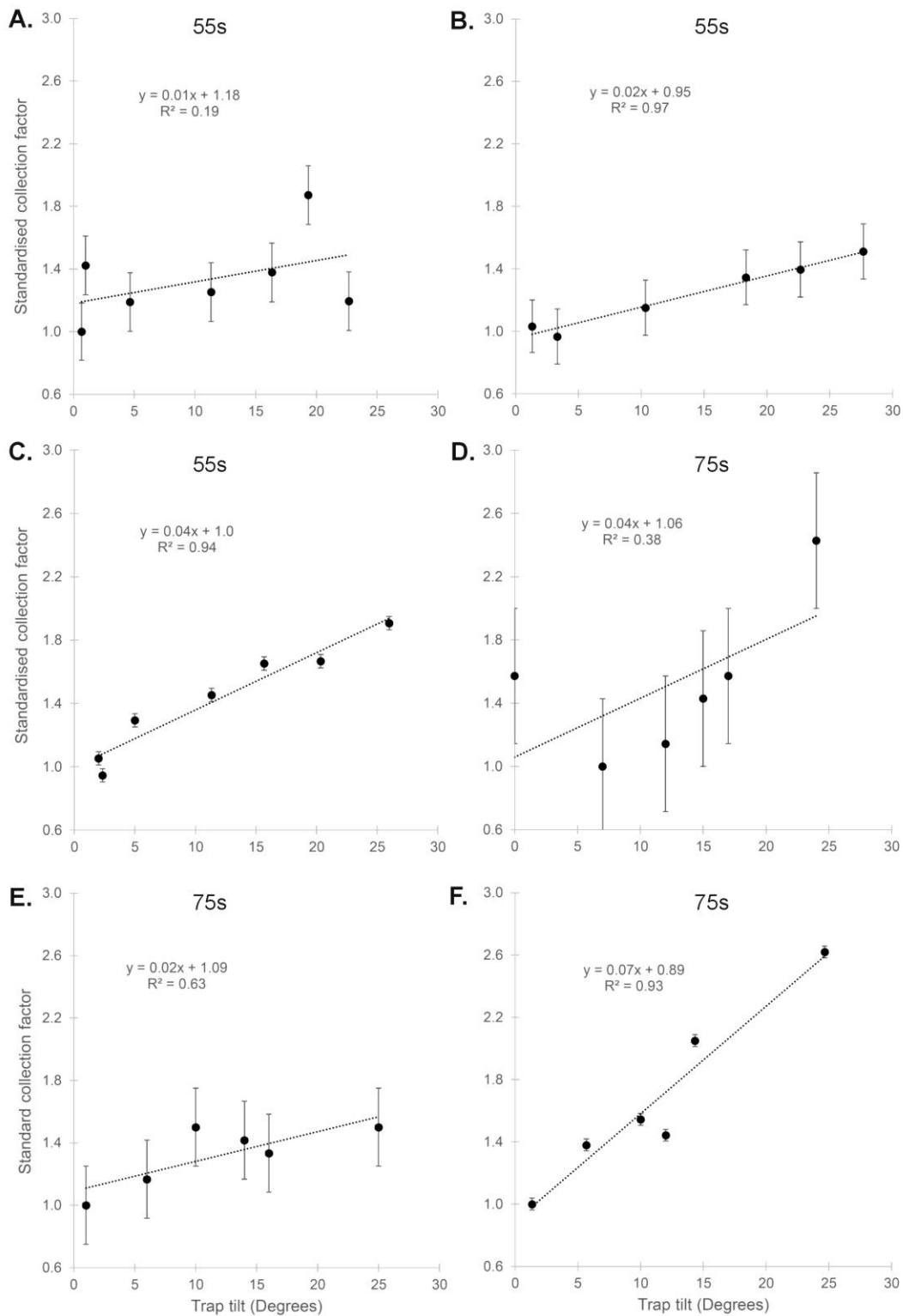
Figure 1.4. Results of the flume experiments on tilt using the 55 mm D (A-C) and 75 mm D (D-F) sediment traps. The standard collection factor is based on the standardisation to the mean value calculated from 0° tilt samples. Vertical bars represent the measurement error (based on sediment mass collected) of each sample.

1.3.6 Field experiments: tilt

The difficulty in conducting controlled laboratory flume experiments to examine the influence of tilt on trap accumulation was further amplified in the field where even higher variability in collection rates were observed (Figure 1.5). Sources of this variability may include non-observed loss of material from blockages in the trap heads, non-controlled effects from orientation to dominant flow directions and local differences in material available (including height above substrate) for resuspension on the substrate between frames. Moreover, trap instability and changes during the experiment may have also influenced accumulation; measured tilts at the end of each deployment ranged from 0° to 43° (± 2°). However, the uncertainty of the accumulation rates of individual samples was lower (relative to the flume experiment data) due to the longer deployment periods. Nevertheless, when the data with observed blockages were excluded, increases in trap collection rates were generally evident with increasing tilts (Figure 1.5). The increase in accumulation with increasing tilt was not as high as in the flume experiments with a 20% increase in accumulation observed for traps > 10° tilt and a 50% increase in accumulation generally observed with tilts > 25°. While the individual results were variable, the 75 mm D traps appear to display higher collection rates (Figure 1.5D) than the 55 mm D traps (Figure 1.5A-C), similar to the flume experiments.
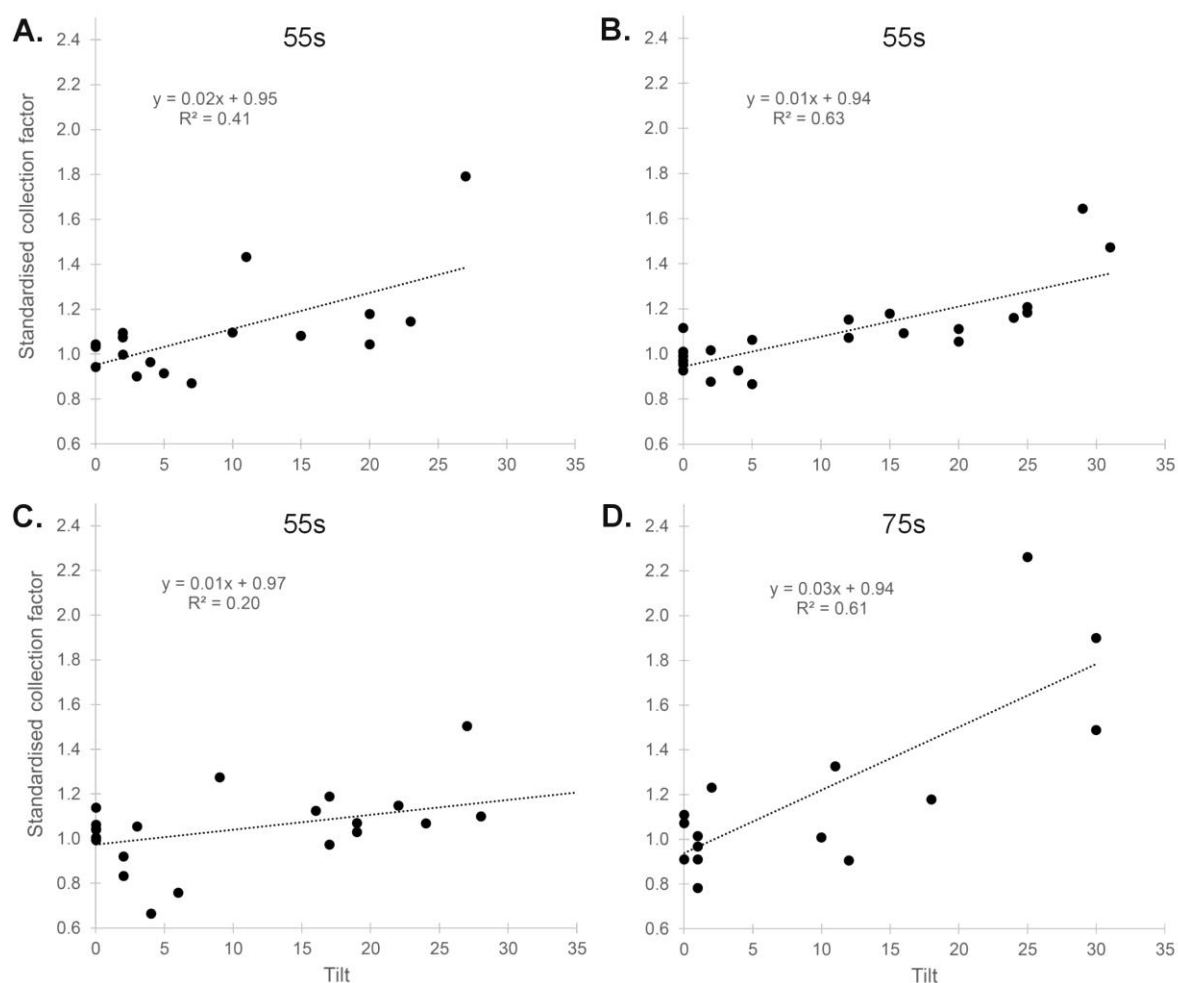
Figure 1.5. Comparisons of field experiment on tilt using the 55 mm D (A-C) and 75 mm D (D) sediment traps. The standard collection factor is based on the standardisation to the mean value calculated from 0° tilt samples.

1.4 Discussion

1.4.1 Trap collection mass measurements: TSS versus total dried mass method

Our data show that the TSS method is suitable (within 10% of the SSC method) to measure sediment trap collection rates despite the relatively large masses collected and the resulting small volume (~ 1-2 ml) that can be subsampled for the analysis (Figure 1.2). Both the SSC and TSS methods likely have constraints that result in an under- or over-estimation of the mass trapped in marine samples.   For example, the SSC method could potentially overestimate the mass trapped if the dissolved salts have not adequately been removed prior to drying or alternatively underestimate mass if material is lost when dissolved salts are being removed (i.e. decanting). The TSS method could overestimate mass if the sample aliquot was taken from a more concentrated section of the sample (i.e. if sample has not been adequately mixed) or similarly underestimate mass particularly if coarser particles (> 1 mm) are present and are 'missed' in subsampling. Indeed, the general underestimation of the TSS method due to the difficulty in capturing a representative sample of the coarser particles (i.e. the larger particles settle before the subsample can be collected) is well established in the literature (e.g. Gray et al. 2000) and is likely amplified by the smaller aliquots (1-2 ml) taken by the pipette in our method. For example, the three outlier points in Figure 1.2 are likely due to this under-sampling (or in the case of the pipette potential exclusion) of the coarser particles and the trend line also suggests that TSS is generally underestimated by 8% compared to the SSC method. In addition, a proportion of very fine particles (< 1.2 µm) could also potentially pass through the GF/C filter paper and hence also produce an underestimation of the TSS method; however, particle size analysis using the salt removed method show (see Figure 1.7 in Chapter 2) that in the Geoffrey Bay and Havannah Island sites there were no particles < 1 µm. In any case, the TSS method provides a reasonable alternative to the SSC method and is optimal when further analysis of SPM in the traps is required (i.e. drying the sample hinders analyses such as microscope, laser diffraction particle size and recovering < 10 µm particles for tracing purposes). In this study we incorporated an uncertainty value of ± 10% into our TSS estimates for the spacing and tilt experiments to account for the possible over and underestimation possible with the two measurement methods.

1.4.2 Trap design and collection rate reproducibility

The data demonstrate that cylindrical traps > 50 mm D with aspect ratios > 6 provide excellent reproducibility on collection rates in coral reef settings and support the recommendations of Storlazzi et al. (2011). The few studies that have applied multiple traps in a field setting have previously reported standard deviations of collection mass within 10% and rarely above 20% (Bloesch and Burns, 1980; Nodder and Alexander, 1999), which is consistent with the results from this study. Indeed, the instances where the reproducibility of the 9D spaced field traps deployed in Geoffrey Bay were higher (>15%) was commonly related to one sample with a higher accumulation relative to the other seven samples. Grain size measurements on these 'higher accumulation' samples compared to other samples in the array showed marked differences in distribution; however, when treated to remove organic and carbonate particles (see Bainbridge et al. in review), the resulting grain size distributions closely matched (data not shown). This finding likely demonstrates the heterogeneity in the resuspension (and subsequent capture in the traps) of the coarser particles at coral reef sites where a trap may

randomly capture a relatively large shell fragment which in turn can considerably influence the final accumulation measurement. Indeed, in comparison to inorganic minerals, biogenic carbonates of equivalent size may have different hydrodynamic properties as a function of mass due to mineralogy or skeletal architecture as well as having a myriad of different shapes which could considerably influence particle size distribution measurements by the laser diffraction method. Hence our data suggest that the removal of organic and carbonate material from the trapped sediment prior to accumulation measurement may further improve the reproducibility on sediment collection rates at coral reef sites.

While the collection efficiency of traps with varying aspect ratios under different flow conditions has perhaps received the most research attention in this field, there is still some uncertainty on the optimal ratio for traps. The seminal flume studies of Garner (1980a) and Butman (1986) suggested cylindrical traps with an aspect ratio of three produced unbiased results that were closest to the 'true' trapping efficiency. Subsequent investigations on the influence of aspect ratio and flow (measured by Reynolds number) on trap collection efficiency suggest that an aspect ratio of somewhere between 5 and 10 is optimal for traps in marine settings due to the more turbulent flows (Lau, 1979; Hawley, 1988; Gardner et al. 1997; Storlazzi et al. 2009, 2011). It is noteworthy that the vast majority of coral reef studies have applied sediment traps with aspect ratios < 5 and hence the collection rates may be underestimated due to saturation, scouring and resuspension out of the traps. Nevertheless, there has been limited research on how collection rates in sediment traps with different aspect ratios perform in such settings and the sediment retention/loss in traps with higher flows is not easily examined, even under laboratory conditions (see White, 1990). In any case, trap aspect ratio presumably becomes more important at sites with greater wave turbulence.

While some studies have shown that trap collection rates are unaffected by the presence or absence of baffles at the trap mouth (e.g. Bloesch and Burns, 1980; Nodder and Alexander, 1999), Butman (1986) suggested they can either slightly decrease trap efficiency and/or reproducibility of collection rates. In marine settings such as coral reefs honeycomb-type baffles (or a 1 cm^2 nylon mesh) have been widely recognised as a necessity to exclude fish and crustaceans from resuspending material within the trap (Storlazzi et al. 2004, 2009; Bothner et al. 2006; Sherman et al. 2013, 2016). Our data using multiple traps show good reproducibility (generally within 10%) with the use of baffles and hence we recommend that their use be advised in protocols for trap design in coral reef settings. In addition, the coating of the traps with antifoul allowed longer deployments (>3 months), preventing the encrustation of traps with various shells and barnacles, and considerably reducing organic growth (i.e. weed/algal growth) and the incidence of trap blockages.

1.4.3 Trap spacing

Both our flume and field sampling experiments consistently show that a 3D spacing array when using multiple traps had similar collection efficiencies to the corresponding 9D spacing array. The two exceptions in the Geoffrey Bay deployments are likely explained by the difference in the mouth position in the water column (i.e. 3D frame was sitting ~ 150 mm higher in the water column than the 9D frame) and highlight that this is an important consideration in trap deployment; this is due to a gradient of increasing suspended sediment concentrations that would be expected closer to the substrate under resuspension events. Our results also match the flume data of Gardner (1980a, 1980b) who recommended 3D spacing for multiple

traps as well as the field experimental data of Nodder and Alexandar (1999) who showed spacing of about 3-trap diameters was sufficient to minimize inter-trap interactions and maintain trapping efficiency among suspended traps at the same depth in the water column. Hence, we suggest the spacing recommendations in Storlazzi et al. (2011) should be revised from the 10D suggestion to 'at least 3D apart'; further investigation on the reproducibility in collection rates for traps with closer spacing would be required to refine this protocol further. Indeed, 3D spacings of multiple traps in coral reef settings may provide better reproducibility than wider spacing of traps especially where there can be considerable spatial heterogeneity in sediment dynamics; however, traps spaced at larger intervals would be more desirable if the heterogeneity of the sediment exposure on a reef site is the study objective. In fact, it appears that the position of the trap mouth in the water column is a much more important factor on the reproducibility of trap collection rates where the collection rates in the first and second Geoffrey Bay deployment doubled in traps sitting 150 mm closer to the seafloor.

1.4.4 Tilt

Our flume and field experiments on the influence of tilt of sediment traps on collection efficiency concur with Gardner's (1980a, 1985) conclusions that increased tilts result in increased sediment collection rates. Our data provide field validation that trap efficiency generally increases with > 5° tilt (and up to ~ 30°), even under multi-directional current regimes. In that regard, our results conflict with the only previous marine field experimental study that concluded traps with tilts between 5° and 20° had lower collection efficiencies (Chiswell and Nodder, 2015). However, we note that Chiswell and Nodder (2015) used conical traps that may behave differently to the cylindrical traps deployed in our study. Our data suggest that cylindrical traps should be deployed vertically and that traps should remain within 5° tilt on retrieval to ensure consistency in SPM collection efficiency. Traps with > 5° tilts should be documented and if needed a 'correction' to trap collection rate may be applied. Future studies should investigate whether trap collection rates can be correlated to directional velocities of currents as suggested by Buesseler et al. (2007) which will provide further insights on trap function.

Grain size measurements of the flume and field tilt experiments provide further insights on the reasons for increased collection rates with increasing tilt (Figure 1.6). For the majority of the experiments with increasing tilt, a decreasing trend across the D10, D50 and D90 grain size distributions was evident, with particularly more negative slopes for the D90 (Figure 1.6). We note that the flume D90 measurements have lower values and gradients compared to the field results, due to the lack of resuspension of larger particles. Indeed, there are two related mechanisms influencing these trends which are related to the fall velocity and fall distance before capture of the particles, resulting in differences in the particle size fractions captured. Firstly, the more variable and steeper gradients for the D90 data with increasing tilt (Figure 1.6) support the contention of a reduced flux of these coarser particles due to being in shorter supply (i.e. heterogeneously distributed) and falling faster through a reducing horizontal orifice area, respectively. Secondly, the decrease in relative fall distance (i.e. the minimum length for a particle to fall to reach the tranquil zone or deposit on the side of the trap for capture) with increased tilt explains the higher collection rates for the slower sinking (i.e. finer) particles (Figure 1.7). Our calculations show that the residence time defined as the time in suspension before coming into contact with the trap wall or zero velocity boundary condition for a 4 μm particle to fall 300 mm (0° tilt) is 340 minutes, compared to 57 minutes to fall 50 mm (30° tilt).

In comparison, a 63 µm particle takes 1.4 minutes to fall 300 mm (0° tilt) and 0.23 minutes to fall 50 mm (30° tilt) (Figure 1.7); demonstrating the preferential accumulation of the finer particles with increasing tilt.
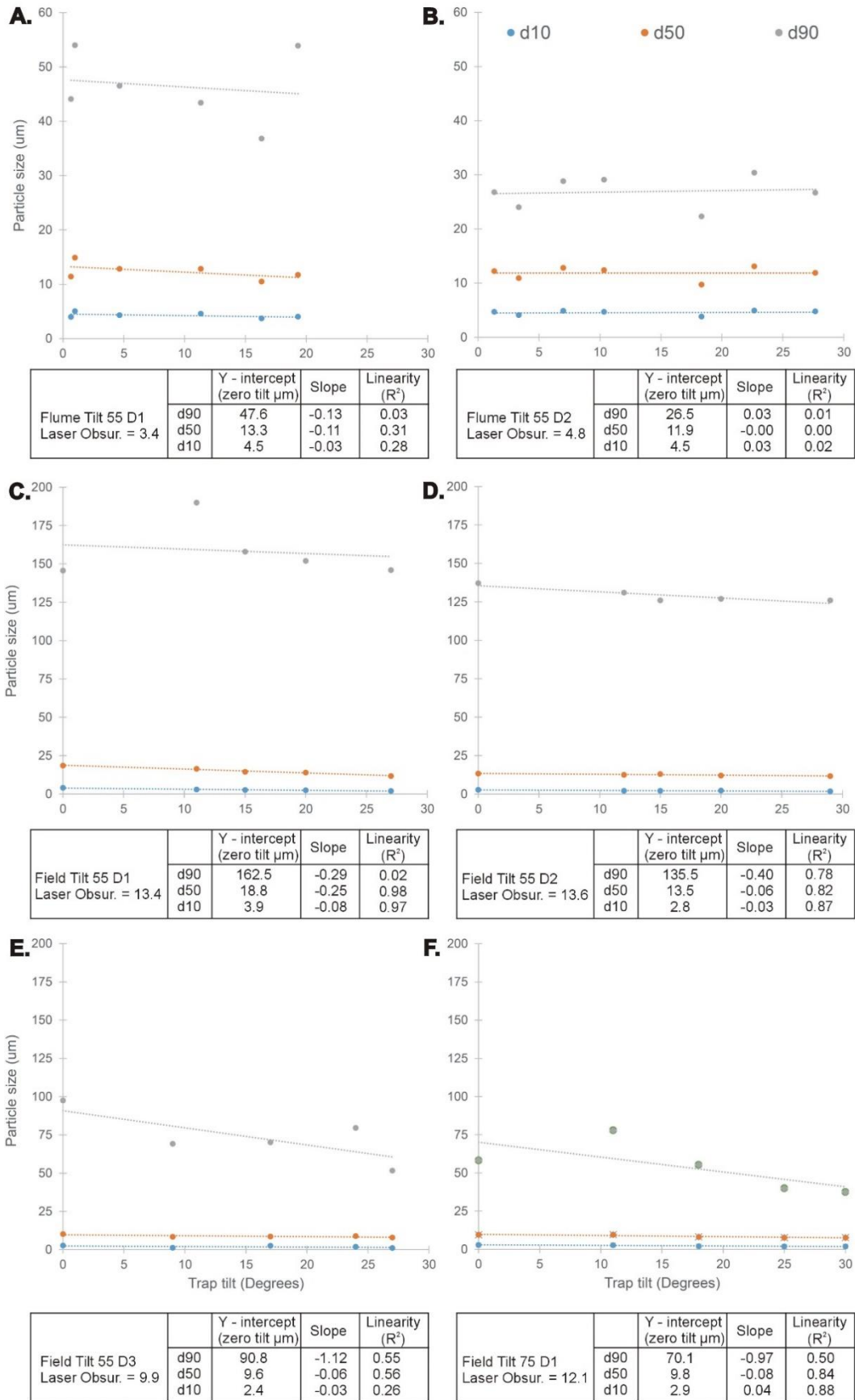
Figure 1.6. Response of the D90 (grey line), D50 (orange) and D10 (blue) particle size measurement to varying tilt for both flume and field settings. Note respective trend statistics for each experiment below each plot.

Tilt	Distance (mm)	Time (min) (4 µm)	Time (min) (16 µm)	Time (min) (63 µm)
0°	300	340	21	1.4
5°	275	310	19	1.3
10°	145	160	10	0.66
15°	100	110	7.1	0.46
20°	75	85	5.3	0.34
30°	50	57	3.5	0.23
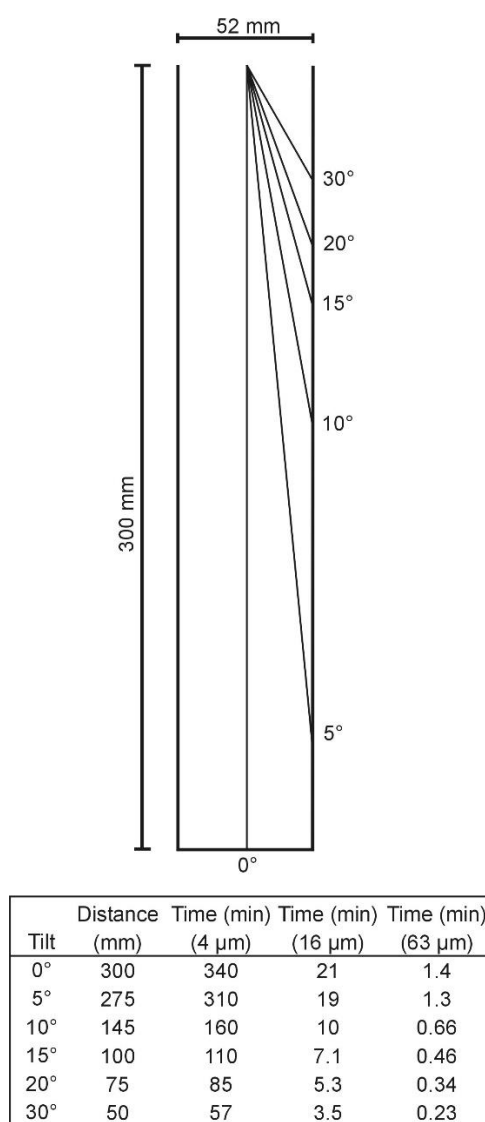
Figure 1.7. Demonstration of the change in fall distance with increasing trap tilt and the relative time changes (Stoke's settling equation using seawater density, viscosity at 25° C) for various grain sizes.

1.4.5 Use of traps in coral reef environments

We show that baffled, antifoul-coated sediment traps with adequate aspect ratios (> 6), spaced at least 3D apart and with tilts < 5° provide precise measurements of sediment collection rates in coral reef settings. However, the application of sediment traps in the marine environment has been questioned due to the recognition that traps do not measure sedimentation (Ridd et al. 2001; Ogston et al. 2004; Storlazzi et al. 2011; Browne et al. 2012). Clearly sediment traps record a combination of sedimentation, sediment resuspension and new sediment delivered to or transported through a sampled site (i.e. sedimentation plus sediment 'in transit' or components of both vertical and horizontal flux) and recent studies have recognised this application (e.g. Cortes and Risk, 1985; Nugues and Roberts, 2003; Malella et al. 2004; Bothner et al. 2006; Smith et al. 2008; Draut et al. 2009; Hernández et al. 2009; Storlazzi et al. 2009, 2011; Sherman et al. 2013; Gowan et al. 2014; Otaño-Cruz et al. 2017). Indeed, Storlazzi et al. (2011) showed that sediment traps recorded an elevated sediment flux which moved past a reef site in Hawaii where no 'sedimentation/deposition' occurred. In that regard,

a sedimentation device deployed at this location would not have recorded this sediment exposure at this site. A possible way forward in coral reef studies would be to pair deployments of sediment traps and sedimentation devices where the subtraction of the sedimentation rate recorded by the device from the sediment trap collection rate would provide a measure of resuspension and delivery of new sediment. In any case, sediment traps on their own provide a measure of sediment exposure and dynamics at coral reef sites and the composition retained by the traps provide valuable data on sediment sources (Storlazzi et al. 2011; Takesue et al. 2009; Takesue and Storlazzi, 2019).

Temporal deployments of sediment traps used at coral reef sites have been applied to examine the contribution of the sediment sources including resuspension of existing SPM versus newly delivered SPM (e.g. Cortes and Risk, 1985; Nugues and Roberts, 2003; Malella et al. 2004; Bothner et al. 2006; Smith et al. 2008; Draut et al. 2009; Hernández et al. 2009; Storlazzi et al. 2009; Sherman et al. 2013; Gowan et al. 2014; Otaño-Cruz et al. 2017). A selection of these studies then compared the level of sediment exposure over a gradient of sites against corresponding coral health measurements to assess the potential negative effects of terrigenous sediments on coral reefs (Cortes and Risk, 1985; Nugues and Roberts, 2003; Smith et al. 2008; Gowan et al. 2014). Other studies have applied traps to provide important insights on sediment dynamics on coral reefs sites to highlight periods where the SPM flux moved past (and offshore) a site (i.e. short exposure period) compared to when newly delivered SPM is deposited on a reef and is available for subsequent resuspension (i.e. longer exposure period) (Bothner et al. 2006; Draut et al. 2009; Storlazzi et al. 2009, 2011). In these studies, trap collection rates during non-flood plume periods were correlated with near bed sediment stress.

1.5 Conclusions

Sediment traps deployed on coral reefs provide important insights on the level of sediment exposure at a site and the material in the trap can also be used for characterisation and source tracing purposes. Where they are coupled with additional instruments they likely provide a greater level of understanding of the spatial and temporal variability in vertical and horizontal sediment flux on coral reefs. While Storlazzi et al.'s (2011) landmark work provided the first protocols for sediment trap design and deployment for coral reefs, we highlight that the trap spacing requirements could be reduced from 10D to 3D with little influence on collection rates. In addition, we recommend traps deployed in coral reef settings contain baffles and that trap tilts are recorded on retrieval (with the collection rates on tilts > 5° given more scrutiny). Despite several decades of research, there remains some uncertainty on trap design specifications as well as the internal dynamics that influence trap collection. These gaps require further research across both controlled flume and well-instrumented field studies to further optimise sediment trap design and deployment protocols.

Acknowledgements

References

APHA 2005. Standard methods for the examination of water and wastewaters, 21st edn., American Public Health Association, American Water Works Association and Water Environment Federation, Washington, USA.

Baker, E.T., Milburn, H.B. and Tennant, D.A., 1988. Field assessment of sediment trap efficiency under varying flow conditions. *Journal of Marine Research*, *46*, 573-592.

Bale, A.J., 1998. Sediment trap performance in tidal waters: comparison of cylindrical and conical collectors. *Continental Shelf Research*, *18*, 1401-1418.

Bainbridge, Z. Lewis, S. Stevens, T. Petus, C., Lazarus, E. Gorman, J. and Smithers, S. in review. Measuring sediment grain size across the catchment to reef continuum: Improved methods and environmental insights. *Marine Pollution Bulletin*.

Bartley, R., Bainbridge, Z.T., Lewis, S.E., Kroon, F.J., Wilkinson, S.N., Brodie, J.E. and Silburn, D.M., 2014. Relating sediment impacts on coral reefs to watershed sources, processes and management: A review. Science of the Total Environment, 468–469C, 1138-1153, http://dx.doi.org/10.1016/j.scitotenv.2013.09.030.

Bloesch, J. and Burns, N.M., 1980. A critical review of sedimentation trap technique. *Schweizerische Zeitschrift für Hydrologie*, *42*, 15-55.

Blomqvist, S. and Kofoed. C. 1981. Sediment trapping—A subaquatic in situ experiment 1. *Limnology and Oceanography*, *26*, 585-590.

Bothner, M.H., Reynolds, R.L., Casso, M.A., Storlazzi, C.D. and Field, M.E., 2006. Quantity, composition, and source of sediment collected in sediment traps along the fringing coral reef off Molokai, Hawaii. *Marine Pollution Bulletin*, *52*, 1034-1047.

Brodersen, K. E., K. J. Hammer, V. Schrameyer, A. Floytrup, M. A. Rasheed, P. J. Ralph, M. Kühl, and O. Pedersen., 2017. Sediment Resuspension and Deposition on Seagrass Leaves Impedes Internal Plant Aeration and Promotes Phytotoxic H2S Intrusion. Frontiers in Plant Science 8.

Browne, N.K., Smithers, S.G., Perry, C.T. and Ridd, P.V., 2012. A field-based technique for measuring sediment flux on coral reefs: application to turbid reefs on the Great Barrier Reef. *Journal of Coastal Research*, *28*, 1247-1262.

Buesseler, K.O., Antia, A.N., Chen, M., Fowler, S.W., Gardner, W.D., Gustafsson, O., Harada, K., Michaels, A.F., Rutgers van der Loeff, M., Sarin, M. and Steinberg, D.K., 2007. An assessment of the use of sediment traps for estimating upper ocean particle fluxes. *Journal of Marine Research*, *65*, 345-416.

Butman, C.A., 1986. Sediment trap biases in turbulent flows: results from a laboratory flume study. *Journal of Marine Research*, *44*, 645-693.

Butman, C.A., Grant, W.D. and Stolzenbach, K.D., 1986. Predictions of sediment trap biases in turbulent flows: a theoretical analysis based on observations from the literature. *Journal of Marine Research*, *44*, 601-644.

Chiswell, S.M. and Nodder, S.D., 2015. Tilt-induced biases in sediment trap functioning. *Journal of Geophysical Research: Oceans*, *120*, 8381-8391.

Cortés, J.N. and Risk, M.J., 1985. A reef under siltation stress: Cahuita, Costa Rica. *Bulletin of Marine Science*, *36*, 339-356.

Dodge, R.E., Aller, R.C. and Thomson, J., 1974. Coral growth related to resuspension of bottom sediments. *Nature*, *247*, 574-577.

Donohue, I. and Garcia Molinos, J., 2009. Impacts of increased sediment loads on the ecology of lakes. *Biological Reviews*, *84*(4), pp.517-531.

Draut, A.E., Bothner, M.H., Field, M.E., Reynolds, R.L., Cochran, S.A., Logan, J.B., Storlazzi, C.D. and Berg, C.J., 2009. Supply and dispersal of flood sediment from a steep, tropical watershed: Hanalei Bay, Kaua'i, Hawai'i, USA. *Geological Society of America Bulletin*, *121*, 574-585.

Erftemeijer, P.L., Riegl A., Hoeksema B. W, and Todd. P. A., 2012. Environmental impacts of dredging and other sediment disturbances on corals: A review. Marine Pollution Bulletin 64, 1737–1765.

Gardner, W.D., 1980a. Sediment trap dynamics and calibration: a laboratory evaluation. *Journal of Marine Research*, *38*, 17-39.

Gardner, W.D., 1980b. Field assessment of sediment traps. *Journal of Marine Research*, *38*, 41-52.

Gardner, W.D., 2000. *Sediment trap sampling in surface waters* (pp. 240-284). Cambridge University Press, Cambridge.

Gardner, W.D., 1985. The effect of tilt on sediment trap efficiency. *Deep Sea Research Part A. Oceanographic Research Papers*, *32*, 349-361.

Gardner, W.D., Richardson, M.J., Hinga, K.R. and Biscaye, P.E., 1983. Resuspension measured with sediment traps in a high-energy environment. *Earth and Planetary Science Letters*, *66*, 262-278.

Gardner, W.D., Southard, J.B. and Hollister, C.D., 1985. Sedimentation, resuspension and chemistry of particles in the northwest Atlantic. *Marine Geology*, *65*, 199-242.

Gardner, W.D., Biscaye, P.E. and Richardson, M.J., 1997. A sediment trap experiment in the Vema Channel to evaluate the effect of horizontal particle fluxes on measured vertical fluxes. *Journal of Marine Research*, *55*, 995-1028.

Gowan, J.C., Tootell, J.S. and Carpenter, R.C., 2014. The effects of water flow and sedimentation on interactions between massive Porites and algal turf. *Coral Reefs*, *33*, 651-663.

Gray, J. R., G. D. Glysson, L. M. Turcios, and G. E. Schwarz (2000), Comparability of suspended-sediment concentration and total suspended solids data, U.S Geol. Surv. Water Resour. Invest. Rep. 00–4191, 14 pp.

Gust, G. and Kozerski, H.P., 2000. In situ sinking-particle flux from collection rates of cylindrical traps. *Marine Ecology Progress Series*, *208* 93-106.

Gust, G., Bowles, W., Giordano, S. and Hüttel, M., 1996. Particle accumulation in a cylindrical sediment trap under laminar and turbulent steady flow: an experimental approach. *Aquatic Sciences*, *58*, 297-326.

Hargrave, B.T. and Burns, N.M., 1979. Assessment of sediment trap collection efficiency. *Limnology and Oceanography*, *24*, 1124-1136.

Hawley, N., 1988. Flow in cylindrical sediment traps. *Journal of Great Lakes Research*, *14*, 76-88.

Hernández, R., Sherman, C., Weil, E. and Yoshioka, P., 2009. Spatial and temporal patterns in reef sediment accumulation and composition, southwestern insular shelf of Puerto Rico. *Caribbean journal of science*, *45*, 138-151.

Jürg, B., 1996. Towards a new generation of sediment traps and a better measurement/understanding of settling particle flux in lakes and oceans: a hydrodynamical protocol. *Aquatic Sciences*, *58*, 283-296.

Kozerski, H.P., 1994. Possibilities and limitations of sediment traps to measure sedimentation and resuspension. *Hydrobiologia*, *284*(1), pp.93-100.

Latrille, F.X., Tebbett, S.B. and Bellwood, D.R., 2019. Quantifying sediment dynamics on an inshore coral reef: Putting algal turfs in perspective. *Marine pollution bulletin*, *141*, 404-415.

Larcombe, P., Ridd, P.V., Prytz, A. and Wilson, B., 1995. Factors controlling suspended sediment on inner-shelf coral reefs, Townsville, Australia. *Coral Reefs*, *14*, 163-171.

Lau, Y.L., 1979. Laboratory study of cylindrical sedimentation traps. *Journal of the Fisheries Board of Canada*, *36*, 1288-1291.

Lough, J.M., Lewis, S.E. and Cantin, N.E., 2015. Freshwater impacts in the central Great Barrier Reef: 1648–2011. *Coral Reefs*, *34*, 739-751.

Mallela, J., Perry, C.T. and Haley, M.P., 2004. Reef morphology and community structure along a fluvial gradient, Rio Bueno, Jamaica. *Caribbean Journal of Science*, *40*, 299-311.

Mapstone, B.D., Choat, J.H., Cumming, R.L. and Oxley, W.G., 1992. The fringing reefs of Magnetic Island: benthic biota and sedimentation-a baseline study: a report to the Great Barrier Reef Marine Park Authority.

Marshall, S.M., Orr, A.P., 1931. Sedimentation on Low Isles Reef and its relation to coral growth. Scientific Reports Great Barrier Reef Expedition, 1(94-133).

Nodder, S.D. and Alexander, B.L., 1999. The effects of multiple trap spacing, baffles and brine volume on sediment trap collection efficiency. *Journal of Marine Research*, *57*, 537-559.

Nugues, M.M. and Roberts, C.M., 2003. Coral mortality and interaction with algae in relation to sedimentation. *Coral reefs*, *22*, 507-516.

Ogston, A.S., Storlazzi, C.D., Field, M.E. and Presto, M.K., 2004. Sediment resuspension and transport patterns on a fringing reef flat, Molokai, Hawaii. *Coral reefs*, *23*, 559-569.

Otaño-Cruz, A., Montañez-Acuña, A.A., Torres-López, V., Hernández-Figueroa, E.M. and Hernández-Delgado, E.A., 2017. Effects of changing weather, oceanographic conditions, and land uses on spatio-temporal variation of sedimentation dynamics along near-shore coral reefs. *Frontiers in Marine Science*, *4*, 249.

Reynolds, C.S., Wiseman, S.W. and Gardner, W.D., 1980. *An annotated bibliography of aquatic sediment traps and trapping methods* (No. 11). Freshwater Biological Association.

Ridd, P.V., Day, G., Thomas, S., Harradence, J., Fox, D., Bunt, J., Renagi, O. and Jago, C., 2001. Measurement of sediment deposition rates using an optical backscatter sensor. *Estuarine, Coastal and Shelf Science*, *52*, 155-163.

Risk, M.J., 2014. Assessing the effects of sediments and nutrients on coral reefs. Current Opinion in Environmental Sustainability, 7, 108-117.

Rogers, C.S., 1983. Sublethal and lethal effects of sediments applied to common Caribbean reef corals in the field. *Marine Pollution Bulletin*, *14*, 378-382.

Rogers, C.S., 1990. Responses of coral reefs and reef organisms to sedimentation. *Marine ecology progress series. 62*, 185-202.

Sherman, C., Hernandez, R., Hutchinson, Y. and Whitall, D., 2013. Chapter 4: Terrigenous sedimentation patterns at reefs adjacent to the Guánica Bay Watershed. *Baseline Assessment of Guánica Bay, Puerto Rico In Support of Watershed Restoration. MD: NCCOS Center for Coastal Monitoring and Assessment-Biogeography Branch, Silver*, 103-122.

Sherman, C., Schmidt, W., Appeldoorn, R., Hutchinson, Y., Ruiz, H., Nemeth, M., Bejarano, I., Motta, J.C. and Xu, H., 2016. Sediment dynamics and their potential influence on insular-slope mesophotic coral ecosystems. *Continental Shelf Research*, *129*, 1-9.

Smith, T.B., Nemeth, R.S., Blondeau, J., Calnan, J.M., Kadison, E. and Herzlieb, S., 2008. Assessing coral reef health across onshore to offshore stress gradients in the US Virgin Islands. *Marine Pollution Bulletin*, *56*(12), pp.1983-1991.

Søndergaard, M., Jensen, J.P. and Jeppesen, E., 2003. Role of sediment and internal loading of phosphorus in shallow lakes. *Hydrobiologia*, *506*(1), pp.135-145.

Stevens, T. 2013. Suspended sediment sampler. Australian Patent AU 2013206318. Canberra: IP Australia.

Storlazzi, C.D., Ogston, A.S., Bothner, M.H., Field, M.E. and Presto, M.K., 2004. Wave-and tidally-driven flow and sediment flux across a fringing coral reef: Southern Molokai, Hawaii. *Continental Shelf Research*, *24*, 1397-1419.

Storlazzi, C.D., Field, M.E., Bothner, M.H., Presto, M.K. and Draut, A.E., 2009. Sedimentation processes in a coral reef embayment: Hanalei Bay, Kauai. *Marine Geology*, *264*, 140-151.

Storlazzi, C.D., Field, M.E. and Bothner, M.H., 2011. The use (and misuse) of sediment traps in coral reef environments: theory, observations, and suggested protocols. *Coral Reefs*, *30*, 23-38.

Storlazzi, C.D., Norris, B.K. and Rosenberger, K.J., 2015. The influence of grain size, grain color, and suspended-sediment concentration on light attenuation: Why fine-grained terrestrial sediment is bad for coral reef ecosystems. *Coral Reefs*, *34*(3), pp.967-975.

Takesue, R.K. and Storlazzi, C.D., 2019. Geochemical sourcing of runoff from a young volcanic watershed to an impacted coral reef in Pelekane Bay, Hawaii. *Science of the Total Environment*, *649*, 353-363.

Takesue, R.K., Bothner, M.H. and Reynolds, R.L., 2009. Sources of land-derived runoff to a coral reef-fringed embayment identified using geochemical tracers in nearshore sediment traps. *Estuarine, Coastal and Shelf Science*, *85*, 459-471.

Weber, M., De Beer, D., Lott, C., Polerecky, L., Kohls, K., Abed, R.M., Ferdelman, T.G. and Fabricius, K.E., 2012. Mechanisms of damage to corals exposed to sedimentation. Proceedings of the National Academy of Sciences, 109(24), E1558-E1567.

White, J., 1990. The use of sediment traps in high-energy environments. *Marine Geophysical Researches*, *12*, 145-152.

Wolanski, E., Fabricius, K., Spagnol, S. and Brinkman, R., 2005. Fine sediment budget on an inner-shelf coral-fringed island, Great Barrier Reef of Australia. *Estuarine, Coastal and Shelf Science*, *65*, 153-158.

Wolanski, E., Fabricius, K.E., Cooper, T.F. and Humphrey, C., 2008. Wet season fine sediment dynamics on the inner shelf of the Great Barrier Reef. *Estuarine, Coastal and Shelf Science*, *77*, 755-762.

U.S. GOFS Report 10. 1989. Sediment trap technology and sampling. Rep. U.S. GOFS Working Group on Sediment Trap Technology and Sampling, November, 1988, G. A. Knauer and V. L. Asper, co-chairs, 94 pp.

CHAPTER 2

Measuring sediment grain size across the catchment to reef continuum: Improved methods and environmental insights

Zoe Bainbridge[1], Stephen Lewis[1], Thomas Stevens[1], Caroline Petus[1], Emily Lazarus[1,2], Jessica Gorman[1,3] and Scott Smithers[1,4]

1 Catchment to Reef Research Group, TropWATER, James Cook University
2 Present address: Alluvium Consulting, Fortitude Valley
3 Present address: Department of Agriculture & Fisheries
4 Environmental Science and Management, College of Science and Engineering, James Cook University

Abstract

Sediments collected within freshwater, estuarine and marine habitats were used to trial various chemical and physical pre-treatments to develop a systematic protocol for grain-size analysis using laser diffraction. Application of this protocol mitigates the influence of bio-physical processes that may transform grain-size distributions, enabling the characterisation and quantification of 'primary' mineral sediments across the complex freshwater-marine continuum to be more reliably assessed. Application of the protocol to two Great Barrier Reef (Australia) river catchments and their estuaries reveals the ecologically relevant <20 μm fraction comprises a larger component of exported sediment than existing methods indicate. These findings are highly relevant when comparing measured data to grain-size-specific modelled sediment loads and water quality targets. Finally, adoption of the protocol also improves the environmental interpretation of the influence of 'terrigenous sediment' in marine settings, including quantification of newly-delivered flood plume sediment.

2.1 Introduction

Grain size is a fundamental measure in the field of sedimentology. It is used to quantify sediment size, composition and texture, to understand geochemical properties, and to infer sediment transport and sorting dynamics (Sperazza et al. 2004; Walling et al. 2000; Blott & Pye 2012; Owens et al. 2016). Within a catchment to reef continuum setting, grain size analysis (GSA) is critical to determine the sediment size fractions that may be transported furthest from the stream mouth into the marine environment, and to define the particles likely to influence water clarity during both flood plume and subsequent resuspension events (Bartley et al. 2014; Bainbridge et al. 2018). Research focused on understanding sediment transport processes and tracing the source of eroded sediments to prioritise remediation sites requires a grain size methodology that can be applied to suspended sediment samples collected across the complex freshwater-marine continuum. This includes particles suspended in freshwater through the catchment, the estuarine mixing zone, and finally within the marine environment. Within each of these zones, physical and biogeochemical processes interact which can alter the composition, nature and transport potential of suspended sediments. Understanding and managing sediment loads is a key component of water-quality management on the Great Barrier Reef (GBR), Australia. However, factors including the transformations above make the measurement and modelling of sediment loads across the freshwater to marine continuum difficult. An improved characterisation of sediment loads being exported from individual GBR rivers, and a better understanding of the nature and significance of varying particulate organic matter contents and dominant grain size on sediment transport are required to reduce uncertainties in load estimations, and to improve how this sediment is monitored and modelled from catchment to reef (Bainbridge et al. 2018).

Several well-established techniques are available to measure sediment grain size, including wet sieving and settling methods (e.g. hydrometer, pipette, rapid sediment analyser), image analysis and laser diffraction (Eshel et al. 2004; Sperraza et al. 2004; Özer et al. 2010; Fisher et al. 2017; Bittelli et al. 2019). Laser diffraction measures the diameter of particles according to the intensity of scattered light (using Mie or Franhofer theory) from a dispersed particulate sample (International Organisation for Standardisation, 2020). Wider access to improved laser diffraction instruments has increased their use in recent years, with advantages over traditional settling techniques including the speed of analysis and the capacity to precisely measure a complete grain-size distribution of the fine sediment fraction (Esher et al. 2004; Özer et al. 2010; Fisher et al. 2017; Bittelli et al. 2019). While standardised GSA procedures and protocols are well-established for analysis of soils, suspended sediment and sediment cores (Walling et al. 2000; Snyder et al. 2004; Özer et al. 2010), the details of sample pre-treatment and GSA procedures for marine sediments are more complex and varied (Loring & Rantala 1992; Rodriguez & Uriarte 2009; Spencer 2017; Romano et al. 2018; Hunt & Jones 2019). Marine sediment pre-treatment and GSA procedures will also vary depending on whether the grain sizes of agglomerated *in situ* particles or the primary constituent particles of which they are composed are the focus (Allen and Thornley, 2004; Spencer, 2017; Hunter & Jones 2019).

Grain size analyses of suspended sediment in streams are regularly performed to determine sediment behaviour, transport and likely sediment fate (Walling et al. 2000). Analytical methods are straightforward, with little pre-treatment of sample typically required as the medium is freshwater, with similar properties to the deionised water routinely used as the

dispersing medium that delivers the sediments into the laser diffraction instrument. Measuring the grain size of marine sediment is far more complex due to changes in ionic strength and the influence of additional components such as microscopic organisms and other organic matter (e.g. plankton, detritus, biogenic silica) and marine carbonates (e.g. coral, mollusc, coralline algae fragments) (Loring & Rantala 1992; Reynolds et al. 2010; Romano et al. 2018). Low sediment concentrations (<5 mg L^{-1}) in offshore flood plume waters present further challenges to the collection of the necessary sample volumes required to satisfy obscuration thresholds for reliable GSA (Bainbridge et al. 2012). The *in situ*, particle aggregate sizes may be required when examining marine sediment transport dynamics, whereas terrigenous sediment transport and source tracing studies require an understanding of the hydrodynamic properties of individual 'primary' sediment grains; investigations of the latter will involve removing the marine components through various sample pre-treatments (Spencer, 2017). Undertaking concurrent *in situ* and treated analyses provides a more thorough understanding of the source, transport, and fate of suspended sediments, and when considered together can provide insights on the bio-physical processes that influence sediments across the catchment to marine continuum.

This study sought to develop a standard sediment grain size methodology for both freshwater and marine environments for application in catchment to reef studies, encompassing freshwater, estuarine, organic-rich flood plume and marine resuspended sediment samples. We use two case study rivers from the Great Barrier Reef (GBR), Australia, including the Tully River located in the Wet Tropics and Burdekin River located in the Dry Tropics. Samples in each location were collected along transects that included: (i) end-of-river (EoR) (freshwater) suspended sediment transported in elevated flow events; (ii) surface water sediment from the adjacent estuary and flood plume during high-flow discharge events; and (iii) sediment captured in marine sediment traps deployed at inshore GBR reef and seagrass habitats. We explore the influence of several different pre-treatments commonly applied to chemically disperse marine sediment samples on grain size results. The treatments examined included the use of Calgon and the removal of salts, organic matter and carbonate material. We show that the application of different treatments can produce highly variable grain-size distributions. A standard approach for the pre-treatment and analysis of sediment for studies that span the freshwater-marine continuum is recommended to ensure consistent and replicated results. Finally, we apply our standard method to demonstrate the importance of sample pre-treatment to accurately measure sediment dynamics across the catchment to marine continuum, and we outline how these new data can be incorporated within the current water-quality monitoring and modelling framework on the GBR.

2.2 Methods

2.2.1 Study region

This study focused on two GBR catchment to reef transects, including the Tully River catchment (1,480 km^2) located in the Wet Tropical region and discharging into the northern GBR, and the larger, seasonally Dry Tropical Burdekin River catchment (130,000 km^2), that drains into the central GBR (Figure 2.1). High rainfall and discharge events, concentrated during the wet season and often associated with tropical cyclones and depressions, dominate the flow regimes of both rivers (Lough et al. 2015). Detailed catchment descriptions are provided in Bainbridge et al. 2009 and 2014. Briefly, the long-term median annual discharge

for the Tully River Basin is 3,536 GL (1986-2018 inclusive; Gruber et al. 2019), with discharge from this river characterised by elevated dissolved inorganic nitrogen loads (Bainbridge et al. 2009). The mostly natural (rainforest) upper catchment drains into a coastal floodplain extensively modified by agricultural expansion (sugarcane, horticulture) in the late 20th century (Lewis et al. in review). In contrast, the Burdekin River has a 'hot semi-arid' climate as defined by the Köppen-Geiger climate classification scheme (Peel et al. 2007), with highly pronounced intra-annual (coefficient of variation 1.3) and also relatively high interannual (coefficient of variation 1.1) river discharge variability (Lewis et al. 2013). The Burdekin long-term median annual discharge is 6,290 GL (range: 246-54,031 GL), calculated over a 93-year gauge record to 2014 (Lough et al. 2015). This catchment is dominated (>90%) by cattle grazing across open woodland pastures. Ground cover is typically low, with soils exposed and erosion prone over much of the catchment (Bartley et al. 2014). The Burdekin catchment is the largest single contributor of suspended sediment to the GBR, exporting an average of four million tonnes of sediment per annum (range 0.004-15.74 over the period 1986 to 2010) (Kuhnert et al. 2012). Targeted management efforts are underway to reduce the suspended sediment load exported from the Burdekin catchment to improve turbidity regimes and water clarity in inshore and mid-shelf GBR environments (Bartley et al. 2014; Fabricius et al. 2014, 2016; Bainbridge et al. 2018).
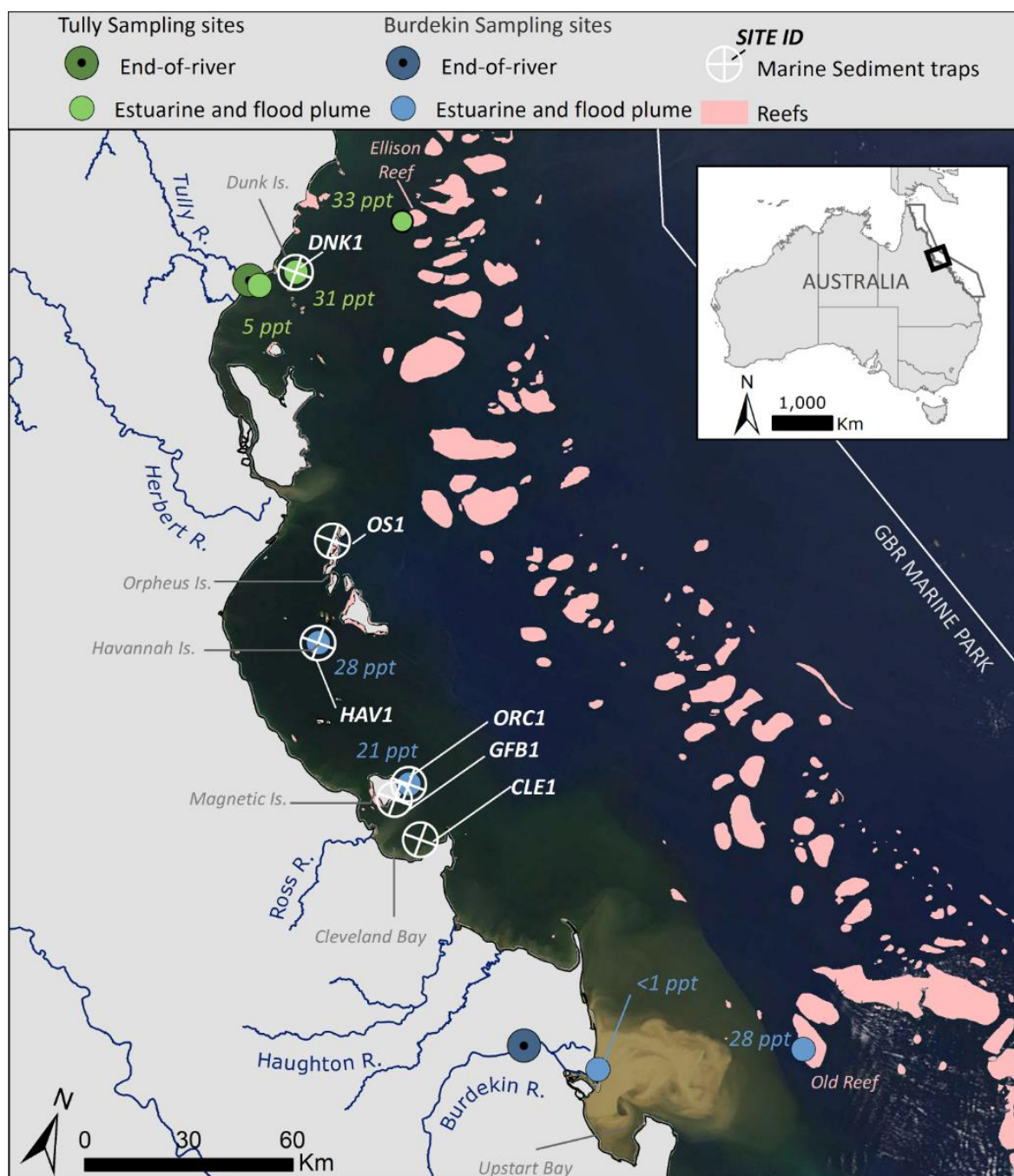
Figure 2.1. MODIS (Aqua true-colour) satellite image captured on the 12th February 2019 following peak discharge at the Burdekin River mouth, highlighting a visible turbid sediment plume and less turbid secondary waters moving northwards along the Queensland coastline. Reefs shown as pink polygons. End-of-river, estuarine and flood plume sampling sites are shown for the Tully (green circles) and Burdekin (blue circles) Rivers, following a salinity gradient from each river mouth to the respective sediment trap sites (crossed circles) within the inshore Great Barrier Reef. Off the Burdekin River mouth, a sample was also collected from flood plume waters which covered Old Reef on the 15th February, 2019. Note the Tully River to Dunk Island sampling sites were collected in a flood plume event during February 2018 (not captured in this image, refer to Supp. Fig. 1c).

2.2.2 Sampling design and collection

This study forms part of a larger Australian Government National Environmental Science Program (NESP) research project aimed at characterising and tracing the origin(s) and fate of environmentally detrimental sediment across two catchment-to-reef transects of the GBR,

including the Tully and Burdekin Rivers. Field sampling campaigns in each transect location targeted:

1) end-of-river (freshwater) suspended sediment sampled during wet season high flow discharge events;

2) surface water suspended particulate matter (SPM) in the adjacent estuary and resultant flood plume generated by these high-flow discharge events; and

3) SPM captured over time in marine sediment traps situated at key inshore reef and seagrass habitats within the inshore GBR. These sediment traps capture a combination of newly delivered flood plume SPM as it is transported across the inshore lagoon and settles from the water column as well as sediments delivered to the traps when benthic deposits composed of previously deposited materials are resuspended during turbulent high-energy periods (Lewis et al. 2020).

Prior to this project, field logistical, technological and analytical constraints have restricted the collection of sufficient sample material for the full characterisation and tracing of terrigenous sediment transported in flood plumes and during subsequent resuspension events within the GBR lagoon. The novel application of the patented SediPump® high-volume filtration system (Stevens, 2019) and SediSampler® sediment trap (Stevens, 2013) have been critical in achieving the collection of sufficient sediment mass to perform the required analyses from:

- end-of-river and flood plume surface waters, *in situ* during high flow events. The SediPump® high-volume filtration system (Integral Aqua Pty Ltd) collects necessary masses (>1 g) of sample material from low sediment concentration water types (refer to section 2.2.6). These included low SPM concentration plume waters (typically <5 mg L^{-1} in salinities 10 PPT or greater; Bainbridge et al. 2012), and rivers of the northern GBR Wet Tropics region with lower sediment concentrations, including the Tully River.

- the subsequent deposition of plume SPM and resuspended material captured within SediSampler® traps fixed at reef/seagrass substrates, with material accumulating over 2-3 month deployment periods. The SediSampler® traps surround an *in situ* instrument array comprising a nephelometer (turbidity), pressure, light and current meters at each site. The traps and arrays were continuously deployed, on rotating 2-3 month deployments between June 2016 and March 2020 (Chapter 1).

The sediment samples collected during this project have been used to characterise the physical, chemical and biological traits of the fine sediments, and to trace their source and transformation, at a level of detail not possible in previous GBR research. Developing a consistent and reproducible methodology for the pre-treatment and analysis for primary grain size of mineral particles in samples collected across this catchment to reef continuum was also essential.

2.2.3 End-of-river (freshwater) samples

Our dataset includes EoR suspended sediment samples from the Burdekin and Tully Rivers captured during high flow events that occurred over the 2016-2017 and 2017-2018 water years, and also the 2018-2019 water year for the Burdekin. Opportunistic, representative samples were also collected from the neighbouring South Johnstone River (Wet Tropics) in

2018, and the Herbert (Wet Tropics), Ross and Haughton (Dry Tropics) Rivers in 2019 (refer to Table 2.6). In total 15 samples were analysed for the Burdekin, three for the Tully, two for the Ross and one each for the neighbouring South Johnstone, Herbert and Haughton Rivers. The Herbert River sample was a composite of daily sampling across the discharge peak from 4th to 7th February, 2019. The grain size methodology development component of this paper focuses mainly on samples collected across the 2019 Burdekin and 2018 Tully transects (EoR, flood plume and marine sediment trap samples).

The EoR sample for the Burdekin River was collected in February 2019 during a prolonged and 'large flood event', with an approximate 1 in 5-year flood return (volume) interval. The Burdekin River discharged 14.5 million ML in the 3-week period between 30 January and 19 February, and peaked at the moderate flood river height classification (Gruber et al. 2020). A manual 'grab' sample collected on the 6th February at Inkerman Bridge (Figure 2.1) during the first of multiple flood peaks that occurred during this event had a suspended particulate matter (SPM) concentration of 470 mg L^{-1} (all SPM concentrations measured using the total suspended solid method).

The Tully EoR sample was collected from the freshwater upstream limit of the estuary on the 9th February 2018 (Figure 2.1) during a catchment wide, moderate-sized flood discharge event. SPM concentrations ran at 17 mg L^{-1} at the time of sample collection; SPM for this smaller Wet Tropics River are clearly much lower than those produced by the larger and drier Burdekin system. To ensure sufficient sediment was collected to perform all analyses outlined below, the standard manual grab sample (for nutrients and suspended sediments) was augmented with another collected using the SediPump® filtration system.

Additional wet season sampling details for the Burdekin (March 2017, March 2018), Tully (January 2017 and March 2018) and the ancillary rivers sampled are provided in Supp. Table 1.

2.2.4 Flood plume samples

Flood plume sampling along the estuarine salinity gradient from the river mouth was conducted immediately following EoR sample collection. Given the large size and duration of the Burdekin flood plume, sample sites targeted the movement of the plume over a number of days guided by near real-time MODIS satellite imagery. Samples were collected when the plume passed over sediment trap and environmental logger sites (HAV1, ORC1) as it moved northwards (11-12th Feb 2019), and later as it moved directly offshore to the mid shelf (Old Reef, 15th Feb 2019) (Figure 2.1). Suspended particulate matter (sediment and organic matter) samples were collected using a 10 L container in plume surface waters (i.e. top 0.5 m) at the low salinity (<1 ppt), high concentration (590 mg L^{-1}) turbid plume site (Figure 2.1). For the three offshore sites where greater mixing with seawater had occurred (i.e. 21-28 ppt), samples were collected using the SediPump® high-volume filtration system to ensure adequate samples sizes to complete the analyses below. Pump durations at each site were 2-3 hours, which includes the time to collect both a surface and depth sample (1-2m above local benthic depth). Only the Old Reef depth sample is discussed in this paper.

Sampling of the plume surface water at the shorter Tully River transect occurred on the 9th February 2018. Sites were located along a salinity gradient transect extending from the

freshwater reaches of the estuary out to the sediment trap and environmental instrument array installed at a nearshore reef off Dunk Island (DNK1) (Figure 2.1). At this most offshore site, surface waters were well mixed and had a salinity of 31 ppt. Using real-time MODIS satellite imagery to track plume movement and guide sampling, an outer plume transect was repeated 5 days later (14th Feb). This sampling campaign targeted Ellison Reef on the mid-shelf, where the plume extent was clearly visible and surface water salinity was measured to be 33 ppt. The DNK1 trap site was also resampled on this second trip, with increased salinity (33 ppt) indicating further mixing of plume surface waters with seawater during the intervening five days. Because SPM concentrations were low across the entire transect the SediPump® filtration system was used to collect all samples.

Additional wet season flood plume sampling of Burdekin (March 2017, March 2018) and Tully (January 2017 and March 2018) river discharge events are reported in Lewis et al. (2018) and are also referred to in this study. Flood plume sampling transect locations and associated wet season water-type mapping (e.g. Devlin et al. 2015 and Petus et al. 2019) for each event are provided in Supp. Figure 1a-e. Wet season water type maps are produced using MODIS true colour satellite imagery reclassified to six distinct colour classes defined by their colour properties (Alvarez-Romero et al. 2012). The wet season water types are regrouped into three water types: primary, secondary and tertiary, and characterised by different concentrations of optically active components (suspended sediment, colour dissolved organic matter and chlorophyll a), which control the colour of the water and influence the light attenuation, and different contaminant concentrations (Petus et al. 2019). In the GBR, the primary water type is typically found in nearshore areas with resuspended sediments and/or inshore regions of river flood plumes and the secondary waters are typical of coastal waters or the mid-region of river plumes. Sampling targeted both primary (brownish to brownish-green turbid water masses) and secondary (greenish to greenish-blue water masses with increased algal content) water types in flood plumes (hereafter 'water type'). Water types are described in further detail in Supp. Material 1.

2.2.5 Marine sediment traps

Six marine trap sediment samples were chosen for grain size method development to represent a range of inshore GBR environmental conditions, including reefal and open sediment field locations, relatively low to high swell exposure and bottom currents, as well as seasonal conditions (Table 2.1). Five SediSamplers® were located in Cleveland and Halifax Bays, on an approximately north-south longitudinal gradient extending from the Burdekin River mouth (Figure 2.1). The most northern SediSampler® was deployed at Dunk Island, ~13 km from the Tully River mouth. Collected samples include mineral sediment, organic matter and marine carbonates deposited within the trap over a ~90 day deployment period. Samples from the five Burdekin sites represent wet season flood (ORC1, CLE1, HAV1) and post wet season (GFB1, OS1) deployments between December 2018 and June 2019. The Dunk Island trap (DNK1) was deployed from December 2017 to February 2018. This site is located on a reef-slope on the western side of the island to capture flood plume material exported from the Tully and nearby rivers.

Representative sub-samples were extracted from each highly-concentrated and well-mixed field sample for the analyses outlined in section 2.2.7 below.

Table 2.1. Environmental settings for the six marine sediment trap sites shown in Figure 2.1.

Environment Key	DNK1	OS1	HAV1	ORC1	GFB1	CLE1
Trap depth below LAT and position	6 m, lower reef slope	10.5 m, mid reef slope	8 m, mid reef slope	15 m, open sediment field	3 m, sub-tidal reef flat	3.5 m, open sediment field
Proximity to dominant catchments or coastline	• 13 km → Tully River • 6 km → main coastline	• 20 km → Herbert River • 14 km → main coastline	• ~160 km → Burdekin River • 23 km → main coastline	• ~115 km → Burdekin River • 19 km → Ross River	• ~115 km → Burdekin River • 13 km → Ross River	• ~110 km → Burdekin River • 13 km → Ross River
Turbidity (NTU)[1]	Moderate	Low	Low	High	Moderate	Very High
Exposure to swell	Exposed to South-Easterly swell	Sheltered	Sheltered	Exposed	Exposed to South-Easterly swell	Semi-exposed
Benthic current (m/s)[2]	Low	High	Moderate	High	Moderate	Very high
Substrate description and image	Weak reef framework with undulating substrate. Thin dynamic mud layer embedded with coral rubble. Abundant turf algae on hard dead corals.	Weak reef framework with massive and encrusting live and dead corals, large undulating reef slope; high current low deposition environment.	Unconsolidated fine carbonates. Complex undulating morphology (intermittent grooves filled with fine sediment), high coral cover (>80% live *Goniopora* sp.).	Unconsolidated, flat, exposed outer bay mobile sediment field. Soft deep mud with poorly sorted large shell grit.	Weak reef framework. Poorly sorted terrigenous/carbonate mix. Abundant macro algae.	Unconsolidated, flat mid-bay site. Thick layer of mobile mud covering poorly sorted shell fragments. Often covered with moderate ephemeral sea grass cover.

[1] Mean site turbidity = Low (<2 NTU) Moderate (2-5 NTU) High (5-15 NTU) Very High (>15 NTU) from Lewis et al. (2020) for the period June 2016 to March 2020 for all sites, except DNK1 (June 2016 to March 2019).

[2] Mean site benthic current (~60cm above substrate) using ten minute average data discontinuous record for the period June 2016 to March 2020 for all sites, except DNK1 (June 2016 to March 2019) from Lewis et al. (2020). Categories = Low (<0.04 m/s) Moderate (0.04-0.8 m/s) High (0.8-0.12 m/s) Very High (>0.12 m/s)

2.2.6 Suitability of the SediPump® sample collection method for grain size analysis

The SediPump® high-volume filtration system (Stevens, 2019) was configured and initially applied in this study to process large volumes of water (> 6 KL) to collect sufficient fine particles for sediment source tracing analyses. The SediPump® houses a replaceable 1 µm string filter, where particulate matter in the water column is filtered and captured within the carousel. Fixed to a small vessel (<6 m), several thousand litres of water are pumped from a targeted section of the water column *in situ* over a short time period (e.g. 2 hours) where a 20 ± 0.5 L min^{-1} filter^{-1} processes 2400 ± 60L. Using this SediPump® set up, 2-4 grams of sediment are typically recovered from plume surface and depth waters with SPM concentrations <5 mg L^{-1} within two hours. This capability presented the opportunity to potentially capture the sample volumes required for additional analyses, including grain size analysis and the larger sample material required for multiple pre-treatment steps. Low concentrations and field logistics have in the past limited sample sizes and the scope of analyses. Full GSA including pre-treatment for organic removal on low SPM concentration flood plume waters has been notoriously difficult, limited by grab samples containing high organic contents (~50%) and relatively low SPM concentrations (i.e. <5 mg L^{-1}). Previous investigations of Burdekin flood plume SPM samples found the grain sizes were mostly larger than 1 µm (Bainbridge et al. 2012), and hence the 1 µm filter used in the Sedipump should capture all particulates in the plume.

To confirm the SediPump® captures the full representative grain-size distribution of sampled waters, point-in-time 'grab' samples were also collected during SediPump® sampling at three sites for comparison. These sites included the Tully flood plume estuarine zone (5 ppt) in 2018 (1-hour pumping time), and the Orchard Rocks (ORC1) and Old Reef sites sampled in the 2019 Burdekin flood plume transect (each pumped for 2 hours). Grain size results are presented for the analysis that included a salt-removal pre-treatment.

2.2.7 Sample pre-treatments

Pre-treatment steps for the samples collected from the EoR, flood plume and marine sites are outlined in Figure 2.2. They include mechanical and chemical dispersion of flocculated particles, and the removal of salt, organic and carbonate materials which may influence the measured sediment grain size. Representative aliquots of each sample were prepared for the number of pre-treatment steps required to process each sample type (i.e. freshwater, estuarine or sediment trap). Each pre-treatment is described further below.
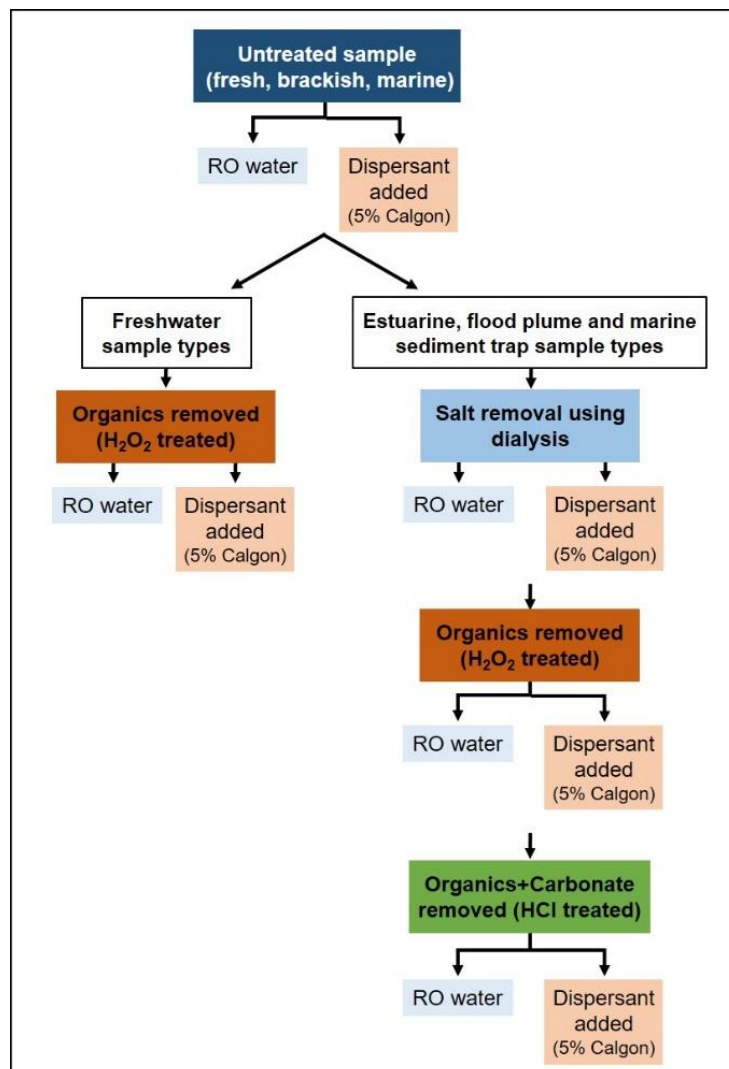
Figure 2.2. Flow chart illustrating the pre-treatment steps undertaken in this study prior to grain size analysis for end-of-river freshwater sample types (left) and estuarine, flood plume and marine sediment traps (right).

Removal of organic matter [All samples]: Hydrogen peroxide (H_2O_2) is commonly used for wet oxidation of organic matter, with minimal damage to the mineral grains of the sample (Vassma et al. 2008; Romano et al. 2018). Concentrated H_2O_2 (30%) was added to a small aliquot of each sample (i.e. 50-100 ml sample) at a 50:50 H_2O_2 to water dilution. Sub-samples were placed in a fume hood and heated in a water bath at 80°C until the active reaction (i.e. bubbling) had ceased. The active reaction duration varied between sample types; organic-rich flood plume samples required repeated H_2O_2 additions and heating time over a number of days whereas those with lower organic contents were usually completed within 24 hours. Finally, whilst remaining in the water bath samples were rinsed and decanted with RO water until H_2O_2 concentrations were <1 mg L^{-1} (measured using Quantofix® peroxide test strips).

Salt removal [Salt-influenced samples]: Dissolved salts were removed using pre-rinsed cellulose membrane visking dialysis tubing. Sediment samples were placed and sealed into the tubing and continuously rinsed with RO water until conductivity <200 µS.cm^{-1} was achieved (measured using an Orion Star A215 meter and 013005MD conductivity cell).

Marine carbonate removal [Marine trap samples only]: Following H_2O_2 treatment above, carbonate present in sediment recovered from the marine traps was digested using HCl acid (1M active concentration) in a water bath at 80°C for 3 to 4 hours until the reaction ceased. Samples were then repeatedly rinsed (≥ 3 times) and decanted with RO water (≥ 1L) to flush the acid (Vaasma et al. 2008; Fisher et al. 2017).

2.2.8 Sample analysis

Sediment grain size analysis

Grain size distributions were determined using a Mastersizer 3000 (Malvern Panalytical) laser diffraction analyser with a lens range of 0.01–3500 µm following the general ISO 13320:2020(E) guidelines (International Organisation for Standardisation, 2020). The Mie diffraction theory was applied, which is most applicable to measuring sediments <50 µm in diameter, typical of our sample types (Sperazza et al. 2004; Özer et al. 2010). A refractive index of 1.52 was used and all samples were ultrasonically dispersed (at 15% power) for 30 seconds in the introduction unit prior to measurement. Each sample was measured by the Mastersizer three times, and following checks for quality assurance (e.g. data quality pass, weighted residual, signal to noise ratio) the average of these measurements was used for reporting. Samples were sieved through a coarse 1400 µm wet mesh sieve before measurement on the Mastersizer to remove large carbonate (shell or coral) fragments in marine samples and leaf/woody debris in freshwater samples. No residual sediment was captured by this coarse sieve from any of our samples.

A small quantity (~5 ml) of the common dispersal agent, Calgon (5% solution sodium hexametaphosphate) was initially trialled and added to a subset of all sample types, following the flow chart in Figure 2.2 developed from the literature.

Microscope analysis (see relevant section below) established the presence of long cylindrical or large circular diatoms in flood plume sediment samples. These diatoms were removed by repeatedly sieving samples through 38 µm sieves before they were re-analysed for mineral grain size on the Mastersizer. In these cases, sieves were carefully checked to ensure no

mineral grains were captured. The Mastersizer determined that most mineral grains were <20 µm in diameter.

Results are presented as grain-size distribution plots (% distribution by volume), and classified underneath each plot as one of four size classes based on the Udden-Wentworth sediment grain size scale (Leeder, 1982): (1) clay (<3.9 µm); (2) very fine and fine silt (3.9-15.6 µm; hereafter referred to as fine silt); (3) coarse silt (15.6-63 µm); and (4) sand (63-2000 µm). Grain size results are also provided in tabular form as D-values (D10, D50, D90) representing the median particle diameter, in µm (i.e. D50 = 50% by volume of the particles is smaller than this diameter), and the particle diameter at the 10th and 90th percentiles (AS 4863.1-2000). For each sample analysed the standard deviation for these D-values (D10, D50, D90) are provided. The proportion of sediment grain size for each measured sample representing the ecologically relevant <20 µm fraction is also reported (see Bainbridge et al. 2018). This <20 µm fraction is often referred to as "fine sediment" within current Great Barrier Reef science and policy documents (e.g. Brodie et al. 2017; McCloskey et al. in review-a).

Microscope analysis
Light microscopy was used to visually assess the effect of each pre-treatment on grain size, flocculation and separation in each sample. A small aliquot (i.e. 1-2 pipette drops) of sub-sample collected at each pre-treatment step was placed on a microscope slide (diluted with RO if required) for visual comparison of a sample across each pre-treatment step undertaken. The ToupView software program (Touptex photonics) was used to capture these images.

Loss-on-ignition (LOI) for organic matter and carbonate content
Sample organic matter content was determined using Standard Method 2540E (APHA, 2012). Briefly, a glass fibre filter paper (flood plume samples) or crucible (sediment trap samples) containing a pre-weighed quantity of each sample (dried at 105°C to remove moisture) was ignited in a Carbolite (AAF1100) ashing furnace at 550°C for 4 to 5 hours, before being reweighed. The weight lost during ignition represents the total volatile solids, an approximation of the organic matter content of each sample (weight % LOI, 550°C).

Marine sediment trap carbonate content (weight % LOI, 950°C) was determined through an additional igniting step to the process above, as described by Heiri et al. (2001). Briefly, following LOI at 550°C, sample crucibles were returned to the ashing furnace and heated at 950°C for at least 6 hours, with the weight lost on ignition representing carbon dioxide release from calcium carbonate. The ratio between CO_2 and $CaCO_3$ molecular weights can then be used to determine the percentage of $CaCO_3$ in the original sample following Equation 1.

Equation 1. $\% \, CaCO_3 = \frac{[\text{Sample weight post 550°C ash - sample weight post 950°C ash}]}{[\text{Dried sample weight post 100°C}]} \times 2.274 \times 100$

2.3 Results

2.3.1 Systematic protocol for sediment grain size analysis across the catchment to reef continuum

Freshwater samples

EoR samples collected in freshwater were uncontaminated by salt water or marine carbonates and required the least pre-measurement preparation. Measurement of the untreated (as collected) sample produces the grain-size distribution (Figure 2.3b,d dark blue series) of all particulate matter carried in suspension at the EoR, including discrete mineral grains, freshwater diatoms and flocculated particles held together by organic matter (Figure 2.3 a and c). Flocs and freshwater diatoms were more common in the Tully River EoR samples (e.g. Figure 2.3c) than those from the Burdekin, where they were only observed in samples collected during the rising stages of the 2017 and 2019 flood events.

Pre-treatment to remove organic matter reduced the number of larger particles. As a result the grain-size distributions of both samples shifted toward the finer size fractions (Figure 2.3b,d orange series) and the D10, D50 and D90 values all decreased (Tables 2.2-2.3). The organic-rich Tully sample (18% organic content) changed the most, with the distribution curve shifting toward the finer fractions and the grain size ranges narrowing from 1.45 to 400 μm and 1.13 to 111 μm in the untreated and treated samples respectively. Grain-size values for the D10, D50 and D90 statistics all decreased by ≥50% (the D50 reduced from 14.6 to 6.6 μm; the D90 from 62 to 22 μm). The untreated Burdekin EoR sample's multi-modal distribution persisted post-treatment, but the proportion of sediments in the main finer-fraction peak increased as coarser sediments dominated by organics were removed by the treatment procedure. Overall the distribution shifted toward the finer fractions; the untreated D50 of 7.4 μm changed to 5.6 μm after treatment (Figure 2.3b).

Calgon addition did not improve measurement precision or alter the grain-size distributions of EoR samples (e.g. Supp. Figure 2a); the relative standard deviation (RSD) was generally <5%, especially for the D10 and D50 statistics. Accordingly, EoR samples were not pre-treated with Calgon.
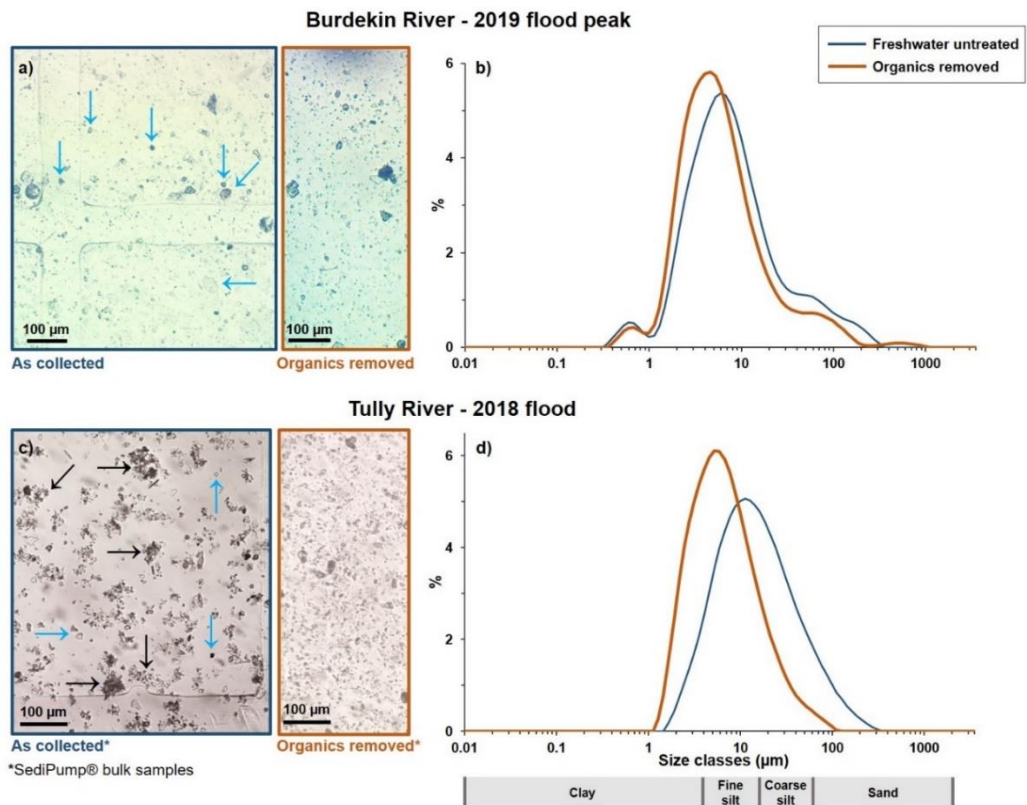
Figure 2.3. Micro-imagery of Burdekin (a) and Tully (c) end-of-river (freshwater) samples collected during respective flood peaks (dark blue border), highlighting the presence of discrete clay, silt and sand-sized mineral grains in both samples (blue arrows), as well as small flocs (black arrows) present in the Tully River sample. The right-hand (orange border) image in each set is the sample post treatment for organic-removal, and shows the removal of binding floc organic matter in the Tully sample, with fine-grained mineral particles now separated. Note the bulk SediPump® sample has been used for this Tully EoR sample analysis, compared to a standard 'grab sample' captured at the Burdekin EoR, with an approximate 25-fold higher SPM concentration (470 mg L^{-1} compared to 17 mg L^{-1} for the Tully EoR). Grain-size distributions for the untreated and organic-removed sub-samples for the Burdekin (b) and Tully (d) EoR samples are also displayed. Mastersizer analysis ranges from 0.01 to 2000 µm (log scale), and represents each distribution as percent volume. A fine, colloidal fraction (<1 µm) is present in the Burdekin multi-modal distribution (b). A vertical scale below the plot represents the proportion of grain sizes within the clay, fine silt, coarse silt and sand size fractions.

Table 2.2. Grain size results for sediment samples collected along the Burdekin River flood plume salinity gradient (6-15/02/19) during a major discharge event in February 2019. Grain size results including the proportion of sample sediments <20 μm and the full grain-size distribution represented by the D10, D50 and D90 (standard deviation in brackets) are presented for the various pre-treatment options for each site including: as collected (i.e. untreated) and salt-, organic- and carbonate removed sub-samples. An additional measurement run for the plume samples that were repeatedly sieved through 38μm mesh is also included. The set of final results used for each sample (i.e. best treatment option) is highlighted.

Sample location from catchment to reef		% organic	Treatment	<20 μm %	Grain size (μm)		
					D10	D50	D90
Freshwater	End-of-river	12%	*As collected*	81	2.4 (±0.01)	7.4 (±0.05)	43 (±5)
			Organics removed	**87**	**2.1 (±0.01)**	**5.6 (±0.09)**	**29 (±5)**
Plume – turbid primary waters	Estuarine mixing zone <1 ppt	15%	*Salt removed*	80	2.3 (±0.01)	7.7 (±0.02)	36 (±1)
			Salt + Organics removed	**89**	**2.2 (±0.00)**	**6.1 (±0.02)**	**21 (±0)**
Plume – secondary waters	Northern plume – 21 ppt surface waters @ ORC1 trap site	~19%	*Salt removed*	50	4.6 (±0.03)	19.9 (±0.35)	142 (±8)
			Salt-Organics removed	55	2.6 (±0.01)	15.9 (±0.27)	101 (±2)
			Salt + Organics removed + <38μm sieved	**83**	**1.4 (±0.01)**	**6.6 (±0.14)**	**34 (±3)**
Plume – secondary waters	Northern plume – 28 ppt surface waters @ HAV1 trap site	~50%	*Salt removed*	41	6.5 (±0.05)	26 (±0.12)	123 (±3)
			Salt + Organics removed	**44**	**4.3 (±0.01)**	**25 (±0.12)**	**97 (±0)**
			Salt + Organics removed + <38μm sieved	**68**	**2.4 (±0.01)**	**11.5 (±0.06)**	**63 (±1)**
			Salt-Organics-Carbonate removed	50	3.6 (±0.03)	19.9 (±0.36)	82 (±2)
Plume – secondary waters	Mid-shelf – 28 ppt (Old Reef)	~50%	*Salt removed*	59	4.9 (±0.04)	15.3 (±0.25)	84 (±2)
			Salt + Organics removed	**58**	**1.3 (±0.06)**	**13.0 (±0.40)**	**81 (±3)**
			Salt + Organics removed + <38μm sieved	**79**	**0.7 (±0.00)**	**6.6 (±0.11)**	**31 (±1)**

Table 2.3. Grain size results for sediment samples collected along the Tully River flood plume salinity gradient (9-14/02/18) during a major discharge event in February 2018. Grain size results including the proportion of sample <20 μm and the full grain-size distribution represented by the D10, D50 and D90 (standard deviation in brackets) are presented for the various pre-treatment options for each site including: as collected (i.e. untreated) and salt- and organic removed sub-samples. The set of final results used for each sample (i.e. best treatment option) is highlighted.

Sample location from catchment to reef		% organic	Treatment	<20 μm %	Grain size (μm)		
					D10	D50	D90
Freshwater	Freshwater estuary – 0.05 ppt	18%	*As collected – freshwater*	62	4.6 (±0.01)	14.6 (±0.10)	62 (±2)
			Organics removed	**88**	**2.6 (±0.01)**	**6.6 (±0.01)**	**22 (±0)**
Plume – primary waters	Estuarine mixing zone – 5 ppt	20%	*As collected – 5 ppt*	68	4.4 (±0.01)	13.6 (±0.06)	40 (±0)
			Salt removed	72	2.9 (±1.53)	10.5 (±0.60)	39 (±1)
			Salt + Organics removed	**71**	**3.2 (±0.01)**	**10.4 (±0.10)**	**45 (±1)**
Plume – secondary waters	Midway to Dunk Is. – 22 ppt	33%	*Salt removed*	61	3.1 (±0.03)	13.4 (±0.20)	103 (±6)
			Salt + Organics removed	**91**	**0.7 (±0.01)**	**4.3 (±0.02)**	**18 (±1)**
Plume – secondary waters	Outer plume – 31 ppt surface waters @ DNK1 trap site	38%	*As collected – 31 ppt*	80	3.0 (±0.00)	7.9 (±0.02)	41 (±1)
			Salt removed	82	2.6 (±0.01)	7.2 (±0.03)	35 (±0)
			Salt + Organics removed	**84**	**0.7 (±0.00)**	**5.4 (±0.01)**	**29 (±0)**
Plume – secondary waters (+5 days)	Outer plume – 33 ppt surface waters @ DNK1 trap site	40%	*Salt removed*	63	3.6 (±0.01)	12.3 (±0.10)	111 (±2)
			Salt + Organics removed	**95**	**1.5 (±0.02)**	**5.2 (±0.04)**	**16 (±1)**
Plume – tertiary waters (+5 days)	Mid-shelf – 33 ppt (Ellison Reef)	29%	*Salt removed*	41	6.2 (±0.05)	26 (±0.15)	163 (±12)
			Salt + Organics removed	**79**	**3.1 (±0.04)**	**8.0 (±0.09)**	**43 (±3)**

Estuarine and flood plume samples

Measurement reproducibility for the untreated (salt-present) estuarine and flood plume samples was generally poor (Supp. Figure 2d). Salt (ionic) interference with the Mastersizer's background or measurement readings, and the low obscuration (i.e. low particle concentrations in the instrument's measurement cell and poor signal-to-noise ratio at the detector) typical of flood plume samples may explain this instability. Additional sonication during measurement or the addition of Calgon (e.g. Supp. Figure 2b) had negligible benefit. Many of the untreated measurement results were therefore discarded because the precisions required to satisfy the ISO 13320:2020(E) guideline (International Organisation for Standardisation 2020) could not be achieved. Some of the Tully case study samples were more stable and are compared below with other treated measurements.

Salts were removed using dialysis tubing (see section 2.2.7) and all plume samples were lightly sonicated (15% for 30 seconds) prior to measurement. The addition of Calgon dispersant did not improve measurement precision or alter the grain-size distribution for flood plume samples (e.g. Supp. Figure 2b) and was therefore included in the processing of flood plume samples. The salt-removed grain-size distributions of flood plume sediments collected from the Burdekin and Tully transects are presented in Figures 2.4-2.6 (light blue series). Replicate measurements on salt-removed samples were generally more stable than for untreated samples. However, the high particulate organic matter content (15-50%) of flood plume samples often bound the primary particles together, producing a peaked unimodal distribution (see Figures 2.4b-d and 2.6d). Once treated to remove the organics the grain-size distributions of these samples generally became multi-modal (refer to orange series in the plots), reducing the D90 grain-size values for each estuarine and flood plume sample across the two case study sets (Tables 2.2 and 2.3). For example, removal of the organic content in the Burdekin estuarine sample (<1 ppt) increased the proportion of particles in the sample falling within the main distribution peak (Figure 2.4a), and reduced the D90 value from 36 to 21 µm (Table 2.2).

The remainder of the Burdekin flood plume samples were collected further offshore in secondary waters characterised by well mixed salinities (21-28 ppt), low SPM concentrations (<5 mg L^{-1}), and organic matter comprising ~20-50% of measured sample particulate matter by mass (Table 2.2; Petus et al. 2019). Accurate measurement of grain size in these samples is particularly challenging and time-intensive, requiring additional treatments beyond standard organic removal. Light microscopy confirmed the presence in many samples of siliceous diatoms (long cylindrical and disc shaped cells shown in Figure 2.5b-c) not removed by the H_2O_2 treatment. Siliceous diatoms can be abundant in samples collected during flood plume associated phytoplankton blooms, as was the case for the sample depicted in Figure 2.5a. Where this occurs the diatoms comprise a coarser grain-size peak around 65-90 µm within the total sample grain-size distribution (Figure 2.5a). Similar peaks of coarse particle fractions were also measured in the other secondary water samples (Figure 2.4b and d orange series). Repetitive sieving of these samples was required to remove the diatoms (due to their rod shape and particle orientation during the sieving process), with light microscopy used to confirm they were mostly removed prior to re-measurement (e.g. Figure 2.5d). Application of this series of pre-treatments greatly refined the grain-size distributions produced for these samples so that they better represent the suspended sediments delivered from the catchments. The peak associated with coarser particles was reduced (orange dashed series

in Figure 2.4b-d) and the D90 grain-size value declined by >50% in all three samples (Table 2.2).

Within the Tully transect samples, the grain-size distributions for two untreated samples are included (Figure 2.6a and c). These samples represent two endmembers of the salinity gradient (5 ppt within the estuary and 31 ppt in the outer secondary waters of the plume) and were more stable than the majority of untreated sample measurements. The grain-size distribution curves are similar for the two measurement runs (i.e. untreated versus salt removed) for each sample (see Figure 2.6a,c dark blue series (untreated) and light blue series (salt-removed)), with a slightly finer D90 value (35 compared to 41 μm) in the salt-removed measurement of the outer plume sample (Table 2.3).

Large flocs binding mineral particles and phytoplankton were again observed using light microscopy in the Tully flood plume samples collected in secondary waters (with salinity >22 ppt and organic contents of 29-40%). Treatment to remove this organic content shifted the main distribution peak to finer grain sizes, and for two samples, created bi-modal distributions with a smaller colloidal peak (Figure 2.6b-d). Similar to the Burdekin secondary water samples, the D90 grain-size value reduced considerably in three of these secondary water samples, from >100 μm to <50 μm (Table 2.3). However, unlike the Burdekin samples the Tully samples were collected a year earlier and were not further analysed for grain-size following sieving to remove the diatoms after treatment. These results therefore include coarse, non-mineral particles that would normally be removed. The proportion of finer mineral grains represented is thus conservative compared to the output expected if diatoms had been removed.

The HCl-digestion treatment used to remove marine carbonates was also trialled on one of the Burdekin secondary water samples (surface waters at HAV1 site) and two Tully plume samples as a potential alternative method to the repeated sieving and microscopy. Light microscopy revealed diatoms were still present after HCl-digestion, and thus this treatment was not applied further to plume samples. Figure 2.5a provides an example of this carbonate-removed distribution (green) curve, which is similar to the organic-removed (orange) measurement. The D10, D50 and D90 results are provided in Table 2.2.
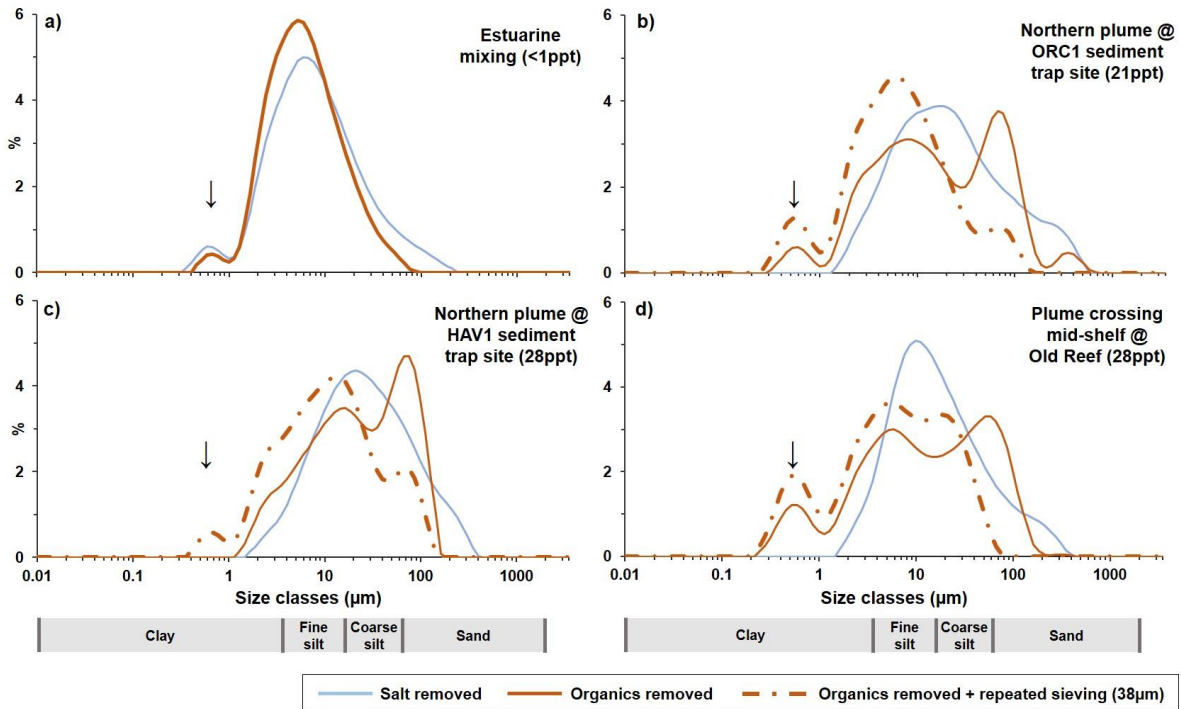
Figure 2.4. Grain-size distributions of samples collected from the Burdekin River flood plume event, 11-15th February, 2019 including: (a) an inner plume sample from the estuarine mixing zone (<1 ppt); northern plume transect collected from surface waters above the Orchard Rocks (b) and Havannah Is. (c) marine sediment trap sites; and (d) the eastern edge of the plume crossing the GBR Mid-shelf (Old Reef). Grain-size distributions analysed on the salt- and organics-removed and additional sieved (38 μm) sub-samples are presented for each site. Arrow on each graph highlights the colloidal fraction present along the plume gradient.
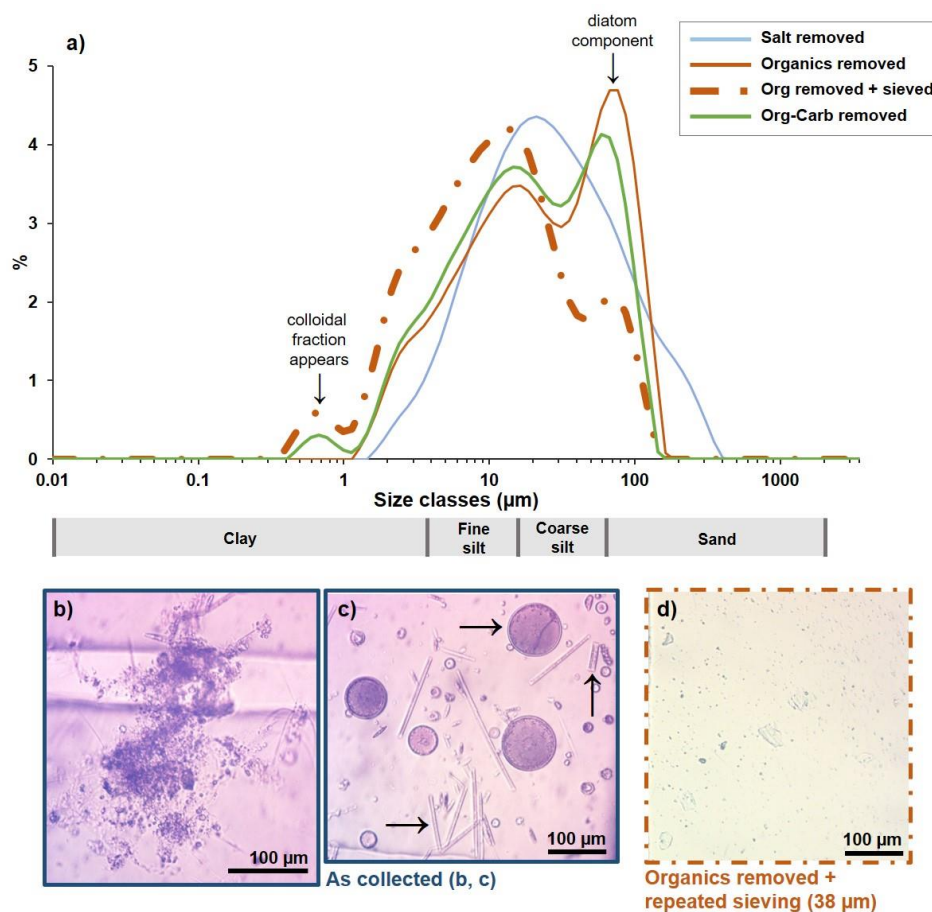
Figure 2.5. Grain-size distributions (a) of northern Burdekin flood plume surface water SPM (12th Feb 2019) collected above the Havannah Island marine sediment trap site following multiple pre-treatments. Associated light microscopy images show this sample: (b) and (c) as collected; (d) post organic-removal and multiple sieving (<38µm) to further remove siliceous diatoms. This plume sample captured a phytoplankton bloom providing a good case study for removal of both organic matter and siliceous diatoms. Image (b) highlights a large floc comprising organic matter binding diatoms and small discrete mineral particles. Diatoms dominate SPM in this water (c), with arrows highlighting disc-shaped (?*Coscinodiscus*) and long cylindrical diatom cells. Most of these diatoms have been removed through pre-treatment steps in (d), highlighting the need for careful sieving in a sub-set of these difficult diatom-rich samples.
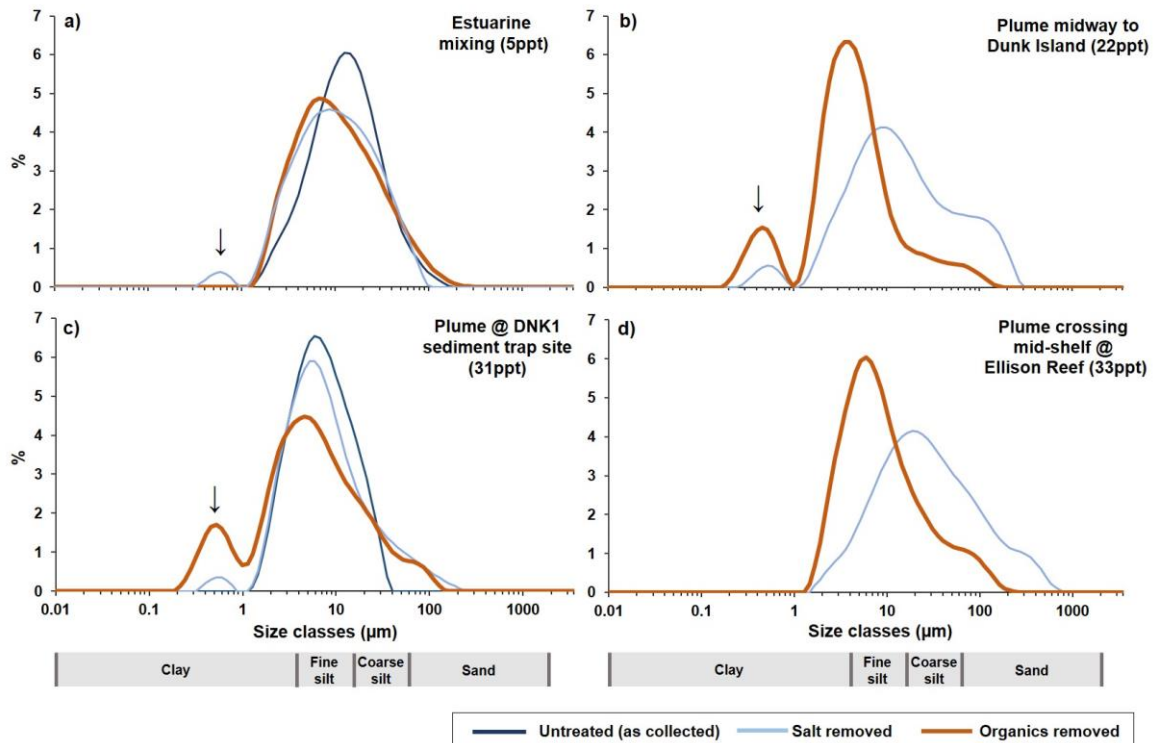
Figure 2.6. Grain-size distributions for samples collected from the Tully River flood plume surface waters on the 9th February, 2018 following EoR peak discharge including: (a) an inner plume sample from the estuarine mixing zone (5ppt); (b) midway to Dunk Island (22ppt) and (c) plume surface waters (31 ppt) above the inshore reef (Dunk Is.) marine sediment trap site. Sample (d) was collected 5 days later (14th February) as the plume crossed the mid-shelf at Ellison Reef (33ppt). Grain-size distributions analysed on the salt- and organic removed sub-samples are presented for all sites. Additional as collected (i.e. untreated) distributions are also presented for (a) and (c).

Marine sediment trap samples

The grain-size distributions determined for untreated and salt-removed samples collected from each of the six marine sediment traps were similar (Figure 2.7a-e dark blue and light blue series), but differed most in the coarser fractions as demonstrated by divergent D90 values and large standard deviations within each treatment set (Table 2.4). The coarser grained CLE1 sample was an exception, with more variable bi-modal distributions between the untreated and salt-removed measurements (Figure 2.7f). For each of these treatment types Calgon addition did not improve measurement reproducibility (e.g. Supp. Figure 2c). However, for samples dominated by coarser grain sizes (i.e. CLE1), the reproducibility of distribution curves was improved by light sonication (15-20%), especially at the coarse end of the curve (i.e. D90).

Pre-treatment to remove organic matter binding primary particles in the marine trap samples (i.e. the flocs visible in the untreated DNK1 sample images Figure 2.8a-b) shifted the grain-size distributions for all samples towards the finer size fractions (Figure 2.7a-f orange series), and lowered the D10, D50 and D90 values for all sites except ORC1 (Table 2.4). The combined pre-treatment H_2O_2 and HCl steps in Figure 2.2 to remove both organics and marine carbonate present (e.g. Figure 2.8c) generally increased the height of the main distribution peak of each sample (Figure 2.7a-f green series) and further lowered the coarser D90 value in all samples (Table 2.4). Combined with Calgon-drop additions and ultrasonic dispersal (at

15%) during measurement, this extensive pre-treatment improved the reproducibility of these sub-samples with improved standard deviations across the D10, D50 and D90 values compared to the less treated runs (Table 2.4). The grain-size reduction across treatments was greatest for DNK1, OS1, HAV1 and GFB1, where D90 values of 95-158 µm in the salt-removed run reduced in the treated run to 24-46 µm (Table 2.4). As a result the proportion of total grain-size <20 µm for each of these four samples increased substantially to 71-86%. In contrast, for the two open sediment field site samples (ORC1, CLE1) the proportion of grains <20 µm did not shift substantially across the different pre-treatments. The coarser grained CLE1 sample showed the most variation across pre-treatment grain-size distributions (Figure 2.7f), and had the largest decrease in D90 value from the salt-removed to full treatment run (163 to 71 µm, respectively).

A pre-treatment to remove carbonate only (i.e. organics remaining in the sample) was trialled with HCl acid digestion-only on the OS1 and CLE1 samples (see Figure 2.7b and f yellow series). Measurements show a coarser D90 value for both samples than for the standard carbonate and organic removed treatment.
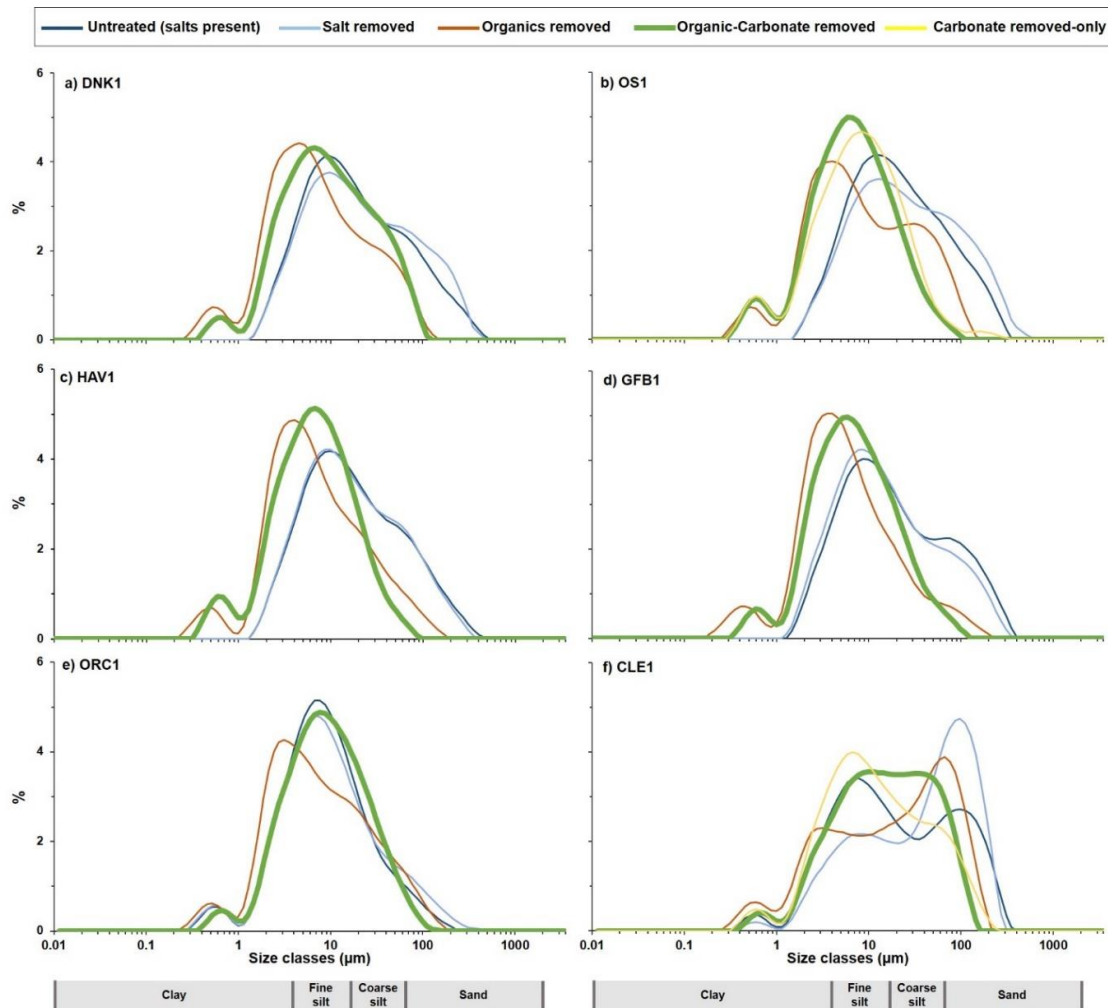
Figure 2.7. Grain-size distributions of six samples collected from marine deployed SediSamplers® including: (a) Dunk Is. (DNK1) trap capturing the Tully River offshore gradient (Dec 2017 to Feb 2018); and five sites within Cleveland and Halifax Bays representing the longitudinal gradient from the Burdekin River mouth including (b) OS1, (c) HAV1, (d) GFB1, (e) ORC1 and (f) CLE1 collected during wet season flooding (c,e,f) and post wet season (b, d) deployments in the period December 2018 to June 2019. Grain-size distributions presented compare pre-treatments including as collected (i.e. untreated) and salt-, organic-, organics + <38µm sieving, organic + carbonate removed. For sites OS1 (b) and CLE1 (f) an additional distribution is presented for carbonate removal-only pre-treatment.

Table 2.4. Sediment grain-size results for various treatments for six marine sediment trap sites during various wet and dry season deployments. The site environment, and proportions of organic and carbonate content for each sample are also provided. Grain-size results including the proportion of sample <20 μm and the full grain-size distribution represented by the D10, D50 and D90 (standard deviation in brackets) are presented for the various pre-treatment options for each site including: as collected (i.e. untreated) and salt-, organic- and carbonate removed sub-samples. The set of final results used for each sample (i.e. treatment option) is highlighted.

Marine sediment trap site	% organic	% carbonate	Environment	Treatment	<20 μm %	D10	D50	D90
DNK1			**Lower reef-slope**	*As collected in marine trap*	55	4.3 (±0.01)	16.9 (±0.06)	117 (±2)
Wet season deployment – 2018 Tully flood plume	7.1%	23%	Exposed in SE swell Low current	*Salt removed*	57	4.1 (±0.12)	15.8 (±0.80)	95 (±6)
				Salt + Organics removed	**77**	**1.9 (±0.01)**	**6.7 (±0.03)**	**43 (±1)**
(Dec'17 – Feb'18)			Weakly consolidated reef framework	***Salt + Organics + Carbonate removed***	71	2.5 (±0.05)	9.7 (±0.02)	46 (±1)
OS1			**Mid reef-slope**	*As collected in marine trap*	50	5.1 (±0.02)	19.9 (±0.1)	112 (±1)
				Salt removed	44	5.3 (±0.05)	25 (±0.85)	158 (±18)
Post wet season deployment	7.1%	35%	Sheltered High current	***Organics removed***	**70**	**1.9 (±0.01)**	**7.8 (±0.05)**	**54 (±1)**
			Weakly consolidated reef framework	***Salt + Organics + Carbonate removed***	85	1.9 (±0.07)	7.0 (±0.06)	26 (±0)
(April-June'19)				*Salt + Carbonate removed only (HCl)*	79	1.9 (±0.23)	8.4 (±1.0)	32 (±8)
HAV1			**Mid reef-slope**	*As collected in marine trap*	56	4.2 (±0.02)	16.3 (±0.17)	102 (±3)
Wet season deployment – 2019 Burdekin flood plume	7.2%	24%	Sheltered Low current	*Salt removed*	57	4.1 (±0.02)	15.8 (±0.23)	95 (±3)
				Salt + Organics removed	**80**	**2.0 (±0.02)**	**6.3 (±0.05)**	**38 (±1)**
(Jan-April '19)			Unconsolidated fine carbonates	***Salt + Organics + Carbonate removed***	86	1.9 (±0.03)	7.0 (±0.06)	24 (±0)
GFB1			**Sub-tidal reef flat**	*As collected in marine trap*	55	4.1 (±0.02)	16.6 (±0.32)	130 (±8)
Post-wet season deployment	8%	15%	Exposed in SE swell Low current	*Salt removed*	60	3.7 (±0.06)	14.1 (±0.53)	105 (±7)
				Salt + Organics removed	**84**	**1.7 (±0.01)**	**5.4 (±0.03)**	**31 (±1)**
(March-June'19)			Weakly consolidated reef framework	***Salt + Organics + Carbonate removed***	83	2.2 (±0.04)	7.1 (±0.09)	28 (±1)
ORC1			**Open sediment field**	*As collected in marine trap*	76	2.6 (±0.09)	9.2 (±0.28)	43 (±3)
Wet season deployment – 2019 Burdekin flood plume	7.5%	7%	Exposed Low to moderate current	*Salt removed*	71	2.6 (±0.08)	9.8 (±0.34)	71 (±5)
				Salt + Organics removed	**76**	**1.9 (±0.02)**	**7.0 (±0.03)**	**45 (±1)**
(Dec'18-Mar'19)			Unconsolidated, flat, exposed outer-bay mobile sediment field	***Salt + Organics + Carbonate removed***	76	2.7 (±0.05)	9.4 (±0.11)	35 (±0)
CLE1			**Open sediment field**	*As collected in marine trap*	55	3.4 (±0.01)	16.4 (±0.10)	134 (±2)
Wet season deployment – 2019 flood major resuspension event	4.4%	8%	Semi-exposed Very high current	*Salt removed*	51	2.6 (±0.10)	19.3 (±0.84)	163 (±9)
				Salt + Organics removed	**49**	**2.1 (±0.04)**	**21 (±0.39)**	**102 (±3)**
(Dec'18-Mar'19)			Unconsolidated, flat mid-bay sediment field	***Salt + Organics + carbonate removed***	56	3.2 (±0.08)	16.1 (±0.20)	71 (±2)
				Salt + Carbonate removed only (HCl)	64	2.8 (±0.06)	11.7 (±0.12)	76 (±1)

As collected (untreated) **Organics removed** **Organics + carbonate removed**
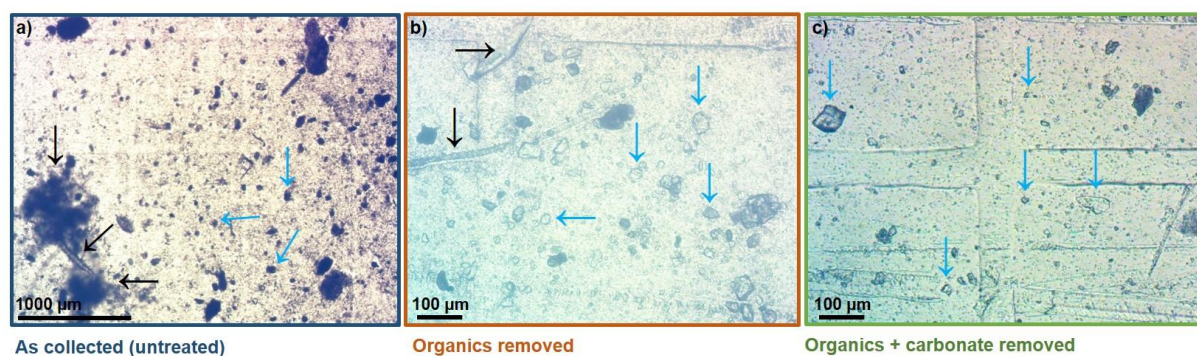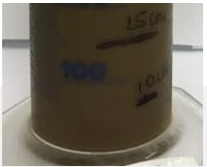
Figure 2.8. Micro-imagery of the DNK1 sediment trap sample from the 2017-18 wet season flood period deployment (07/12/17-15/02/18): (a) as collected (untreated); and following (b) organic removal and (c) both organic-carbonate removed. A wider view of the untreated sample highlights the presence of large flocs, plankton (both black arrows) and grain particles (blue arrows), with organic matter binding particles removed in (b) and showing a magnified view (note change in scale) of discrete grains of various sizes, and the presence of some remaining plankton (black arrows). Finally, with carbonate grains and fragments removed, a large range of clay to coarse sized grains are observed (blue arrows). The cross-pattern of the counter cell is also clearly visible on (b) and (c).

SediPump® filtration system for bulk sediment collection

The comparison of grain-size distributions from the SediPump® bulk sample and the manual point-in-time 'grab' samples concurrently collected at the three flood plume sampling sites show close agreement (Table 2.5). For all three samples the SediPump® sample had a slightly wider distribution than the point-in-time 'grab', confirming that this new collection method captures particles of all size ranges. For example, the grain-size range (D10 and D90) for the Old Reef site was 5.9 and 81 µm for the 'grab' sample, and 4.9 and 84 µm for the SediPump® sample. The proportion of total sample <20 µm in grain-size was also similar or slightly higher in the SediPump® sample compared to the grabs for all three sites e.g. 50% compared to 45% in the Orchard Rocks (21 ppt) sample. The quantity of particulate material that can be captured within the SediPump® 1 µm filter compared to the 'grab' sample as collected is shown in Table 2.5.

Table 2.5. Comparison of grain-size results for a SediPump® concentrated 'bulk' sample and the corresponding manual point-in-time 'grab' sample collected at three study plume samples. Sample characteristics, SPM concentration (mg L^{-1}), organic content (%) and imagery of both the 'grab' sample and concentrated SediPump® sample are also included. Sites include the February 2018 Tully flood plume estuary site and two February 2019 Burdekin secondary water type flood plume samples collected at Orchard Rocks (ORC1) and Old Reef (refer to Figure 2.1 and Supp. Figure 1c). Grain-size results are from salt-removed sub-samples (i.e. organics present).

Sample	Sample type	Sample collection method	SPM conc. (mg L^{-1})	% Organic	% <20 µm	Grain size (µm)			Images of recovered sample	
						D10	D50	D90	Grab (point in time)	SediPump® bulk
Flood plume – 5 ppt in estuary surface waters	Discrete particles, flocs (50-100µm), some plant debris	Grab sample	20	~20	73	3.5	12.3	31		
		SediPump® bulk sample (1 hr pump)	-	-	72	2.9	10.5	39		
Flood plume – 21 ppt surface waters at ORC1 trap site	High organic matter (plankton/ detritus)	Grab sample	<3	~19	45	6	22.8	135		
		SediPump® bulk sample (3 hr pump)	-	-	50	4.6	19.9	142		
Flood plume – 28 ppt surface waters at Old Reef, Mid Shelf	High organic matter (plankton /detritus)	Grab sample	<3	~50	47	5.9	21.5	81		
		SediPump® bulk sample (2 hr pump)	-	-	59	4.9	15.3	84		

2.3.2 Sediment grain size across the GBR catchment to reef continuum

Freshwater samples

Samples from the Wet Tropics rivers contained consistently higher organic contents (16-23%) than those collected from Dry Tropics streams (11-14%), largely attributed to a higher abundance of flocculated particles and freshwater diatoms. Tully EoR samples were collected at peak-of-flow in three moderate-sized discharge events, including January 2017 (peak ~8.5 m) and February and March 2018 (peaks of 8 and 9 m, respectively, measured at the Euramo gauge: 113006A). An opportunistic sample was also collected on the South Johnstone River

in 2018. Pre-treatment to refine these samples to primary particles considerably increased the measured proportion of fine sediment (<20 µm) (Table 2.6). For example, at the peak of flood in January 2017, pre-treatment for organic removal increased the proportion of mineral grains <20 µm from 44 to 77%. The treated grain-size range (bounded by the D10 and D90 statistics incorporating 80% of the sample grain sizes) for Tully sediments (2.6 to 30 µm) was smaller than for the South Johnstone sample (3.4 to 70 µm). The grain-size range for the Herbert sample collected across the discharge peak (composite from 4-7th February 2019) was 4.1 to 38 µm.

The Burdekin EoR site was repeatedly sampled across minor to large discharge events during the 2017, 2018 and 2019 wet seasons, representing different flow stages and sediment sources within each year sampled (Table 2.6). For the fifteen samples analysed, organic content (11-14%) and the proportion of mineral grains <20 µm (81-93%) remained relatively consistent for the treated samples (Tables 2.2 and 2.6). The largest increases in the fine sediment fraction between the untreated and treated samples occurred in those collected during the March 2017 event, a drought-breaking and rapid flood associated with Tropical Cyclone Debbie. Treatment of the rising stage sample collected during this event increased the proportion of fine sediment (<20 µm) from 49 to 89% (Table 2.6). The grain-size distribution for all Burdekin samples ranged from 1.9 ± 0.5 µm at the D10 to 24 ± 7 µm at the D90 (average of annual averages in Table 2.6), with a slightly finer D10 measured in all 2018 event samples. The 2018 event was exclusively sourced from the Upper Burdekin catchment area which passed through the Burdekin Falls Dam. All measured Burdekin suspended sediment samples contained a characteristic multi-modal distribution (e.g. Figure 2.3b), with a small mini peak at ~0.5 µm, representing a colloidal fraction (<1 µm). A similar colloidal fraction component was also observed in suspended sediment samples from the neighbouring Haughton and Ross River EoR sites collected opportunistically for sediment source tracing purposes. Organic contents of suspended sediment for the Haughton River (13%) and Ross River (11-12%) were similar to the Burdekin (11-14%), however the fine <20 µm sediment fraction comprised only 63-69% of all grain sizes measured in these samples (Table 2.6). Ross River sediments contained a larger coarse component than Burdekin samples, with a D10 to D90 range of 10.5 to 75 µm, and sand (>63 µm) comprising around ~12% of all mineral grains.

Table 2.6. Grain-size distributions for samples collected at a number of Great Barrier Reef catchment end of river (EoR) freshwater sites collected under the broader NESP research project. Collection dates, hydrograph flow stage, total suspended solid concentrations (mg L^{-1}) and organic content (%) are also provided. The proportion of fine sediment (<20µm) in freshwater samples analysed as collected and following treatment for organic-removal are presented, as well as the grain-size distribution on treated samples.

GBR Catchment	Site coordinates (DD)	Date	Hydrograph stage	TSS (mg L^{-1})	Organic content	Proportion grain size <20 µm		Grain size (µm)		
						As collected	Organics-removed	D10	D50	D90
Burdekin EoR – 2017	-19.64, 147.40	29/03/17	Rising rapidly	748	13%	49	89	1.9	5.6	22
		30/03/17	Steady peak	1810	11%	70	85	2.5	7.4	26
		31/03/17	falling steadily	884	12%	66	90	2.1	6.5	20
		mean					*88*	*2.1*	*6.5*	*22*
Burdekin EoR – 2018	-19.64, 147.40	03/03/18	Rising	998	12%	77	90	1.8	5.3	20
		04/03/18 am	Rising	681	12%	76	89	1.8	4.9	21
		04/03/18 pm	Rising	644	12%	76	82	1.0	5.6	32
		05/03/18	Sustained peak	534	12%	89	90	0.7	4.4	21
		06/03/18	falling	554	13%	93	93	1.7	4.4	15
		mean					*90*	*1.4*	*4.9*	*22*
Burdekin EoR – 2019	-19.64, 147.40	11/01/19	Local Bogie R source	820	13%	88	92	2.0	5.4	18
		31/01/19	Rising	740	14%	76	86	2.4	6.7	25
		05/02/19	Rising	500	12%	89	86	2.0	5.6	31
		06/02/19	Peak 1	470	12%	81	87	2.1	5.6	28
		07/02/19	Rising to peak 2	504	-	87	92	2.1	5.3	18
		11/02/19	Falling	330	12%	87	81	2.3	6.7	40
		14/02/19	Falling	137	12%	75	85	2.4	6.2	28
		mean					*87*	*2.2*	*5.9*	*27*
Haughton EoR - 2019	-19.55, 147.11	06/02/19	Falling after flood peak	167	13%	62	69	2.8	11	48
Ross EoR – 2019	-19.28, 146.83	02/02/19	Early dam release	170	12%	44	67	2.7	10	75
		06/02/19	Sustained dam release	79	11%	66	63	1.9	11	82
Herbert EoR – 2019	-18.63, 146.17	4-7/02/19	Around peak	-	-	50	69	4.1	14	38
Tully EoR – 2017	-18.02, 146.05	11/01/17	Peak	39	18%	44	77	3.6	11	30
Tully EoR – 2018	-18.02, 146.05	09/02/18	Around peak	17	18%	62	88	2.6	6.6	22
		12/03/18	Around peak	25	16%	39	81	2.8	8.9	28
South Johnstone Arm – 2018	-17.61, 145.99	08/02/18	Falling after flood peak	35	23%	25	60	3.4	14	70

Estuarine and flood plume samples

Along the 2019 Burdekin flood plume gradient, the pre-treatment refining these samples to primary particles resulted in significant increases in the measured proportion of fine sediment (<20 µm), with the treated grain size ranging from 68-89% along this plume gradient (Table 2.2). The grain-size distribution of the sample collected in the seawater mixing zone (<1 ppt) was narrowest, with a D10 to D90 range from 2.2 to 21 µm (Table 2.2, Figure 2.4a). This sample lacked the smaller coarse peak (around ~100 µm) present in the EoR freshwater sample collected immediately upstream (Figure 2.3.b). The samples collected further along the salinity gradient from secondary water types had more variable and coarser grain-size distributions ranging from 0.7 to 63 µm (Table 2.2, Figure 2.4b-d). These traits probably reflect

the presence of residual diatoms not removed by pre-treatment and sieving due to the long cylindrical shape of the diatoms, which can pass through the sieve at the right angle. This is likely the case for the phytoplankton bloom sample collected at the HAV1 site, which had the largest D90 value. Median grain size (D50) for the plume samples ranged from 6.1 to 11.5 μm. The colloidal fraction (<1 μm) characteristic of all Burdekin EoR samples was evident in each of the flood plume samples following sample pre-treatment but was not measured in the corresponding untreated salt removed samples (Figure 2.4a-d black arrows).

Across the Tully transect, flood plume waters were characterised by relatively low SPM concentrations, generally <10 mg L^{-1}, and high organic contents (20-40%) (Table 2.3). The plume sampled at the seawater mixing zone (5 ppt) had the highest SPM concentration (20 mg L^{-1}) and a treated grain-size range (D10 to D90) of 3.2 to 45 μm (Table 2.3, Figure 2.6). Treated grain-size distributions for secondary water samples collected further along the salinity gradient increased in salinity and organic content, with fine sediment (<20 μm) comprising 71-95% of all grain sizes measured. These results were consistent with sampling of 2017 Tully River secondary waters at Dunk Island (DNK1 trap site) and Bedarra Island, where treated samples were also dominated by the fine sediment fraction (92 and 99% respectively; Lewis et al. 2018).

Marine sediment trap samples

Across the six marine sediment trap samples, silt-sized grains (3.9-63 μm) dominated mineral sediment, comprising 69-78% of the total sample (Figure 2.7). Clay-sized grains (<3.9 μm) comprised 14% in CLE1, 19% in ORC1 and 27-30% in GFB1, HAV1, DNK1 and OS1. The proportion of sand grains (>63 μm) was highest for the CLE1 sample at 13%, and comprised only 1.0-2.6% in the other five samples. A colloidal fraction (<1 μm) was present in all six treated samples and ranged from 2.4% (at CLE1) to 8.2% (at DNK1) of all grain sizes across the sample set (Figure 2.7a-f).

The organic contents of the six sediment trap samples were lower than established for the EoR and plume samples, comprising 7.1-8.0% of all captured material in five of the six samples (Table 2.4). The high energy CLE1 site was an exception, with organics comprising only ~4% of captured material during the wet season deployment at this open sediment field site within Cleveland Bay. This sample had the widest and coarsest mineral grain-size distribution of all six trap samples following full treatment for organic and carbonate removal with a D10 to D90 range of 3.2 to 71 μm (Table 2.4). This coarser grain-size distribution is clearly demonstrated by a unique distribution curve in Figure 2.7f (green line). Pre-treatment for removal of organic content-only also revealed a carbonate component notably coarser than observed at other sites (see Figure 2.7f orange line), with a D90 value of 102 μm (Table 2.4). Carbonate comprised 8% of total sediment accumulated over this deployment. The proportion of fine sediment (<20 μm) was smallest for this sample, comprising only 56% of all grain sizes measured. A second site (ORC1 situated off Magnetic Is.) also located within an open sediment field displayed very different grain-size results (Figure 2.7e). Unlike the CLE1 sample, pre-treatment on the ORC1 sample did not greatly reduce the untreated finer grain-size distribution, with only a small shift in the D10 to D90 range from 2.6 to 43μm (untreated) to 2.7 to 35 μm (full treated) (Table 2.4). Fine sediment (<20 μm) comprised 76% of all grain sizes measured in this sample.

Mineral grain-size distributions were finest for the two sheltered mid reef-slope sites (OS1 and HAV1) and the sub-tidal reef flat site (GFB1), with D10 to D90 ranges of 1.9 to 26 μm, 1.9 to 24 μm and 2.2 to 28 μm, respectively (Table 2.4). Carbonate contents were also highest for samples from the two mid reef-slope sites, comprising 35% of the post-wet season sample collected at OS1 and 24% of the wet season HAV1 sample. The northern most trap (DNK1) was positioned on a lower leeward reef-slope at Dunk Island. The 2017-2018 wet season sample there had a grain-size range of 2.5 to 46 μm (D10-D90; Table 2.4) and a carbonate content of 23%.

2.4 Discussion

2.4.1 A systematic protocol for measuring terrigenous sediment grain size across the catchment to reef continuum

The chemistry and biology of the water in which sediments are suspended varies from catchment to reef, and suspended sediments are influenced by a range processes and additions as they move through the continuum. The measurement and interpretation of sediment grain size across river to reef gradients is therefore complex. Depending on the specific objectives of the research and location within the continuum samples are collected, particular sample pre-treatments will be required if the identification of primary mineral grains is necessary. Here, suspended sediment samples collected from end-of-river (freshwater), flood plume (estuary) and marine habitats were used to develop a systematic protocol (Figure 2.9) for the reproducible and consistent measurement of mineral grain size in marine-influenced sediment samples that yields results directly comparable to those derived from the analysis of instream sediments.

For freshwater environments, pre-treatment is required to remove the organic component to eliminate the bias of flocculated particles so that a true representation of primary particle size is revealed. This is especially important where organic matter comprises >15% of the total particulate content. The most complicated pre-treatment regime must be applied to samples collected in mixed salinity estuarine and flood plume settings. In addition to the organics that may be present, biogenic silica particles (i.e. diatom valves) can obscure the grain size signature of primary sediments, and thus must be removed. This requires additional sieving and microscope checking (outlined in Figure 2.9; see also section 2.2.8), or additional chemical stripping that was beyond the scope of this study (e.g. Vaasma et al. 2008). Fine sediments deposited in marine settings exposed to mixed carbonate and terrigenous inputs, such as the marine trap sites in this study, must be chemically and physically pre-treated to remove both organic and carbonate components (i.e. coral or shell fragments) if the primary mineral particles are the focus. Paired grain size analyses on corresponding untreated sub-samples for freshwater EoR samples and a salt-removed sub-sample for marine samples is also recommended to provide a measure of how the particles behave in transport, and to inform their potential settling capacity. This information can support modelling of sediment transport in estuarine and inshore marine waters (Manning et al. 2017), but cannot replace time-intensive and costly *in situ* or laboratory-based analysis of particle settling rates. Below we apply the processes recommended above to demonstrate new insights on sediment transport and fate across the Great Barrier Reef catchment to marine continuum.
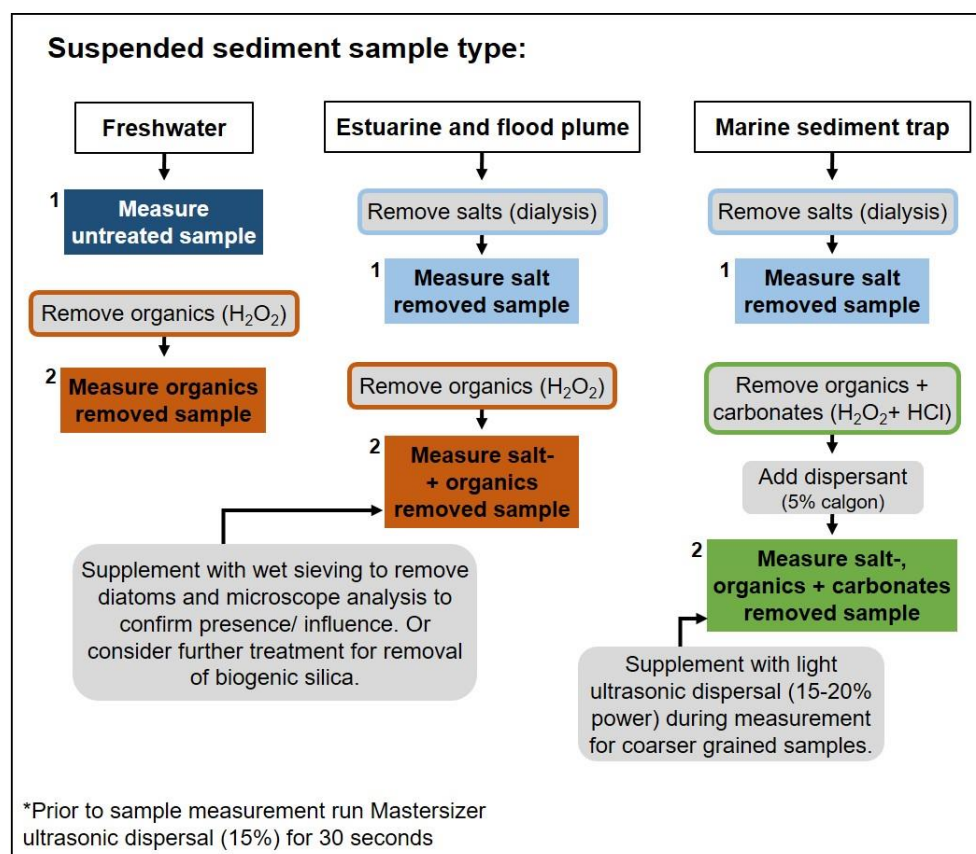
Figure 2.9. A systematic protocol for sediment pre-treatment and grain size analysis for end-of-river freshwater, estuarine and marine sediment trap samples. Each sample type has two proposed Mastersizer analysis runs, labelled 1 and 2 accordingly.

2.4.2 New insights into fine sediment transport along the catchment to reef continuum

Improved characterisation of GBR end-of-river fine sediment

Suspended sediments carried by Wet and Dry Tropics rivers were determined to have distinct compositional differences that influence their measured grain size characteristics. Those from the Wet Tropics contain higher organic content (>16% of SPM), and the organics combine with mineral particles to form larger flocs within the freshwater reaches. Wet Tropics rivers typically carry high dissolved inorganic nitrogen loads (Bainbridge et al. 2009; McCloskey et al. in review-b) that are likely contributing to instream floc formation by freshwater bacteria during downstream sediment transport (Bainbridge et al. 2018). Removing organic matter from samples collected in both the Tully (2017, 2018) and Johnstone Rivers (2017) increased the proportion of fine sediment (<20 µm) by 25-40%, with the mineral-only component containing 60-88% of fine silt and clays particles finer than 20 µm (Table 2.6).

In comparison, organic matter comprised only 11-14% of EoR suspended sediments measured in the Dry Tropics streams (Burdekin, Haughton and Ross Rivers) (Table 2.6). Burdekin EoR sediment has been well characterised across three minor-large discharge events (2017–2019). Recent results show fine sediment (<20 µm fraction = 88% ±4%) dominates export from this catchment, in accord with earlier (2009–2011) sampling during a wetter period (Bainbridge et al. 2012). Removing the organics to improve characterisation of the mineral fraction is not as critical as for Wet Tropics samples as the <20 µm fraction

dominates untreated Burdekin samples (79 ±11%) before the organics are removed. Drought-breaking and/or extreme, rapid flooding may be an exception, where EoR sediment may carry elevated organic particulate loads (i.e. Tropical Cyclone induced rapid rise on 29/03/17, Table 2.6). Light microscopy of Burdekin EoR samples collected during the 2017–2019 discharge events revealed a high concentration of mineral grains of varying sizes, and less common but present in some events, flocculated particles and freshwater diatoms. The average Burdekin EoR sediment grain-size range across 2017–2019 was remarkably consistent across the three events given the different catchment source contributions (Table 2.6). Despite the trapping influence of the Burdekin Falls Dam, particularly on the coarser grain component (Lewis et al. 2013), EoR sediment was no finer in the 2018 event sourced from above the BFD than in the other two sampled events.

The grain-size distributions of Tully EoR samples (3.0 ± 0.5 to 27 ± 4 µm) were slightly coarser than for the Burdekin EoR, although further sampling and characterisation of Tully River sediments are required. Burdekin EoR sediments also include a colloidal fraction (<1 µm) that is reflected in the finer D10 grain size compared to the Tully samples. For both rivers the mud fraction (<63 µm) comprised 95-100% of all mineral particles exported, with a greater 'coarse silt' component measured in Tully (16-32%) compared to Burdekin (mean of 15%) samples.

Improved characterisation of fine sediment transported within the GBR

The efficiency of the SediPump® high-volume filtration system in capturing the full grain-size distribution of suspended sediment and associated particulate matter was demonstrated in this study (section 2.3.1). Using this device enabled the collection and analysis of particles from low suspended sediment concentration waters (<10 mg L^{-1}), such as in secondary water types, which have previously been difficult to collect and describe. The particulate sample mass collected by this device at a single sampling location (e.g. 2-4 grams) allows full characterisation of terrigenous sediments and associated particulate matter, and permits changes in SPM as it is transported across EoR, estuarine and flood plume environments to be fully documented. Of importance, for the first time in the GBR, plume samples have been collected in secondary water types at seagrass and coral reef locations on both inshore and mid-shelf environments (e.g. Old Reef, Ellison Reef), allowing characterisation and source tracing of this material.

Grain-size analysis and identification of the mineral component of SPM within these secondary waters is limited by the presence of organic matter binding sediment grains, including live bacteria (i.e. plankton) and fungi, and detritus (Bainbridge et al. 2012; Manning et al. 2017). The pre-treatment procedure used in this study overcomes these challenges, allowing the grain size distribution of mineral particles transported by rivers and exported into the GBR lagoon to be reliably and accurately measured. By removing most of the organic matter (confirmed by micro-imagery), our results show clay and fine silt grains <20 µm (i.e. fine sediment) are preferentially transported within both Burdekin and Tully primary and secondary water types (Tables 2.2 and 2.3, Figures 2.10-2.11). Whilst some biogenic silica (diatoms) residuals remain despite rigorous pre-treatment and wet sieving steps, these data likely overestimate the coarser grain sizes. Mineral grains were measured in secondary waters transported as far as the GBR mid-shelf, including Old Reef and Ellison Reef, both ~50 km off the coast from the Burdekin and Tully river mouths, respectively (Figures 2.11-2.12). The concentrated SediPump® samples collected within surface and depth (10 m) plume waters that reached Old Reef in February 2019 highlight the distribution of terrigenous SPM

throughout the water column, down to the seafloor (Figure 2.12). Micro-imagery of these samples (Figure 2.12) also documents the presence of both discrete mineral grains and flocculated particles. In the context of water-quality guidelines, these low SPM concentrations (i.e. <5 mg L^{-1}) can still substantially impact benthic light availability; the Secchi disc depth measured at Old Reef during sampling was <1.5 m.

Conceptual summaries of Burdekin and Tully catchment to reef continuum sediment characteristics are provided in Figures 2.10 and 2.11, respectively. These figures synthesise all data collected during discharge events from 2017-2019 (Burdekin) and 2017-2018 (Tully), and classified by water type colour classes developed for the GBR (Petus et al. 2019). The Tully EoR suspended sediment concentrations are an order of magnitude lower than for the Burdekin. However, once terrigenous material is transported into the GBR lagoon, SPM characteristics (concentration, % <20 μm minerals, organic content and presence of larger flocs) become comparable within both primary (colour classes 1-4) and secondary (colour classes 5) water types of the two river plumes. As SPM concentrations decrease, organic matter and flocculated particles increase in quantity and size, dominating secondary waters. Comparison grain-size analysis on the salt-removed sub-set of these secondary water type samples shows these flocculated particles easily reach 100-165 μm in size as measured at the D90 (i.e. large floc aggregates), and that at least some finer mineral grains (i.e. clay and colloidal sizes) are also bound together in transport, as organic removal from these samples reveals a finer D10 mineral grain-size (Tables 2.2 and 2.3; see also arrows at colloidal fraction in Figures 2.3-2.4). The marine sediment traps situated at offshore locations designed to intercept typical secondary water movements of the Burdekin and Tully River plumes, including Orchard Rocks (115 km from Burdekin River) and Dunk Island (13 km from Tully River) have also been included for the associated wet season deployments (Figures 2.10-2.11). Trap material contained a lower (<10%) organic content than secondary surface waters collected above these trap locations, with increased presence of diatoms and larger floc aggregates in the Dunk Island trap compared to other deployment periods outside of plume influence (Lewis et al. 2020). Of the mineral component, the treated <20 μm fraction comprised 76% (Orchard Rocks) and 71% (Dunk Island). Trap accumulation rates were 65 and 23 mg.cm^{-2}.day^{-1}, respectively compared to the corresponding previous dry season deployment at each site of 35 and 10 mg.cm^{-2}.day^{-1}, respectively (Lewis et al. 2020). Further tracing analysis is required to confirm the river catchment source of this material.
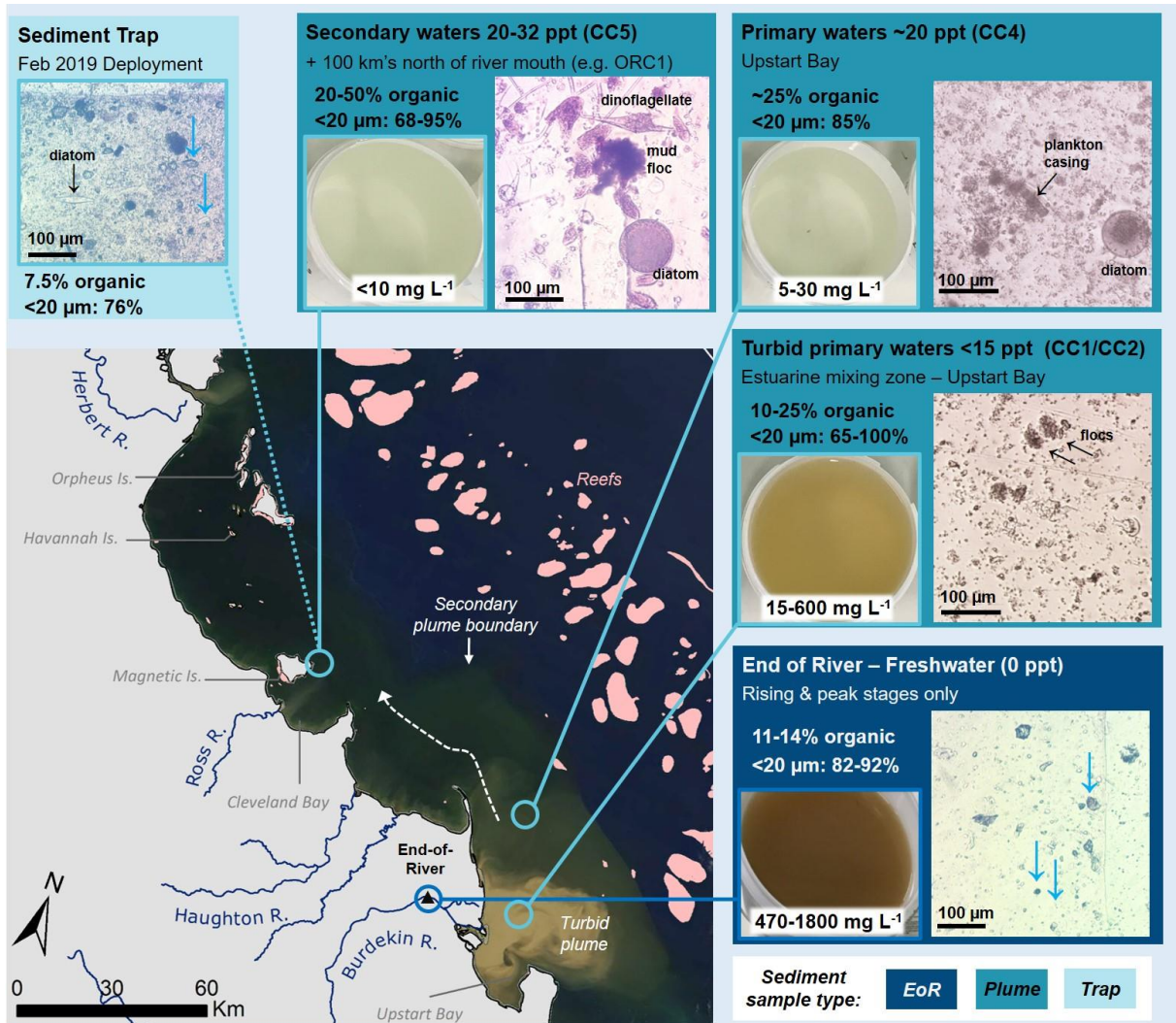
Figure 2.10. Sediment characteristics across the Burdekin catchment to reef continuum, highlighting distinct flood plume water types and summarising data collected during river discharge events that occurred in 2017, 2018, and 2019. End of river (freshwater), flood plume water types and a sediment trap site that captured these flood plume events are all presented, anticlockwise from bottom right (refer to legend). The water type colour classification scheme from Petus et al. (2019) is used to describe plume waters from Colour Class 1 (CC1) to Colour Class 5 (CC5). Each water type box includes micro-imagery of a representative sediment sample and the ranges of salinity, organic content and proportion of fine sediment (<20 μm) measured within each zone. The suspended sediment concentration/suspended particulate matter range (mg L^{-1}) is also displayed on an image of a typical "grab sample" collected at each of the end of river and flood plume water types (with increasing salinity and decreasing SPM concentration). The MODIS satellite image was captured on the 12th February and is used here to generally represent plume transitions along a salinity gradient from the river mouth. Refer to Supplement for tabulated data.
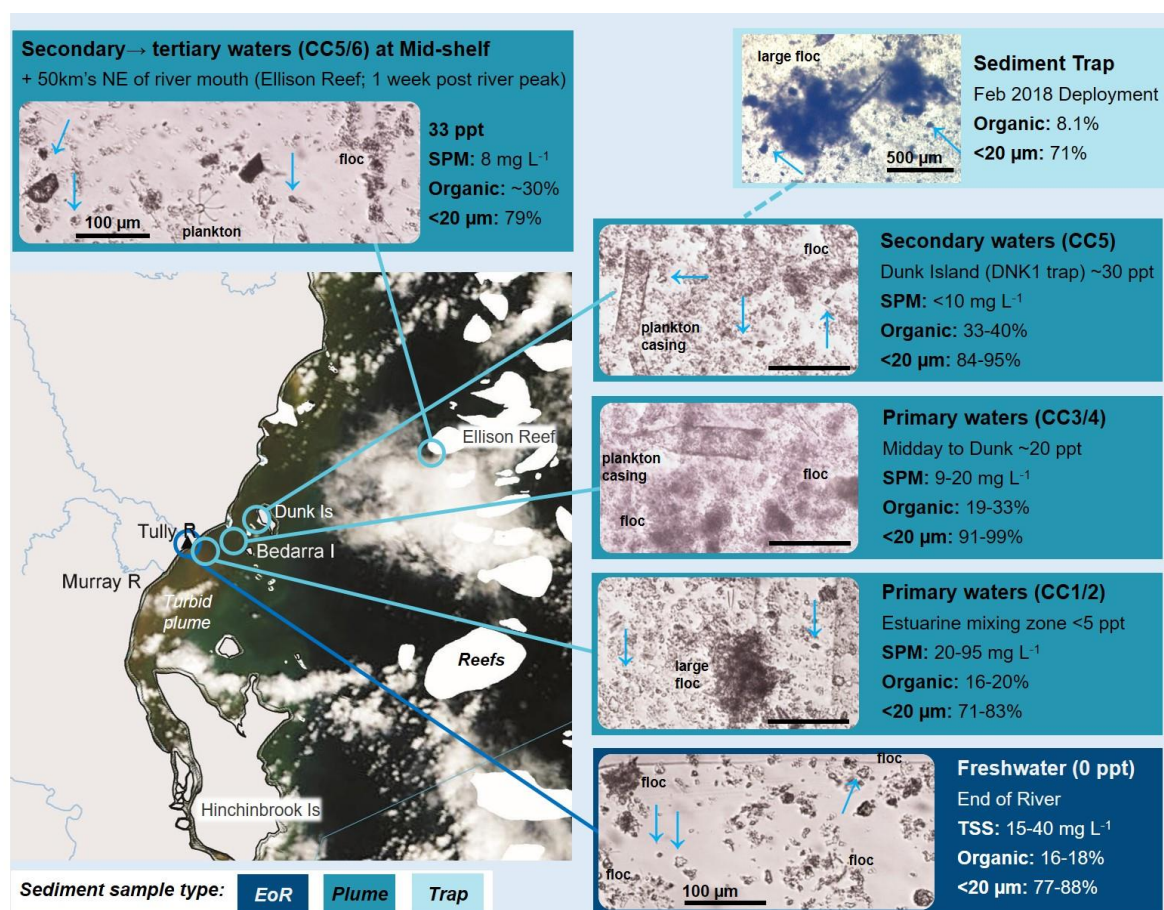
Figure 2.11. Sediment characteristics across the Tully catchment to reef continuum, highlighting distinct flood plume water types and summarising data collected during river discharge events that occurred in 2017 and 2018. End of river (freshwater), flood plume water types and a sediment trap site that captured these flood plume events are all presented, anticlockwise from bottom right (refer to legend). The water type colour classification scheme from Petus et al. (2019) is used to describe plume waters from Colour Class 1 (CC1) to Colour Class 6 (CC6). Each water type box includes micro-imagery of a representative sediment sample and the ranges of salinity, suspended sediment concentration (TSS)/suspended particulate matter (SPM) range (mg L^{-1}), organic content (%) and proportion of fine sediment (<20 µm) measured within each of these zones. All micro-imagery was captured from the concentrated SediPump® sample, with features labelled and blue arrows highlighting mineral particles. The scale bar represents 100 µm unless otherwise indicated. The MODIS satellite image was captured on the 12th January 2017 and is used here to generally represent plume transitions along a salinity gradient from the river mouth. Refer to Supplement for tabulated data.
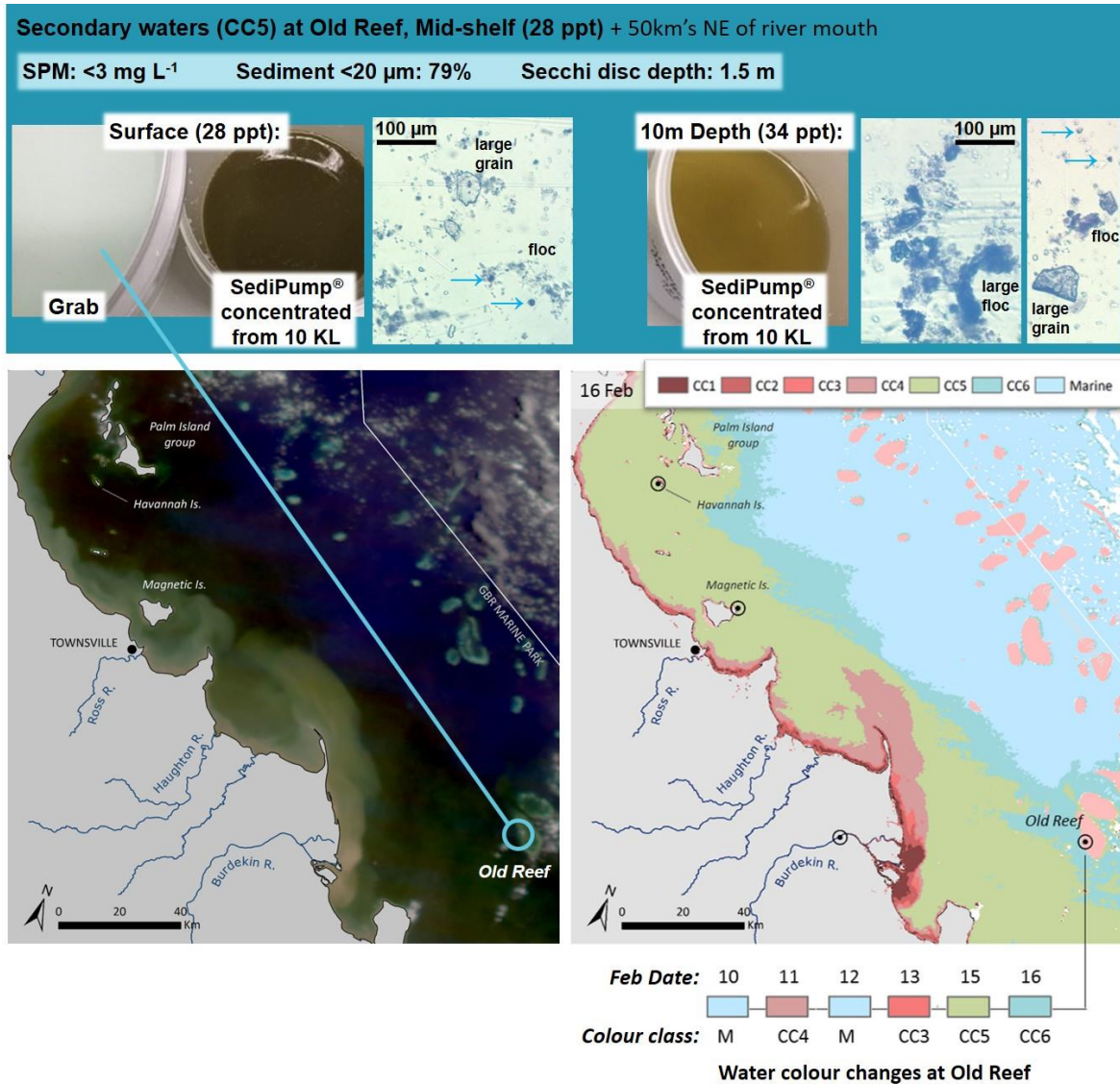
Figure 2.12. Burdekin plume sediment characteristics in secondary waters at Old Reef, mid-shelf collected on the 15th February, 2019, including SPM (suspended particulate matter), mineral sediment grain size <20 μm and Secchi disc depth (m). Micro-images of sample collected at the plume surface (left, top panel) and at 10 m depth (right, top panel) illustrate the sediment and particulate organic matter present in the concentrated SediPump® sample, with blue arrows highlighting mineral particles. The surface "grab" sample is also shown for comparison. The MODIS satellite image (bottom left panel) captured on the 16th February shows the location of Old Reef NE of the Burdekin River mouth. The water type colour class map (bottom right panel) highlights the changes in water type over the period 10th to 16th February.

Improved quantification of fine sediment influence and fate within the GBR lagoon

Clear spatial distinctions in the grain size and sediment composition were detected at the six environments targeted by sediment traps. The fine to coarsely grained carbonate content in trapped sediment samples ranged from 7.0 to 35%, with the highest values recorded at the mid reef slope sites at Orpheus Island (OS1) and Havannah Island (HAV1) in the Palm Island Group. Samples collected from these sheltered locations also contained the greatest proportion of fine sediment (<20 μm) within the mineral component (85% and 86%, respectively) (Table 2.4). In contrast, the sample collected at the higher energy mid-bay sediment field site within Cleveland Bay (CLE1) was characterised by coarse mineral and carbonate grains. Sediments from this site had the lowest proportion of fine sediment (56%

<20 µm), a much larger sand fraction (13%) than all other sites, and pre-treatment for organic and carbonate removal refined this distribution considerably more than for any other site (Table 2.4). Sediment from the Orchard Rocks (ORC1) site, a deep (>15 m) and wave exposed outer bay mobile sediment field setting was much finer; fine sediment comprised 76% of the mineral component, with sample pre-treatment having little influence on grain-size distribution shape or range. The compositions of sediments collected at each trap were associated with the type of sediment in the surrounding environment and its potential for resuspension. Factors affecting this include proximity to sediment source (i.e. river mouth versus coral reef/carbonate bank), the local exposure or resuspension energy, settling behaviours of the particles and other aspects such as local structure, benthos and bioturbation, and water depth.

This methodology builds on earlier studies of GBR sediments where the carbonate component has been removed (e.g. Orpin et al. 2004) and also highlights the additional influence of sample organic matter (4-8% measured in this study) in aggregating particles and skewing the grain-size distribution to coarser grain sizes. Removing the organics allows the seasonal influence of "terrigenous" sediment to be more accurately examined, and the addition of newly delivered sediments can be quantified through normalisation to mineral-only accumulation rates. It is this fine <20 µm terrigenous sediment that presents the greatest ecological risk to phototrophic benthos such as corals and seagrasses through a disproportional influence on light attenuation and the settling of these organic-rich and often sticky and difficult to disperse fine particles (Fabricius et al. 2003; Bainbridge et al. 2018).

The marine sediment characterisation methodology outlined here is currently being applied to several marine monitoring sites and provides new insights into sediment composition across a range of inshore GBR environments (Lewis et al. 2020). Understanding changes in sediment composition and total accumulation will allow quantification of newly delivered flood plume material at these sites during active wet season flows, and isolating the influence of other marine factors. This methodology has benefit for understanding the relative role of marine ecosystem exposure to mineral grains exported from catchments and can assist with targeted management decisions, such as consideration of potential sites for restoration efforts and to improve *in situ* and laboratory-based experiments focused on turbidity and sedimentation effects on GBR marine species.

2.4.3 Implications for reporting fine sediment transport across Catchment to Reef Programs

The improved characterisation of sediments being transported by two GBR rivers during wet season discharge events, including key mineral size fractions, provide important data for current GBR catchment modelling efforts under the Australian and Queensland Governments Paddock to Reef Program. The GBR Dynamic SedNet model (implemented in Source) generates fine sediment (<20 µm) loads for each of the 35 GBR rivers, including the Burdekin and Tully Rivers (McCloskey et al. in review-a). Correction for the analysis of the 'mineral' only grain-size distribution (i.e. organic removal) provides normalisation to a true suspended sediment load for GBR rivers that can be directly compared to grain-size-specific sediment load targets, and for improved validation of modelled fine sediment loads. This is particularly important for the Wet Tropics rivers where the higher particulate organic content and aggregation of particles results in an over-estimation of coarser grain sizes for comparison

against grain-size specific modelled loads. With the Burdekin EoR fine sediment (<20 µm) contribution now well characterised (88 ± 4%), the current best measured average SPM load of 4 million tonnes (Kuhnert et al. 2012) equates to approximately 3.52 ± 0.16 million tonnes of fine sediment, which is close to the GBR Dynamic SedNet modelled load of 3.77 million (McCloskey et al. in review-a).

Our EoR, estuarine and flood plume sediment characterisation data will also provide valuable input parameters for the eReefs fine sediment transport and biogeochemical model components (Steven et al. 2019). At present the quantification and variation in sediment composition (grain sizes, bioavailability or organic content) across the major GBR rivers are not well constrained, and are identically set for each river despite the variability along the coast in geography, climate, land use and water quality loadings. These data can also be incorporated into further improvements of the "fluff/dust"-layer (Margvelashvili et al. 2018), and how this "new sediment" is modelled over subsequent months within the inshore GBR.

This study demonstrates the need for standardised reporting of sediment grain size analysis for samples collected across rivers, flood plumes, and marine settings, which is currently lacking. Variability in grain-size distributions established for untreated and pre-treated samples demonstrates the need for more consistent reporting in mineral-sediment grain size which will help deliver improved clarity for grain-size specific catchment loads, meeting water quality targets, dredging compliance monitoring and offsets. Ideally at a minimum the treated <20 µm fraction and proportion of sample organic content are both required. Future research should examine additional sample pre-treatments to remove biogenic silica in flood plume samples as well as investigate the reproducibility of our method by applying other GSA techniques. Expansion of this work to quantify sediment grain size across all GBR rivers would also be highly valuable for validation of current modelling efforts.

Acknowledgements

References

Allen, JR., Thornley, DM., 2004. Laser granulometry of Holocene estuarine silts: effects of hydrogen peroxide treatment. The Holocene 14(2), 290-5.

Álvarez-Romero, J.G., Devlin, M., Teixeira da Silva, E., Petus, C., Ban, N.C., Pressey, R.L., Kool, J., Roberts, J., Cerdeira, S.,Wenger, A., Brodie, J., 2013. Following the flow: a combined remote sensing-GIS approach to model exposure of marine ecosystems to riverine flood plume. Journal of Environmental Management 119, 194-207.

APHA 2012, Standard Methods for the Examination of Water and Waste Water. 22nd Edition, American Public Health Association, American Water Works Association, Water Environment Federation.

Bainbridge, Z., Brodie, J., Faithful, J., Sydes, D., Lewis, S., 2009. Identifying the land-based sources of suspended sediments, nutrients and pesticides discharged to the Great Barrier Reef from the Tully-Murray Basin, Queensland, Australia. Marine and Freshwater Research 60(11), 1081-90.

Bainbridge, ZT., Wolanski, E., Alvarez-Romero, JG., Lewis, SE. and Brodie, JE., 2012. Fine sediment and nutrient dynamics related to particle size and floc formation in a Burdekin River flood plume, Australia. Marine Pollution Bulletin 65, 236-248.

Bainbridge, ZT., Lewis, SE., Smithers, SG., Kuhnert, PM., Henderson, BL., Brodie, JE., 2014. Fine-suspended sediment and water budgets for a large, seasonally dry tropical catchment: Burdekin River catchment, Queensland, Australia. Water Resources Research 50, 9067-87.

Bainbridge, Z., Lewis, S., Bartley, R., Fabricius, K., Collier, C., Waterhouse, J., Garzon-Garcia, A., Robson, B., Burton, J., Wenger, A., Brodie, J., 2018. Fine sediment and particulate organic matter: a review and case study on ridge-to-reef transport, transformations, fates, and impacts on marine ecosystems. Marine Pollution Bulletin 135, 1205-20.

Bartley R, Bainbridge ZT, Lewis SE, Kroon FJ, Wilkinson SN, Brodie JE, Silburn DM., 2014. Relating sediment impacts on coral reefs to watershed sources, processes and management: A review. Science of the Total Environment 468, 1138-53.

Brodie, J., Baird, M., Waterhouse, J., Mongin, M., Skerratt, J., Robillot, C., Smith, R., Mann, R., Warne, M., 2017. Development of basin-specific ecologically relevant water quality targets for the Great Barrier Reef. TropWATER Report No. 17/38, James Cook University, Published by the State of Queensland, Brisbane, Australia. 68 pp.

Bittelli, M, Andrenelli, MC., Simonetti, G., Pellegrini, S., Artioli, G., Piccoli, I., Morari, F., 2019. Shall we abandon sedimentation methods for particle size analysis in soils?. Soil and Tillage Research 185, 36-46, doi.org/10.1016/j.still.2018.08.018.

Blott, SJ. and Pye, K. 2012. Particle size scales and classification of sediment types based on particle size distributions: Review and recommended procedures. Sedimentology 59, 2071-2096.

Cooper, M, Lewis, SE, Smithers, SG 2017. Spatial and temporal dynamics of suspended sediment causing persistent turbidity in a large reservoir: Lake Dalrymple, Queensland, Australia. Marine and Freshwater Research 68(7), 1377-90.

Devlin, M., Petus, C., Teixeira da Silva, E., Tracey. D., Wolff, N., Waterhouse, J., Brodie, J., 2015. Water Quality and River Plume monitoring in the Great Barrier Reef: An Overview of Methods Based on Ocean Colour Satellite Data. Remote Sensing 7, 12909-12941; doi:10.3390/rs71012909

Eshel, G, Levy, GJ, Mingelgrin, U, Singer, MJ. 2004. Critical evaluation of the use of laser diffraction for particle-size distribution analysis. Soil Science Society of America Journal. 2004 68(3), 736-43.

Fabricius, K.E., Wild, C., Wolanksi, E., Abele, D. 2003. Effects of transparent exopolymer particles and muddy terrigenous sediments on the survival of hard coral recruits. Estuarine, Coastal and Shelf Sciences 57, 613-621.

Fabricius, KE., Logan, M., Weeks, S., Brodie, J., 2014. The effects of river run-off on water clarity across the central Great Barrier Reef. Marine Pollution Bulletin. 84(1-2), 191-200.

Fabricius, KE., Logan, M., Weeks, SJ., Lewis, SE. and Brodie, J., 2016. Changes in water clarity in response to river discharges on the Great Barrier Reef continental shelf: 2002-2013. Estuarine, Coastal and Shelf Science 173, A1-A15.

Fisher, P., Aumann, C., Chia, K., O'Halloran, N., Chandra, S., 2017. Adequacy of laser diffraction for soil particle size analysis. PLoS One 12(5), 1-20.

Garzon-Garcia, A., Burton, J.M., Lewis, S., Bainbridge, Z., Dehayr, R., Moody, P., Brodie, J. In review. The bioavailability of nitrogen associated with sediment in riverine plumes entering coastal environments of the Great Barrier Reef. Marine Pollution Bulletin. (Chapter 7 of this Report).

Gruber, R., Waterhouse, J., Logan, M., Petus, C., Howley, C., Lewis, S., Tracey, D., Langlois, L., Tonin, H., Skuza, M., Costello, P., Davidson, J., Gunn, K., Lefevre, C., Shanahan, M., Wright, M., Zagorskis, I., Kroon, F., Neilen, A., 2019. Marine Monitoring Program: Annual Report for Inshore Water Quality Monitoring 2017-18. Report for the Great Barrier Reef Marine Park Authority, Great Barrier Reef Marine Park Authority, Townsville.

Gruber, R., Waterhouse, J., Logan, M., Petus, C., Howley, C., Lewis, S., Tracey, D., Langlois, L., Tonin, H., Skuza, M., Costello, P., Davidson, J., Gunn, K., Lefevre, C., Moran, D., Robson, B., Shanahan, M., Zagorskis, I., Shellberg, J. and Neilen, A., 2020. Marine Monitoring Program: Annual Report for Inshore Water Quality Monitoring 2018-19. Report for the Great Barrier Reef Marine Park Authority, Great Barrier Reef Marine Park Authority, Townsville.

Heiri, O., Lotter, A.F., Lemcke, G., 2001. Loss on ignition as a method for estimating organic and carbonate content in sediments: reproducibility and comparability of results. Journal of paleolimnology, 25(1), 101-110.

Hunt, S. and Jones, HF., 2019. Sediment grain size measurements are affected by site-specific sediment characteristics and analysis methods: implications for environmental monitoring. New Zealand Journal of Marine and Freshwater Research 53(2), 244-57.

International Organisation for Standardisation. 2020. ISO 13320:2020(E) Particle size analysis – Laser diffraction methods. Geneva: ISO.

Kuhnert, P., Henderson, B., Lewis, S., Bainbridge, Z., Wilkinson, S., Brodie, J.E. 2012. Quantifying total suspended sediment export from the Burdekin River catchment using the loads regression estimator tool. Water Resour Res 48, doi: 10.1029/2011WR011080

Leeder, M.R. 1982, Sedimentology; process and product. Chapman and Hall, London.

Lewis, S., Bainbridge, Z. Stevens, T. Garzon-Garcia, A. Chen, C. Burton, J. Bahadori, M. Rezaei Rashti, M. Gorman, J. Smithers, S. Olley, J. Moody, P. Dehayr, R., 2018. Sediment tracing from the catchment to reef 2016 to 2018: Flood plume, marine sediment trap and logger data time series. Report to the National Environmental Science Program. Reef and Rainforest Research Centre Limited, Cairns (94pp.).

Lewis, S.E., Bartley, R., Wilkinson, S.N., Bainbridge, Z.T., Henderson, A.E., James, C.S., Irvine, S.A., Brodie, J.E. in review. Land use change in the river basins of the Great Barrier Reef, 1860 to 2019: A foundation for understanding environmental history across the catchment to reef continuum. Marine Pollution Bulletin.

Lewis, S. et al. 2020. What's really damaging the Reef? Tracing the origin and fate of the ecologically detrimental sediment. NESP Report Project 5.8. Report to the National Environmental Science Program Reef and Rainforest Research Centre Limited, Cairns.

Loring, TH. and Rantala RTT., 1992. Manual for geochemical analyses of marine sediments and suspended particulate matter. Earth-Science Reviews 32, 235-283.

Lough, JM., Lewis, SE., Cantin, NE., 2015. Freshwater impacts in the central Great Barrier Reef: 1648–2011. Coral Reefs 34, 739-51.

McCloskey, G.L., Baheerathan, R., Dougall, C., Ellis, R., Bennett, F.R., Waters, D., Darr, S., Fentie, B., Hateley, L.R., Askildsen, M. in review-a. Modelled estimates of fine sediment and particulate nutrients delivered from the Great Barrier Reef catchments. Marine Pollution Bulletin.

McCloskey, G.L., Baheerathan, R., Dougall, C., Ellis, R., Bennett, F.R., Waters, D., Darr, S., Fentie, B., Hateley, L.R., Askildsen, M. in review-b. Modelled estimates of Dissolved Inorganic Nitrogen exported to the Great Barrier Reef. Marine Pollution Bulletin.

Manning, A.J., Whitehouse, R.J.S., and Uncles, R.J. 2017. 'Suspended particulate matter: the measurement of flocs'. In Uncles, R.J. and Mitchell, S.B. eds., 2017. Estuarine and coastal hydrography and sediment transport. Cambridge University Press, 211-260.

Margvelashvili, N., Andrewartha, J., Baird, M., Herzfeld, M., Jones, E., Mongin, M., Rizwi, F., Robson, B.J., Skerratt, J., Wild-Allen, K. and Steven, A., 2018. Simulated fate of catchment-derived sediment on the Great Barrier Reef shelf. Marine Pollution Bulletin 135, 954-962.

Owens, PN., Blake, WH., Gaspar, L., Gateuille, D., Koiter, AJ., Lobb, DA., Petticrew, EL., Reiffarth, DG., Smith, HG., Woodward, JC., 2016. Fingerprinting and tracing the sources of soils and sediments: Earth and ocean science, geoarchaeological, forensic, and human health applications. Earth-Science Reviews 162, 1-23.

Özer, M., Orhan, M., Isik, NS., 2010. Effect of particle optical properties on size distribution of soils obtained by laser diffraction. Environmental and Engineering Geoscience 16(2), 163-173.

Peel, M.C., Finlayson, B.L. McMahon, T.A., 2007. Updated world map of the Köppen-Geiger climate classification, Hydrol. Earth Syst. 11 1633-1644, doi.org/10.5194/hess-11-1633-2007.

Petus, C., Waterhouse, J., Lewis, S., Vacher, M., Tracey, D., Devlin, M., 2019. A flood of information: Using Sentinel-3 water colour products to assure continuity in the monitoring of water quality trends in the Great Barrier Reef (Australia). Journal of Environmental Management 248, 109255.

Poppe, LJ, Eliason, AH, Fredericks, JJ, Rendigs, RR, Blackwood, D, Polloni, CF., 2000. Grain size analysis of marine sediments - methodology and data processing. In: USGS East-Coast sediment analysis: procedures, database and georeferenced displays. US Geological Survey Open-File Report 00-358. https://pubs.usgs.gov/of/2000/of00-358/index.htm.

Reynolds, RA., Stramski, D., Wright, VM., Wozniak, SB. 2010. Measurements and characterization of particle size distribution in coastal waters. Journal of Geophysical Research 115, 1-19.

Rodríguez, JG, Uriarte A., 2009. Laser diffraction and dry-sieving grain size analyses undertaken on fine-and medium-grained sandy marine sediments: a note. Journal of Coastal Research 25(1), 257-64.

Romano, E., Magno, M.C., Bergamin, L., 2018. Grain size of marine sediments in the environmental studies, from sampling to measuring and classifying. A critical review of the most used procedures. ACTA International Measurement Confederation (IMEKO) 7(2), 10-15, doi.org/10.21014/acta_imeko.v7i2.537.

Shepard, F.P., 1954, Nomenclature based on sand-silt-clay ratios: Journal of Sedimentary Petrology, 24, 151-158.

Snyder, NP., Allen, JR., Dare, C., Hampton, MA., Schneider, G., Wooley, RJ., Alpers, CN., Marvin-DiPasquale, MC., 2004. Sediment grain-size and loss-on-ignition analyses from 2002 Englebright Lake coring and sampling campaigns. U.S. Geol. Surv. Open File Rep., 2004-1080, 46 pp. https://pubs.usgs.gov/of/2004/1080/of2004-1080.pdf

Spencer, K.L. 2017, 'Estuarine deposited sediments: sampling and analysis', in. RJ. Uncles & SB. Mitchell (ed.), Estuarine and coastal hydrography and sediment transport, Cambridge University Press, Cambridge, pp153-178.

Sperazza, M., Moore, JN. and Hendrix, MS. 2004, High-resolution particle size analysis of naturally occurring very fine-grained sediment through laser diffractometry. Journal of Sedimentary Research 74(5), 736-743.

Steven, A.D., Baird, M.E., Brinkman, R., Car, N.J., Cox, S.J., Herzfeld, M., Hodge, J., Jones, E., King, E., Margvelashvili, N. and Robillot, C. 2019. eReefs: An operational information system for managing the Great Barrier Reef. Journal of Operational Oceanography, 12. S12-S28.

Stevens, T. 2013. Suspended sediment sampler. Australian Patent No. 2013206318. Canberra: IP Australia.

Stevens, T. 2019. International Patent Application PCT/AU2019/051436 Improved Sampler and Method

Walling, DE., Owens, PN., Waterfall, BD., Leeks, GJL., Wass, PD., 2000. The particle size characteristics of fluvial suspended sediment in the Humber and Tweed catchments, UK. The Science of the Total Environment 252, 205-222.

Williams, ND., Walling, DE., Leeks, GJL., 2007. High temporal resolution in situ measurement of the effective particle size characteristics of fluvial suspended sediment. Water Research 41, 1081-1093.

Vaasma, T. 2008. Grain-size analysis of lacustrine sediments: a comparison of pre-treatment methods. Estonian Journal of Ecology 57 (4), 231-243, doi: 10.3176/eco.2008.4.01.

Supplementary Figures and Material

Supplementary Figure 1. Burdekin and Tully River flood plume sampling locations and associated water types mapped using corresponding MODIS satellite imagery for each day the flood plume was sampled in the field. Burdekin: 31st March 2017 (a), 6th (estuarine sites) and 13th (northern sites) March 2018 (b) and 11-15th February 2019 (c). Tully River: 11th January 2017 (d), 9th & 14th February 2018 (e).
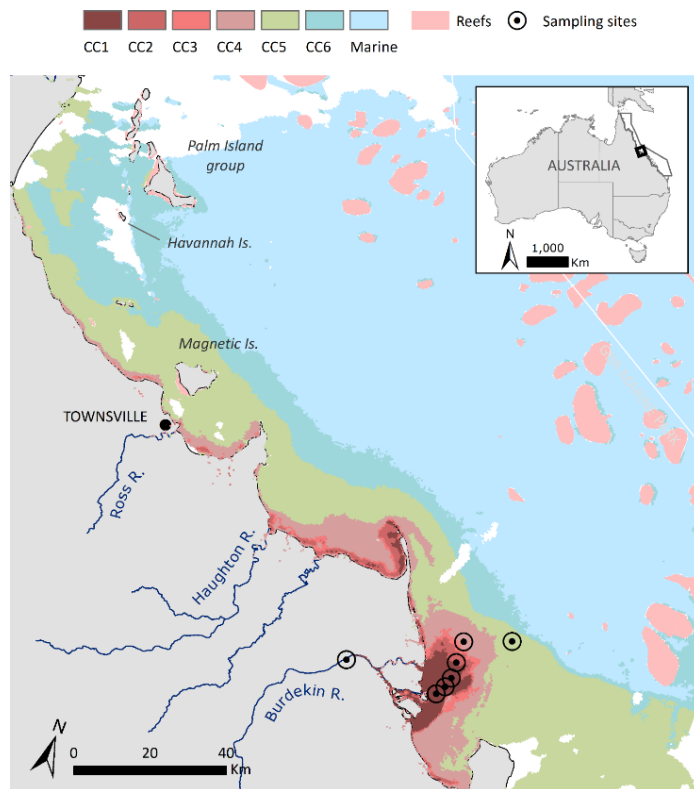
(a) Modis Aqua water type maps and Burdekin plume sample location: 31st of March 2017. Reefs shown as pink polygons.
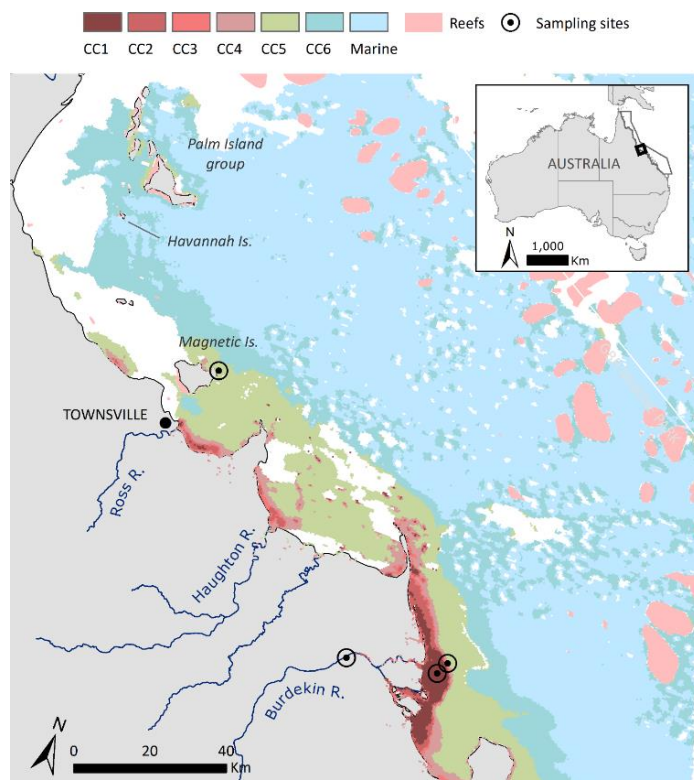
(b) Modis Aqua water type maps and Burdekin plume sample location: 6th of March 2018. Source: Modis-Aqua satellite. White patches represent locations where cloud cover has prevented satellite imagery capture.
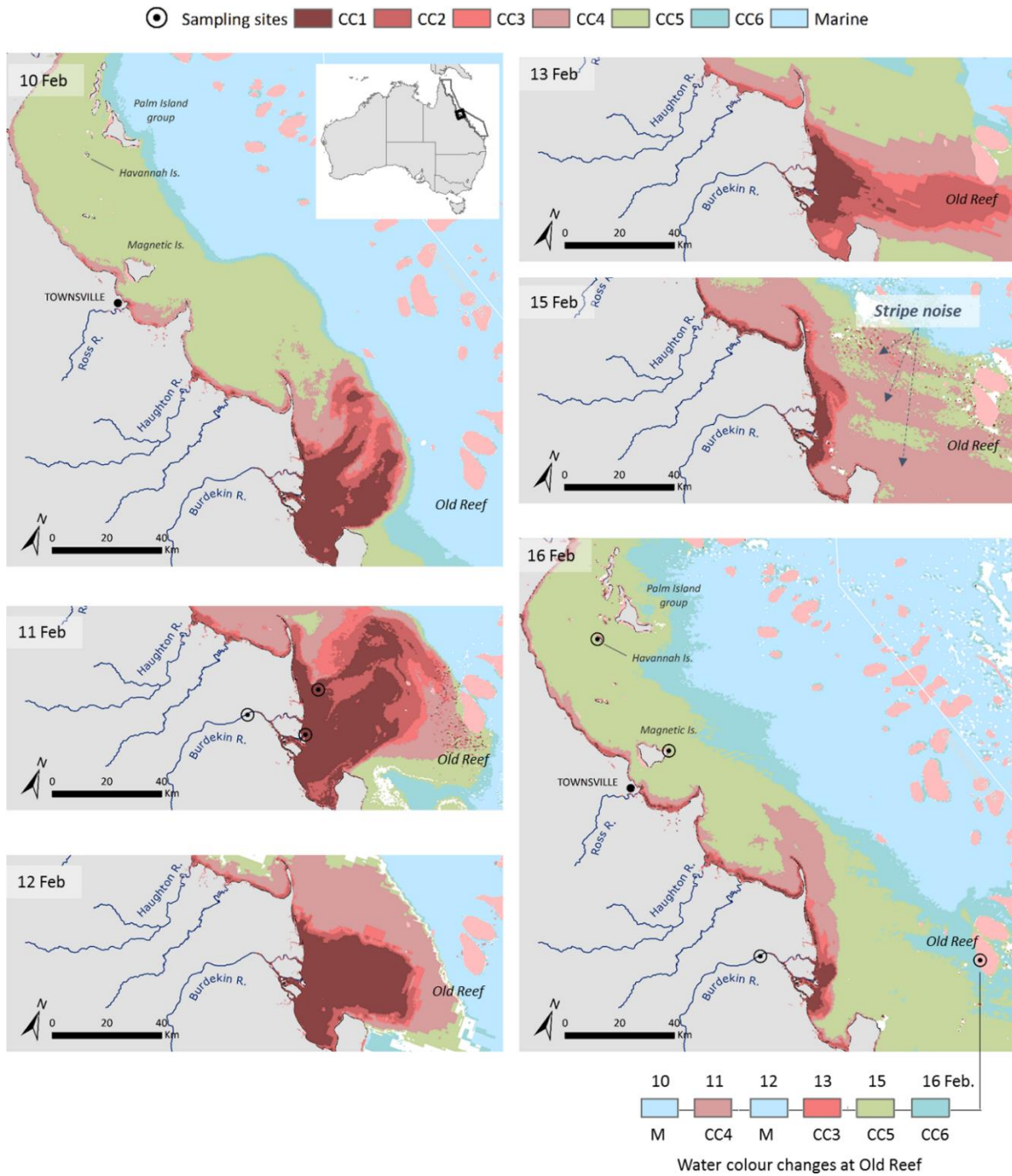
(c) Time series of water type maps showing Burdekin primary plume movements between the 10th and the 16th of Feb 2019. Sample collected on the 11th of February are overlaid on the 11th of February map and samples collected on the 12th (Havannah Is. and Orchard Rocks, Magnetic Is.) and 15th (Old Reef) of Feb are overlaid on the 16th of February map. Bottom plot underline changes in water colour at the Old reef between the 10th and the 16th of Feb 2019. Images of the 10, 11 and 16th of Feb: Modis Aqua and of the 12, and 13th of February: MODIS-terra satellite.
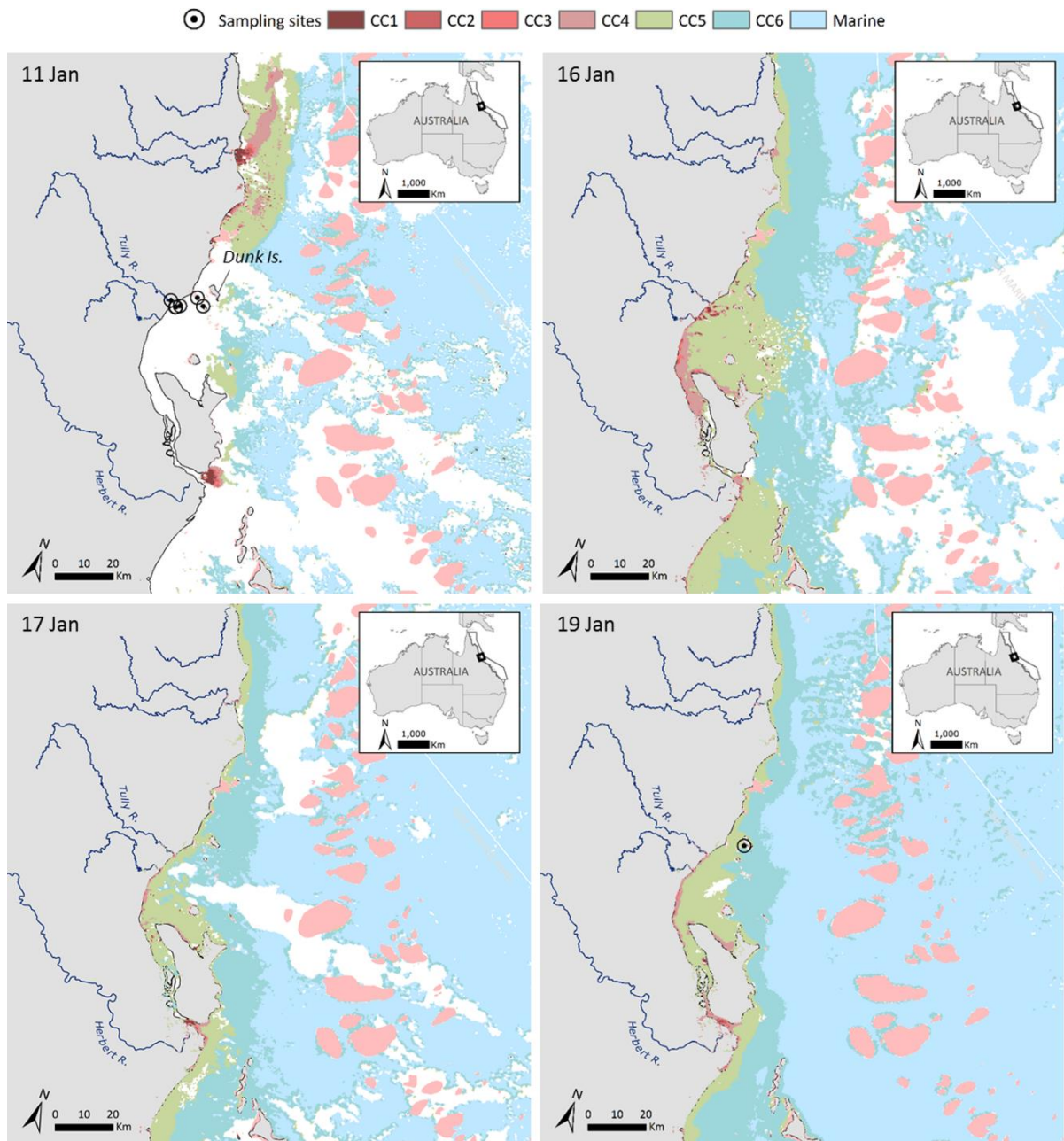
(d) Time series of water type maps showing Wet Tropics water type movements between the 11th and the 19th of January 2017. Samples collected along the Tully River transect on the 11th and 19th of January are overlaid on the 11th and 19th of January maps, respectively. Source: Modis-Aqua satellite. White patches represent locations where cloud cover has prevented satellite imagery capture. Reefs shown as pink polygons.
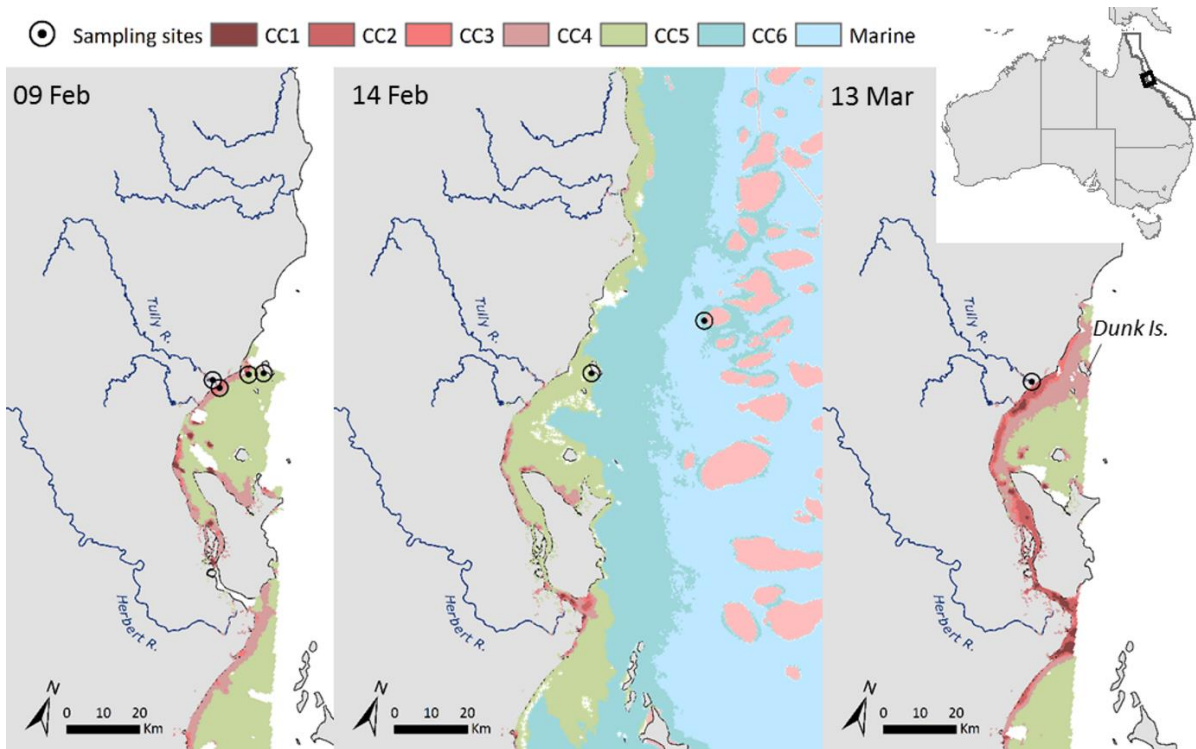
(e) Tully 2018 (left and middle) Modis Aqua water type maps and samples collected the 09 and 14 Feb 2018, right Modis Aqua water type maps of the 13th of March 2018 and samples collected the 12th of March 2018.

Supplementary Figure 2. Example of various sonication and dispersant treatments for freshwater and salt-removed samples.
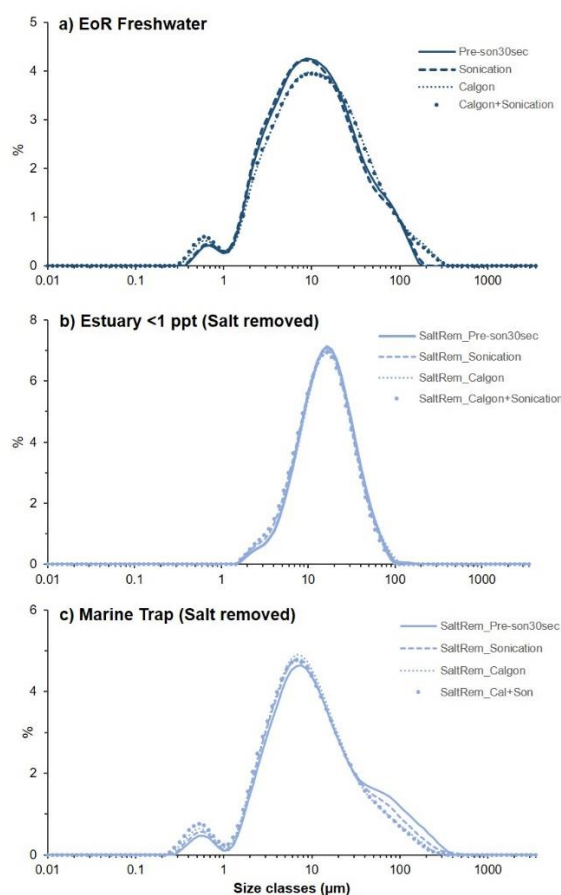
Supplementary material 1: Wet season water type maps

Wet season water type maps are produced using MODIS true colour imagery reclassified to six distinct colour classes defined by their colour properties. The wet season water types are regrouped into three water types (primary, secondary and tertiary) characterised by different concentrations of optically active components (suspended sediment, colour dissolved organic matter and chlorophyll a), which control the colour of the water and influence the light attenuation, and different pollutant concentrations (e.g., Petus et al. 2019):

• Primary water type (colour classes 1–4): Corresponds to the brownish to brownish-green turbid water masses. These waters have high nutrient and phytoplankton concentrations but are also enriched in sediment and dissolved organic matter and have reduced light levels. They are typical for nearshore areas or inshore regions of flood river plumes.

• Secondary water type (colour class 5): Corresponds to the greenish to greenish-blue water masses and are typical of coastal waters dominated by algae, but also with some dissolved matter and some fine sediment present. Relatively high nutrient availability and increased light levels due to sedimentation favour an increased coastal productivity in this water type. This water type is typical for the coastal waters or the mid-region of river plumes.

• Tertiary water type (colour class 6): Transitional, greenish-blue water mass with slightly above ambient turbidity and nutrient concentrations. This water type is typical for areas towards the open sea or offshore regions of flood river plumes.

Supplementary Table 1. Summary EoR and flood plume sediment grain size excel spreadsheet. Please email first author for copy.

CHAPTER 3

Examining turbidity regimes on the inner Great Barrier Reef: quantifying the influence of newly delivered riverine sediments

Stephen Lewis[1], Thomas Stevens[1], Cassandra James[1], Zoe Bainbridge[1], Scott Smithers[1,2]

[1] Catchment to Reef Research Group, TropWATER, James Cook University
[2] Environmental Science & Management, College of Science & Engineering, James Cook University

3.1. Introduction

Sediment loads delivered to the Great Barrier Reef (GBR) lagoon have increased markedly from most Natural Resource Management Regions since the arrival of Europeans (McCloskey et al. 2017). However, the impact of these elevated sediment loads on key GBR ecosystems including coral reefs and seagrass meadows is still contested. Sedimentologists argue that the accumulation of a substantial sediment wedge along the inshore GBR since sea levels stabilized in the mid-Holocene provides an abundance of sediment for resuspension which is the dominant control on turbidity regimes in the GBR (Larcombe et al. 1995; Orpin and Ridd, 2004; Larcombe and Ridd, 2018). They contend that inshore turbidity is driven by resuspension and not limited by sediment supply, and that any extra sediment delivered from river catchments has negligible influence on sediment exposure in the GBR (Larcombe et al. 1995; Larcombe and Woolfe, 1999; Orpin and Ridd, 2004; Larcombe and Ridd, 2018). In contrast, another body of research has been developed to suggest that the newly exported sediment is more physically and biologically active both during and in the months following delivery to the GBR (Fabricius et al. 2013, 2014, 2016). While the bulk (~80 to 90%) of the mud-sized (< 63 µm) sediment exported from the rivers with relatively higher sediment loads such as the Burdekin is deposited and largely retained near the river mouth (Lewis et al. 2014; Delandmeter et al. 2015), a portion of the finer sediment fraction (< 20 µm) travels further within the river flood plumes and forms organic-rich sediment floc aggregates (Bainbridge et al. 2012, in review/chapter 2). It is postulated that these organic-rich sediments eventually settle on the seafloor as a 'fluffy/fluff layer' but are more easily resuspended in the following months relative to the more compacted Holocene wedge sediments (Fabricius et al. 2016; Bainbridge et al. 2018; Margvelashvili et al. 2018). Indeed, this hypothesis has been supported by turbidity data recorded at inshore coral reefs (Fabricius et al. 2013), measurements of spatial and temporal variability in satellite-derived photic depth (Fabricius et al. 2014, 2016) and sediment modelling (Margvelashvili et al. 2018). Nonetheless, Larcombe and Ridd (2018) argue that more empirical evidence is required before this hypothesis can be accepted. Larcombe and Ridd (2018) justify their assertion on the basis that large public investment would be needed to remediate erosion-prone landscapes if these areas were the source of the suspended sediments driving elevated turbidity.

To date, measuring the contribution of the newly delivered sediment relative to the background resuspension of the existing sediment bed has proven difficult. Indeed, a number of parameters such as wind speed, wind direction, wave height, wave period, water depth (tidal range) and water currents need to be considered as well as river discharge and load parameters (Fabricius et al. 2013, 2014, 2016). Such parameters are combined in a statistical model to remove the influences of waves and tides on sediment resuspension so that the influence of the recently delivered sediment can be calculated (Fabricius et al. 2014, 2016). Larcombe and Ridd (2018) argue based on the empirical data of Fabricius et al. (2013) that the increase in turbidity from flood plumes 'appears to be no more than 1 NTU rise in turbidity for perhaps a few days of each year, so is very small indeed and there is no evidence that it is of ecological importance', although they did not consider the changes in turbidity in the months following the flood plume. Schaffelke et al. (2018) point out that the 1 NTU increase postulated by Larcombe and Ridd (2018) is unsubstantiated and that more recent work by Fabricius et al. (2014, 2016) also found similar relationships between sediment load and turbidity. In response Larcombe and Ridd (2019) argue that there is still no evidence of the ecological importance of a rise in turbidity and that the dataset should be re-analysed. In any case, new data collected in this project highlight that relatively small changes in concentrations of suspended particulate matter (~ 1 mg.L^{-1}) or turbidity (1-2 NTU) can result in large changes in Secchi Disc Depth (Lewis et al. chapter 4) and in PAR light profiles (Lewis et al. chapter 5).

Clearly there is a need to re-examine the influence of newly delivered sediment on sediment exposure in the inshore GBR through a systematic approach. This approach includes site selection to cover relevant inshore-offshore water quality gradients as well as to capture and quantify spatial and temporal variations in sediment composition to examine changes between the dry and wet seasons. Indeed the influence of wind and waves on bottom shear is the critical determinant on resuspension and a more direct measure of this shear would be optimal to better account for the direct resuspension contribution. This study set up seven monitoring locations in the inshore GBR to take continuous readings of turbidity, light, pressure (RMS) and current along with sediment traps to capture spatial and temporal variation in sediment exposure with increasing distance from the Burdekin River mouth including an inshore-offshore transect, and off the Tully River in the Wet Tropics. Our dataset not only provides new insights on the spatial and temporal influence of newly delivered sediment and associated particulate nutrients along the inshore GBR but also looks to quantify the the sediment fractions most likely to cause ecosystem decline and their sources within catchments.

3.2 Methods

3.2.1 Site selection and instrument setup

Sites were selected to cover key ecosystems (coral reefs and seagrass meadows) from an alongshore gradient off the Burdekin River mouth which is a common pathway for its freshwater river plume (Figure 1). In addition, an inshore-offshore gradient was selected in Cleveland Bay to examine sediment exposure regimes on the fore reef slopes on a turbid zone platform reef at ~ 5 m depth (Middle Reef), a turbid inshore fringing reef slope (5 m) (Geoffrey Bay) and a deeper inshore site (~16 m) located at the transition between the inner and middle shelves (Orchard Rocks) (Figure 1). We also established sites off Dunk Island to examine the

influence of Wet Tropics rivers (predominately the Tully River but also the Herbert River on occasion) on inshore coral reef sites (Figure 3.1).

Seven of the sites (Cleveland Bay, Middle Reef, Geoffrey Bay, Orchard Rocks, Havannah Island (1), Orpheus Island and Dunk Island (1)) were set up with a frame containing a nephelometer which took continuous 10-min interval measurements of turbidity, PAR light, depth and pressure (RMS) as well as a current meter (1 second measurements) and four 55 diameter SediSampler® (Integral Aqua Pty Ltd) sediment traps (see Chapter 1) surrounding the nephelometer (Figure 3.2). Four additional sites (Havannah Island toe (immediately offshore from Havannah Island (1)), Havannah Island (2), Pelorus Island and Dunk Island (2)) were established (Figure 3.1) with 3 equally-spaced (~ 5 m apart) sediment traps; these sites were designed to examine the broader variation in sediment exposure related to the nephelometer sites across Dunk Island and Halifax Bay. Depending on logistics and time of year (i.e. wet versus dry seasons) sites were typically changed over and serviced every 2 to 5 months. Details on the deployments at each of the sites are provided in the appendix.

Several flood events of various magnitudes and large resuspension events were recorded over the total logger monitoring period (Cleveland Bay deployments: 1st June 2016 to 23rd March 2020; Halifax Bay deployments: 7th June 2016 to 26th March 2020; Dunk Island deployments 7th June 2016 to 29th March 2019). Specifically, the large flood events captured off the Tully River relevant to our Dunk Island logger site occurred in January 2017, January to March 2018 and January to February 2019. The flood events relevant to our loggers across Cleveland and Halifax Bays included March 2018 and January to February 2019. A major resuspension event linked to the passage of ex-Tropical Cyclone Penny occurred in December 2018 to January 2019. A summary of these events is provided in Table 3.1.

Table 3.1. Summary table outlining the key event periods over the logger deployments.

Site locations	Key flood events	Key resuspension events
Cleveland Bay (Cleveland Bay, Middle Reef, Geoffrey Bay, Orchard Rocks)	**2017:** no large flood (TC Debbie plume went south); **2018:** 7/3/18 to 13/3/18; **2019:** 27/1/19 to 12/2/19; **2020:** no large flood	**2018:** 24/12/18-8/1/19 (Ex TC Penny)
Halifax Bay (Havannah Island, Orpheus Island)	**2017:** no large flood (TC Debbie plume went south); **2018:** 7/3/18 to 13/3/18; **2019:** 27/1/19 to 12/2/19; **2020:** no large flood	**2018:** 24/12/18-8/1/19 (Ex TC Penny)
Dunk Island	**2017:** 8/1/17 to 11/1/17; **2018:** 16/1/18 to 19/1/18, 24/1/18 to 26/1/18, 4/2/18 to 9/2/18, 8/3/18 to 12/3/18, 24/12/18 to 2/1/19; **2019:** 26/1/19 to 11/2/19	**2018:** 6/12/18-12/12/18
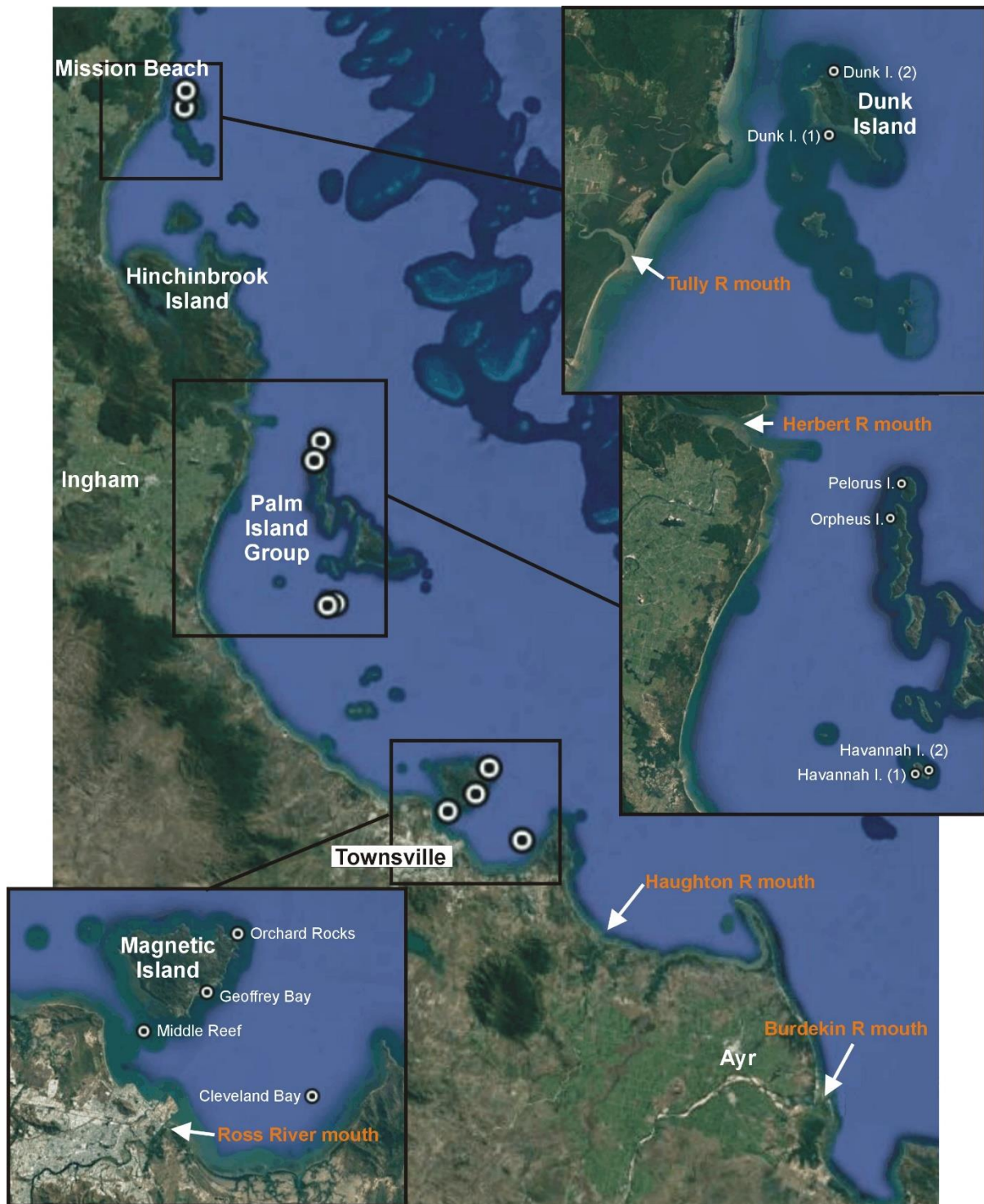
Figure 3.1. Map of sampling sites in this project.
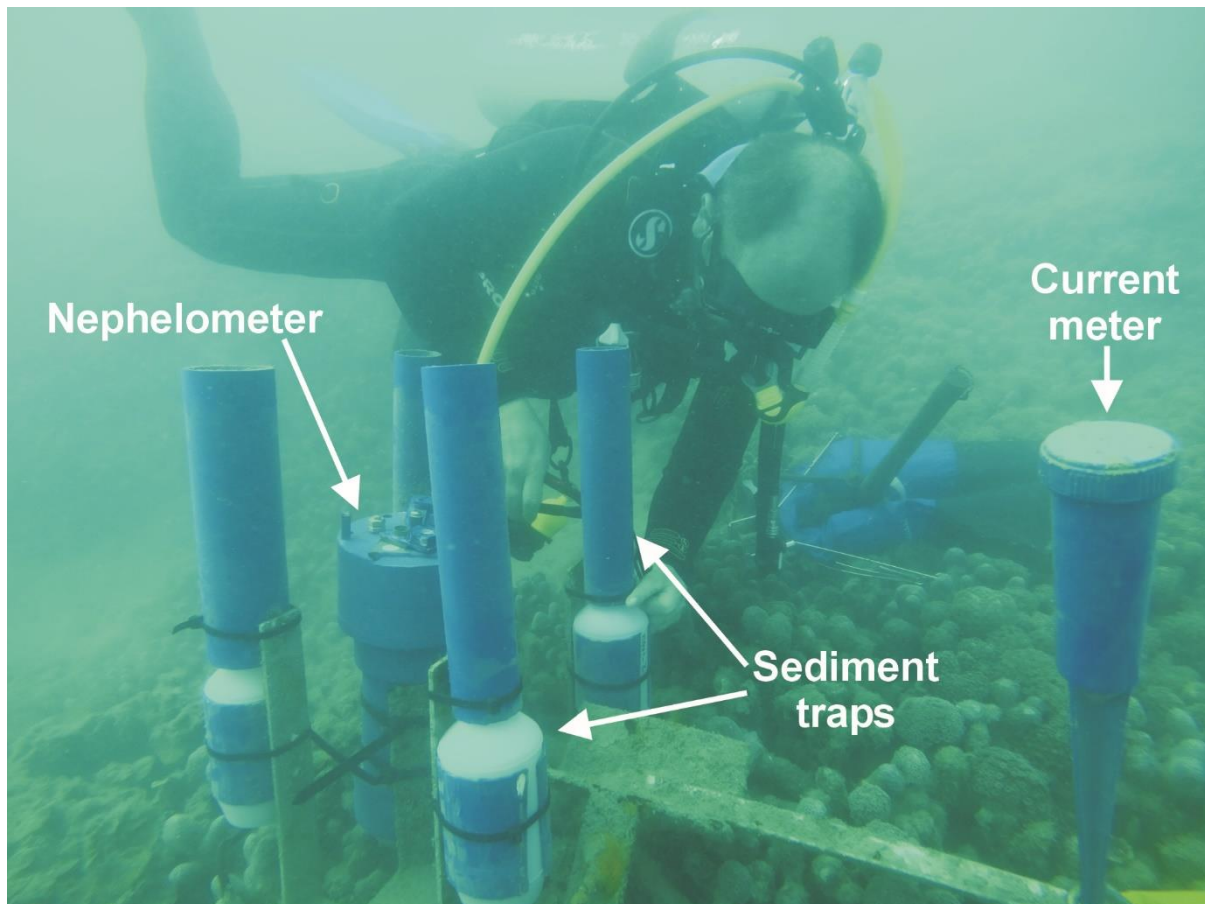
Figure 3.2. Typical instrument set up at the seven sites with nephelometer, current meter and sediment traps (Photo: Ian McLeod).

3.2.2 Nephelometer deployment and processing

Prior to each deployment the nephelometers were serviced (check the cleaning wipers were functioning, check for leaks and painted with antifoul) and calibrated for pressure, turbidity and light. Following retrieval, the data from the nephelometer were downloaded and processed using software developed by the Marine Geophysics Laboratory, James Cook University. This processing software applies the latest calibration data (i.e. converts the raw NTU measurements to calibrated or equivalent NTU ('NTUe' where two plates (on the '45' and '57' grey scale) are used to correct for the offset voltage between each instrument: Larcombe et al. 1995; raw pressure measurements to depth and; raw light data to PAR light) and only captures the period when the instrument was deployed (i.e. in the water column) as well as applying a 'zero point' correction factor. Periods where the sensor failed or was fouled were removed and 'spikes' or 'low level fouling' which were not logically viable in the environment were identified and manually removed. In that regard, a systematic approach was established to better process these data. Once the obvious sensor malfunction, fouling and anomalous spiking were removed, more subtle sensor behaviour could be investigated. These subtle influences included low level fouling patterns on the NTU (turbidity) readings which largely involved a small continuous increase in NTU readings commonly in the order of 1-2 NTU over the 2-hour window between wiping intervals; the lowest NTU reading occurred either on the wipe or the second 10-minute reading following the wipe. Hence once this pattern was identified the lowest NTU reading was then checked against the corresponding NTU from the

deposition sensor (if not fouled; the deposition sensor is a nephelometer facing vertically) and retained if deemed reasonable while the data surrounding it was deemed to be fouled and removed. The turbidity (NTU) data were converted to suspended sediment concentration (SSC) using the relationships for each site developed in Lewis et al. (2018). On a few occasions the PAR light measurement by the instrument 'drifted' over the deployment period; data were manually corrected for this drift. We note that the RMS pressure data is a 'root mean square' reading of 10 depth measurements taken 1 second apart at 10-minute intervals. The full data time series for each site was then plotted and visually inspected to further check for any anomalies (i.e. clear outliers) not previously identified.

3.2.3 Current meter deployment and processing

The Marotte HS current meter, produced by the Marine Geophysics Laboratory, James Cook University, was deployed at the seven sites coupled with the nephelometer and the SediSampler® sediment traps. Prior to each deployment, the current meters had their batteries replaced and were painted with antifoul paint. Once retrieved, the raw data were downloaded and then processed using software developed by the Marine Geophysics Laboratory, James Cook University. The initial processing used the software to calculate 10-min average current conditions to match the nephelometer dataset. These data are provided to the eAtlas, although as statistical analysis of these data showed no apparent relationship to turbidity variability they have not been considered further in this report. However, additional processing of the higher resolution data (i.e. 1 second intervals) for the Dunk Island time series was performed and the data normalised to root mean square (RMS) to capture the variability in the movement of the current meter. This approach has been used to demonstrate a potential new method to capture bed shear stress as an indicator of resuspension (see Statistical processing of logger data section). Indeed, the RMS of the current meter is likely a closer and more direct measure of bed shear stress (i.e. recording variability in back and forth, side-to-side horizontal water movements) which is the ultimate cause of wave-generated turbidity. In contrast, the RMS (pressure) sensor is recording the variability in depth readings (i.e. recording variability in the up and down, vertical water depth movements) over 10 second windows every 10 mins (i.e. not continuous like the current RMS).

3.2.4 Sediment trap processing

Once retrieved from the field, the sediment trap samples (in 1 L containers) were placed immediately on ice and refrigerated at 4° C on return to the laboratory. Each sample was transferred to a 2 L container and well-mixed aliquots were taken for the TSS method (30 ml), microscopy and nutrient (250 ml) analysis (these aliquots were kept refrigerated (TSS, microscopy) or frozen (nutrients) prior to analysis). The samples were transferred to a glass cylinder and photographed and the colour was determined on a Munsell colour chart. The remaining sample was transferred to the 2 L container, left to settle with the clear supernatant decanted and the concentrated sample poured into dialysis tubing to remove the salts from each sample. Aliquots (30 ml) from the salt removed sample were then taken for grain size analysis.

TSS analysis
A 1 to 2 ml well-mixed aliquot from each trap was pipetted into a filtering manifold which was prefilled with 250 ml of RO water for total suspended solid (TSS) analysis. This method vacuum filters known volumes of sample onto pre-weighed Whatman GF/C filter papers

(nominal pore size 1.2 μm) which were dried overnight in a 103–105°C oven and reweighed to provide a concentration in g.L^{-1}. This approach compared favourably with the suspended sediment concentration (SSC) or dry weight method (for further details see Chapter 1).

Microscopy

Subsamples from the sediment traps were taken and placed on a microscope slide and viewed under a light microscope. The ToupView software program (Touptex photonics) was used to capture images (see Bainbridge et al. in review). In particular, we were particularly interested in documenting the presence/absence of the large sediment floc aggregates as well as diatoms captured by the traps over the deployment periods.

Grain size analysis

The salt-removed subsamples from the sediment trap samples were analysed on a Malvern Mastersizer 3000 at James Cook University. Two separate analysis runs were performed according to the protocols outlined in Bainbridge et al. (in review/chapter 2). Briefly, the first run involved the direct measurement of the salt removed sample on the instrument following sieving to 1.2 mm while the second run was performed following sequential treatment with H$_2$O$_2$ (to remove organics) and HCl (to remove carbonates) in a heated 80° C bath. The former measurement provides an indication of the behavior of the particles in the water column that were captured by the sediment trap while the latter measurement provides an indication of the primary grain size of the mineral particles. For further detail on the methods including machine settings the reader is referred to Bainbridge et al. (in review/chapter 2). For the purpose of this report we present the results of the treated grain size analysis separated into the clay (< 4 μm), fine silt (4 – 16 μm), coarse silt (16 – 63 μm) and sand (> 63 μm) fractions.

Loss on ignition analysis

Salt-removed dried samples from the sediment trap deployments were weighed after drying in a crucible in a 105° C oven. The samples were then added to a Carbolite (AAF1100) ashing furnace and heated to 550° C for 4-5 hours and then reweighed and then were reheated in the furnace at 950° C and reweighed. The weight difference between the 550° C and 105° C treatments reflect the total organic matter of the sample while the difference between 950° C and 550° C (multiplied by 2.274) provide a measure of the carbonate content (see Bainbridge et al. in review/chapter 2 for further details). The data from this analysis provided a measure of the proportions of mineral (i.e. terrigenous), organic and carbonate content to be determined for each sediment trap sample.

Nutrient analysis

The 250 ml aliquots from the sediment trap samples were analysed for total organic carbon (TOC), total nitrogen (TN) and total phosphorus (TP) contents at the Department of Environment and Science Laboratory. Nitrogen and phosphorus concentrations were determined in accordance to *Standards Australia and Standards New Zealand* (1998). The methods *5210 D APHA AWWA (2012)* were followed to determine the amount of carbon using an automated carbon analyser.

3.2.5 Statistical analysis of logger data

Due to the extensive collection of high temporal resolution 'big' data from this project we sought further statistical analysis to better quantify the influence of newly delivered sediment

at our sites. This intensive statistical analysis component moved beyond the initial methodology proposed in the original project brief and hence for this report we only consider the Dunk Island dataset as a demonstration of the potential for this approach. In that regard, we utilised the turbidity data time series (note for this analysis we used the calibrated NTUe data) for our Dunk Island (1) site coupled with additional turbidity logger data measured at Dunk Island (situated close to the Dunk (2) site see Figure 3.1) by the Australian Institute of Marine Science (AIMS) for the Great Barrier Reef Marine Park Authority's (GBRMPA) Marine Monitoring Program (MMP). These turbidity data collectively allow an additional QA/QC check of the broader trends in resuspension events around Dunk Island. In turn, these data are used as the 'base' to establish correlations with other predictive data such as RMS pressure from the nephelometer, the current meter data (averaged and RMS), wind data (speed and direction) measured at Cardwell Parade and tidal height data measurements from Clump Point. To derive weekly wind speed and direction averages for the full time series plots, wind direction was decomposed into west/east and north/south components which are then averaged and recombined to produce an average weekly direction. The weekly average wind speed is the simple scalar average of the speed observations.

Generalised additive mixed models (GAMM) were used to model NTUe as a function of different covariates (primarily RMS pressure and RMS current). The GAMMs model relationships in data as non-linear functions using smooth functions with the default penalized thin plate regression splines used as the smoother. Model assumptions were checked using standard diagnostic tools available in the R packages (e.g. gam.check, autocorrelation function plots). For naïve models (these are GAMs and not GAMMs), we assumed that the observations are independent. These naïve models were used to estimate the autocorrelation coefficient (the rho value) which is then used in subsequent AR1 models taking into account temporal tendencies in the data (i.e. a model that estimates influence of preceding measurements on the current measurement in a series).

For the GAMM models we used the R package 'mgcv' (Wood, 2006) and various other packages for visualizing data ('ggplot2' (Wickham, 2016) and 'gratia' (Simpson, 2020). We used the bam function with discrete = TRUE and family ="scat". Bam is a less memory intensive version of a gam (Wood et al. 2015). The NTUe data in its raw form is fat/heavy tailed and skewed and so the initial model diagnostics assuming Gaussian distribution were poor. The "scat" family is designed to deal with data that are heavy tailed (i.e. more data located at the extremes than would be expected for a normal distribution). The "discrete" term provides another function that speeds up the processing when dealing with large datasets. Percentiles were used to remove outliers; while various standardised approaches were trialled they were found to remove too much data and so working with the percentiles allowed outliers to be more easily identified and removed without overpruning the data. The lower range removed was generally <1% and the upper percentile was 99.5%. Both NTU and the predictor datasets were then log transformed.

Firstly, we explored various predictors of NTUe as a function of different lags in the RMS current meter data. Initial data exploration was undertaken using various time lags (10 minutes, 30 minutes, 1 hour, 3 hours and 12 hours). Subsequent analysis focused on two contrasting lag periods; the ten minutes prior to each NTUe recording and the three hours prior to each NTUe recording and different metrics of those lags (i.e. mean, 90th percentile and 95th percentile). The three hour lag performed better than ten minute lag (and indeed the other

time-periods considered) but there was little difference between the mean, 90th and 95th percentile current RMS (they were all highly correlated) and so the 95th percentile were selected as it performed marginally better as a predictor. Secondly, naïve models were run relating NTUe to both RMS current and RMS pressure separately with no autocorrelation error assumed. We then used an autocorrelation function from the "itsadug" package (van Rij et al. 2020) to explore whether there was structure in the naïve model residuals. This analysis did suggest structure in the residuals and hence an AR1 model was subsequently included (see below) to reduce the effects of autocorrelation.

The final models were then run for the full time series including an AR1 as described above. Each deployment was specified as the start of an event and the deployments were considered as a random effects structure (to account for differences in deployments due, for example, to differences in instruments between deployments and/or calibration settings). These model runs were done for both RMS current 3-hour lag and RMS pressure.

3.3 Results

3.3.1 Logger time series and sediment composition data

Our logger time series data from the Cleveland Bay site clearly show the influence of the 2018 and 2019 flood events on the suspended sediment concentration (SSC) record from the Burdekin River (Figure 3.3). While the site was notoriously difficult to capture a continuous time series due to its shallow (~ 5 m depth) and open sediment field location which resulted in regular disruptions in virtually every deployment (i.e. traps knocked over, broken or lost, regular loss of current meters and losses/failures of the nephelometer), the available time series provide important insights on the role of resuspension and the delivery of new sediment. Specifically the SSC time series show the influence of regular spikes in the absence of river discharge which highlight the influence of resuspension; however, the two highest peak SSC readings both coincided with flooding from the Burdekin River (Figure 3.3). In addition, the SSC time series in (at least) the 3 months following the 2019 floods show much higher concentrations relative to the response shown by the RMS pressure sensor (i.e. fairly low RMS spikes compared to large SSC fluctuations). This result indicates that the newly delivered sediment associated with the floods has continued to influence the turbidity regime in this area for several months after the event.

Interestingly, the instruments also recorded a major resuspension event just prior to the 2019 floods which produced a similar SSC signal (and light response) to the 2019 flood event. Indeed, the PAR light sensor at this shallow site showed virtually no light reached the bottom for 15 days during the large resuspension event and for 17 days during the Burdekin (and Townsville region) floods. Furthermore, light levels were similarly suppressed in the months following the 2019 floods coinciding with the elevated SSC resuspension events. While there are occasions in other parts of the record where light levels are suppressed, these events were much shorter lived with light conditions typically improving within a few days. In any case, the light time series provide insights on conditions that would result in lengthy periods where no/little light would be expected to reach the seafloor and provide support for the reductions in seagrass meadow area in Cleveland Bay following large and consecutive Burdekin River discharge events (Petus et al. 2014; Lambert et al. 2020). The normalised accumulation rates measured in the sediment traps also show the second highest rates for

the deployment coinciding with the large resuspension event and the 2019 floods and the rates remained elevated (relative to previous deployments – third highest in the series) for the subsequent deployment between March and June 2019 when there was no flooding and no large rough weather events (Figure 3.3). However, the highest accumulation rates in the traps occurred in the final deployment between December 2019 and March 2020 when there were no large river discharge events, but possibly a large resuspension event. Unfortunately, the nephelometer failed over this deployment and the current meter had broken off at its base and was lost so we lack direct measurements over this period for assessment.
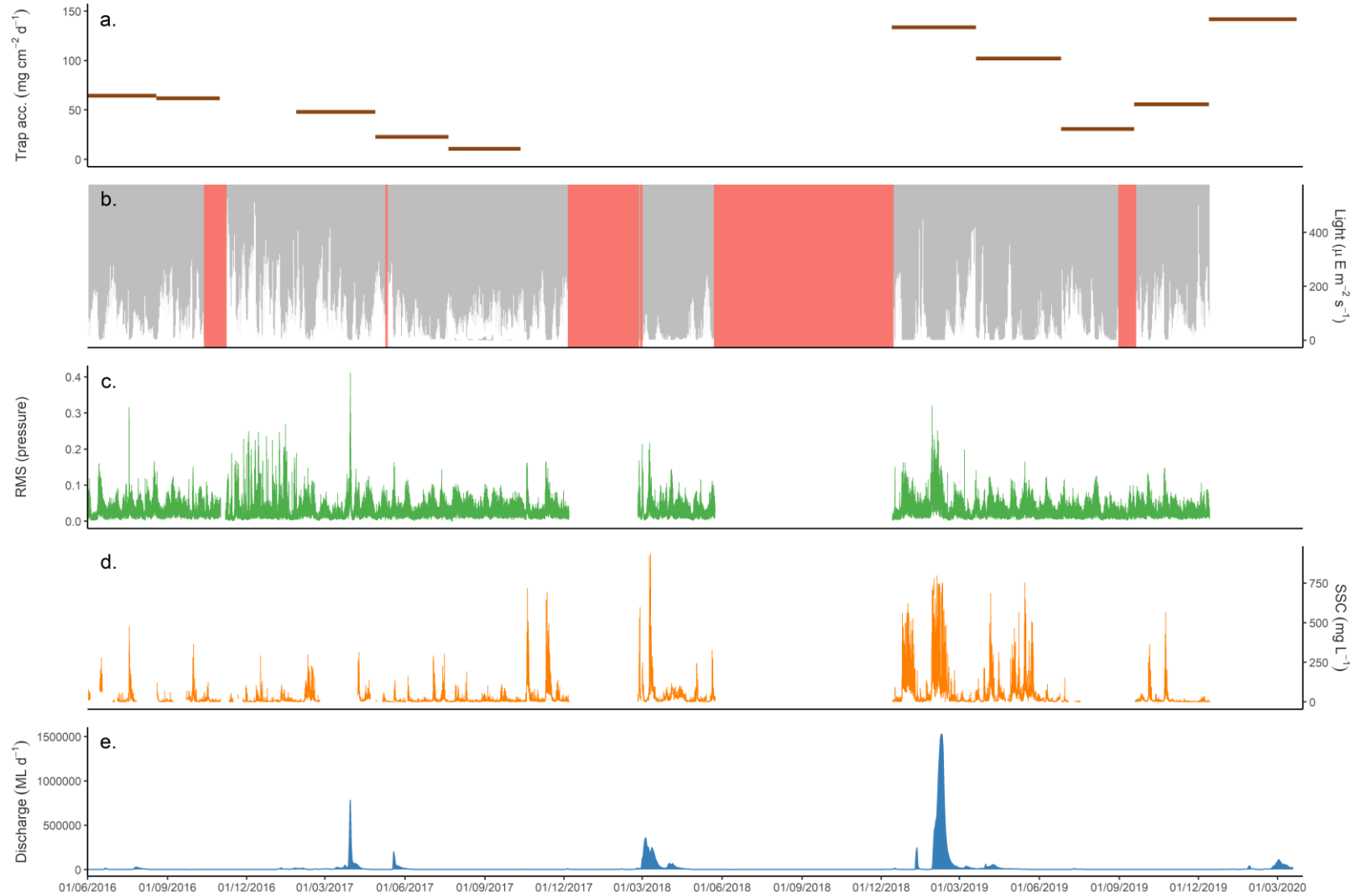
Figure 3.3. Logger time series and trap accumulation rates for the Cleveland Bay site (mean depth = 3.5 m) including: trap accumulation rates (in mg.cm^{-2}.day^{-1}) for each deployment (a), PAR light data (b), RMS pressure data (c), suspended sediment concentration data (d) and Burdekin River discharge data (e). The orange shading in the light data refer to periods where the instrument fouled and hence no reliable data are available for those periods.

The Middle Reef time series (Figure 3.4) appear to show a different response to the flood events compared to the Cleveland Bay dataset. While the SSC time series was quite patchy due to instrument failures and fouling of the sensor, data were captured during the 2017 and 2018 wet seasons. In those cases, the SSC response during the flood periods was lower than the resuspension events when no flooding occurred. Unfortunately, the turbidity sensor failed in the 2019 flood and so we have no quantifiable influence of this flood at this site and the large resuspension event that proceeded it. In contrast, a reliable time series has been developed with the sediment accumulation rates in the traps at this site with rates ~ 2-fold higher in the traps deployed during the deployment with the large resuspension event and the 2019 flood (Figure 3.4). Unlike the Cleveland Bay site, the accumulation rates declined greatly in the subsequent deployment period following the 2019 floods and were also amongst the lowest in the December 2019 to March 2020 deployment. This finding indicates that a large flux of sediment must have passed through the site during the 2019 flood, although that material was not available for subsequent resuspension as it had either transited past the site or it had deposited and compacted in a well-baffled area. The PAR light data reveal periods of relatively higher and lower light levels, although it appears that while light levels can be suppressed for periods under high resuspension and turbidity, there is generally at least some light that reaches the bottom on most occasions of this shallow ~ 5 m depth site (Figure 3.4).
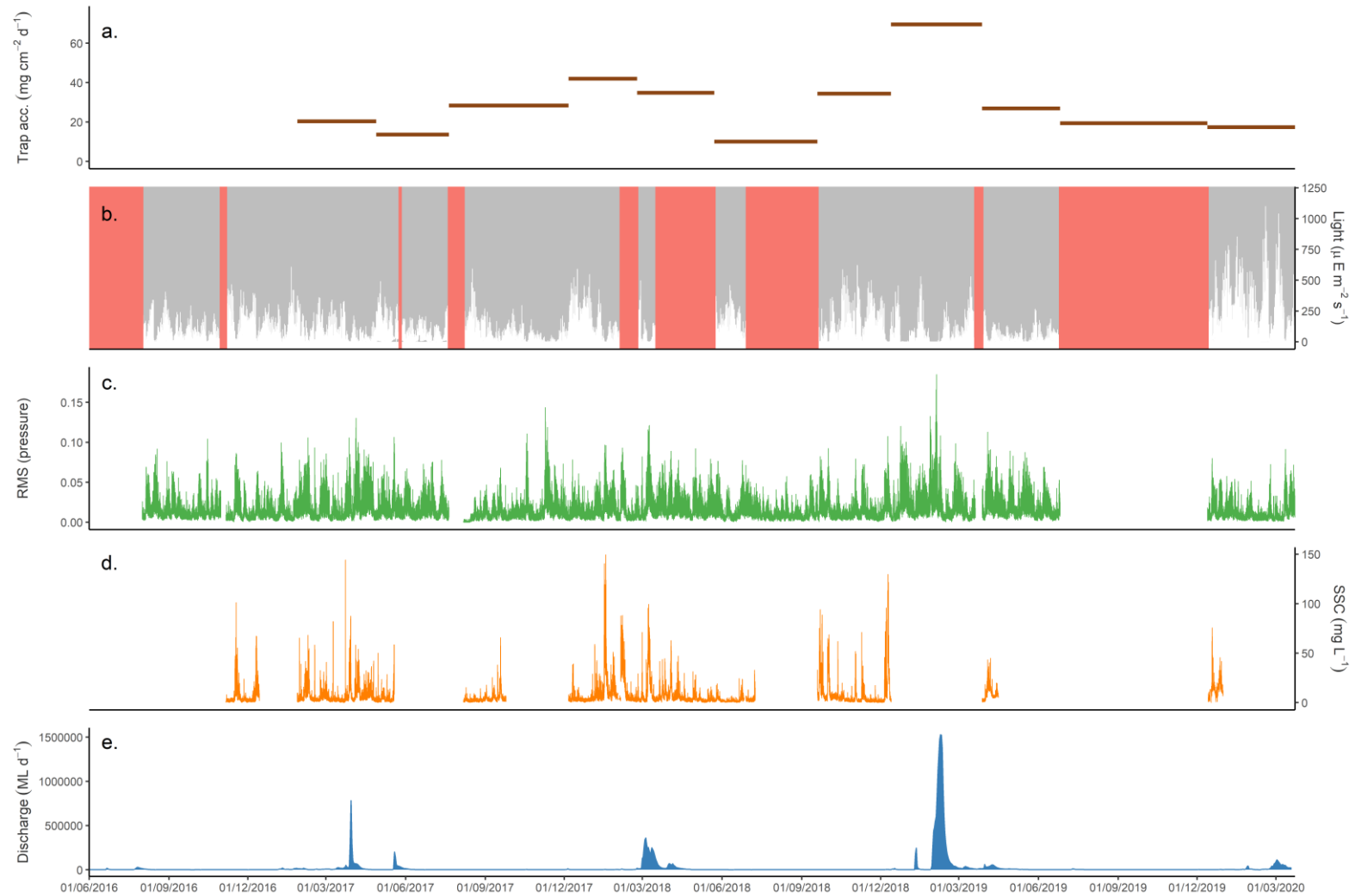
Figure 3.4. Logger time series and trap accumulation rates for the Middle Reef site (mean depth = 4.0 m) including: trap accumulation rates (in mg.cm⁻².day⁻¹) for each deployment (a), PAR light data (b), RMS pressure data (c), suspended sediment concentration data (d) and Burdekin River discharge data (e). The orange shading in the light data refer to periods where the instrument fouled and hence no reliable data are available for those periods.

The Geoffrey Bay time series highlight the important influence of the 2019 flood event at this site (Figure 3.5). By far the highest SSC readings were recorded during this event with concentrations exceeding 50 mg.L^{-1} on the 3rd February 2019 between 4:50 am and 1:50 pm (i.e. 9 hours) with a peak of 342 mg.L^{-1} at 9:00 am. Elevated SSCs > 10 mg.L^{-1} were recorded between the 27th January 2019 and 5th February (i.e. 10 days). Very low light conditions were also recorded at the site for this period with 10 continuous days of light levels < 1 µE.cm^{-2} (Figure 3.5). The large resuspension event prior to the 2019 flood observed in the Cleveland Bay series (Figure 3.3) appears to have been largely 'missed' in the Geoffrey Bay SSC time series which remain < 10 mg.L^{-1} over that period. However, a ~ 7 day period of suppressed light at the end of December 2019 coincides with this event (Figure 3.5). The influence of the 2019 flood is also evident in the accumulation rates in the sediment traps which were > 2-fold (and mostly > 3-fold) higher for this deployment than determined for all other trap deployments. In addition, the second highest accumulation rates were recorded in the subsequent deployment period between March and June 2019, again suggesting that the newly delivered sediment continued to influence this site in the following resuspension events (Figure 3.5). In comparison, it appears that the smaller 2017 and 2018 Burdekin River floods had little influence at the Geoffrey Bay site, with only minor fluctuations in SSC and light, and no detectable response in the sediment trap data (Figure 3.5).

The composition of the material captured by the sediment traps show the highest accumulations of mineral, organic and carbonate material coincide with the deployment containing the large 2019 floods and the large resuspension event associated with ex-Tropical Cyclone Penny (Figure 3.6). Interestingly, the grain size composition of the organic and carbonate removed sediment show little variability over the time series with no apparent trends coinciding with flood or resuspension events (Figure 3.6). The composition of particulate organic carbon in the traps also reveal that the higher concentrations do not always coincide with flood periods; this may reflect the variability in macroalgae cover at this site. The highest total nitrogen and total phosphorus concentrations in the traps coincided with the 2019 flood event (Figure 3.6), although like total organic carbon, the variability in the these concentrations did not appear to follow any wet or dry season trends.
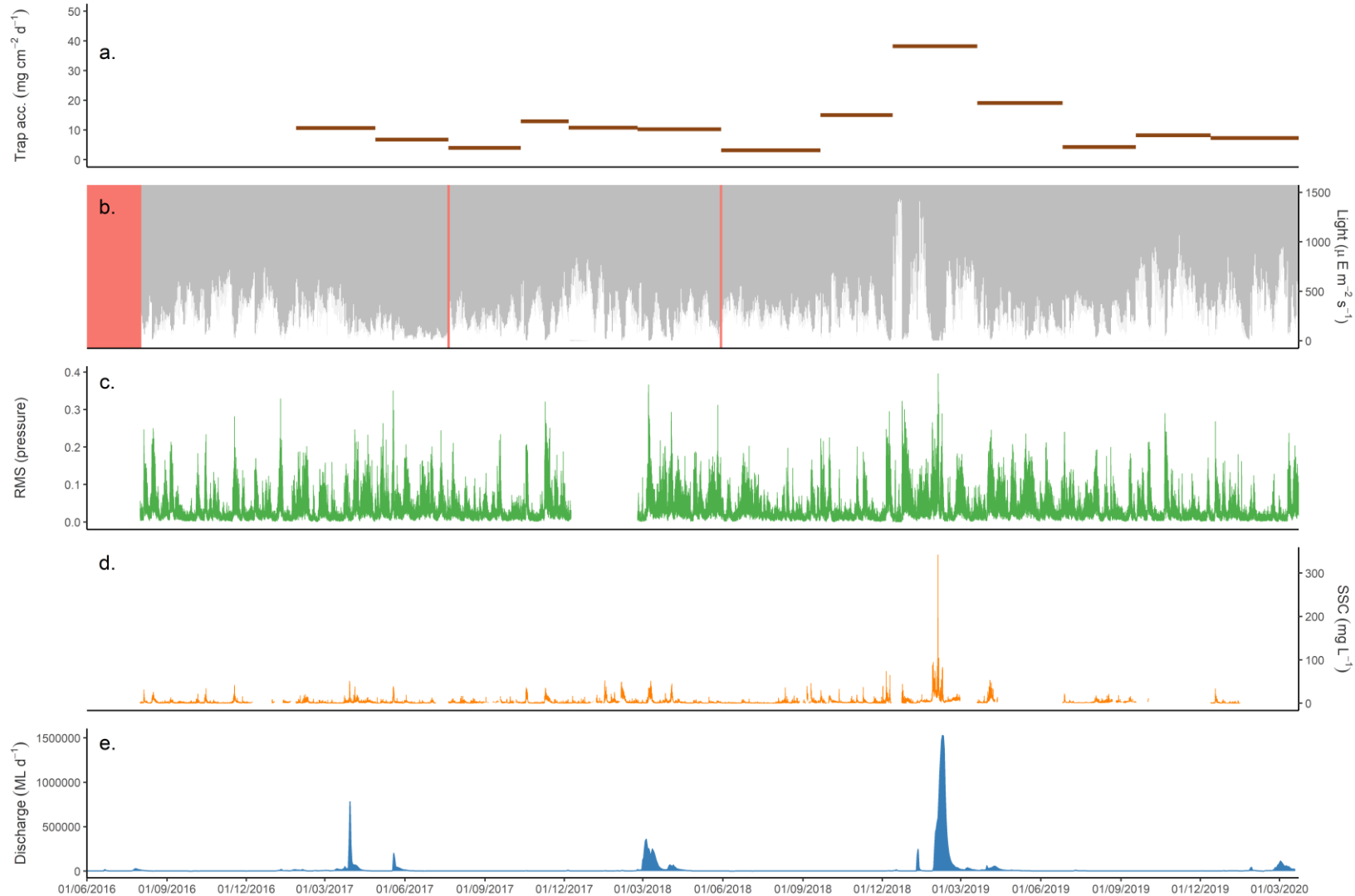
Figure 3.5. Logger time series and trap accumulation rates for the Geoffrey Bay site (mean depth = 3.0 m) including: trap accumulation rates (in mg.cm⁻².day⁻¹) for each deployment (a), PAR light data (b), RMS pressure data (c), suspended sediment concentration data (d) and Burdekin River discharge data (e). The orange shading in the light data refer to periods where the instrument fouled and hence no reliable data are available for those periods.
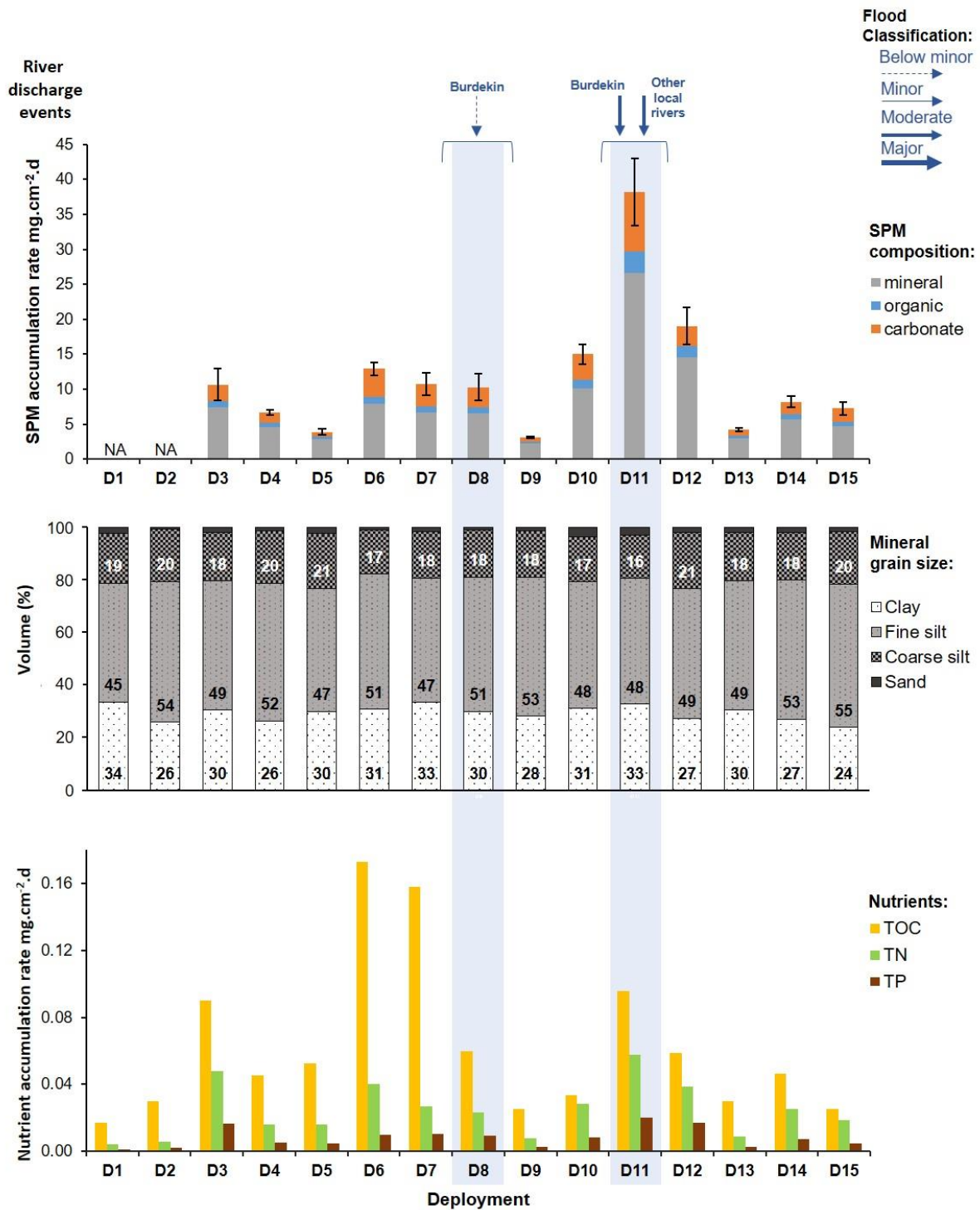
Figure 3.6. Sediment trap compositional time series data for the Geoffrey Bay logger site.

The Orchard Rocks SSC data were hampered by sensor fouling and malfunction, particularly over the latter part of the time series. Hence SSC for the key periods during the 2018 Burdekin flood and the large 2019 flood were not recorded at this site. The available SSC time series show that this open field, exposed, deeper water site (~ 16 m depth) is regularly influenced by elevated SSC events (Figure 3.7). These events are more likely current-derived events than wave driven resuspension due to the increased depth. In addition, the greater depth and the regular spikes in SSC produce persistent low light conditions at this site. The sediment

accumulation rates measured in the traps do appear to reveal seasonal differences over the time series (Figure 3.7). With the exception of the outlier in deployment 6 (October to December 2017) where the frame sunk into the substrate (the frame was moved and re-levelled for the subsequent December 2017 changeover), the highest accumulation rates coincided with the 2019 flood event with the next highest accumulation rates measured in the subsequent deployment between March and June 2019. Similar to the Cleveland Bay site (Figure 3.3), elevated accumulation rates were also recorded in the December 2019 to March 2020 deployment despite little flood influence over that period (Figure 3.7).

The composition of the sediment traps for the Orchard Rock time series displays relatively high variability across accumulation rates, particle size and nutrient composition (Figure 3.8). Excluding deployment 6 where the frame sunk into the substrate, the two highest accumulation rates coincided with two deployments associated with the 2019 floods and the subsequent deployment which also had highly elevated total organic carbon, total nitrogen and total phosphorus contents. Interestingly, the deployment following the 2019 floods (deployment 11) had considerably higher nutrient concentrations compared to the deployment within the flood period. Indeed, this site likely captures sediment being winnowed out of the bay and hence this result may provide insights on the length of time that the newly delivered sediment is 'active' within Cleveland Bay (i.e. up to 4 months following the flood). The variability in the particle size fractions produced some unexpected results with the lowest clay (< 4 μm) content (19%) of the time series coinciding with the 2019 floods; however, this period also coincided with the large resuspension event driven by ex-Tropical Cyclone Penny (Figure 3.8). In contrast, the deployment following the 2019 flood had the highest clay contents (35%) of the time series (excluding deployment 6).
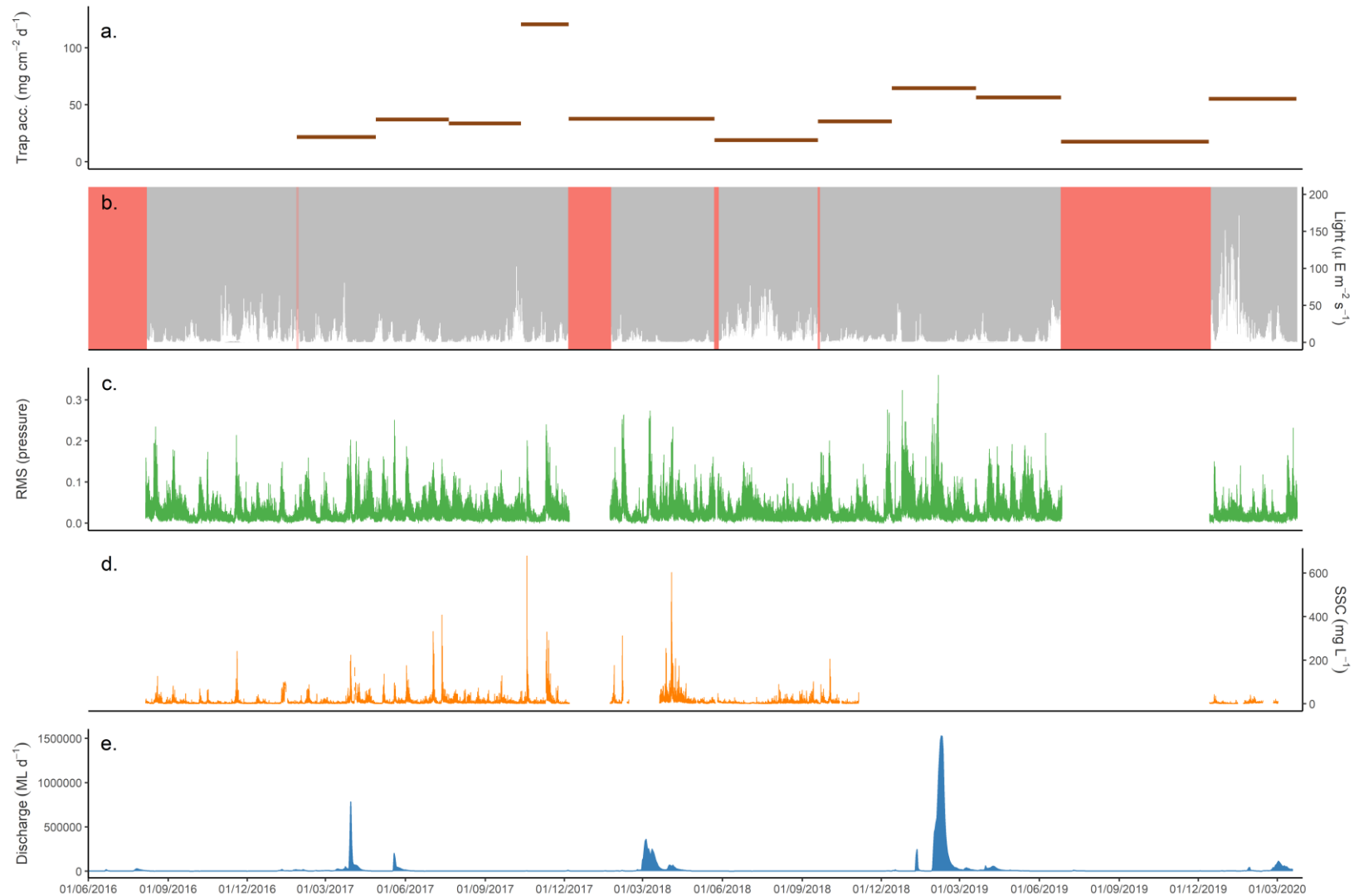
Figure 3.7. Logger time series and trap accumulation rates for the Orchard Rocks site (mean depth = 15 m) including: trap accumulation rates (in mg.cm⁻².day⁻¹) for each deployment (a), PAR light data (b), RMS pressure data (c), suspended sediment concentration data (d) and Burdekin River discharge data (e). The orange shading in the light data refer to periods where the instrument fouled and hence no reliable data are available for those periods.
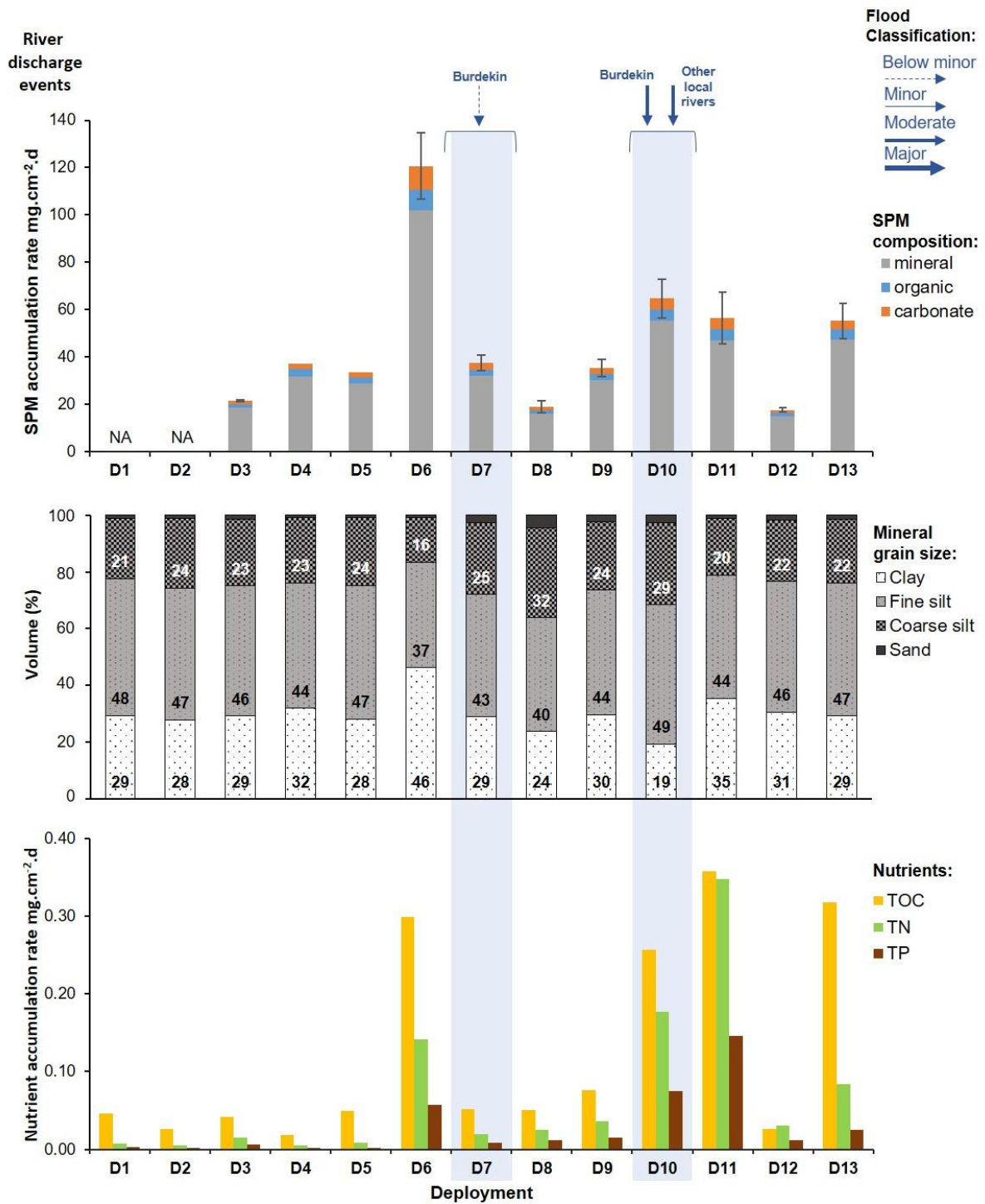
Figure 3.8. Sediment trap compositional time series data for the Orchard Rocks logger site.

The Havannah Island SSC time series show the strongest response to the 2018 and 2019 flood events with concentrations peaking > 150 mg.L^{-1}, albeit for short periods. During the 2018 Burdekin flood, concentrations > 5 mg.L^{-1} were recorded between 7th March 2018 and 10th March 2018 (i.e. 4 days) with two-three shorter intervals with highly elevated concentrations > 30 mg.L^{-1} during this period (Figure 3.9). During the larger 2019 floods SSC > 5 mg.L^{-1} was recorded between the 2nd and 4th February 2019 (i.e. 3 days). Elevated SSC events > 5 mg.L^{-1} were also evident at this site in the absence of floods that covered similar time periods (i.e. a few days), although the highly elevated SSC > 100 mg.L^{-1} were only recorded during the period of flooding (Figure 3.9). Importantly, it appears that SSCs were not elevated in the resuspension events that followed the flooding periods, suggesting that the influence of the new sediment on turbidity regimes only occurs during the flood event at this site. Light conditions at this site were suppressed during both the flooding and resuspension events, although the periods of reduced light were only evident over a few days (Figure 3.9). The accumulation rate data from the sediment traps reveal a seasonal-type signal with higher rates during the wet season months and lower rates in the dry season. However, the rates in the traps influenced by the flooding events were not elevated compared to other wet season trap deployments that coincided with no flooding periods of note (Figure 3.9).

The sediment composition from the traps deployed at the Havannah Island site appear to display more elevated accumulation rates and nutrient contents during the wet season relative to the dry season (Figure 3.10). While elevated accumulation rates and nutrient contents coincide with the 2018 and 2019 flooding periods, similarly elevated accumulation rates and nutrient contents occurred in the previous deployment period that was not influenced by river discharge events. Indeed, the deployment containing the finest particle size distribution (90% clay and fine silt) coincided with the deployment before the 2018 flood period (deployment 7) which also contained the highest measured total accumulation rate, total organic carbon, total nitrogen and total phosphorus contents (Figure 3.10). Further investigation is required to examine the possible drivers for this change; while similarly elevated accumulation rates were measured at the Havannah Toe site (just downslope from this site), the accumulation rates measured at the Havannah 2 site (on other side of island) were lower than those measured in deployment coinciding with the 2018 and 2019 floods.
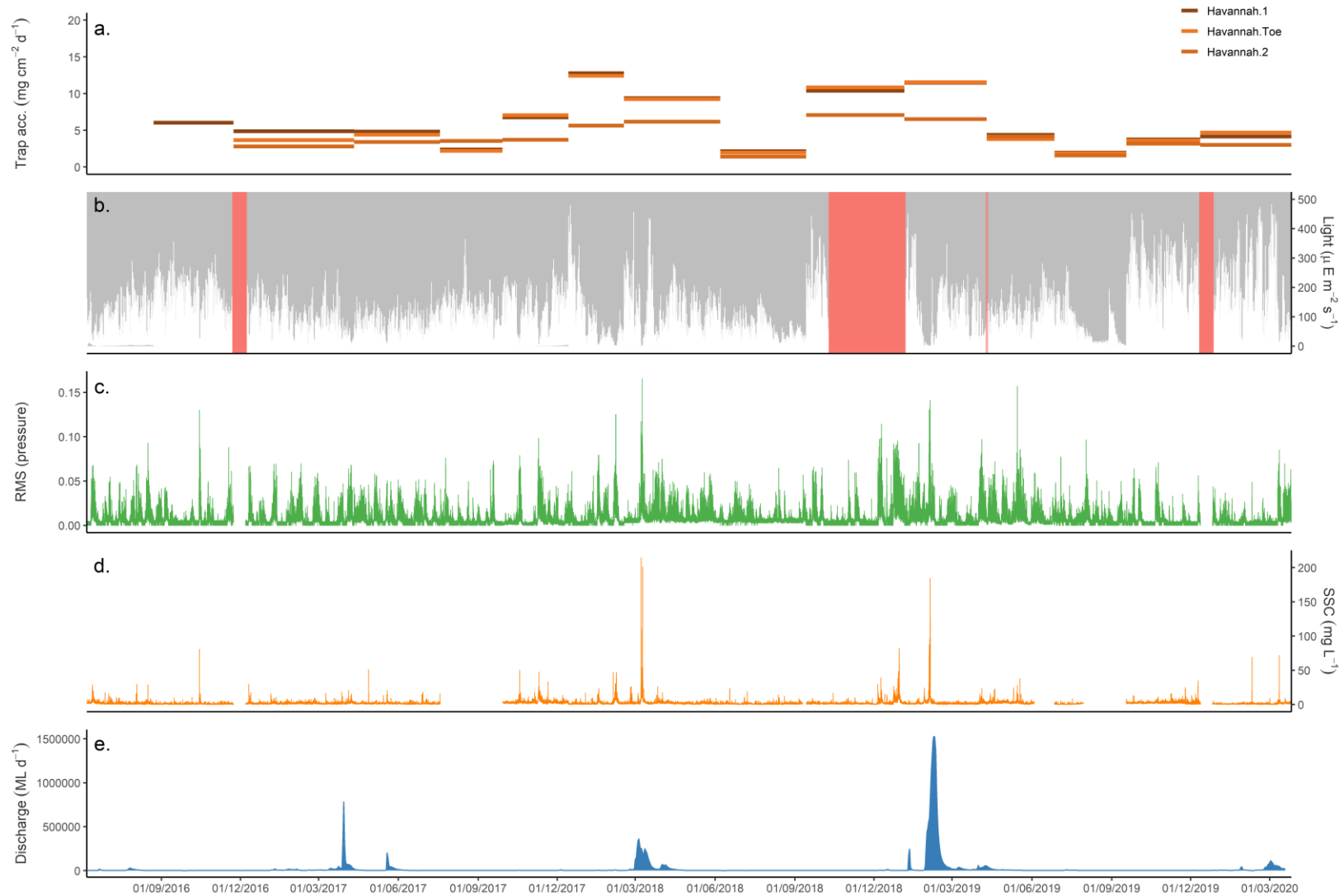
Figure 3.9. Logger time series and trap accumulation rates for the Havannah Island site (mean depth = 8.0 m) including: trap accumulation rates (in mg.cm^{-2}.day^{-1}) for each deployment (a), PAR light data (b), RMS pressure data (c), suspended sediment concentration data (d) and Burdekin River discharge data (e). The orange shading in the light data refer to periods where the instrument fouled and hence no reliable data are available for those periods.
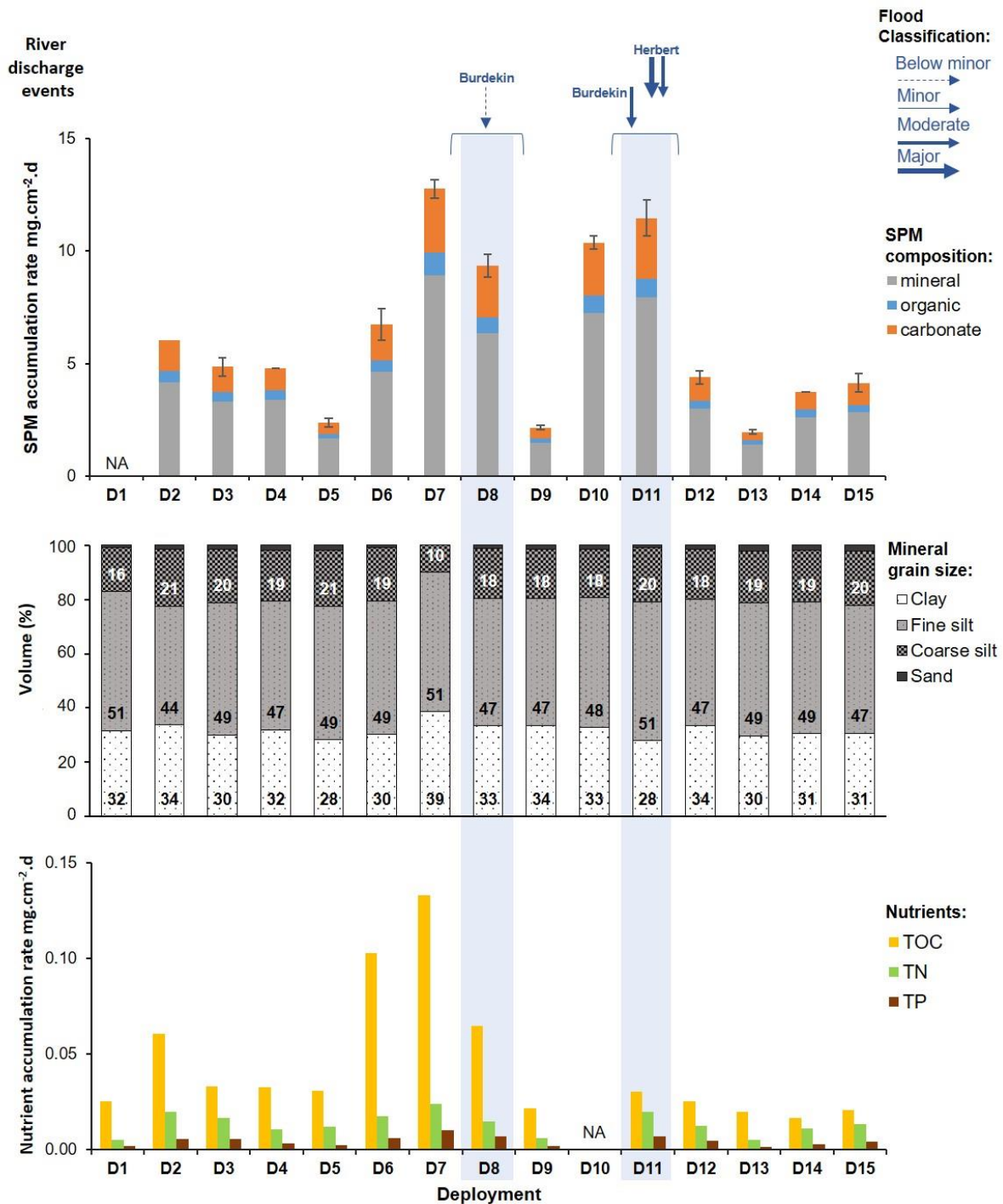
Figure 3.10. Sediment trap compositional time series data for the Havannah Island (1) logger site.

The Orpheus Island time series showed similar patterns to the Havannah Island series with the 2018 and 2019 flood periods recording SSC spikes > 100 mg.L^{-1} (Figure 3.11). For the 2018 and 2019 flood events SSCs > 5 mg.L^{-1} were recorded between the 8th March and 12th March 2018 (5 days) and between the 2nd and 8th February 2019 (7 days), respectively. However, in comparison to the Havannah Island SSC dataset, the Orpheus Island site is a little deeper (i.e. 10 m versus 12 m, respectively) and is more sheltered and hence experiences

fewer resuspension events and the lowest SSCs recorded across our seven sites (Figure 3.11). Based on the visual inspection of the record there appears to be potentially elevated SSC in the resuspension events that occurred immediately following both the 2018 and 2019 floods, although further statistical analysis is required to quantify if this is significant. Interestingly, the light conditions at this site reduced greatly in the ~ 3 months following the 2018 flood event (Figure 3.11). Unlike the SSC data, the highest sediment accumulation rates in the traps at both the Orpheus and Pelorus Island sites do not coincide with major flooding events (Figure 3.11).
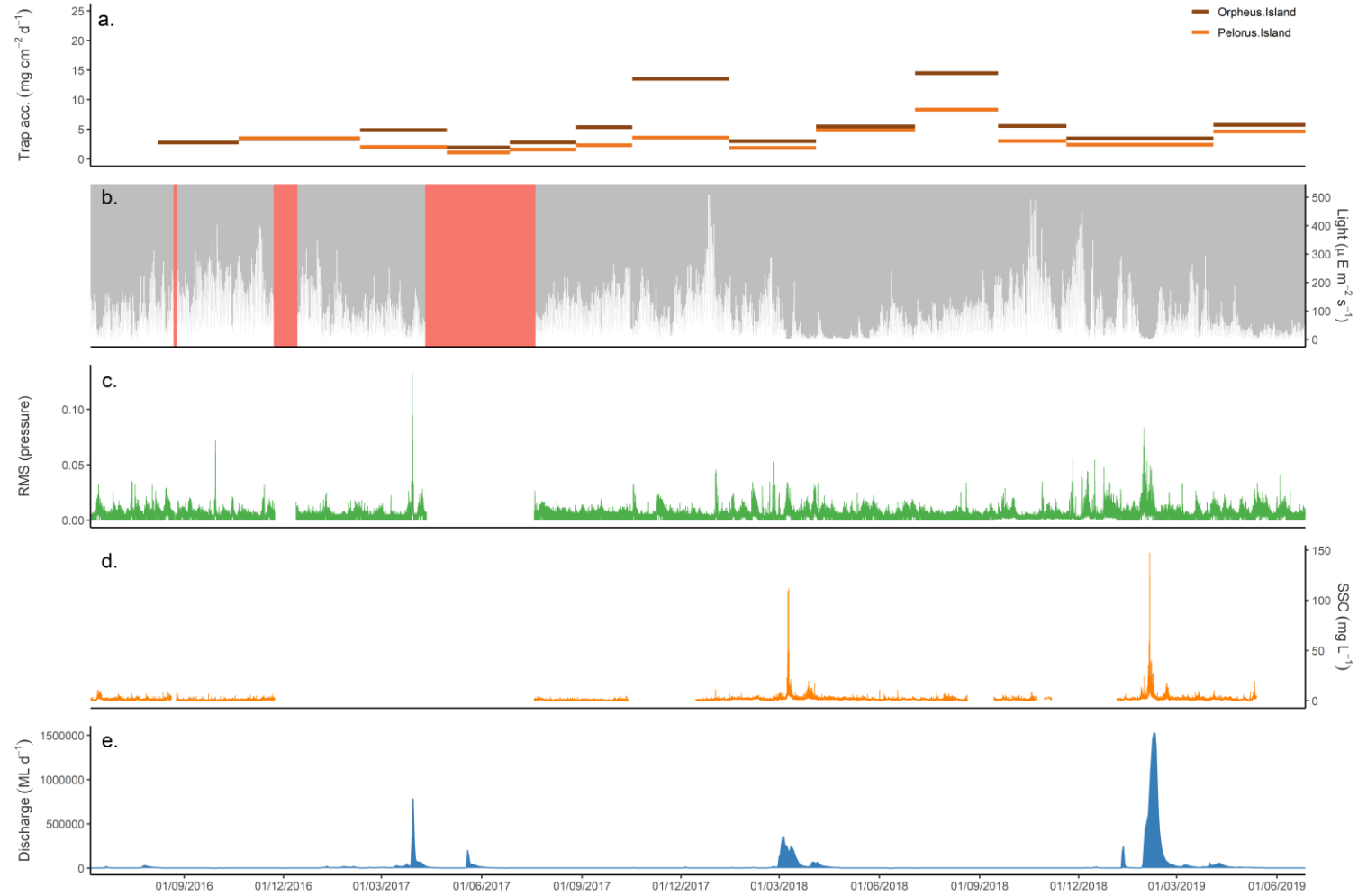
Figure 3.11. Logger time series and trap accumulation rates for the Orpheus Island site (mean depth = 10.5 m) including: trap accumulation rates (in mg.cm^{-2}.day^{-1}) for each deployment (a), PAR light data (b), RMS pressure data (c), suspended sediment concentration data (d) and Burdekin River discharge data (e). The orange shading in the light data refer to periods where the instrument fouled and hence no reliable data are available for those periods.

The Dunk Island time series show a more complicated pattern than the other plots largely due to the more frequent flow events from the Tully River (Figure 3.12) as well as the occasional possible influence from the Herbert River. However, in accord with most of the other time series, the peak SSCs > 100 mg.L^{-1} coincide exclusively with flood events (this case from the Tully River). The logger at Dunk Island is situated < 13 km from the mouth of the Tully River (Figure 3.1) and hence even smaller flow events would influence this site under the right environmental conditions (i.e. wind direction to drive the plume to this site). There appears to be elevated SSC relative to the RMS pressure reading in the months following the large flooding events, although further statistical processing is required to confirm this response (see next section). In general, the peak light conditions at the site occur towards the end of the dry season prior to the larger Tully River discharge events (Figure 3.12). Interestingly, the sediment accumulation rates in the sediment traps at both the Dunk (1) and Dunk (2) sites (Figure 3.1) during the November 2017 to February 2017 deployment were > 3.5 fold higher than all the other deployments. The higher sediment accumulation rates in the traps coincided with the larger flooding events from the Tully River (Figure 3.12).

The sediment composition data for each trap deployment period also highlight the influence of the flood events at this site (Figure 3.13). Specifically, the microscopy analysis reveal that while small sediment flocs are present throughout the time series, large sediment floc aggregates (i.e. marine snow) are only found within the traps deployed over the large flooding periods (Figure 3.13). Moreover, these periods also coincide with higher accumulation rates of total organic carbon, total nitrogen and, to a lesser extent, total phosphorus in the sediment traps (Figure 3.13) which generally reflect the higher sediment accumulation rates. Indeed, there was generally higher masses of mineral, organic and carbonate suspended particulate matter in the traps coinciding with these large flood events (Figure 3.13). Interestingly, there was little change in the treated mineral grain size across the time series which was unexpected (i.e. we would have hypothesised that the grain size would have become finer coinciding with the flood events) (Figure 3.13).
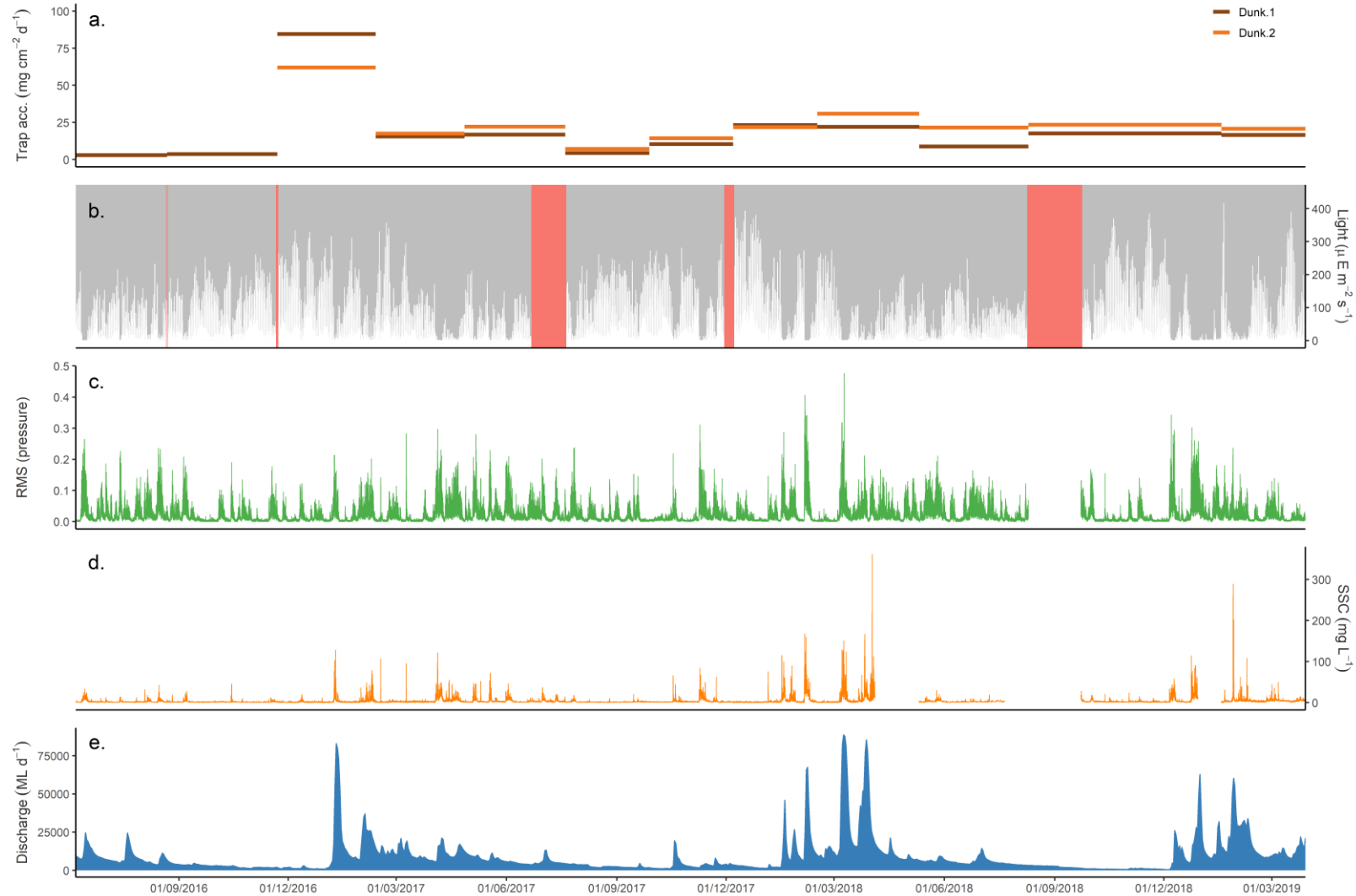
Figure 3.12. Logger time series and trap accumulation rates for the Dunk Island site (mean depth = 6.0 m) including: trap accumulation rates (in mg.cm^{-2}.day^{-1}) for each deployment (a), PAR light data (b), RMS pressure data (c), suspended sediment concentration data (d) and Tully River discharge data (e). The orange shading in the light data refer to periods where the instrument fouled and hence no reliable data are available for those periods.
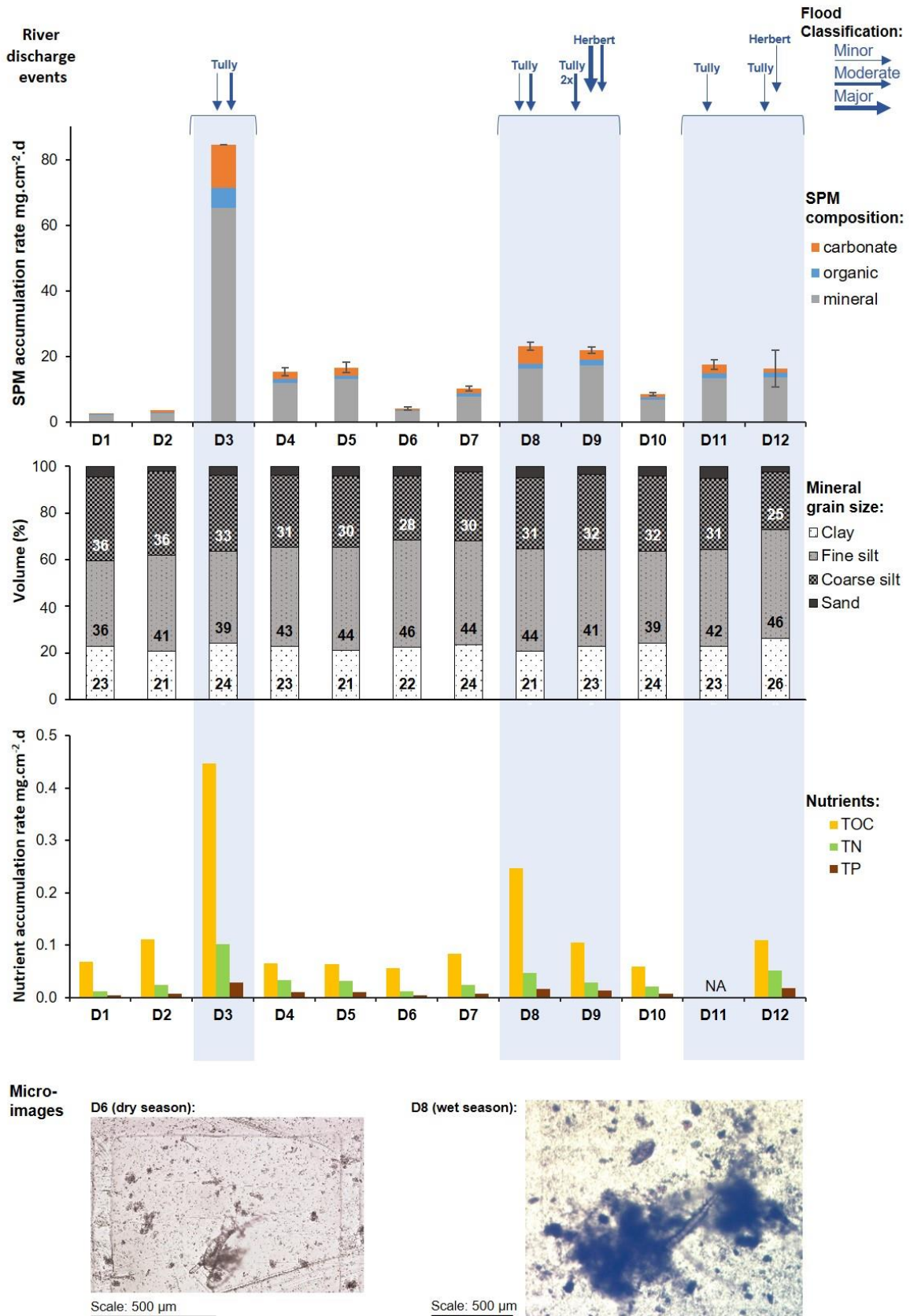
Figure 3.13. Sediment trap compositional time series data for the Dunk Island (1) logger site.

3.3.2 Statistical analysis of the Dunk Island logger data

Due to the more complicated time series for the Dunk Island site (Figure 3.12), we undertook additional statistical analysis to better unravel the influence of newly delivered sediment at this location. This section outlines the systematic approach that we plan to develop further for the remainder of the sites in a future publication. Our first analysis involved the additional scrutiny of turbidity data and specifically whether our data were recording locally restricted turbidity fluctuations or reflecting a more regional island/bay wide response. Here we drew on the AIMS logger data taken for the GBRMPA's MMP to compare with our time series (Figure 3.14); the AIMS logger is located on the other side of Dunk Island (400 m from our Dunk (2) site: Figure 3.1) and hence it potentially records the influence of different wind-driven resuspension events (i.e. northerly versus south-easterly). The two overlapping data series show good agreement in the turbidity fluctuations over the June 2016 to March 2019 series and confirm that the large events recorded in our dataset were regional island/bay wide events (Figure 3.14). Indeed, this finding provides an additional QA/QC measure for our data and also helps fill gaps in the time series when our logger fouled or failed to record.
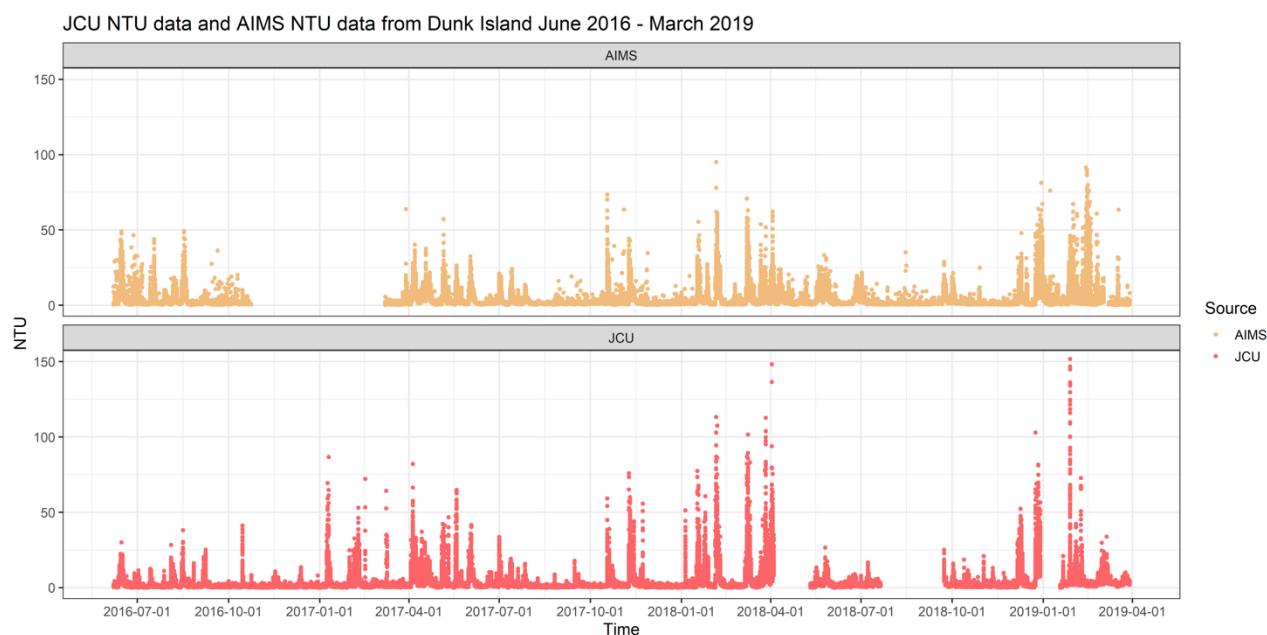
Figure 3.14. The MMP AIMS turbidity time series (orange dots: top panel) compared to our turbidity time series (red dots: bottom panel) for the Dunk Island. The AIMS Marine Monitoring Program site is located on the northern side of the island ~400 m from our Dunk 2 trap site while the JCU site is located on the south western side (Dunk 1 trap site).

We then considered the key factors that drive sediment resuspension in the GBR. We developed a conceptual diagram of these key processes including the site characteristics, physical forces that cause resuspension and the drivers that influence these forces as well as the measurements we had available to quantify them (Figure 3.15). We used this model to guide our subsequent analysis.
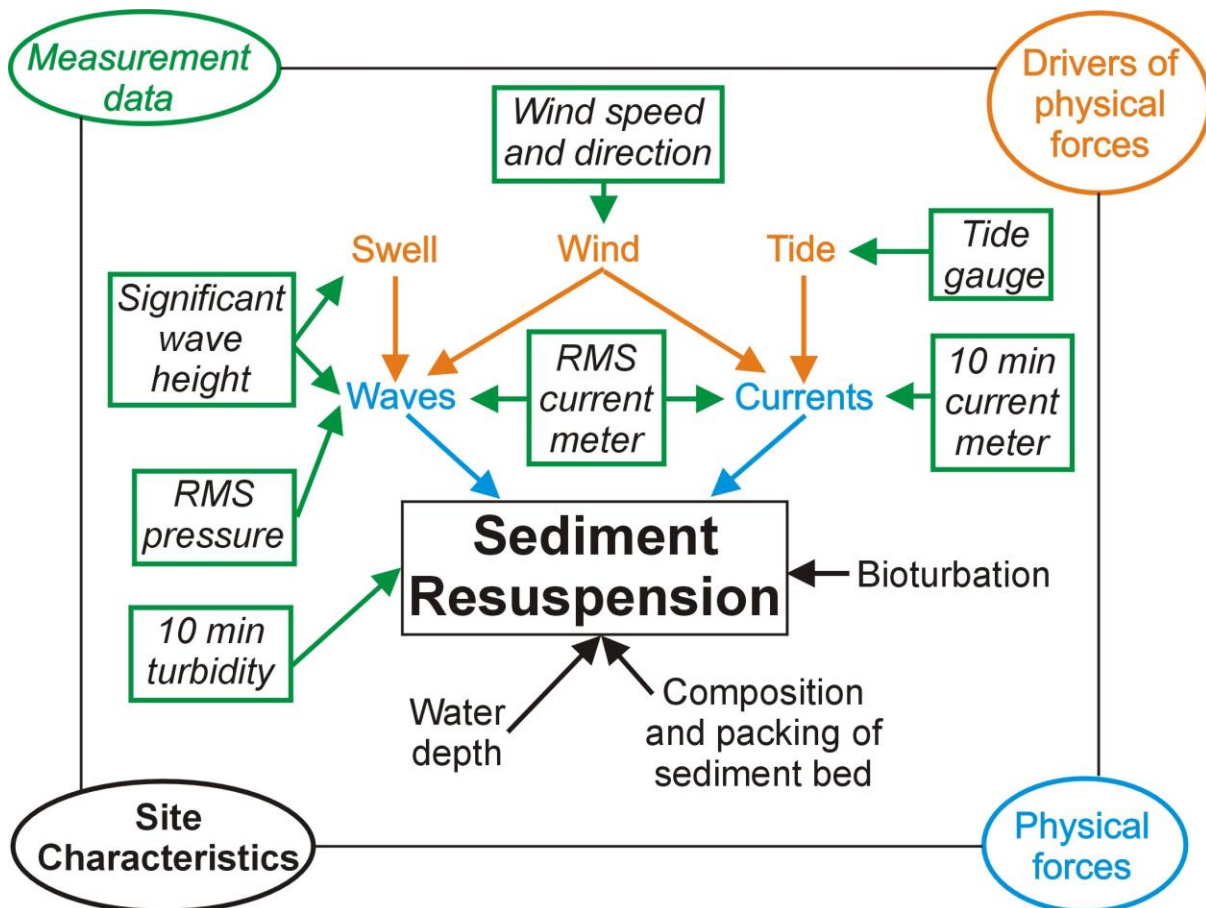
Figure 3.15. Conceptual diagram of the key influences on sediment resuspension in the GBR and the measurements that were available to constrain each component.

The Dunk Island time series was then plotted alongside additional environmental measurements that help to explain turbidity-generated wave resuspension taken from our NESP project (i.e. average current and current meter RMS) as well as from the nearest wind (from Cardwell Parade) and tidal (from Clump Point) measurements Figures 3.16-3.18. The full time series (June 2016 to March 2019) is presented in Figure 3.16, while enlarged periods of interest are presented in Figures 3.17 and 3.18. Collectively, while the data highlight the complexity of interpreting a number of parameters that may influence resuspension and turbidity, the potential of the RMS current meter record (here plotted as 10 min lagged data) to predict turbidity is shown with strong responses between increased current RMS and turbidity. In some cases, there is good agreement between the RMS current meter and the RMS pressure outputs such as in the August 2018 to March 2019 deployment period (Figure 3.17). However, at other time periods such as the June 2016 to April 2017 deployment period, the RMS current and RMS pressures show less agreement (Figure 3.18). The average current meter data smoothed at 10 min intervals appear to respond to periods of elevated unidirectional tidal currents specifically during the spring tide periods (Figures 3.16-3.18).
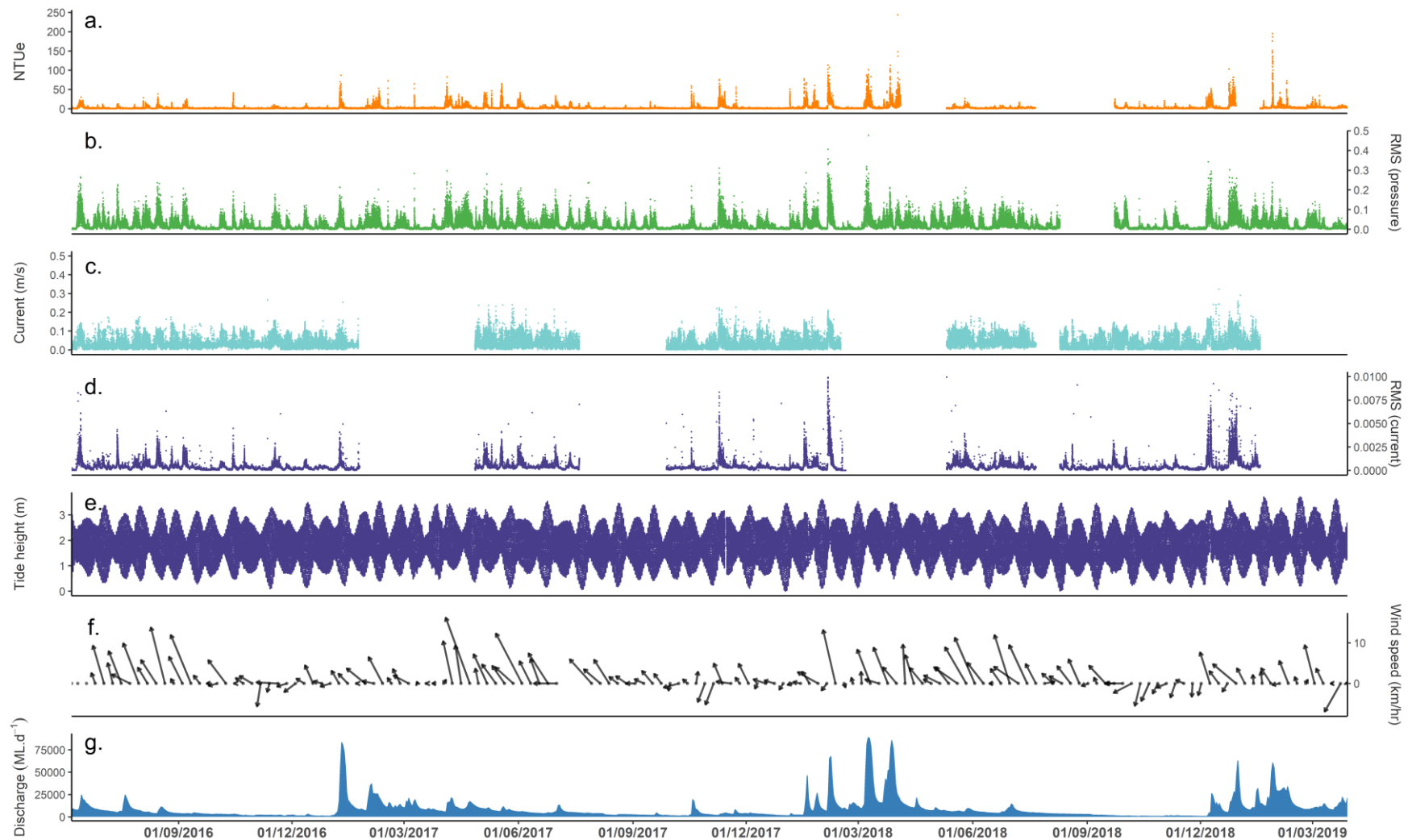
Figure 3.16. Full time series (June 2016 to March 2019) of the Dunk Island logger site including turbidity (note in NTU: a), RMS of the pressure sensor (b), 10 min averaged current (c), RMS of the current meter (d), water (tide) level height (e), weekly average wind speed and direction (f) and Tully River discharge at the Euramo gauge (g).
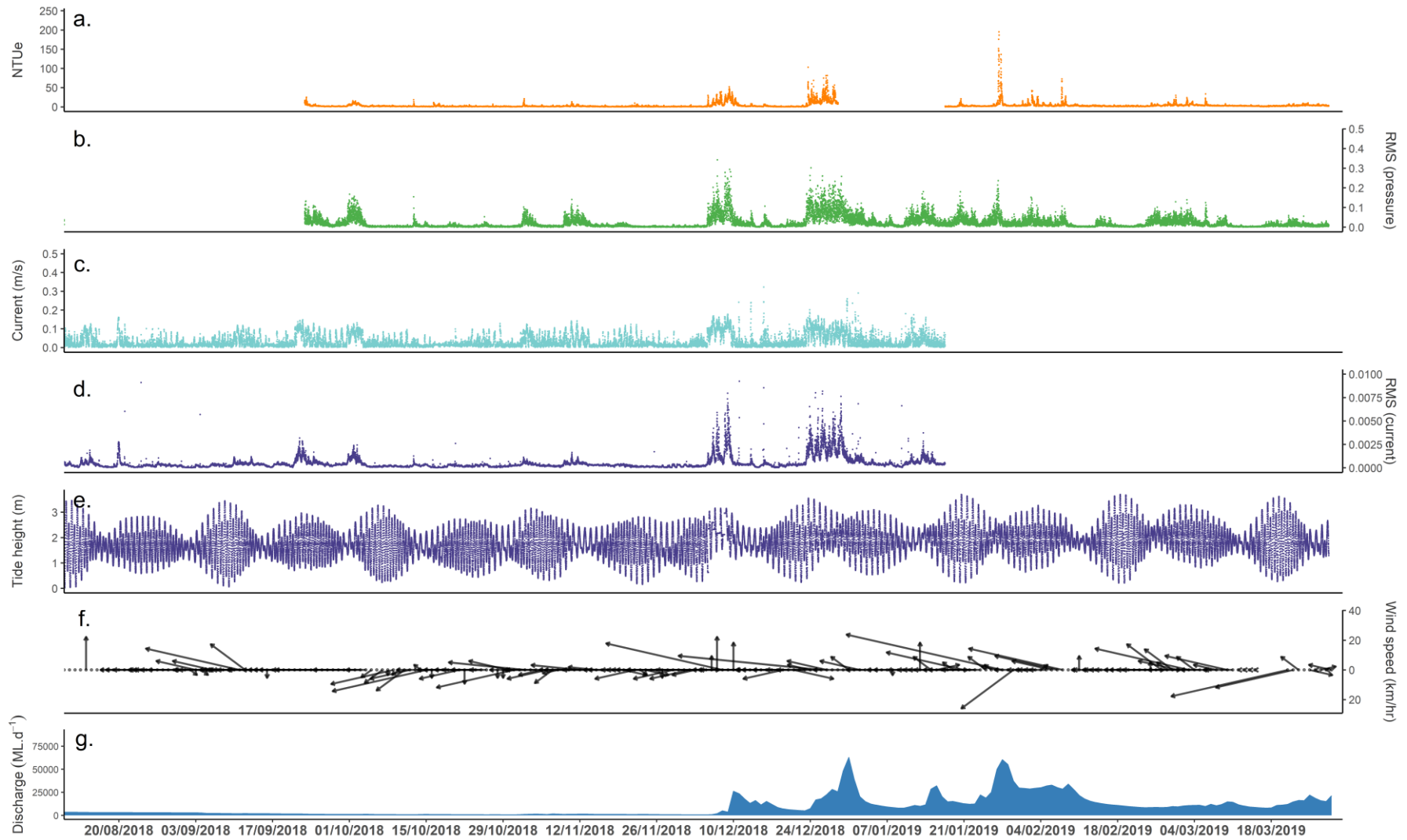
Figure 3.17. An enlarged version of the Dunk Island time series between August 2018 and March 2019. Note the wind speed and direction plots (f) are based on daily data.
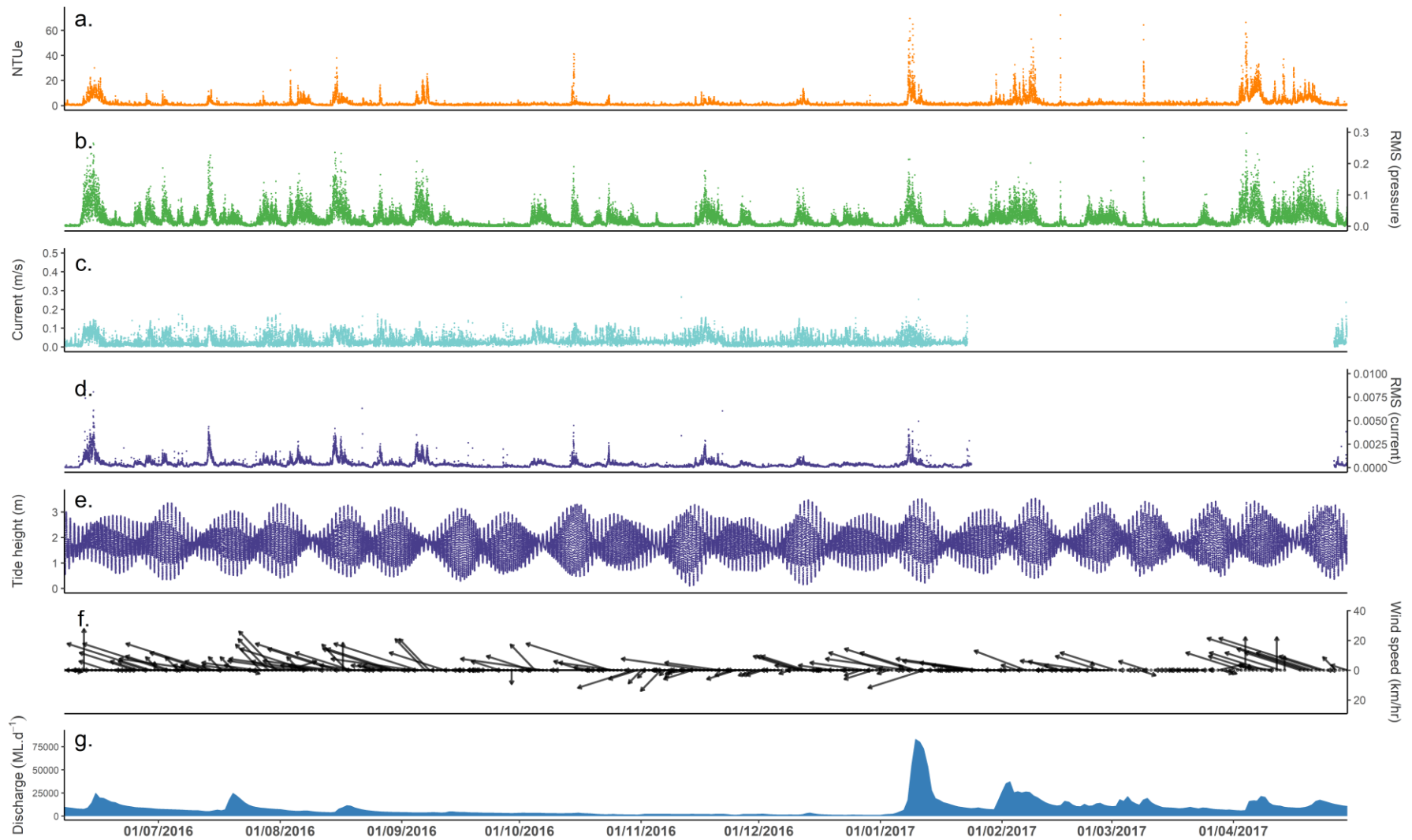
Figure 3.18. An enlarged version of the Dunk Island time series between June 2016 and April 2017. Note the wind speed and direction plots (f) are based on daily data.

Statistical analysis of the data series plotted in Figure 3.16 first included a correlation matrix to visualise the data, remove data outliers, and provide a first approximation of the strength and significance of the correlations for the various parameters with turbidity (not shown). To provide an indication of the influence of river flow events on turbidity at our Dunk Island site we directly overlaid the Tully and Herbert discharge over the turbidity time series (Figure 3.19). The plots highlight that in most cases the elevated turbidity readings (i.e. > 50 NTU) coincide with discharge events from the Tully River (Figure 3.19). However, there were occasions when elevated turbidity (>20 NTU) occurred with no little/low flow river discharge. In many cases these turbidity episodes closely followed a river discharge event, although some (e.g. ~ November 2016) do occur towards the end of the dry season in the absence of any large recent river discharges (Figure 3.19). These data also suggest that fairly small flow events from the Tully River (< 25,000 ML.day^{-1}) may still drive the turbidity conditions at the Dunk Island site.

Generalised Additive Mixed modelling (GAMM) was used to investigate the key factors affecting turbidity. Relationships were explored between the 10 min turbidity time series and the parameters that constrained the physical forces and drivers of turbidity as identified in the conceptual diagram (Figure 3.15). Recognising relationships between turbidity and potential drivers are unlikely to be instantaneous, various successively larger antecedent periods prior to each turbidity reading were explored (10 minutes, 30 minutes, 1 hour, 3 hours and 12 hours). The model including the three hour lag resulted in the highest deviance explained compared to the other time periods explored (Table 3.2). Under future analysis these lags will also be explored for other predictors such as RMS pressure. We also explored the use of various metrics such as the mean, D90 and D95 for the same lag periods. The D95 (95th percentile) of the RMS current meter data (3 hour lag) resulted in a slightly higher deviance explained compared to the mean for the 3 hour lag. Model assumptions were checked using standard diagnostic tools available and the results for the model with the highest explained deviance (the RMS current meter 3 hour lag D95) are provided in the appendix.

Another consideration in building the models is the availability of data during critical periods of interest. The pressure sensor data had less periods of sensor/data loss during discharge events compared with the current meter data (Figure 3.20). Hence we also developed a model using the RMS pressure data and compared this with the best performing model from the current meter data. Overall, the model relating RMS pressure to NTUe performed far more poorly than the RMS current models (Figure 3.20, Table 3.2). The goodness-of-fit statistic (percentage deviance explained) for the RMS pressure model was 18.7 which is a generalization of r^2. In contrast, the RMS current models captured between 26% and 46% of the local turbidity variation depending upon the antecedent period explored (Table 3.2). These results suggest that the approach using the RMS of the current meter data could be useful to capture the turbidity influence driven by resuspension events (Figure 3.21).
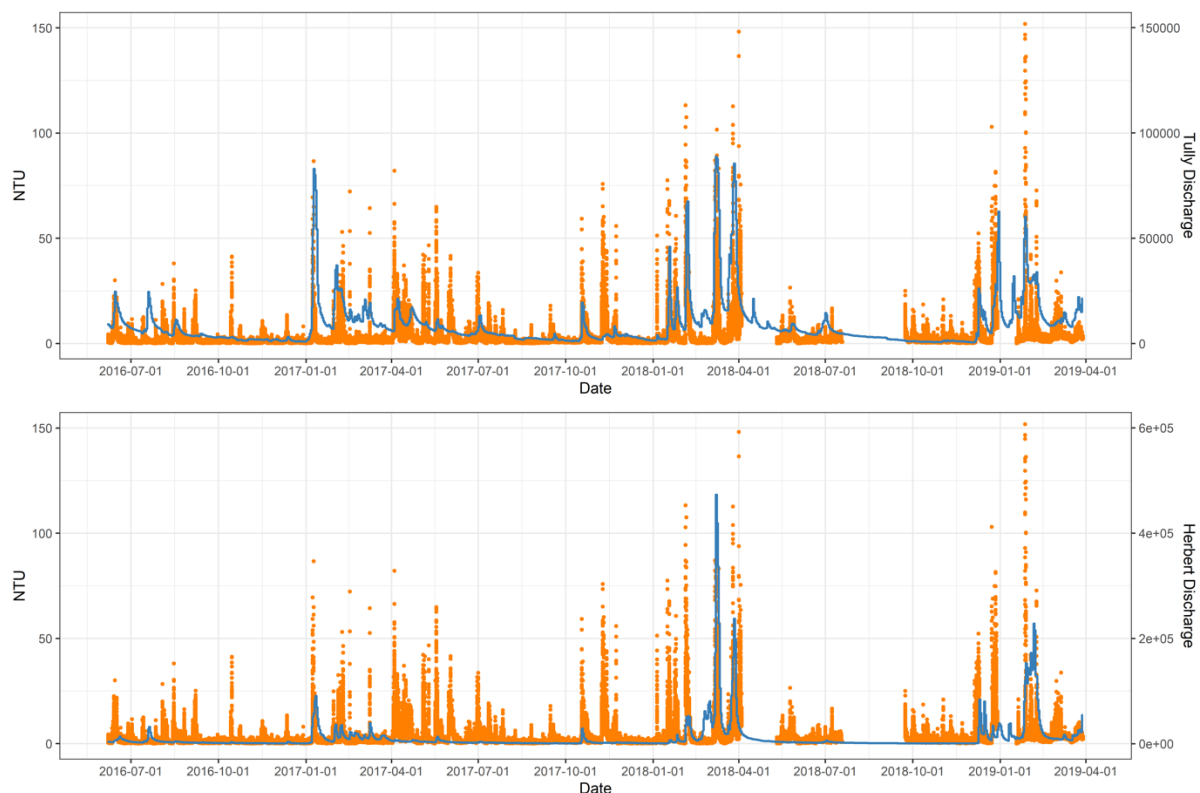
Figure 3.19. Our turbidity time series from Dunk Island overlaid with Tully River (top panel) and Herbert River (bottom panel) daily discharge data (data in ML per day).

Table 3.2. A summary of results for selected GAMMs using the 'scat' family with first order autoregressive terms included. edf: effective degrees of freedom.

Measurement	period	Deviance explained	Adjusted R2	edf	Covariates
RMS pressure	10 minutes	18.7	0.236	8.717	s(log(RMS pressure))
				6.96	s(deploys)
Current speed	10 minutes	7.15	0.078	4.766	s(Speed)
				6.863	s(deploys)
RMS current 10	10 minutes	26.9	0.335	7.994	s(log(RMS current 10 mins lag D50))
				6.931	s(deploys)
		26.4	0.33	7.433	s(log(RMS current 10 mins lag D95))
				6.933	s(deploys)
RMS current 10	1 hour	38.9	0.472	7.99	s(log(RMS current 1 hr lag D50))
				6.923	s(deploys)
		38.2	0.465	8.243	s(log(RMS current 1 hr lag D95))
				6.925	s(deploys)
RMS current 3 hrs	3 hours	45.8	0.55	8.198	s(log(RMS current 3 hr lag D95))
				6.93	s(deploys)
		44.8	0.54	8.115	s(log(RMS current 3 hr lag D50))
				6.927	s(deploys)
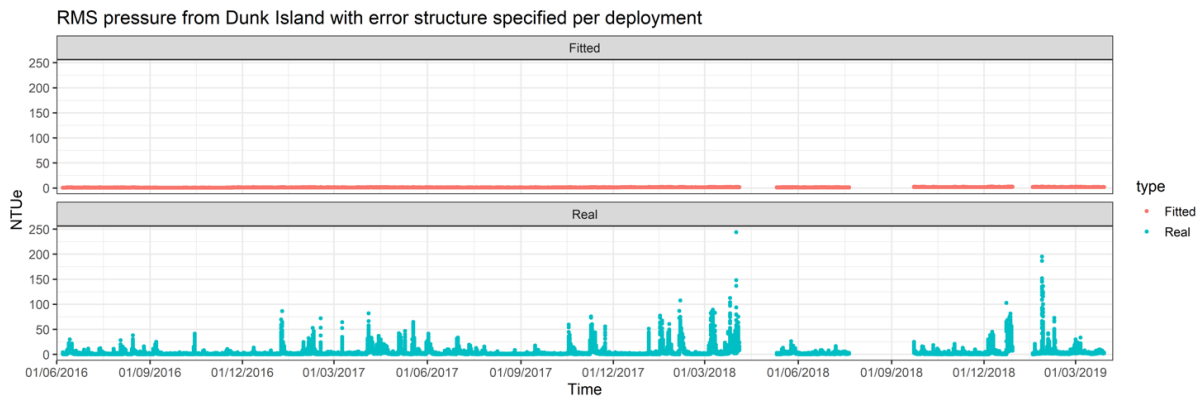
Figure 3.20. The fitted turbidity predicted by the RMS pressure model (red line, top panel) compared to the measured turbidity readings (blue line, bottom panel).
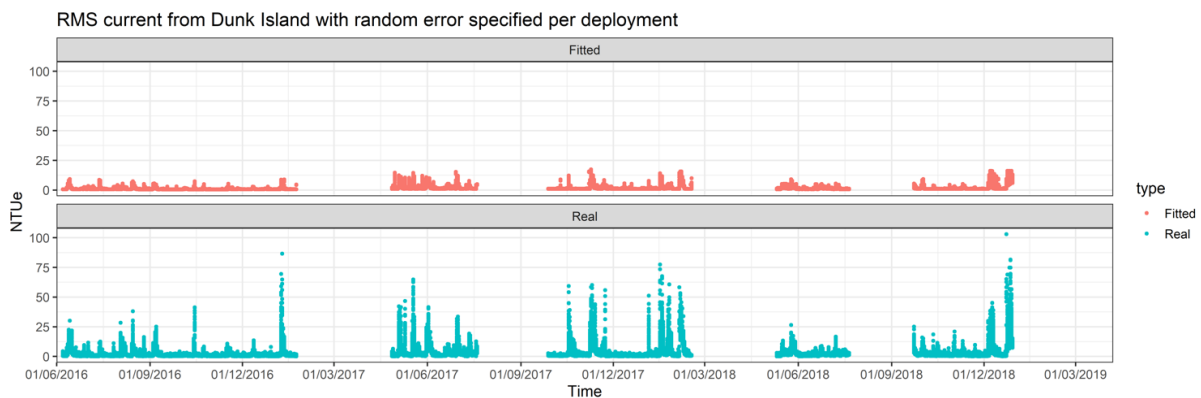
Figure 3.21. The fitted turbidity predicted by the RMS current model (red line, top panel) compared to the measured turbidity readings (blue line, bottom panel).

The residuals extracted from the GAMMs reflect the variation in turbidity after the extraction of wave (RMS pressure) and current (RMS current) signals thus representing variation in turbidity that could not be explained by the drivers included in the models. This unexplained variation may be due to factors not included in the model such as sediments delivered from river discharge events and also other local site factors such as bioturbation. When the residuals from the RMS current model (3 hour lag D95) are plotted against the Tully River flow data (Figure 3.22), they appear to highlight the importance of small 'first flush' style events (and subsequent resuspension events) on the turbidity regimes at Dunk Island. For example, in the case of elevated turbidity in early November 2017 (4th/5th November), the corresponding MODIS satellite imagery (not shown) suggests a resuspension event with brown-coloured water within the area. Both the RMS pressure and RMS current are elevated in this period and support a resuspension event (Figure 3.15) but it seems that the resuspension was over and above what could be explained by local conditions. Notably field sampling occurred in the area for the GBRMPA's MMP on October 20th 2017 with a 'first flush' being documented and hence this subsequent 'resuspension-only' event may have been influenced by this preceding small discharge event. Unfortunately, the critical periods when the current meter failed including during or shortly after the 2017, 2018 and 2019 key flow events prevented further detailed analysis (Figure 3.22). However, we believe this approach has considerable

promise in the ability to quantify the influence of the newly delivered sediment at our other monitoring sites where a more continuous record of current meter data are present.
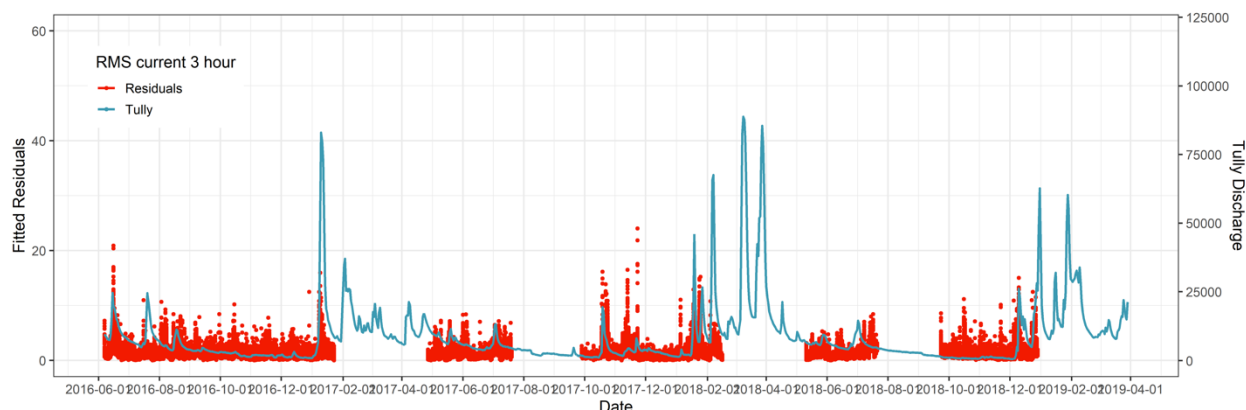
Figure 3.22. Model residuals when the predicted turbidity using the RMS current model (i.e. Figure 3.18) is subtracted from the measured turbidity.

3.4 Discussion

Collectively our time-series data demonstrate the influence of newly delivered sediment in flood plumes at all sites where the highest SSC coincided directly with the flood event (i.e. Cleveland Bay, Geoffrey Bay, Havannah Island, Orpheus Island, Dunk Island) and/or the highest accumulation rates in the sediment traps (e.g. Middle Reef, Geoffrey Bay and Dunk Island and possibly Cleveland Bay and Orchard Rocks). However, key differences were evident at the sites that reflected the length of influence of the newly delivered fine sediment. Based on these data and those in other chapters of this report, this discussion will conceptually define three separate impacts of the newly delivered sediment in the inshore GBR and hence what we consider the 'most damaging sediment'. Finally, we will consider the way forward to further improve the understanding of turbidity regimes in the GBR.

The three types of impact of newly delivered fine sediment to the GBR include:

1. The increased suppression of light in shallow (~ 5 m depth), turbid environments both during the flood plume and the months afterwards. For considerable impact to occur, typically consecutive large flooding periods is required over 2-3 years (for example Cleveland Bay seagrass meadow).

2. The pulsed delivery and subsequent deposition of flood plume sediment and associated particulate nutrients to inshore coral reef sites and resultant increase in macroalgae cover and decrease in live coral cover (for example Havannah Island site).

3. The chronic persistent turbidity (and reduced photic depth) for long periods as a result of wave and current disturbance (resuspension) of the sediment bed or new sediment delivery in areas where flood delivered influx takes longer to export and/or areas with longer water/sediment residence times (for example Whitsunday Island Group).

3.4.1 Cleveland Bay case study example (shallow, turbid location)

The logger and sediment trap data from Cleveland Bay highlight the influence of the 2019 floods as well as a large resuspension event on the turbidity and bottom light conditions (Figure 3). Collectively, these events completely suppressed the light reaching the bottom for nearly 5 weeks and the increased turbidity and sediment exposure (i.e. increased accumulation in the sediment traps) in the ~ 3 months following this event further suppressed light conditions for longer periods. Similar trends were also observed at the Geoffrey Bay and Dunk Island sites (and also likely at the Orchard Rocks site but not enough data were available for a definitive attribution). Now we have better defined the characteristics of the turbidity and sediment exposure regime, the key questions then relate to our ability to quantify the anthropogenic sediment contribution at the Cleveland Bay site and the potential impacts on the benthos, in this case, seagrass meadows. In that regard, a strong relationship has previously been established between the flood plume influence and sediment load from the Burdekin River on seagrass condition in Cleveland Bay (Petus et al. 2014; Lambert et al. 2020). Indeed, modelling of the influence of the sediment load on seagrass meadow area and condition in Cleveland Bay show a considerable impact following consecutive years with large flow and sediment discharge from the Burdekin River (Lambert et al. 2020). Furthermore, the modelling also shows the improvements in seagrass meadow area and condition in simulations of reduced catchment loads, which highlights the influence of the anthropogenic load (Lambert et al. 2020). Hence it appears at these locations, the impact of sediment exposure on the sites involves large resuspension or flood events to continuously reduce light over consecutive years; this applies particularly to seagrass meadows which have the ability to draw on short term energy reserves under reduced light conditions.

3.4.2 Havannah Island case study example (high influx of sediment during flood only)

Our logger time series from Havannah Island reveal very large spikes in SSC (> 150 mg.L^{-1}) that coincide with the flood events in 2018 and 2019 (Figure 3.9). The data show that elevated SSC conditions at this site persists for a few days before returning to background concentrations. We note that while the optical backscatter turbidity (i.e. NTUe) measurements were calibrated to SSC using 'wet season' sediment collected in the sediment traps, the concentrations recorded by the loggers during these flood events could be 'overestimated' based on the larger floc size (see Gibbs and Wolanski, 1992) and higher organic concentrations (Larcombe et al. 1995) likely co-occurring during these flood plume conditions. The accumulation data in the sediment traps also suggest that suspended sediment exposure at this site is also likely only elevated during the period of the flood plume and there is limited influence of any resuspension of the 'newly delivered sediment'. Similar trends were also noted at the Orpheus Island site (Figure 3.11). However, in the months following the 2019 flood event, Havannah Island experienced high coverage of macroalgae over the inshore coral reef that had not previously been observed at this site (Figure 3.23, T. Stevens, personal observation). We postulate that the delivery of the elevated SSCs measured by the logger in this event may have deposited across the reef framework and help fuel a macroalgae bloom in the months after the flood. The reef framework would act as a baffle to reduce the influence of sediment resuspension at this site but the deposited sediment would provide a source of nutrients for the macroalgae. Importantly, in the subsequent deployment periods the macroalgae coverage reduced and the reef recovered. However, we note a more persistent change to macroalgae dominance could occur if an additional stressor coincided with this

event such as bleaching or physical damage from a cyclone. We note that peak SSCs during the flood periods were also observed at several other sites (i.e. Cleveland Bay, Geoffrey Bay and Dunk Island) and hence similar promotions of macroalgae growth would be possible (at least at the coral reef sites).

Mid Sept 2018
- > 80% live coral cover

Late June 2019
- Shift to macro algae cover following 2019 floods
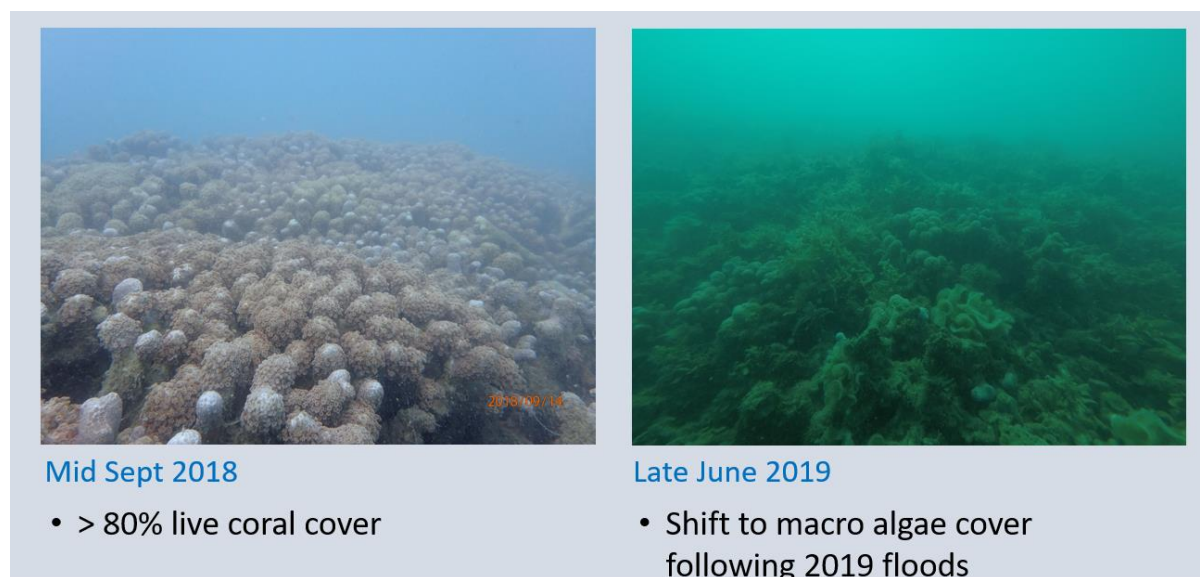
Figure 3.23. Photos of the Havannah Island site prior to the 2019 flood (left panel) and after the 2019 flood (right panel) (photos: Tom Stevens).

The highly elevated SSC (or SPM) (> 100 mg.L^{-1}) indicated by these loggers during the flood plume periods also need to be scrutinised. All direct flood plume water quality measurements in the GBR show that the salinity of the waters by the time they reach these logger locations in Cleveland and Halifax Bays is > 20 PSU; the SPM concentrations of these waters are < 20 mg.L^{-1} with one exception, and mostly < 10 mg.L^{-1} (see Figure 2.9 in Lewis et al. 2018). The exception was a sample collected in Cleveland Bay during the 2008 Burdekin plume which had a SPM concentration of 73 mg.L^{-1} with a salinity of 32.7 PSU. As this measurement is an outlier (e.g. Lewis et al. 2018) it has never previously been considered as a genuine plume concentration; indeed the sampling in the 2008 plume coincided with very rough weather conditions > 20 knots and it may be assumed that resuspension influenced the sample. However, on reflection, the other samples collected along this transect (as well as samples collected in 2007 which also coincided with similar rough conditions) at similar water depths all yielded much lower SPM concentrations. Hence it is possible that certain concentrated 'suspended sediment pockets' exist in flood plumes which rarely get sampled in monitoring programs. The high temporal resolution logger data show that these peak concentrations (> 100 mg.L^{-1}) last perhaps only a few hours. Another possibility is that there may be the presence of a sediment-enriched bottom nepheloid layer associated with the river plumes that is recorded by the instrument loggers (as they are situated near the sea floor) but is 'missed' in the plume monitoring programs where most samples in the GBR have been collected from the surface waters. The development of a sediment-enriched 'turbidity front' associated with a lower nepheloid layer has been documented in the Herbert River plume (Wu et al. 2006). The remaining possibly is that the turbidity loggers are 'overestimating' the SPM concentration due to the different composition of the sediment in the plume (i.e. dominated by organic rich flocs); however, SPM measurements from our logger sites (i.e. at depth) during flood plumes

do agree with the corresponding logger turbidity data (although these measurements were taken when SPM concentrations were < 5 mg.L^{-1}).

3.4.3 Persistent turbidity issues (Whitsunday Island Group)

The third type of sediment impact relates to persistent turbidity issues which may develop in in areas where flood delivered influx takes longer to export and/or areas with longer water/sediment residence times following either the influx of new sediment or the disturbance and redistribution (i.e. resuspension) of the existing sediment bed. Here small sediment flocs (and other SPM) cause subtle low-level increases in the water column (see Lewis et al. chapter 4). While these increases may represent a relatively small change in concentration (i.e. 1 NTU or 1 mg.L^{-1}) the influence on light conditions can be large. As measurements from across an environmental gradient in the Whitsunday Island Group show, the variation between the outer sites with Secchi Disc Depth of 9.0 and 9.5 m coincided with SPM concentrations between 0.17 and 0.50 mg.L^{-1} (turbidity between 0.4 to 0.8 NTU) while the Secchi Disc Depth was 4.0 m at Seaforth Island with SPM concentrations between 0.5 and 1.5 mg.L^{-1} (turbidity between 2.1 to 3.5 NTU). In fact, the skipper of the sampling vessel recalled that visibility at the outer sites was frequently up to 20 m (e.g. could see the boat anchor hitting the bottom in 20 m) and hence the SPM concentrations we measured at these outer sites may have also been 'elevated' relative to such conditions where Secchi Disc Depth reaches ~ 20 m. Such changes in SPM concentrations (i.e. likely in the order of 0.1 to 0.2 mg.L^{-1}) in these scenarios would not be measurable by standard TSS/SSC analysis and hence we recommend that either direct Secchi Disc Depth or light logger measurements be undertaken to better capture this variability.

3.5 Conclusions

Our logger and sediment compositional data clearly highlight the influence of newly delivered SPM in river flood plumes, although the spatial response to the SPM over the longer period is more variable. Variability due to the flood/discharge size is also apparent spatially across the sites, with some locations showing little influence from the smaller 2018 Burdekin flood while others show a marked response; all sites were influenced by the SPM delivered in the 2019 flood event. Based on these findings, we have developed site specific potential impacts of SPM in inshore marine environments of the GBR. We recommend future studies need to examine if a 'sediment-enriched' plume front or a bottom nepheloid layer exists in flood plumes to support the large turbidity spikes recorded by the logger. We plan to conduct statistical analysis of our dataset to more clearly distinguish the influence of newly delivered sediment in the GBR. In addition, future modelling of these potential impacts need to better quantify the role of the anthropogenic component of the SPM at inshore sites.

ACKNOWLEDGEMENTS

References

Bainbridge, Z.T. Wolanski, E. Álvarez-Romero, J.G. Lewis, S.E. Brodie, J.E. 2012. Fine sediment and nutrient dynamics related to particle size and floc formation in a Burdekin River flood plume, Australia. *Marine Pollution Bulletin* 65, 236-248.

Bainbridge, Z. Lewis, S. Bartley, R. Fabricius, K. Collier, C. Waterhouse, J. Garzon-Garcia, A. Robson, B. Burton, J. Wenger, A. Brodie, J. 2018. Fine sediment and particulate organic matter: a review and case study on ridge-to-reef transport, fates, and impacts on marine ecosystems. *Marine Pollution Bulletin* 135, 1205-1220.

Bainbridge, Z. Lewis, S. Stevens, T. Lazarus, E. Gorman, J. Smithers, S. in review. Methods to best measure sediment grain size across the catchment to reef continuum. *Marine Pollution Bulletin*.

Delandmeter, P. Lewis, S. Lambrechts, J. Deleernsijder, E. Legat, V. Wolanski, E. 2015. 3D modelling of the transport and fate of riverine fine sediment exported to a semi-enclosed system. *Estuarine, Coastal and Shelf Science* 167, 336-346.

Fabricius, K.E., De'ath, G., Humphrey, C., Zagorskis, I. and Schaffelke, B., 2013. Intra-annual variation in turbidity in response to terrestrial runoff on near-shore coral reefs of the Great Barrier Reef. *Estuarine, Coastal and Shelf Science*, *116*, pp.57-65.

Fabricius, K.E., Logan, M., Weeks, S. and Brodie, J., 2014. The effects of river run-off on water clarity across the central Great Barrier Reef. *Marine pollution bulletin*, *84*(1-2), pp.191-200.

Fabricius, K.E., Logan, M., Weeks, S.J., Lewis, S.E. and Brodie, J., 2016. Changes in water clarity in response to river discharges on the Great Barrier Reef continental shelf: 2002–2013. *Estuarine, Coastal and Shelf Science*, *173*, pp.A1-A15.

Gibbs, R.J. and Wolanski, E., 1992. The effect of flocs on optical backscattering measurements of suspended material concentration. *Marine Geology*, *107*(4), pp.289-291.

Lambert, V., O'Brien, K., Collier, C., Brodie, J., Adams, M.P., Baird, M., Bainbridge, Z., Carter, A., Lewis, S., Saunders, M., Rasheed, M. (2020) *Connecting Sediment Load Targets to Ecological Outcomes for Seagrass.* Report to the National Environmental Science Program. Reef and Rainforest Research Centre Limited, Cairns (153pp.).

Larcombe, P., Ridd, P.V., Prytz, A. and Wilson, B., 1995. Factors controlling suspended sediment on inner-shelf coral reefs, Townsville, Australia. *Coral reefs*, *14*(3), pp.163-171.

Larcombe, P. and Ridd, P., 2018. The need for a formalised system of Quality Control for environmental policy-science. *Marine pollution bulletin*, *126*, pp.449-461.

Larcombe, P. and Ridd, P., 2019. The need for a formalised system of Quality Assurance for Environmental Policy-Science and for improved policy advice to Government on the Great Barrier Reef. Reply to–"Support for improved quality control but misplaced criticism of GBR science" by Britta Schaffelke, Katharina Fabricius, Frederieke Kroon, Jon Brodie, Glenn De'ath, Roger Shaw, Diane Tarte, Michael Warne, Peter Thorburn (Marine Pollution Bulletin 129: 357–363, 2018). *Marine Pollution Bulletin*, *143*, pp.50-57.

Larcombe, P. and Woolfe, K.J., 1999. Increased sediment supply to the Great Barrier Reef will not increase sediment accumulation at most coral reefs. *Coral reefs*, *18*(2), pp.163-169.

Lewis, S.E., Olley, J., Furuichi, T., Sharma, A. and Burton, J., 2014. Complex sediment deposition history on a wide continental shelf: Implications for the calculation of accumulation rates on the Great Barrier Reef. *Earth and Planetary Science Letters*, *393*, 146-158.

Lewis, S., Bainbridge, Z. Stevens, T. Garzon-Garcia, A. Chen, C. Burton, J. Bahadori, M. Rezaei Rashti, M. Gorman, J. Smithers, S. Olley, J. Moody, P. Dehayr, R. (2018) *Sediment tracing from the catchment to reef 2016 to 2018: Flood plume, marine sediment trap and logger data time series.* Report to the National Environmental Science Program. Reef and Rainforest Research Centre Limited, Cairns (94pp.).

Orpin, A.R. and Ridd, P.V., 2012. Exposure of inshore corals to suspended sediments due to wave-resuspension and river plumes in the central Great Barrier Reef: a reappraisal. *Continental Shelf Research*, *47*, pp.55-67.

Petus, C., Collier, C., Devlin, M., Rasheed, M. and McKenna, S., 2014. Using MODIS data for understanding changes in seagrass meadow health: a case study in the Great Barrier Reef (Australia). *Marine environmental research*, *98*, pp.68-85.

McCloskey, G., Waters, D., Baheerathan, R., Darr, S., Dougall, C., Ellis, R., Fentie, B., Hateley, L. 2017. Modelling pollutant load changes due to improved management practices in the Great Barrier Reef catchments: updated methodology and results – Technical Report for Reef Report Card 2014, Queensland Department of Natural Resources and Mines, Brisbane, Queensland.

Margvelashvili, N., Andrewartha, J., Baird, M., Herzfeld, M., Jones, E., Mongin, M., Rizwi, F., Robson, B.J., Skerratt, J., Wild-Allen, K. and Steven, A., 2018. Simulated fate of catchment-derived sediment on the Great Barrier Reef shelf. *Marine pollution bulletin*, *135*, pp.954-962.

Schaffelke, B., Fabricius, K., Kroon, F., Brodie, J., De'ath, G., Shaw, R., Tarte, D., Warne, M. and Thorburn, P., 2018. Support for improved quality control but misplaced criticism of GBR science. Reply to viewpoint "The need for a formalised system of Quality Control for environmental policy-science" by P. Larcombe and P. Ridd (Marine Pollution Bulletin 126: 449–461, 2018). *Marine pollution bulletin*, *129*(1), pp.357-363.

Simpson, G.L. 2020. gratia: Graceful 'ggplot'-Based Graphics and Other Functions for GAMs Fitted Using 'mgcv'. R package version 0.4.1. https://CRAN.R-project.org/package=gratia

van Rij, J., Wieling, M., Baayen, R. and van Rijn, H. 2020. "itsadug: Interpreting Time Series and Autocorrelated Data Using GAMMs." R package version 2.4.

Wickham, H. 2016. ggplot2: Elegant Graphics for Data Analysis. Springer-Verlag New York.

Wood, S. N. *(*2006*).* Generalized additive models: An introduction with R*.* Boca Raton, FL*: CRC Press.*

Wood, S. N., Goude, Y. & Shaw, S. Generalized additive models for large data sets. *J. R. Stat. Soc. Ser. C Appl. Stat.* **64**, 139–155 (2015).

Wu, J., Ametistova, L., Heron, M., Lemckert, C.J. and Kalangi, P., 2006. Finite dispersal of a separative nepheloid plume by an internal hydraulic jump in a tropical mountainous river estuary. *Journal of Geophysical Research: Oceans*, *111*(C11).

APPENDIX: LOGGER METADATA RECORDS

Table A.1. Cleveland Bay deployment summary.

Deployment	Date in	Date out	Deployment length	Total grams trapped	Trap accumulation rate (mg/cm2/day)
1	1/06/2016	19/08/2016	79	110	64.3
2	19/08/2016	31/10/2016	73	97.5	61.7
3	31/10/2016	27/01/2017	88	Blockage	
4	27/01/2017	28/04/2017	91	94.4	47.9
5	28/04/2017	21/07/2017	84	41.3	22.7
6	21/07/2017	12/10/2017	83	19.1	10.6
7	12/10/2017	6/12/2017	55		
8	6/12/2017	23/02/2018		Traps lost	
9	23/02/2018	23/05/2018	89	Traps lost	
10	23/05/2018	19/09/2018		Traps lost	
11	19/09/2018	13/12/2018	No deployment		
12	13/12/2018	20/03/2019	97	280.5	133.6
13	20/03/2019	26/06/2019	98	216.4	102.0
14	26/06/2019	18/09/2019	84	55.8	30.7
15	18/09/2019	13/12/2019	86	103.6	55.6
16	13/12/2019	23/03/2020	101	310	141.8

Table A.2. Middle Reef deployment summary.

Deployment	Date in	Date out	Deployment length (Days)	Total grams trapped	Trap accumulation rate (mg/cm2/day)
1	1/06/2016	31/10/2016	152	Blockages	
2	31/10/2016	27/01/2017	88	Blockages	
3	27/01/2017	28/04/2017	91	40	20.3
4	28/04/2017	21/07/2017	84	24.7	13.6
5	21/07/2017	6/12/2017	138	84.6	28.3
6	6/12/2017	23/02/2018	79	71.8	42.0
7	23/02/2018	23/05/2018	89	67	34.8
8	23/05/2018	19/09/2018	119	25.9	10.1
9	19/09/2018	13/12/2018	85	63.3	34.4
10	13/12/2018	28/03/2019	105	158	69.5
11	28/03/2019	26/06/2019	90	52.3	26.8
12	26/06/2019	13/12/2019	170	71.3	19.4
13	13/12/2019	23/03/2020	101	38	17.4

Table A.3. Geoffrey Bay deployment summary.

Deployment	Date in	Date out	Deployment length	Total grams trapped	Trap accumulation rate (mg/cm2/day)
1	1/06/2016	31/10/2016	152	Blockages	
2	31/10/2016	27/01/2017	88	Blockages	
3	27/01/2017	28/04/2017	91	21	10.7
4	28/04/2017	21/07/2017	84	12.3	6.8
5	21/07/2017	12/10/2017	83	7.1	4.0
6	12/10/2017	6/12/2017	55	15.4	12.9
7	6/12/2017	23/02/2018	79	18.4	10.8
8	23/02/2018	30/05/2018	96	21.3	10.2
9	30/05/2018	21/09/2018	114	7.7	3.1
10	21/09/2018	13/12/2018	83	27	15.0
11	13/12/2018	20/03/2019	97	80.2	38.2
12	20/03/2019	26/06/2019	98	40.4	19.0
13	26/06/2019	18/09/2019	84	7.7	4.2
14	18/09/2019	13/12/2019	86	15.3	8.2
15	13/12/2019	23/03/2020	101	15.9	7.3

Table A.4. Orchard Rocks deployment summary

Deployment	Date in	Date out	Deployment length	Total grams trapped	Trap accumulation rate (mg/cm2/day)
1	1/06/2016	31/10/2016	152	Blockages	
2	31/10/2016	27/01/2017	88	Blockages	
3	27/01/2017	28/04/2017	91	42.5	21.6
4	28/04/2017	21/07/2017	84	67.4	37.1
5	21/07/2017	12/10/2017	83	60.2	33.5
6	12/10/2017	6/12/2017	55	143.7	120.7
7	6/12/2017	23/05/2018	168	136.7	37.6
8	23/05/2018	19/09/2018	119	48.8	18.9
9	19/09/2018	13/12/2018	85	65.2	35.4
10	13/12/2018	20/03/2019	97	135.7	64.6
11	20/03/2019	26/06/2019	98	119.7	56.4
12	26/06/2019	13/12/2019	170	64.8	17.6
13	13/12/2019	23/03/2020	101	120.7	55.2

Table A.5. Havannah Island deployment summary.

Deployment	Date in	Date out	Deployment length	Total grams trapped	Trap accumulation rate (mg/cm2/day)
1	7/06/2016	23/08/2016	77	Blockages	
2	23/08/2016	23/11/2016	92	12	6.0
3	23/11/2016	11/04/2017	139	14.6	4.9
4	11/04/2017	19/07/2017	99	10.3	4.8
5	19/07/2017	29/09/2017	72	3.7	2.4
6	29/09/2017	14/12/2017	76	11.1	6.7
7	14/12/2017	16/02/2018	64	17.7	12.8
8	16/02/2018	7/06/2018	111	22.5	9.4
9	7/06/2018	14/09/2018	99	4.6	2.1
10	14/09/2018	5/01/2019	113	25.4	10.4
11	5/01/2019	10/04/2019	95	23.6	11.5
12	10/04/2019	27/06/2019	78	7.4	4.4
13	27/06/2019	18/09/2019	83	3.5	1.9
14	18/09/2019	12/12/2019	85	6.9	3.7
15	12/12/2019	26/03/2020	105	9.4	4.1

Table A.6. Orpheus Island deployment summary.

Deployment	Date in	Date out	Deployment length	Total grams trapped	Trap accumulation rate (mg/cm2/day)
1	7/06/2016	23/08/2016	77	Blockages	
2	23/08/2016	23/11/2016	92	5.5	2.8
3	23/11/2016	11/04/2017	139	10.1	3.4
4	11/04/2017	19/07/2017	99	10.4	4.9
5	19/07/2017	29/09/2017	72	3	1.9
6	29/09/2017	14/12/2017	76	4.6	2.8
7	14/12/2017	16/02/2018	64	7.4	5.3
8	16/02/2018	7/06/2018	111	32.5	13.5
9	7/06/2018	14/09/2018	99	6.4	3.0
10	14/09/2018	5/01/2019	113	13.4	5.5
11	5/01/2019	10/04/2019	95	29.8	14.5
12	10/04/2019	27/06/2019	78	9.4	5.6
13	27/06/2019	12/12/2019	168	12.6	3.5
14	12/12/2019	26/03/2020	105	13	5.7

Table A.7. Dunk Island deployment summary.

Deployment	Date in	Date out	Deployment length	Total grams trapped	Trap accumulation rate (mg/cm2/day)
1	7/06/2016	22/08/2016	76	4.7	2.9
2	22/08/2016	22/11/2016	92	7.3	3.7
3	22/11/2016	12/02/2017	82	150	84.5
4	12/02/2017	27/04/2017	74	24.7	15.4
5	27/04/2017	20/07/2017	84	30.4	16.7
6	20/07/2017	28/09/2017	70	6.5	4.3
7	28/09/2017	7/12/2017	70	15.7	10.4
8	7/12/2017	15/02/2018	70	35.1	23.2
9	15/02/2018	11/05/2018	85	40.5	22.0
10	11/05/2018	10/08/2018	91	17.1	8.7
11	10/08/2018	18/01/2019	161	61.3	17.6
12	18/01/2019	29/03/2019	70	25	16.5
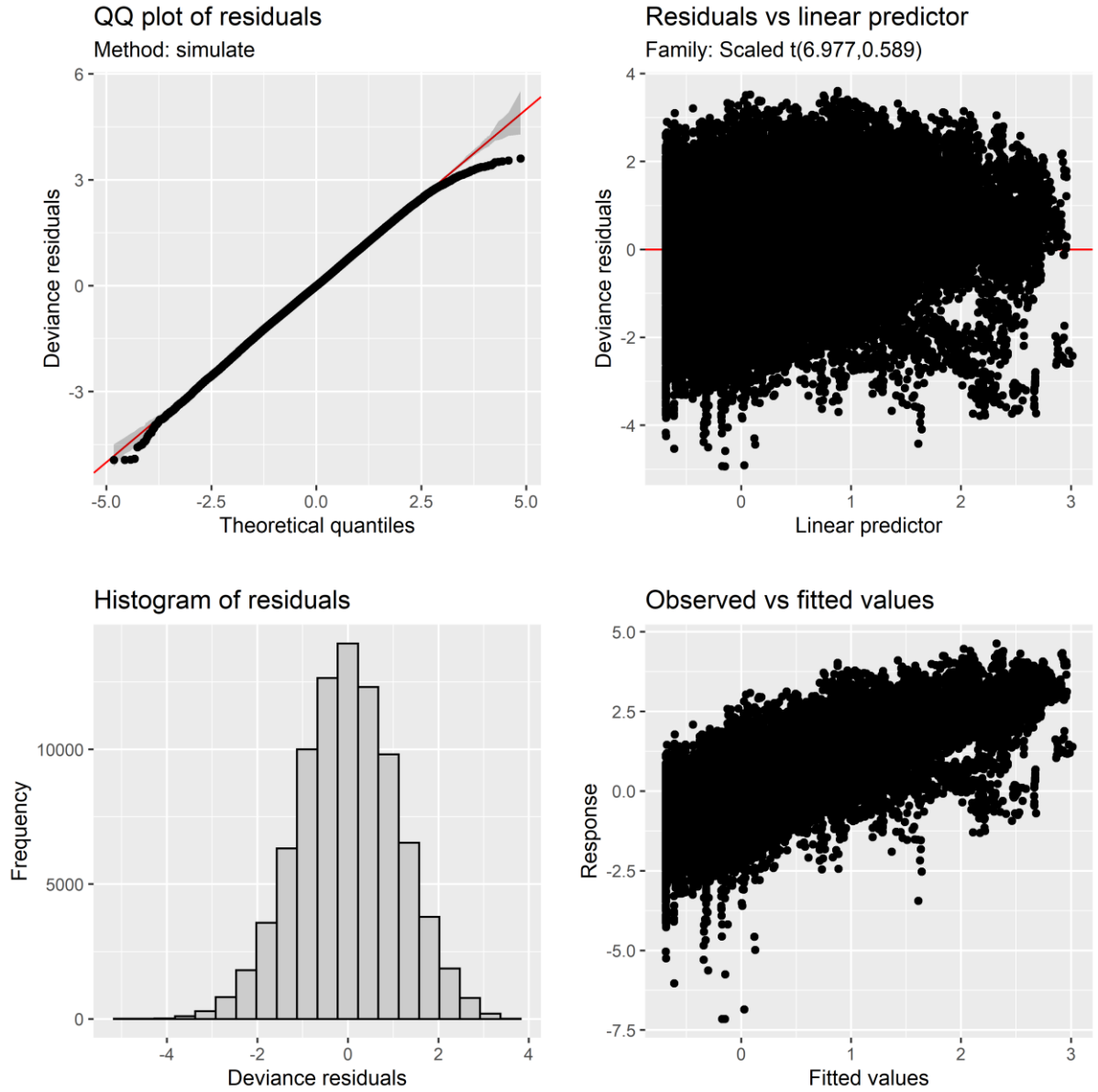
Figure A.1. Model diagnostics for the final model run of the residuals for the current meter RMS data (3 hour lag data) and turbidity.

CHAPTER 4

Characterising the sediment that causes 'persistent turbidity' through the Whitsunday Island Group

Stephen Lewis[1], Zoe Bainbridge[1], Thomas Stevens[1], Scott Smithers[1,2], Mark Raven[3] and Jon Olley[4]

[1] Catchment to Reef Research Group, TropWATER, James Cook University
[2] Environmental Science & Management, College of Science & Engineering, James Cook University
[3] Centre for Australian Forensic Soil Science, CSIRO Land and Water
[4] Australian Rivers Institute, Griffith University

4.1 Introduction

Tourism and community groups within the Whitsunday region have reported persistent turbidity issues within the waters surrounding the Whitsunday Island Group since the 2007-2011 period (Baird et al. 2019; Cantin et al. 2019). Anecdotal accounts from tourism operators suggest that the water clarity at several key coral reef locations has declined since this period and failed to recover. Over this same interval the abundance and community composition of juvenile corals measured on inshore coral reefs in the Whitsunday region reduced (Thompson et al. 2014). Several possible sources of the suspended particulate matter (SPM) responsible for the reduced water clarity have been proposed, including: port dredging operations (including Abbot Point and/or Hay Point); increased sediment supply from the local (Pioneer, Proserpine and O'Connell Rivers) and regional (Fitzroy River) catchments; and the resuspension of previously deposited fine sediments during cyclonic events. However, to date no sediment samples have been collected from the area to characterise the SPM and determine its source.

Previous investigations have examined long term continuous turbidity logger records (since ~ 2005) from the Great Barrier Reef Marine Park Authority's Marine Monitoring Program (MMP); conducted remote sensing of vertical light attenuation using MODIS satellite data; applied coral core geochemistry and; performed e-Reefs modelling in an attempt to quantify the change in water clarity and identify the potential cause (Baird et al. 2019; Cantin et al. 2019). In that regard, the long term turbidity records and the remote sensing of vertical light attenuation which extend back to the early to mid-2000s indicate no significant change over this timeframe (Baird et al. 2011). In contrast, the coral core records reveal increased terrestrial influence in the 2011-2017 period compared to the previous 1992-2010 period, but the increase was no more significant than the earlier 'wetter' periods in the longer term record which extends back to the mid-1800s (Cantin et al. 2019). Sediment modelling in the eReefs framework suggests that the large flooding in 2011 drove the delivery of new sediments into the Whitsunday Islands and these sediments have remained in the area. The eReefs model suggests that the Fitzroy River plume (and associated suspended sediment) in 2011

measurably influenced the Whitsunday Island Group, while the Pioneer and O'Connell Rivers also delivered SPM to the inner section (or western side) of the Whitsunday Island Group (Baird et al. 2019). In addition, modelling of the very fine sediment material (i.e. the "dust" or "fluffy" material) suggests it may have contributed to the enhanced turbidity during this most recent wetter period (Baird et al. 2019). While these recent investigations make a case for attributing the increased and persistent turbidity issues noted since the mid-2000s to the delivery of newly delivered sediment into the Whitsunday Island Group they did not directly examine the potential influence of dredging or resuspension events. We note that Cantin et al. (2019, p. 7) suggests the coral coring sites "appear to be influenced more strongly by marine resuspension events than direct flood plume inputs". Importantly, at least five tropical cyclones affected the Whitsunday Island Group between 2007 to 2017 including Tropical Cyclones Ului (2010: impacted Airlie Beach), Anthony (2011: impacted Bowen), Yasi (2011: impacted Mission Beach but effects felt down the coast – Whitsunday area received category 2-3 intensity), Dylan (2014: impacted Airlie Beach) and Debbie (2017: impacted Airlie Beach).

Previous research in the Whitsunday Island Group has documented clear 'inshore-offshore' gradients in coral reef development (and maximum depth of development) (van Woesik et al. 1999; Cooper et al. 2007), terrestrial signals in the geochemistry of coral cores (Lewis et al. 2012), water quality parameters (Udy et al. 2005; Cooper et al. 2007), species assemblages of benthic foraminifera (Uthicke and Nobes, 2008; Uthicke et al. 2012), photophysiology of symbiotic dinoflagellates in *Pocillopora damicornis* (Cooper and Ulstrup, 2009) and macrobioeroder densities in hard corals (Le Grand and Fabricius, 2011). There is some evidence that these gradients have been influenced by land use change since the arrival of Europeans (e.g. Lewis et al. 2012; Uthicke et al. 2012), although coral accretion and compositional studies from fringing reefs in the region also highlight considerable natural variability over longer Holocene scales (Ryan et al. 2016a; 2016b; 2018). Indeed, sedimentological research in the Whitsunday Island Group show a large accumulation (up to 20-30 m thick) of siliciclastic (terrigenous) sediments in certain locations, the bulk of which was likely deposited between 10.5 and 6.5 thousand years ago as sea-level rise flooded the continental shelf following the last ice age (Heap et al. 2002). More recent (i.e. past 4 thousand years) deposits may also have formed as the Whitsunday Island Group acts as an effective trap to capture transient sediment from the open areas of the mid shelf (Heap et al. 2002) as well as potentially from the catchments (Baird et al. 2019).

For this current study we collected both benthic grab and surface and depth suspended particulate matter (SPM) samples from key inner/western (i.e. Pine and Seaforth Islands) and offshore (Blue Pearl and Manta Ray Bays) sites of the Whitsunday Island Group during the 2019 dry season (Figure 1). An additional benthic grab sample was collected from the southern side of Hook Island in an area where considerable terrigenous sediment accumulation has been documented (see Heap et al. 2002). Our objectives were to characterise the SPM that is causing persistent turbidity issues in the Whitsunday Island Group in terms of particle size, mineralogy and geochemistry and to compare these to benthic grab samples. The resultant dataset provides new insights on the 'persistent SPM' in the Whitsunday Island Group and allows more targeted research to be developed to identify the cause and possible strategies to manage this SPM.

4.2 Methods

4.2.1 Site selection

Four sites were selected to undertake SPM sampling following consultation with tourism operators and scientists working in the region. These sites included Blue Pearl Bay and Manta Ray Bay which were sampled on the 9th September 2019 and Seaforth and Pine Islands which were sampled on the 15th September 2019 (Figure 1). A benthic grab sample from the southern section of Hook Island was also collected on the 9th September 2019 (Figure 1). These sites broadly represent the clearer mid shelf outer zone of the Whitsunday Island Group (Blue Pearl and Manta Ray Bays) and the inner more turbid area of the region (Seaforth and Pine Islands). We aimed to collect samples in 15 to 20 m water depth at each of sites.

Figure 4.1. Map of sampling sites in this project through the Whitsunday Island Group.

4.2.2 Sediment sampling

The SediPump® (Stevens, 2019; Integral Aqua Pty Ltd) was used to capture > 0.5 g SPM from the water column necessary to perform the suite of analysis to characterise the SPM. The SediPump® allows large volumes of water (~10,000-14,000 L) to be filtered over 2.5 to 3 hours of operation through a nominal 1 µm string filter to recover ~ 0.4 to 5.0 g of material (Bainbridge et al. In review, Chapter 2). Due to the relatively low SPM concentrations in the water column at the time of sampling (< 4 mg.L^{-1}), such characterisation or tracing would previously have not been possible without the SediPump®. Surface (top 50 cm) and depth (1-2 m from substrate) water column samples were taken from the four SediPump® sampled sites. The

string filters were placed in a 10 L container with site water and, on return to the laboratory, cut to release the SPM. The samples were transferred into dialysis tubing to remove salts, subsampled for grain size and then washed through a 38 µm sieve prior to analysis.

A standard Van Veen grab sampler was used to collect the benthic sediment samples. At least two casts were taken and the sediment sample thoroughly mixed in a bucket before being subsampled into a plastic bag. Salts were removed from the samples with RO water prior to initial analysis (grain size) and the < 10 µm fraction was then recovered via the settling method for mineralogy and geochemistry analysis (Bainbridge et al. 2016). A benthic grab sample could not be collected at Manta Ray Bay due to the hard substrate.

4.2.3 Water column measurements

Water samples were collected at the surface (top 50 cm) and depth (1-2 m from substrate) at SediPump® sampled sites. The surface samples were collected with a 10 L container while the depth samples were collected with a 5 L Niskin bottle. Samples were taken for total suspended solids (TSS i.e. SPM), volatile suspended solids (VSS) as an approximation of particulate matter organic content (% organic), turbidity, total organic carbon and dissolved organic carbon analyses. A 0.45 µm filter attached to a syringe was used to filter the sample for dissolved organic carbon. Secchi Disc Depth (m) measurements were also taken at the SediPump® sampled sites.

4.2.4 Sediment analysis

Microscopy analysis
Subsamples of the SPM collected by the SediPump® were taken and placed on a microscope slide and viewed under a light microscope. The ToupView software program (Touptex photonics) was used to capture these images (see Bainbridge et al. in review).

Grain size measurements
The salt-removed subsamples from the SPM samples and the benthic grab samples were analysed on a Malvern Mastersizer 3000 at James Cook University. Two separate analysis runs were performed according to the protocols outlined in Bainbridge et al. (in review). Briefly, the first run involved the direct measurement of the salt removed sample on the instrument following sieving to 1.2 mm while the second run was performed following sequential treatment with H_2O_2 (to remove organics) and HCl (to remove carbonates). The former measurement provides an indication of the behavior of the particles in the water column while the latter measurement provides an indication of the primary grain size of the mineral particles. For further detail on the methods including machine settings the reader is referred to Bainbridge et al. (in review/chapter 2).

Clay mineralogy
The salt removed < 38 µm particle size fraction from the SediPump® samples and the < 10 µm fraction of the benthic grab samples were analysed for clay mineralogy by X-Ray Diffraction (XRD) at the CSIRO Adelaide laboratory. The sample analysis involves multiple XRD runs at various angles and samples were run as sequential treatments including 'as received', glycol treatment, heating at 300° and 500° C. The combination of the measurements provides a detailed and quantifiable analysis of the specific clay minerals in

the samples. Minerals that originate from marine production (i.e. shell and coral fragments) such as aragonite, calcite and high Mg-calcite were removed from the final mineralogy plots. We also note that biogenic silica (diatoms) and plankton are amorphous to XRD analysis so they are not identified or included in the semi-quantitative analysis. We present the full mineralogical summary (minus the marine minerals) as a table. However, for tracing purposes we focused on the three dominant clay minerals of smectite, kaolinite and illite and presented each as a proportion of a combined 100% in the plots.

Geochemistry

The salt removed < 38 μm particle size fraction from the SediPump® samples and the < 10 μm fraction of the benthic grab samples were analysed for major and trace element geochemistry using ICP-MS. The major element data were converted to weight percent oxides and summed. The summed weights were then corrected to 100% (i.e. exclude the loss on ignition). The same correction factors were applied to the trace element and the rare earth element (REE) data. The REE and yttrium (Y) were normalised to the MUd from Queensland (MUQ) standard (see Kamber et al. 2005). For further characterisation of potential sources selected REEs and Y were plotted against CaO where CaO represents the level of 'dilution' of the sample due to the presence of shell fragments (hence this approach corrects for this influence).

4.3 Results

4.3.1 Water column measurements

Our sampling was designed to be conducted in the dry season to capture the SPM that causes 'persistent turbidity' with the first sampling date coinciding with a 15 knot S/SE wind regime. The second day of planned sampling (Seaforth and Pine Islands) was postponed due to a strong wind warning and was sampled 6 days later when conditions permitted sampling. The Secchi Disc Depth measurements from the water column of the SediPump® sites reflected the inshore-offshore water clarity gradient with the offshore sites having much better water clarity (9.0 m and 9.5 m at Blue Pearl and Manta Ray Bays, respectively) compared to the inner or western sites (4.0 m and 3.0 m at Seaforth and Pine Islands, respectively).

The TSS and turbidity analyses reflect the Secchi Disc Depth measurements with the lowest concentrations at the offshore sites (SPM < 0.5 mg.L^{-1}; turbidity < 1.0 NTU) compared to the inner/western sites (SPM ~ 0.7 to 3.0 mg.L^{-1}; turbidity 1.0 to 3.5 NTU) (Figure 4.2). Organic content (as measured by VSS) generally made up a relatively low proportion of the SPM sample with slightly higher concentrations measured in the inner/western sites (Figure 4.2). Importantly, the results highlight how a relatively small change in SPM/turbidity corresponds to relatively large change in Secchi Disc Depth. The results also demonstrate the utility of the SediPump® to capture sufficient material for analysis from low concentration waters.

The organic carbon analysis shows fairly similar dissolved organic carbon (DOC) concentrations (~ 0.9 to 1.2 mg.L^{-1}) across the sites while particulate organic carbon (POC) concentrations tended to be higher in the surface samples (Figure 4.3). Interestingly, very little POC was measured in the depth samples from Blue Pearl Bay, Seaforth Island and Pine Island sites (Figure 4.3) despite the VSS readings indicating that organic matter was present in these samples (Figure 4.2).
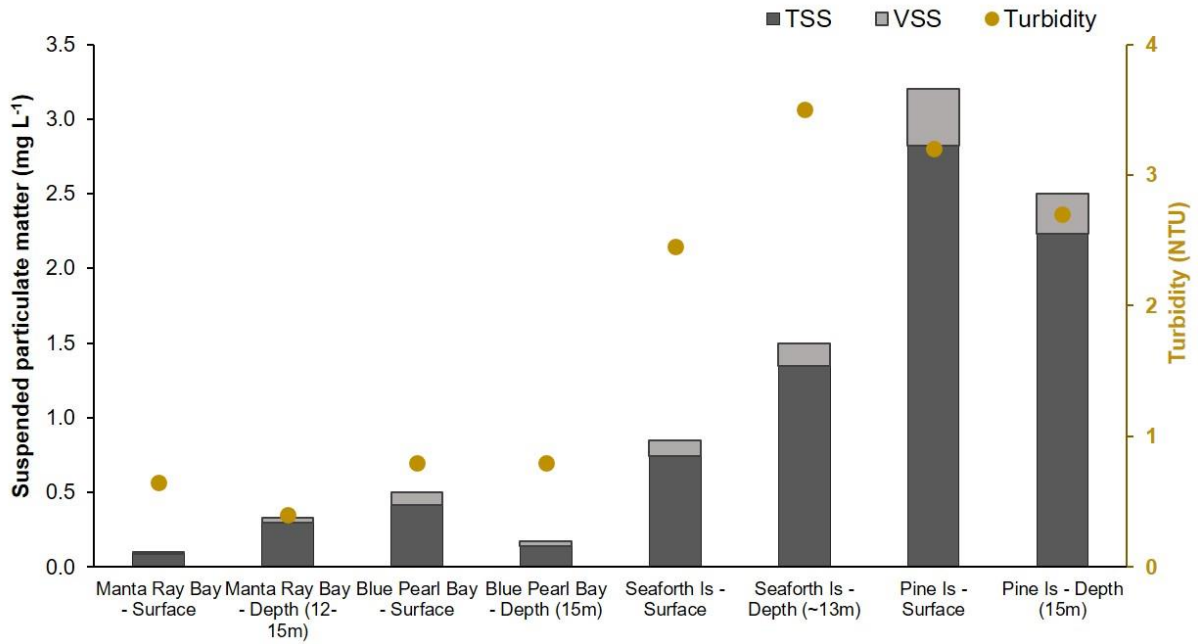
Figure 4.2. Suspended particulate matter composition including TSS and VSS (as an approximation of organic content) analyses, and turbidity measurements (right axis) for surface and depth water column samples collected at each site.
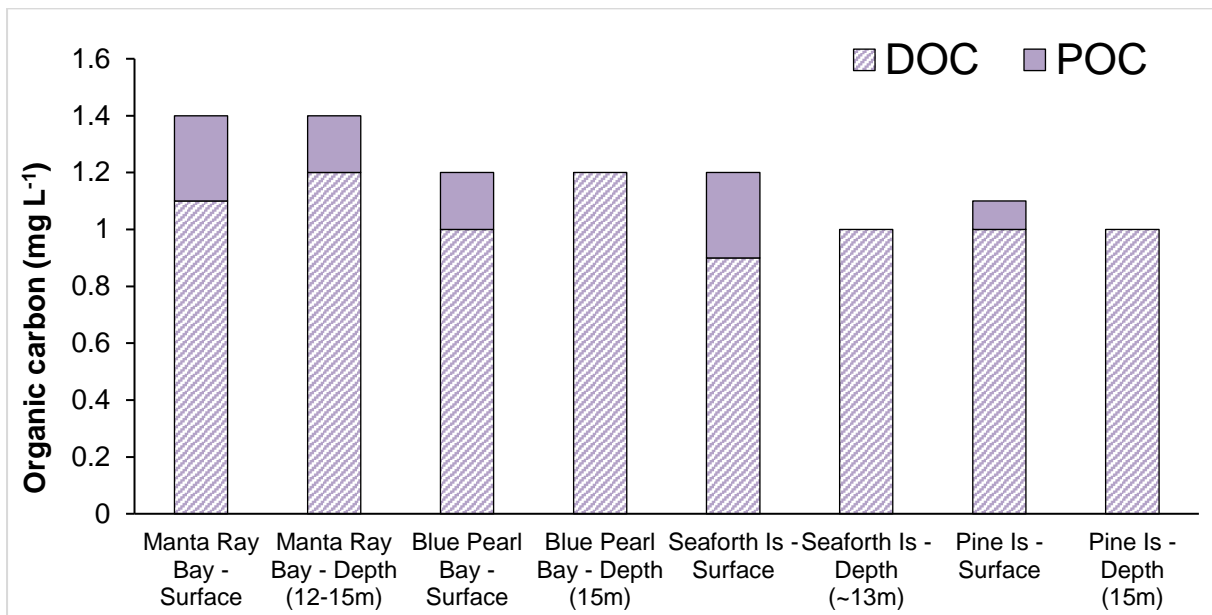
Figure 4.3. Total organic carbon measurements (separated into dissolved organic carbon: DOC and particulate organic carbon: POC) for surface and depth water column samples collected at each site.

4.3.2 Microscopy analysis

Under the microscope, the SPM in the surface samples reveal a mixture of individual mineral particles, fine shell fragments, small sediment flocs and diatoms (Figure 4.4). The images from the inner/western more turbid section of the Whitsunday Island Group (Figure 4.4a-b) show more individual mineral particles and less sediment bound flocs relative to the less turbid offshore locations (Figure 4.4c-d), although the particles in the images suggest a fairly similar range of grain sizes.

a) Seaforth Island – Surface waters

b) Pine Island – Surface waters

c) Manta Ray Bay – Surface waters

d) Blue Pearl Bay – Surface waters
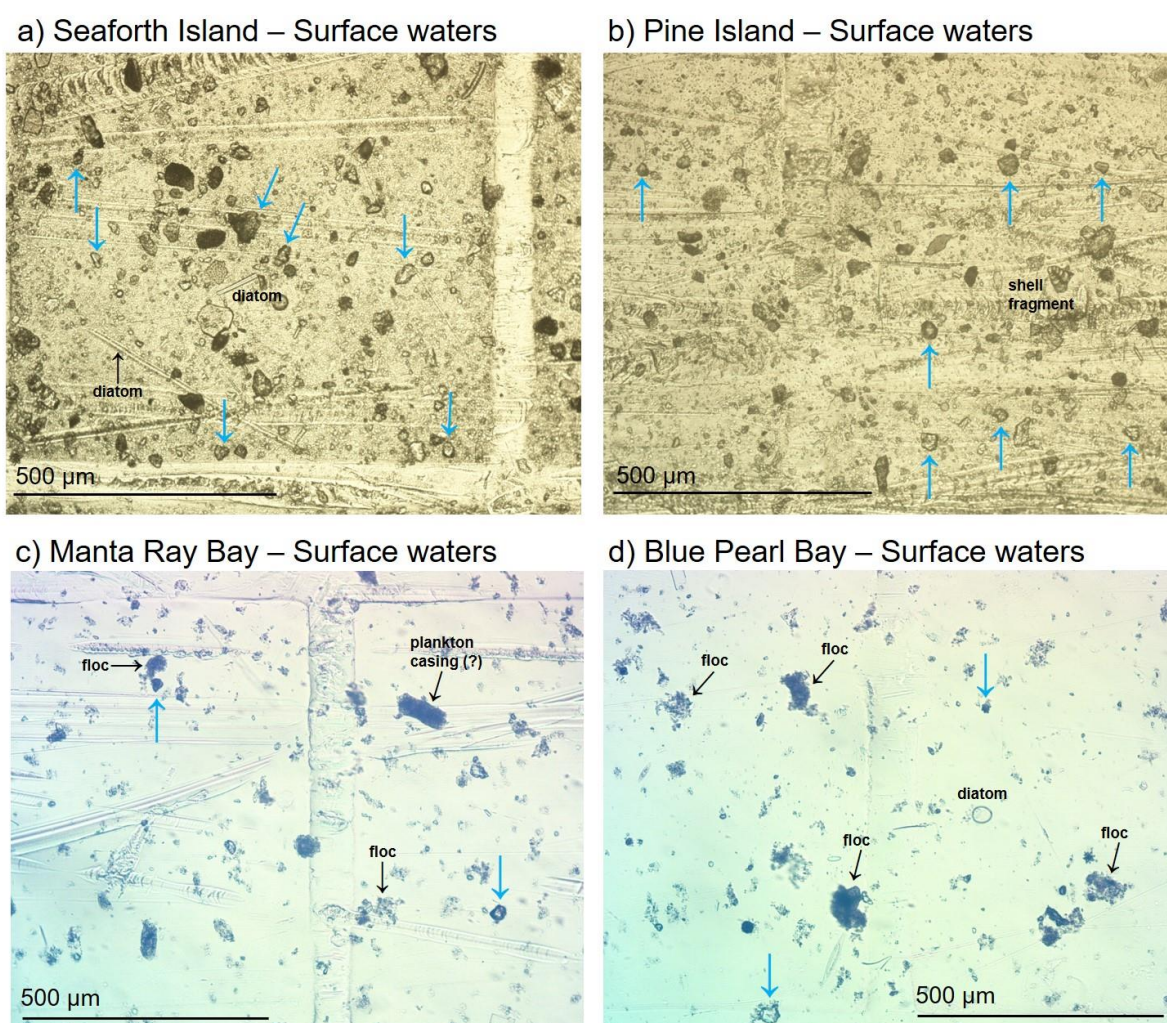
Figure 4.4. Microscope images of the SPM in the surface SediPump® samples across the four sites. Flocs, diatoms and shell fragments are labelled, with examples of discrete mineral particles also identified with blue arrows.

4.3.3 Grain size

Grain size distributions from the SediPump® samples show that the SPM material in the surface and depth waters were identical at each site (depth samples not shown). The difference between the untreated (SPM) and treated (Mineral) grain size distributions was greater in the outer sites (Figure 4.5c) compared to the inshore/western sites (Figure 4.5a). This pattern is congruent with microscopy observations which revealed a higher relative abundance of small sediment flocs at the outer sites. Similarly, the untreated and treated

bottom benthic grab sediment samples from the outer sites showed a greater change in the coarser distribution (Figure 4.5d) compared to the inshore/western sites (Figure 4.5b). Importantly, when the treated (Mineral) grain size distributions are overlaid for the four surface SediPump® sites, the grain size distributions are virtually identical (Figure 4.6a). The coarser mineral fraction (~ >10 μm up to 100 μm) in these treated SPM samples is likely related to the presence of biogenic silica (i.e. diatoms see Figure 4.4) which could not be removed by the H_2O_2 and HCl treatments (see Bainbridge et al. in review). An additional treatment to remove the biogenic silica component would potentially yield further insight on the terrigenous-only SPM at these sites. Similar grain size distributions were also evident across the sites in the treated bottom benthic grab samples (Figure 4.6b).
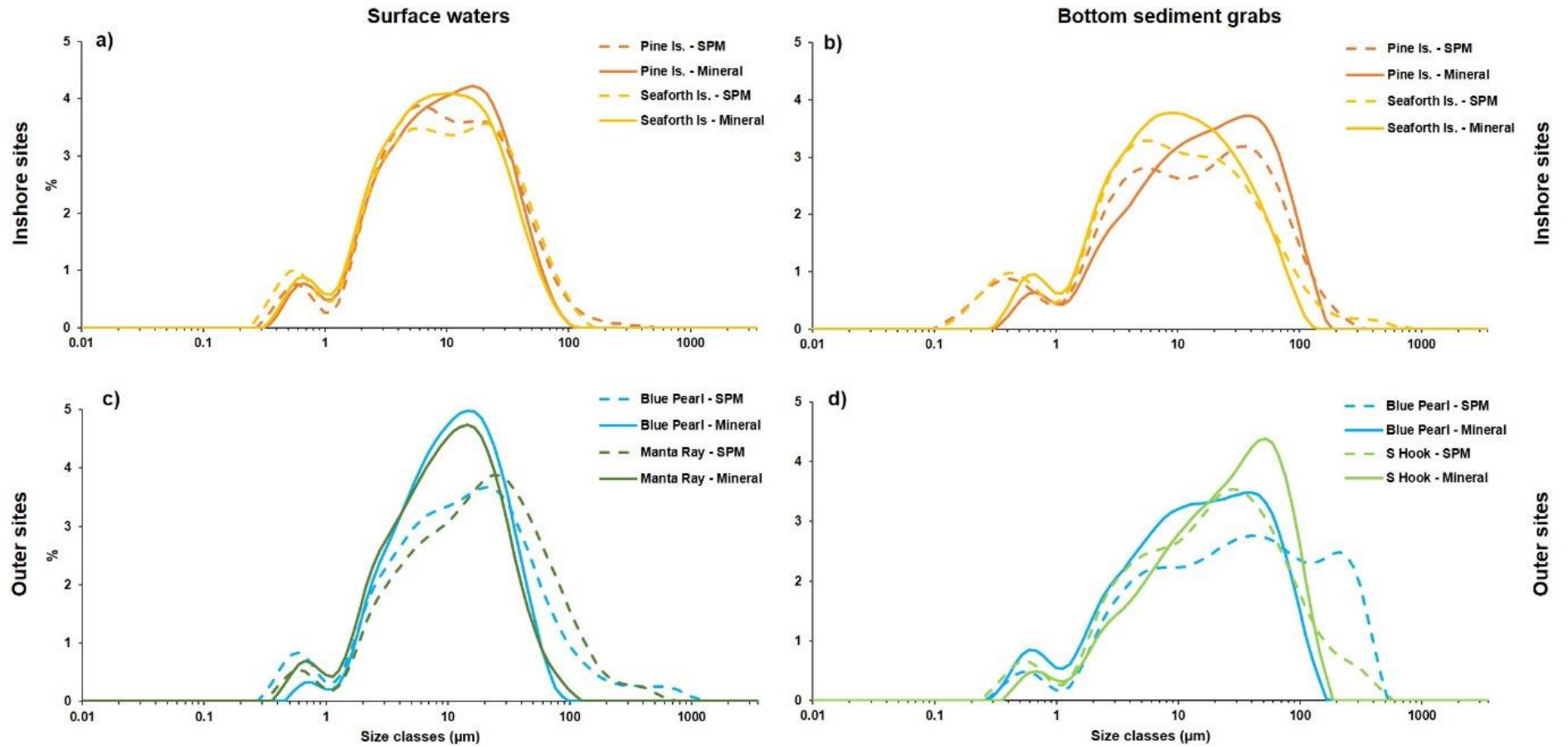
Figure 4.5. Grain size distributions of the surface SPM samples from the inshore sites (a) and the outer sites (c) including the salt removed untreated sample (SPM) and the H$_2$O$_2$ and HCl treated sample (Mineral). The same treatments are shown for the bottom benthic sediment grab samples from the inshore sites (b) and the outer sites (d).
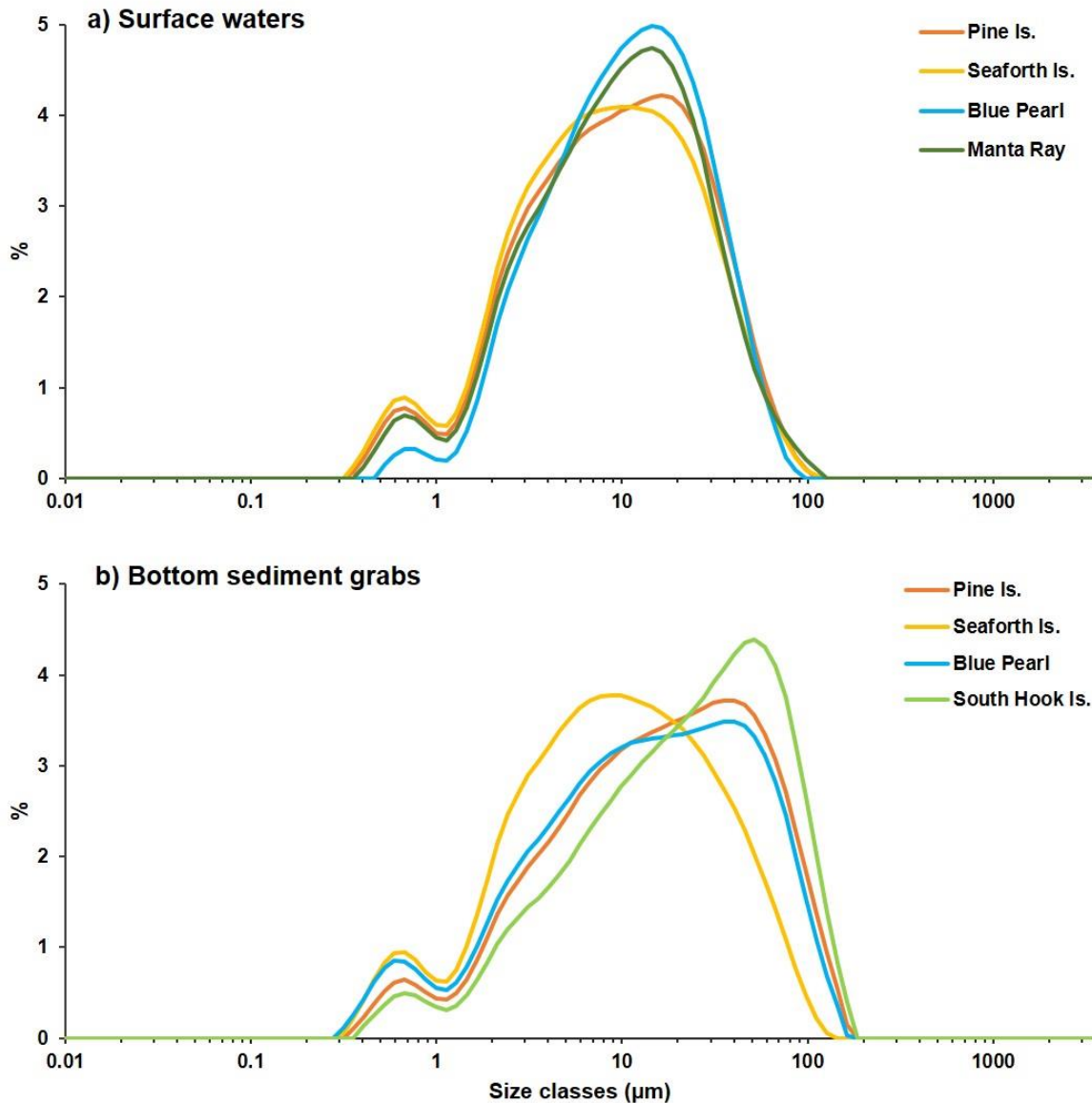
Figure 4.6. Grain size distributions of the surface treated suspended sediment (i.e. 'mineral') samples from the four sites (a) and the bottom benthic sediment grabs (b).

4.3.4 Clay mineralogy

The mineralogy results suggest that the SPM and benthic sediments across all sites originated from similar parent materials from the mainland and/or the surrounding islands and shelf sites. Clays (smectite, kaolinite and illite) dominated the mineralogy, especially for the inner/western sites (87-90% of the total minerals with higher kaolinite), with smaller quantities of quartz, albite and orthoclase (Table 4.1). Quartz comprised 5 to 19% by weight of the mineral composition across the sites. A greater quantity of the coarser non-clay minerals (quartz, albite and orthoclase) as well as the clay mineral illite were present in the SPM samples (both surface and depth) as these samples were recovered only to the < 38 µm fraction because sample size was limited by the low concentration marine waters (i.e. < 4 mg.L^{-1}). In comparison, the larger volumes of material retrieved using the bottom sediment grab samples allowed recovery to < 10 µm with a greater proportion of finer clay minerals as a result. The benthic sediment

grab sample from the mud bank at the south of Hook Island yielded slightly higher quartz and less illite than the other sites (Figure 4.7). Because of the < 38 μm particle size in the SPM samples, the proportion of illite relative to smectite and kaolinite is much higher in these samples compared to the benthic grabs as illite can be > 10 μm (Figure 4.7). However, there is broad similarity in the proportions of the clay minerals in the SPM samples (Figure 4.7) as well as in the benthic grab samples (Figure 4.8).

Table 4.1. Bottom sediment samples mineralogy – averages, RSD

	Smectite	Kaolin	Illite	Quartz	Albite	Orthoclase
Mean (%)	28	39	19	9	4	1
Std Dev	1.23	1.84	3.73	2.46	0.79	0.61
RSD	0.04	0.05	0.20	0.28	0.19	0.67
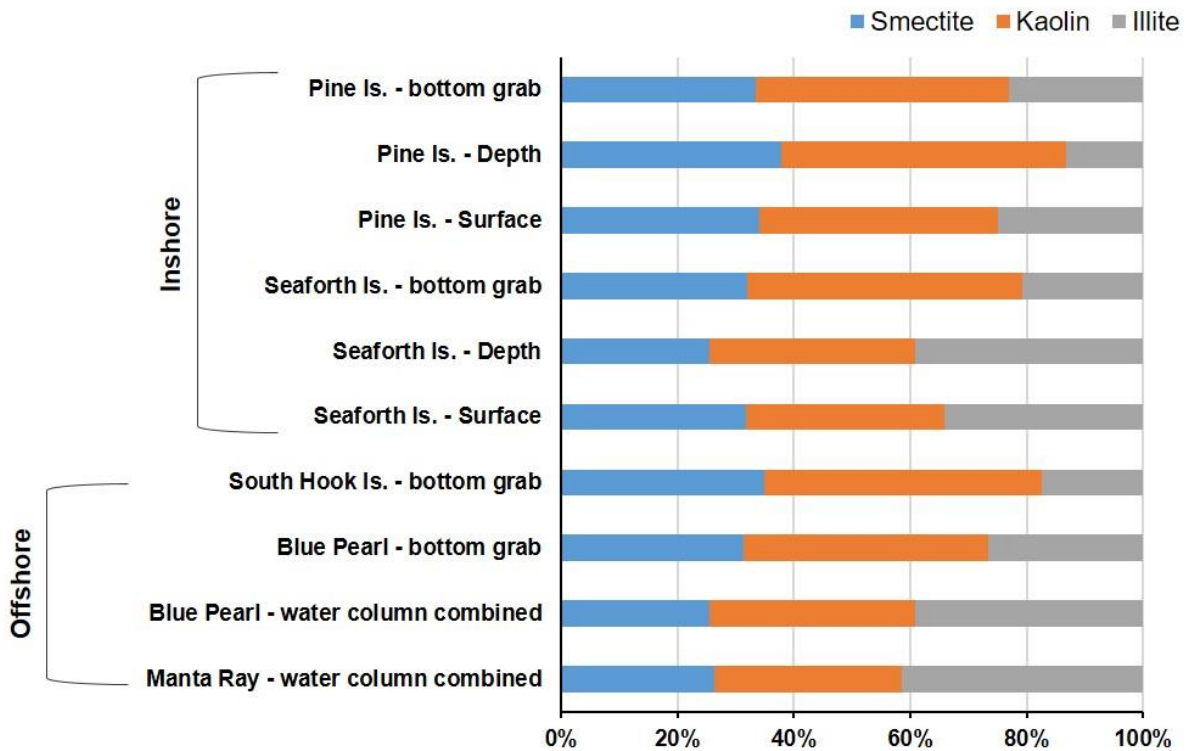
Figure 4.7. Clay mineralogy analysis for the SPM (< 38 μm) and benthic grab (< 10 μm) samples.
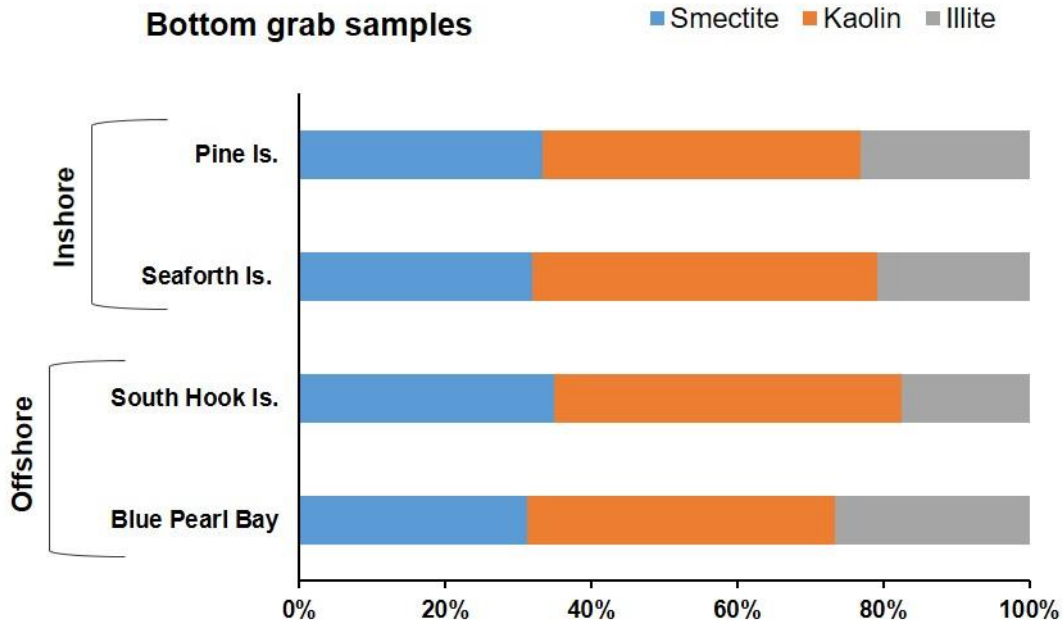
Figure 4.8. Clay mineralogy analysis for the < 10 μm fraction on the benthic grab samples.

4.3.5 Geochemistry

The results from the major and trace element analysis also support the interpretation that the sediment sources are similar across the Whitsunday Island Group. With the exception of the Al_2O_3 and CaO, the major elemental oxides have close to identical concentrations across the samples taken at individual sites (i.e. surface and depth SPM SediPump® samples and the benthic grab samples) as well as across the Whitsunday Island Group (Figure 4.9). The variability in the Al_2O_3 and CaO data likely reflect variable marine carbonate contributions to the site material which reflect when more shell/coral material is present. Extra carbonate material results in a slight relative increase in CaO and a corresponding decrease in Al_2O_3 and vice versa (Figure 4.9). When normalised to the MUQ standard, the REE and Y data show that all SPM and benthic grab sediments represent a terrestrial/terrigenous source that is characteristic of a typical flat line pattern across the series (i.e. little enrichment/depletion across the light to heavy REE series) (Figure 4.10). While these data suggest some potential subtle variations in source material across the Whitsunday Island Group, the actual variations in the data from the individual sites appear similar (or even greater) than the REE and Y patterns across the broader area (Figure 4.10). Importantly, based on these data we conclude the sediment suspended in the water column and in collected benthic grabs from across the broad Whitsunday Island Group are derived from similar source materials. A possible exception occurs with the SPM from the Blue Pearl Bay site which appears to plot on a different trend line when selected REE and Y are plotted against CaO (Figure 4.11). All the other sites including the benthic grab sample from Blue Pearl Bay plot along a trend line that provides an additional line of evidence that they have the same source(s) material (Figure 4.11).
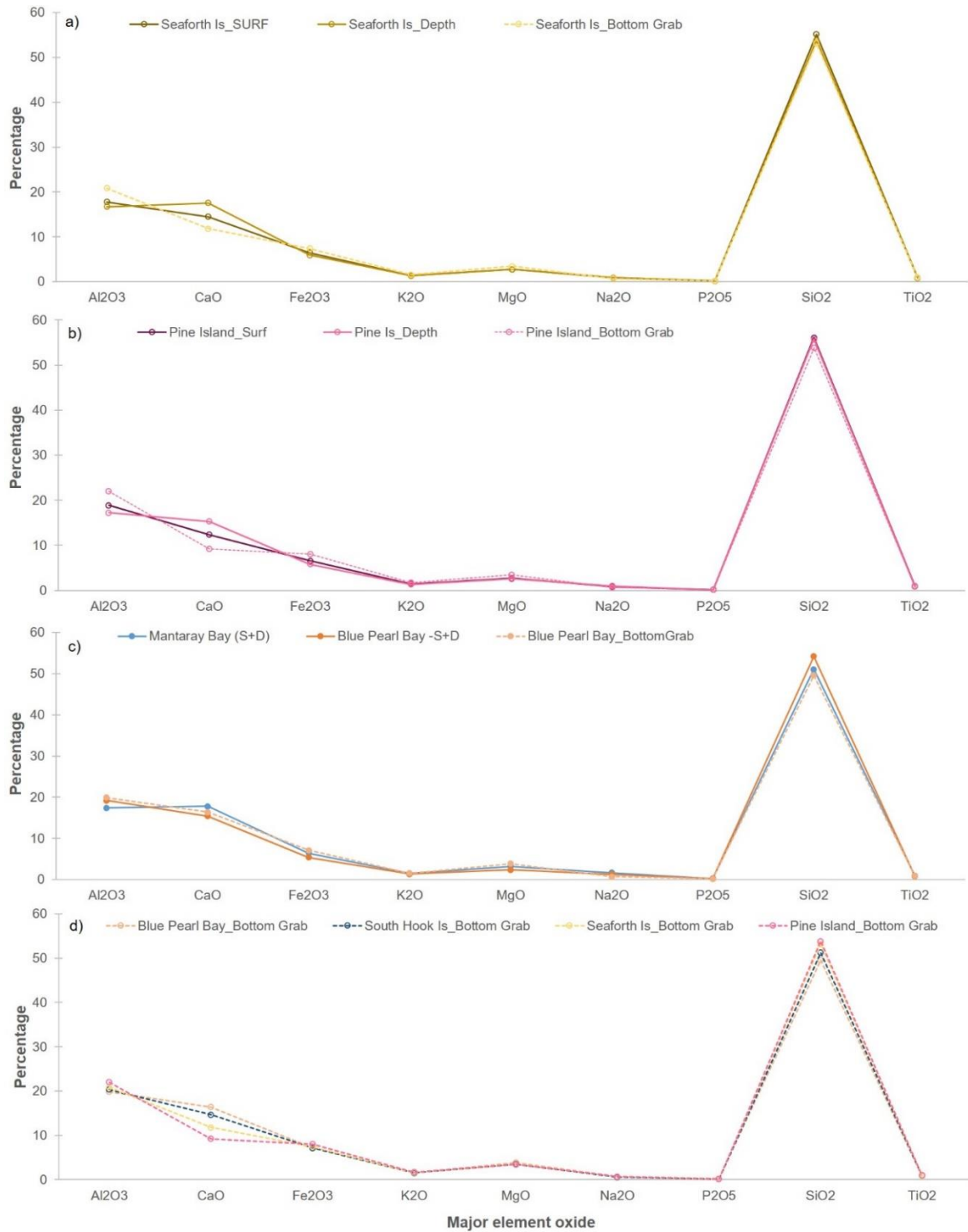
Figure 4.9. Major element oxide data for the surface and depth SPM samples as well as the benthic grab samples for the Seaforth Island site (a), Pine Island site (b), Manta Ray and Blue Pearl Bay sites (c) and all the benthic grab samples (d).
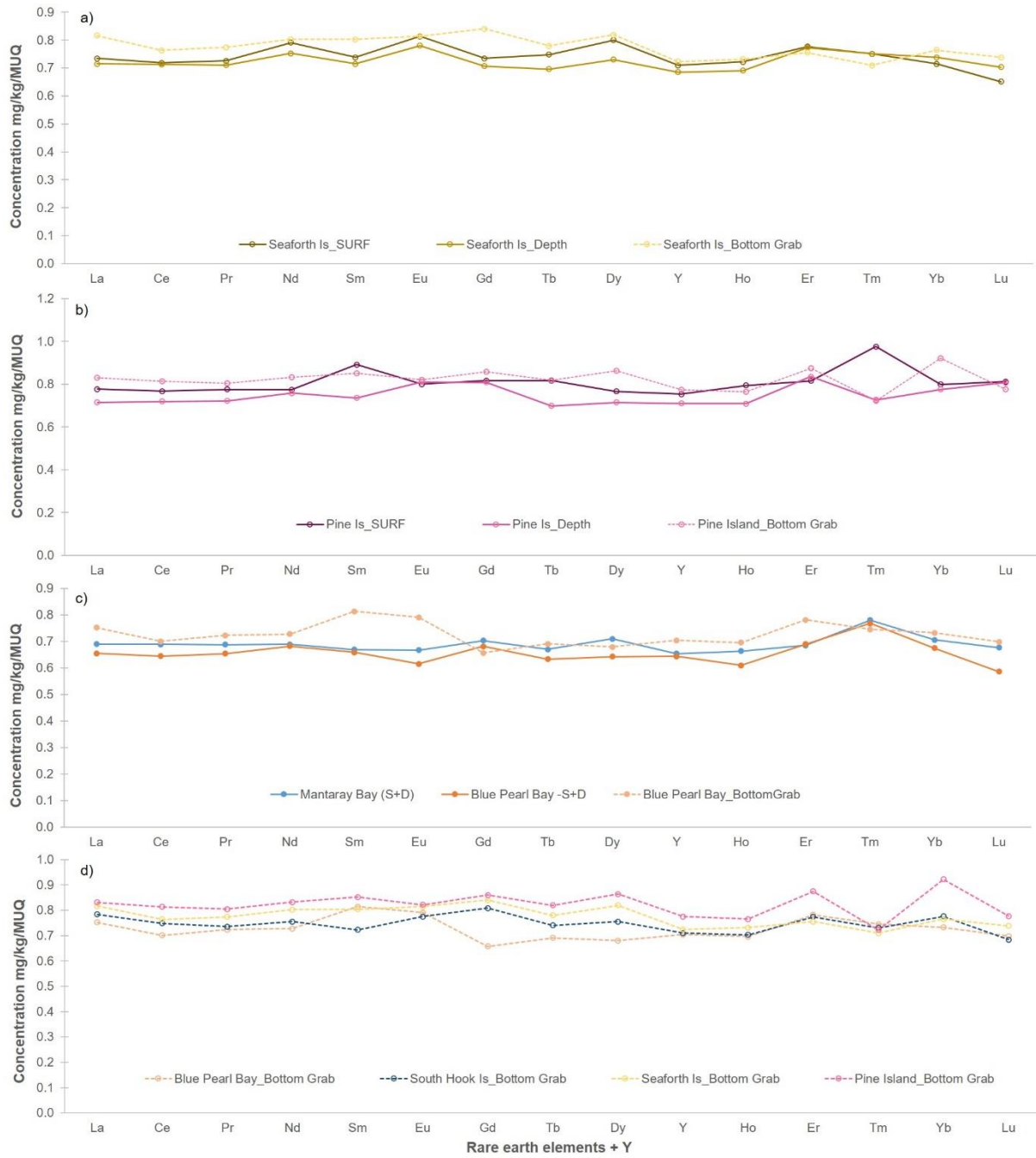
Figure 4.10. MUQ-normalised Rare Earth Element (REE) plus yttrium (Y) data for the surface and depth SPM samples as well as the benthic grab samples for the Seaforth Island site (a), Pine Island site (b), Manta Ray and Blue Pearl Bay sites (c) and all the benthic grab samples (d).
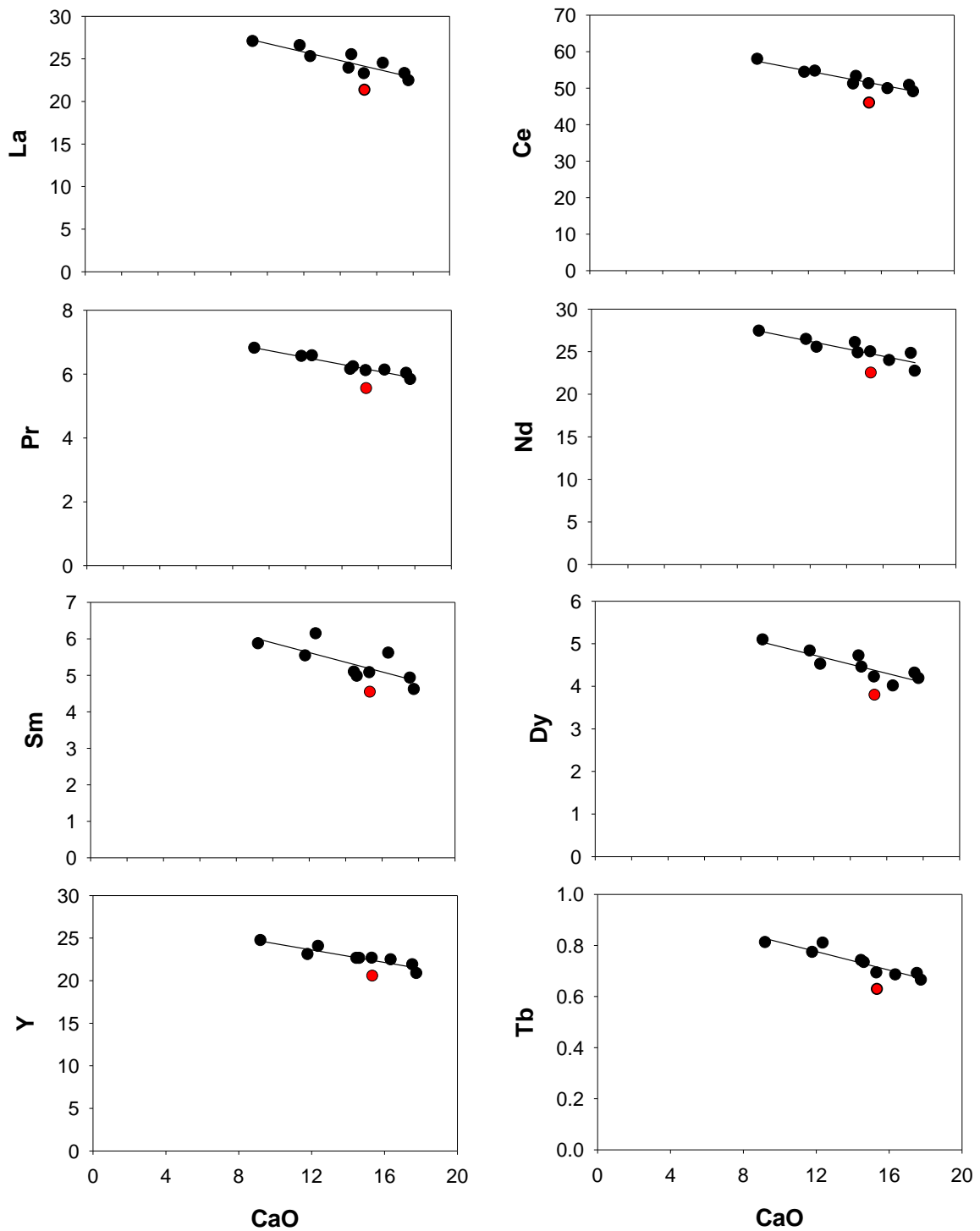
Figure 4.11. Selected Rare Earth Element (REE) plus yttrium (Y) data for the surface and depth SPM samples and benthic grab samples plotted against CaO. In each plot the data, with the exception of the Blue Pearl Bay-Surf/Depth sample (shown in red), are inversely correlated with CaO and are consistent with single regression lines. This indicates that, with the exception of the Blue Pearl Bay-Surf/Depth sample, the samples REE and Y concentrations are consistent with them being derived from a common terrestrial source or mix of sources and changes in element concentrations are related to changes in marine derived carbonate concentrations.

4.4 Discussion and Conclusions

Our case study provides new insights on the potential origins of the SPM in the waters surrounding the Whitsunday Island Group. This study was constrained by the limited number of sites which could be visited due to the two allocated field days and the need for 3 hours of SediPump® collection at each site to collect sufficient material for analytical characterisation. Nonetheless, our design allowed the variability in the physical and chemical composition of the SPM and benthic grab samples to be assessed over a broad area of the Whitsunday region, including the more turbid inner/western zone and the clearer outer/offshore zone. In that regard, our data clearly document the 'water quality gradient' described by Cooper et al. (2007) where what some would consider a 'small change' in SPM concentrations (i.e. 1 to 2 mg.L^{-1}) can produce a large change in water clarity. Specifically Secchi Disc Depths of 9.0 to 9.5 m were recorded for the clearer outer/offshore sites (Manta Ray and Blue Pearl Bays) with SPM concentrations between 0.17 and 0.50 mg.L^{-1} (turbidity between 0.4 to 0.8 NTU) while the Secchi Disc Depth was 4.0 m at Seaforth Island with SPM concentrations between 0.5 and 1.5 mg.L^{-1} (turbidity between 2.1 to 3.5 NTU) (Figure 4.2). Our observations clearly demonstrate that subtle relatively small changes in SPM concentrations in the order of 1 mg.L^{-1} can greatly influence water clarity.

A key question remains regarding the capability to detect and quantify changes in water clarity in the Whitsunday Island Group since 2007/2011 to support (or reject) the anecdotal accounts of reduced water clarity since that time. The luminescent line measurements in coral cores and hydrodynamic and sediment modelling in eReefs indicate the Whitsunday region experienced increased terrestrial influence over the period 2007/2011 to 2018 (Baird et al. 2019; Cantin et al. 2019). However, attempts to quantify the changes in water clarity from available turbidity logger data and coral geochemistry records have thus far proved challenging (Baird et al. 2019; Cantin et al. 2019). Our results suggest that these difficulties may reflect the combined difficulties in the precise measurement of low level concentrations and turbidity in marine environments and the fact that very small changes, some potentially lower than the detection limits of routine methodologies, can produce large changes in water clarity. In that regard, regular measurements of Secchi Disc Depth or continuous PAR light logger data may provide more reliable measures of water clarity change than deriving it from measurements of SPM. For example, an anecdotal account provided by the boat operator chartered for our sampling told of how ~ 10-15 years ago "you could see the anchor hit the bottom in 20 m of water" at the Blue Pearl Bay site. He also recounted that he perceived this was a rarer occurrence in recent times. Our monitoring data show that despite the lower SPM concentrations at the offshore sites at Blue Pearl Bay and Manta Ray Bay, they contained more small sediment flocs than the inshore sites highlighted by both the microscope imagery (Figure 4.4) and the greater changes between the untreated SPM and treated mineral grain size measurements (Figure 4.5). However, the clay mineral tracing and geochemistry data suggest that the terrestrial/terrigenous origin of the inorganic particles are similar between the outer/offshore sites and the inner/western sites (Figures 4.7-4.10), with the possible exception of the Blue Pearl Bay SPM.

Our finding that the origin of the terrigenous sediment through clay mineralogy and geochemical tracing appears broadly consistent across our monitoring locations suggests that the SPM and benthic sediments are fairly well-mixed throughout the Whitsunday Island Group. Moreover, the similarity in the character and composition of the sediments between the SPM

and benthic samples point towards a resuspension origin of the suspended matter. Collectively, these findings show that despite the complex hydrodynamic conditions (i.e. currents, potential sediment sources etc.) throughout the Whitsunday Island Group (Hamner and Hauri, 1977; Wolanski and Hamner, 1988; Blake, 1994; Wolanski et al. 1996; Stewart et al. 2000; Baird et al. 2019), the terrigenous SPM and benthic sediments all appear to have similar origin. This finding appears to contradict Baird et al.'s (2019) postulation that the inner/western parts (i.e. Pioneer, O'Connell and Fitzroy Rivers) and outer/offshore sections (i.e. Fitzroy River) of the Whitsunday region had different sediment sources. However, detailed clay mineralogy and geochemical measurements are required for these specific source rivers to ensure these different river sources can be distinguished using mineralogy and geochemical tracers. Indeed the possibility of a different SPM source for Blue Pearl Bay site also needs further investigation.

Importantly, the similarity of the SPM and benthic terrigenous sediments across the Whitsunday Island Group suggest one dominant source (or a well-mixed combination of sources – with the possible exception of Blue Pearl Bay SPM) which means that targeted management could take place if the source can be identified. Although it is not possible to identify the specific source(s) of the terrigenous sediments nor the cause for the purported 'persistent turbidity' in this study, we can suggest a way toward a more definitive answer. Firstly, river tracing work on the potential sediment sources in the area (i.e. Pioneer, O'Connell, Proserpine and Fitzroy Rivers) should be performed to establish signatures that distinguish each source that can then be compared to our dataset. Should a dominant river source be identified than further finer scale tracing work in that catchment can be completed to better target sediment remediation efforts to particular erosion hotspots. Secondly, dredge spoil materials should also be characterised and traced to compare with our dataset to examine if a dredging source is plausible. If a dredging source is identified then management of dredging operations could then be reviewed and modified. Thirdly, detailed sediment modelling (e.g. SLIM 3D or similar) in the Whitsunday Island Group may provide further insights on the influence of the resuspended sediments in the Whitsunday Island Group. This modelling would examine the hypothesis that a considerable volume of benthic sediments have been disturbed during a cyclone event over this period (or indeed over multiple cyclonic events) and, due to the complex hydrodynamic flushing in the region, these sediments are taking lengthy periods to settle and compact on the seabed. In addition, identification and examination of the available sediment sinks in the region should also be performed in this modelling exercise to determine if any recent changes have taken place. For example, the 'mud bank' at the southern end of Hook Island has been identified as a major Holocene sediment repository (Heap et al. 2002) but the question remains whether this repository is still active in more recent times. A case in Moreton Bay off Brisbane suggests that former river palaeochannels have recently been infilled which has resulted in a redistribution of fine sediment deposition in the bay (Coates-Marnane et al. 2016; Lockington et al. 2017). If the scenario that cyclone resuspension has resulted in increased persistent turbidity in the waters surrounding the Whitsunday Island Group and that suitable accommodation space for the sediments to settle and compact is still available, then a targeted management response may be some form of adaptive management approach to encourage increased sediment deposition and retention; this could include purpose built engineering structures on the substrate, seagrass planting and other substrate protection measures. However, if suitable accommodation space has been recently compromised, then the most appropriate (but probably seen as unorthodox)

management response would be to sensitively harvest and relocate deposited fine to recreate new accommodation space in the former depositional areas via dredging.

Given the similarity between the benthic and SPM samples and that our sampling campaign occurred in September (i.e. later in dry season) where the 'fluffy/dust' sediment layer from the previous wet season would potentially have been compacted (Fabricius et al. 2016), we would postulate that the cyclone resuspension hypothesis would be the most likely contributor to the perceived persistent turbidity issue. Hence along with the modelling, we also recommend tracing of sources and OSL dating in sediment cores from the major depositional areas. This approach would ascertain if sediment sources have changed over time as well as to establish if sediment accumulation rates at these sites have recently been compromised in that the accommodation space for the fine sediments has been exhausted. We would also recommend the establishment of a targeted monitoring program in the region with continuous PAR light logger readings as well as a coordinated community led Secchi Disc Depth program to better quantify changes in water clarity in space and time.

Acknowledgements

References

Bainbridge, Z. Lewis, S. Smithers, S. Wilkinson, S. Douglas, G. Hillier, S. Brodie, J. 2016. Clay mineral source tracing and characterisation of Burdekin River (NE Australia) and flood plume fine sediment. *Journal of Soils and Sediments* 16, 687-706.

Bainbridge, Z. Lewis, S. Stevens, T. Lazarus, E. Gorman, J. Smithers, S. in review. Methods to best measure sediment grain size across the catchment to reef continuum. *Marine Pollution Bulletin*.

Baird, M. Margvelashvili, N. Cantin, N. 2019. Historical context and causes of water quality decline in the Whitsunday region. CSIRO Oceans and Atmosphere Report.

Blake, S.G., 1994. *Processes controlling sediment and nutrient concentrations in the Whitsunday Islands area: Implications for fringing reef communities* [PhD Thesis]. Department of Geology, James Cook University, Townsville.

Cantin NE, Wu Y, Fallon S and Lough JM (2019) Historical records of terrestrial sediment and flood plume inputs to the Whitsunday Island region from coral skeletons: 1861-2017. Australian Institute of Marine Science, Townsville, Qld. (30pp).

Coates-Marnane, J., Olley, J., Burton, J. and Sharma, A., 2016. Catchment clearing accelerates the infilling of a shallow subtropical bay in east coast Australia. *Estuarine, Coastal and Shelf Science*, *174*, pp.27-40.

Cooper, T.F. and Ulstrup, K.E., 2009. Mesoscale variation in the photophysiology of the reef building coral Pocillopora damicornis along an environmental gradient. *Estuarine, Coastal and Shelf Science*, *83*(2), pp.186-196.

Cooper, T.F., Uthicke, S., Humphrey, C. and Fabricius, K.E., 2007. Gradients in water column nutrients, sediment parameters, irradiance and coral reef development in the Whitsunday Region, central Great Barrier Reef. *Estuarine, Coastal and Shelf Science, 74*(3), pp.458-470.

Fabricius, K.E. Logan, M. Weeks, S.J. Lewis, S.E. Brodie, J. 2016. Changes in water clarity in response to river discharges on the Great Barrier Reef continental shelf: 2002-2013. *Estuarine, Coastal and Shelf Science* 173, A1-A15.

Hamner, W.M., Hauri, I.R., 1977. Fine-scale surface currents in the Whitsunday Islands, Queensland, Australia: Effect of tide and topography. Australian Journal of Marine and Freshwater Research 28, 333-359.

Heap, A.D., Dickens, G.R., Stewart, L.K. and Woolfe, K.J., 2002. Holocene storage of siliciclastic sediment around islands on the middle shelf of the Great Barrier Reef Platform, north-east Australia. *Sedimentology*, *49*(3), pp.603-621.

Kamber, B.S., Greig, A. and Collerson, K.D., 2005. A new estimate for the composition of weathered young upper continental crust from alluvial sediments, Queensland, Australia. *Geochimica et Cosmochimica Acta*, *69*(4), pp.1041-1058.

Le Grand, H.M. and Fabricius, K.E., 2011. Relationship of internal macrobioeroder densities in living massive Porites to turbidity and chlorophyll on the Australian Great Barrier Reef. *Coral Reefs*, *30*(1), pp.97-107.

Lewis, S.E. Brodie, J.E. McCulloch, M.T. Malella, J. Jupiter, S.D. Stuart-Williams, H. Lough, J.M. Matson, E.G. 2012. An assessment of an environmental gradient using coral geochemical records, Whitsunday Islands, Great Barrier Reef, Australia. *Marine Pollution Bulletin* 65, 306-319.

Lockington, J.R., Albert, S., Fisher, P.L., Gibbes, B.R., Maxwell, P.S. and Grinham, A.R., 2017. Dramatic increase in mud distribution across a large sub-tropical embayment, Moreton Bay, Australia. *Marine pollution bulletin*, *116*(1-2), pp.491-497.

Raven, M.D., Self, P.G. and Gomez-Camacho, R. (2020) XRD Report – Clay Mineralogy of Sediment Samples from the Whitsunday Islands. CSIRO, Australia.

Ryan, E.J. Smithers, S.G. Lewis, S.E. Clark, T.R. Zhao, J-x. 2016a. Chronostratigraphy of Bramston Reef reveals a long-term record of fringing reef growth under muddy conditions in the central Great Barrier Reef. *Palaeogeography Palaeoclimatology Palaeoecology* 441, 734-747.

Ryan, E.J. Smithers, S.G. Lewis, S.E. Clark, T.R. Zhao, J-x. 2016b. The influence of sea level and cyclones on Holocene reef flat development: Middle Island, central Great Barrier Reef. *Coral Reefs* 35, 805-818.

Ryan, E.J. Smithers, S.G. Lewis, S.E. Clark, T.R. Zhao, J-x. 2018. The variable influences of sea level, sedimentation and exposure on Holocene reef development over a cross-shelf transect, central Great Barrier Reef. *Diversity* 10(4), 110; doi:10.3390/d10040110.

Stevens, T. 2019. International Patent Application PCT/AU2019/051436 Improved Sampler and Method.

Stewart, L.K., Heap, A.D., Woolfe, K.J., 2000. Evaluating the influence of tidal currents on the distribution of silt in Nara Inlet, central Great Barrier Reef, Australia. Sedimentary Geology 136, 59-69.

Thompson, A., Schroeder, T., Brando, V.E. and Schaffelke, B., 2014. Coral community responses to declining water quality: whitsunday Islands, Great Barrier Reef, Australia. *Coral Reefs*, *33*(4), pp.923-938.

Udy, J., Gall, M., Longstaff, B., Moore, K., Roelfsema, C., Spooner, D.R. and Albert, S., 2005. Water quality monitoring: a combined approach to investigate gradients of change in the Great Barrier Reef, Australia. *Marine Pollution Bulletin*, *51*(1-4), pp.224-238.

Uthicke, S. and Nobes, K., 2008. Benthic Foraminifera as ecological indicators for water quality on the Great Barrier Reef. *Estuarine, Coastal and Shelf Science*, *78*(4), pp.763-773.

Uthicke, S., Patel, F. and Ditchburn, R., 2012. Elevated land runoff after European settlement perturbs persistent foraminiferal assemblages on the Great Barrier Reef. *Ecology*, *93*(1), pp.111-121.

Van Woesik, R., Tomascik, T. and Blake, S., 1999. Coral assemblages and physico-chemical characteristics of the Whitsunday Islands: evidence of recent community changes. *Marine and Freshwater Research*, *50*(5), pp.427-440.

Wolanski, E., Hamner, W.M., 1988. Topographically controlled fronts in the ocean and their biological influence. Science 241, 177-181.

Wolanski, E., Asaeda, T., Tanaka, A., Deleersnijder, E., 1996. Three-dimensional island wakes in the field, laboratory experiments and numerical models. Continental Shelf Research 16, 1437-1452.

CHAPTER 5

The dissipation of suspended particulate matter in river flood plumes and implications for marine ecosystems: case studies from the Great Barrier Reef

Stephen Lewis[1], Caroline Petus[1], Dieter Tracey[1], Zoe Bainbridge[1], Cassandra James[1], Lucas Langlois[1], Jane Waterhouse[1], Jon Brodie[2], Thomas Stevens[1], Jane Mellors[1], Scott Smithers[1,3], Michelle Devlin[4], Renee Gruber[5]

[1] Catchment to Reef Research Group, TropWATER, James Cook University
[2] ARC Centre of Excellence for Coral Reef Studies, James Cook University
[3] Environmental Science & Management, College of Science & Engineering, James Cook University
[4] Centre for Environment, Fisheries and Aquaculture Science, Lowestoft, UK
[5] Australian Institute of Marine Science, Townsville

5.1 Introduction

The influence of newly-delivered suspended particulate matter (SPM) exported from coastal catchments on marine ecosystems of the Great Barrier Reef (GBR) has received considerable attention over several decades. While it is widely accepted that sediment loads exported from the GBR catchment area have increased considerably since European settlement (c. 1850) (on average 5.5 fold increase: Kroon et al. 2012), the impact of this 'new anthropogenic sediment' on turbidity and light regimes in the GBR remains contentious (e.g. Woolfe and Larcombe, 1998; Larcombe and Woolfe, 1999; Orpin and Ridd, 2012; Fabricius et al. 2013, 2014a, 2016; Lewis et al. 2014; Bainbridge et al. 2018). There is general agreement that SPM delivered via riverine flood plumes increases turbidity and decreases light in the GBR during the period of flood plume exposure (e.g. Petus et al. 2014; 2018; Lewis et al. chapter 3). In the months following a flood the newly settled particles are more easily resuspended back into the water column compared to the existing sediments which are relatively more compacted on the seafloor (e.g. Fabricius et al. 2013, 2014, 2016; Lewis et al. chapter 3) and thus they may continue to effect turbidity and light available to benthos well after the delivery event. The duration of exposure to primary plume (i.e. brownish coloured waters in satellite true colour images) waters (characterised by elevated SPM concentrations and reduced light) on parts of the inshore GBR has been correlated with reductions in seagrass meadow area (Petus et al. 2014a) and linked to declining coral reef health (Thompson et al. 2014; Petus et al. 2016; Ceccarelli et al. 2019). These views are, however, not universally accepted. Some researchers question the attribution of negative impacts to new sediment delivered in flood plumes, suggesting that wind-driven resuspension of the existing Holocene terrigenous sediment wedge controls SPM concentrations along the inner GBR (Woolfe and Larcombe, 1998; Larcombe and Woolfe, 1999; Orpin and Ridd, 2008).

The initial area influenced by newly delivered SPM is controlled by the movement and coverage of the flood plume in the GBR as well as the dispersal of the SPM within the plume. The movement and composition of flood plumes in the GBR have been well researched and include investigations directly measuring plume waters (e.g. Wolanski and Jones 1981; Wolanski and van Senden, 1983; Taylor, 1996; Devlin et al. 2001; Devlin and Brodie, 2005; Wu et al. 2006; Wolanski et al. 2008; Brodie et al. 2010; Bainbridge et al. 2012; Howley et al. 2018); remote sensing studies of flood plume water types, including analysis of plume frequency, exposure and risk (e.g. Burrage et al. 2002; Devlin and Schaffelke, 2009; Devlin et al. 2012, 2015; Schroeder et al. 2012; Álvarez-Romero et al. 2013; Petus et al. 2016, 2018, 2019); and modelling analyses (King et al. 2002; Delandmeter et al. 2015; Margvelashvili et al. 2018; Xiao et al. 2019). While the lateral dispersal of SPM over surface plume waters of the estuarine mixing zone has been well described in several manuscripts (Devlin et al. 2001; Devlin and Brodie, 2005; Brodie et al. 2010; Bainbridge et al. 2012; Howley et al. 2018), the dispersal of SPM within the water column has received comparatively less focus. The available empirical data on the dispersal of SPM within the water column in GBR plumes provide seemingly contradictory findings. Some observations document that SPM is concentrated within the buoyant low-salinity section of the upper water column (Taylor, 1996), others report that SPM appears to be well-mixed at various depths (Taylor, 1997; Bainbridge et al. 2012), while others report concentrated SPM towards the bottom water column (i.e. development of nepheloid layer) (Wu et al. 2006; Wolanski et al. 2008). Indeed, all scenarios have been reported in the international literature and are related to variability in river discharge and distance offshore (as well as water temperature and density in more temperate settings) whereby the SPM becomes trapped (and potentially concentrated relative to the riverine source) in plume frontal zones (e.g. Geyer et al. 2004).

The quantification of the relative influence of SPM from river plumes compared to the suspended sediment contributed through wind-driven resuspension of existing Holocene bay fill deposits has yielded conflicting findings (Larcombe and Woolfe, 1999; Orpin et al. 1999; Wolanski et al. 2008; Orpin and Ridd, 2012; Fabricius et al. 2013). Earlier studies applied the turbidity profiles of Taylor (1996) from the Barron River plume where SPM levels (equivalent to < 10 mg.L^{-1}) were concentrated in the buoyant upper 2 m of the water column. These measurements combined with the plume area were used to calculate the mass of sediment carried in plumes (Larcombe and Woolfe, 1999; Orpin et al. 1999). This first order sediment budget calculation suggested that the sediment mass dispersed in wind-driven resuspension events may be 'several orders of magnitude' higher compared to SPM supplied in river flood plumes on the inner GBR (Larcombe and Woolfe, 1999; Orpin et al. 1999). Wolanski et al. (2008) subsequently showed that SPM delivered in the Tully River plume was well mixed throughout the water column and was decoupled from the buoyant low salinity wedge with possibly higher SPM concentrations towards the seafloor; similar findings have been reported for other river plumes in the GBR including the Herbert (Wu et al. 2006), Burdekin (Bainbridge et al. 2012) and in another plume from the Barron following Tropical Cyclone Sadie (Taylor, 1997). Turbidity sensors, light loggers and sediment traps deployed by Wolanski et al. (2008) during the 2007 Tully flood plume showed increased sediment exposure and considerable reductions in light irradiance (i.e. no light beyond 4 m depth for 10 days). Orpin and Ridd (2012) offered an alternative interpretation of this dataset suggesting that wind-driven resuspension played the dominant role during this event citing, among other factors, the higher SPM concentrations measured in the offshore plume waters than measured in the Tully River.

More recently, detailed statistical modelling has been applied on *in situ* turbidity logger (Fabricius et al. 2013) and satellite photic depth (Fabricius et al. 2014, 2016) datasets which strongly demonstrated the influence of newly delivered sediment on turbidity regimes in the GBR.

The vast majority of research on terrigenous sediment dynamics in the GBR lagoon has been confined to the inner shelf. This was based on the following three assumptions: 1) it was long-assumed that river plumes rarely reached the mid and outer shelf zones (Devlin et al. 2001; Devlin and Brodie, 2005); 2) it was considered that only 'very little' SPM was carried by plumes beyond the inner shelf (Lambeck and Woolfe, 2000; Larcombe and Carter 2004) and; 3) wave-driven sediment resuspension and the 'terrigenous sediment wedge' are constrained to depths shallower than 22 m (i.e. the inner shelf; Orpin et al. 1999). However, recent modelling using satellite photic depth (Fabricius et al. 2014, 2016) and eReefs (Margvelashvili et al. 2018) indicate that newly-delivered sediment from plumes can influence light regimes out to the mid and possibly even some parts of the outer GBR shelf (see also Petus et al. 2018). Clearly there is a need for research efforts to provide empirical data on the influence of SPM carried in river plumes on more offshore parts of the GBR. Furthermore, the influence of what has previously been considered 'low' river plume SPM concentrations (i.e. < 5 mg.L^{-1}) (e.g. Larcombe and Woolfe, 1999; Orpin and Ridd, 2012) on light availability need additional examination. Indeed Wolanski et al. (2008) reported that fringing reefs below 4 m depth offshore from the Tully River received no light for 10 days during the 2007 plume event.

This study draws on samples collected offshore from the Tully and Burdekin Rivers to examine the dispersal of SPM within river plumes over the estuarine mixing zone under different environmental conditions. Our case study uses satellite imagery time series to document the spatial and temporal variability of plumes in the GBR including the frequency and duration with which they influence the mid-shelf. We examine the amount of light reduction caused by plume waters, including new data from the mid-shelf, and quantify the length of the events and their exposure on the mid-shelf. We show that flood plumes can greatly reduce euphotic depth when the plume impinges on the mid-shelf. Finally we produce a first-order sediment budget for sediment transport in plumes discharged from Wet and Dry Tropics catchments, and consider the implications of the post-European increased sediment supply on the light regimes in the GBR.

5.2 Methods

5.2.1 Marine Monitoring Program background

The flood plume data presented in this study have been collected through the Great Barrier Reef Marine Park Authority's Marine Monitoring Program (MMP) which was established in 2005. The water quality component of the MMP examines the condition and trend of various physiochemical and nutrient parameters measured multiple times at established sites over the year with a particular focus on the wet season (e.g. Gruber et al. 2019). From 2005 to 2014, the surface waters of flood plumes were monitored, targeting variations in the salinity gradient over the estuarine mixing zone with sites chosen in the field based on visual changes in the plume or systematic changes in salinity (i.e. 0, 5, 10, 15, 20, 25, 30 PSU intervals). A review of the program led to the establishment of set locations which are sampled at the surface and at depth (typically 1 to 2 m from the seafloor) throughout the year in both ambient and flood

plume conditions. This new design allows direct inter- and intra-annual comparisons to be made in ambient conditions and in flood plumes to examine spatial and temporal trends in water quality condition. The sites in each region were selected to cover a gradient from the major river mouths. This case study focuses on the sites off the Tully and Burdekin Rivers which have been well-sampled by the MMP and collaborative NESP Project. The main dataset presented was collected in the 2018/19 field season for the Burdekin River and include data from Old Reef (mid-shelf reef offshore from the Burdekin River), and the 2017/18 field season for the Tully River, including data from Ellison Reef (mid-shelf reef offshore from the Tully River).

5.2.2 Burdekin plume 2019

Major flooding was recorded in the Herbert, Black-Ross and Haughton basins including severe flooding in and around Townsville in February 2019. The Burdekin River peaked at the moderate flood level on the 8th February 2019 and discharged 17.5 million ML over the 2018/19 water year (1 Oct 2018 to 30 September 2019), of which 14.5 million ML was discharged in the 3-week period between 30 January and 19 February 2019 (Figure 5.1). This discharge volume is considered a 'very large event' for the river (Lewis et al. 2006) and has a frequency of approximately 1 in 5-years.

Sampling of the Burdekin River flood plume for this program targeted plume waters along the MMP defined event sites over the 11-12th February, 20-21st February and 6-7th March with some additional sampling undertaken at the NESP sediment trap and environmental logger deployment sites (i.e. Orchard Rocks and Havannah Island; Chapter 3). As the flood plume from the Burdekin River moved directly offshore (as opposed to northwards along the coast due to low winds) during its peak flow, an additional transect of sites was sampled out to Old Reef (mid-shelf) on the 15th February.
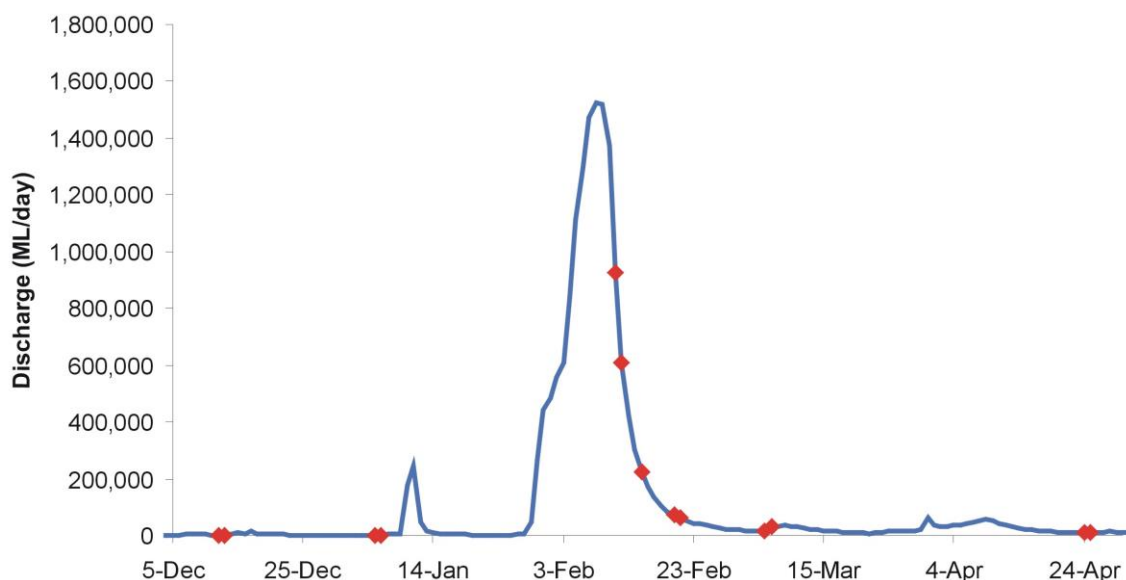
Figure 5.1. River discharge (in ML per day) from 5 December 2018 to 30 April 2019 for the Burdekin (Clare end of river gauge 120006B). Red diamonds show when sampling occurred offshore from the river mouths (including routine monitoring periods).

5.2.3 Tully plume 2018

The Wet Tropics region experienced an above average wet season in 2017/18 with major flooding occurring in many rivers including the Herbert and Tully Rivers. In fact, the Tully River had two major flow events (peaked on the 10th March and 28th March 2018, respectively) as well as two moderate level flow events (peaked on 19th January and 7th February, respectively) and one minor event (peaked on 27th January). The total discharge for the water year (1st October to 30th September) was 4.2 million ML for the Tully River (Figure 5.2) and 6.4 million ML for the Herbert River (above average water years for both rivers).

Poor weather restricted sampling of the Tully flood plume in 2018 on several occasions, shortening times on the water or delaying sampling until a few days after peak river flows. However, intensive sampling of the Tully plume waters across the estuarine mixing zone over January to March 2018 was conducted, including one visit to Ellison Reef on the 14th February (Figure 5.2).
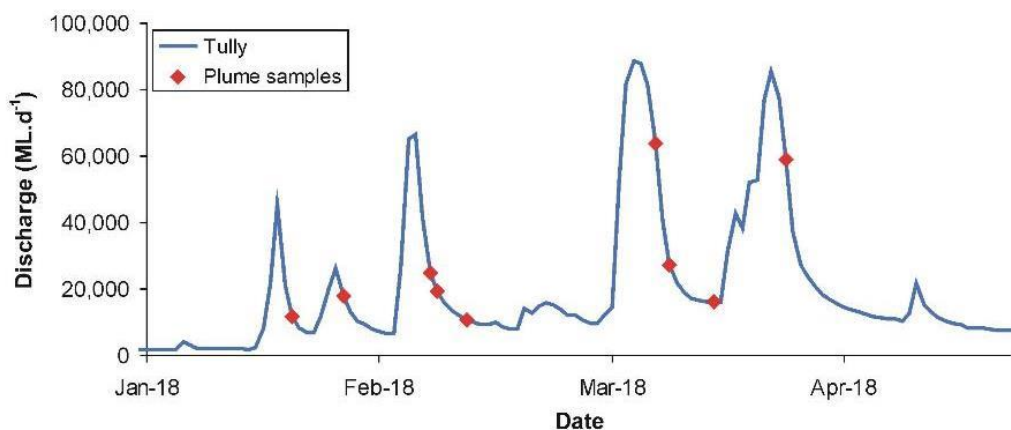
Figure 5.2. River discharge (in ML per day) from 1 January 2018 to 30 April 2018 for the Tully at Euramo gauge (gauge 113006A). Red diamonds show when sampling occurred offshore from the river mouths (including routine monitoring periods).

5.2.4 Plume sampling

At each location depth profiles were performed using a conductivity-temperature-depth (CTD) probe from SeaBird Electronics (SBE-19Plus) equipped with sensors for temperature, salinity, depth and Photosynthetically Active Radiation (PAR). The profiles were carried out from the sunny side of the boat and the probe was kept for 3 min at the water surface for sensor stabilisation before starting the downcast. Under the MMP, these casts are normally processed and largely used to provide information for the remote sensing component of the Program. They are also used to refine the loading maps for suspended sediment and dissolved inorganic nitrogen dispersal and exposure in the Great Barrier Reef. The CTD casts also provide valuable data on the plume mixing in the marine environment and the PAR light availability under sampled conditions. The raw cast data were downloaded and the initial data collected as the instrument equilibrates at the surface were discarded (i.e. the instrument is held ~ 1 m below the surface for ~ 3 mins so the sensors can equilibrate). Both the down-casts and up-casts were plotted to examine the reproducibility of the data at each site (not shown). In most cases, the down- and up- casts were very similar, although differences in the sharpness and depth of the salinity profile were evident where a strong salinity gradient in the

water column occurred. In those circumstances it is likely the down-cast (and subsequent upcast) disturbed the water column where a more 'smoothed/mixed' profile was produced in the upcast. Based on this finding we favoured the downcast data; however, as the downcast data misses the upper ~ 1 m of the water column due to the equilibration step, the upcast data of the upper 1 to 1.5 m of water column was patched onto the downcast data to produce a full profile of the water column.

5.2.5 Suspended Particulate Matter sampling and analysis

SPM samples were collected in a 10 L container at the surface and a 5 L Niskin bottle for depth samples (typically 1-2 m from the seafloor) before being transferred into a 1 L bottle. The samples were kept refrigerated at 4° C and analysed by the Total Suspended Solids (TSS) method using the standard gravimetric filtration method (Method 2540D; APHA, 2005). Known volumes of sample were vacuum filtered onto pre-weighed 0.4 µm polycarbonate filter papers and dried overnight in a 103–105°C oven.

5.2.6 MODIS satellite processing

Time series of wet season water-type maps were produced using daily MODIS-Aqua (hereafter, MODIS) quasi-true colour (hereafter true colour) imagery reclassified to six distinct colour classes defined by their colour properties (Álvarez-Romero et al. 2013; see also Petus et al. 2019). These classes are typical of colour gradients existing across coastal waters, including river plumes during the wet season. To complement this dataset, MODIS-Terra true colour images are also occasionally downloaded from the National Aeronautics and Space Administration (NASA)'s EOSDIS worldview website) and processed to daily water type maps. MODIS-Terra are only used when MODIS-Aqua data are too cloudy or unavailable. Available MODIS data are biased toward clear, non-cloudy days, and may underrepresent water quality conditions in regions of higher rainfall and cloudiness like the Wet-Tropics (i.e. Tully River). These images allow the frequency and exposure of flood plumes to be determined across the inner, mid and outer shelf of the GBR (e.g. Petus et al. 2019).

5.3 Results

5.3.1 Plume extent

Our observations of the plume discharge and dispersal from the Tully and Burdekin Rivers are consistent with previous descriptions in the GBR (e.g. Devlin et al. 2001; Devlin and Brodie, 2005; Devlin and Schaffelke, 2009). Specifically, the spatial extent of the plume is predominantly driven by river discharge volume and the offshore wind speed and direction. The 17-year record of satellite imagery shows the frequency of exposure to primary plume waters (colour classes 1-4) delivered from the Tully and Burdekin Rivers across two cross-shelf transects extending from the coast to the outer shelf (Figure 5.3). Analyses of this record indicate that the Tully flood plume reached the mid-shelf on 12 of the 17 years examined (once every 1.4 years) while the Burdekin plume reached the mid-shelf on 8 of the 17 years examined (once every 2.1 years) (Figure 5.3). The annual analysis suggests that the Burdekin plume reached Old Reef on 3 occasions in the 17 year record (once every 5.7 years). We note that these frequencies do not provide a measure of the duration of inundation (i.e. frequency multiplied by time = exposure) which is likely more important when considering ecological

consequences. In that regard, the data suggest that while mid-shelf events from the Tully were more frequent they were typically shorter-lived compared to the Burdekin, where during larger events mid-shelf exposure to primary plume waters is more prolonged (e.g. 2008, 2011 events in Figure 5.3). This point is demonstrated by the weekly and daily exposure maps for the Tully and Burdekin plumes in 2018 and 2019, respectively (Figure 5.3). During the large 2018 Tully plume the mid-shelf was exposed to primary plume waters for at least 1 day (and up to 6 days; note cloud cover prevented a more accurate analysis) whilst the large 2019 Burdekin River plume exposed the mid-shelf to primary plume waters for at least 6 days (and up to 8 days). However, it is important to note that the combined influence of primary (colour classes 1 to 4) plus secondary (colour class 5; i.e. greenish colours on the satellite true colour imagery) plume waters from both the Tully and Burdekin Rivers on the mid-shelf may persist for as long as 8 weeks (Figure 5.3).
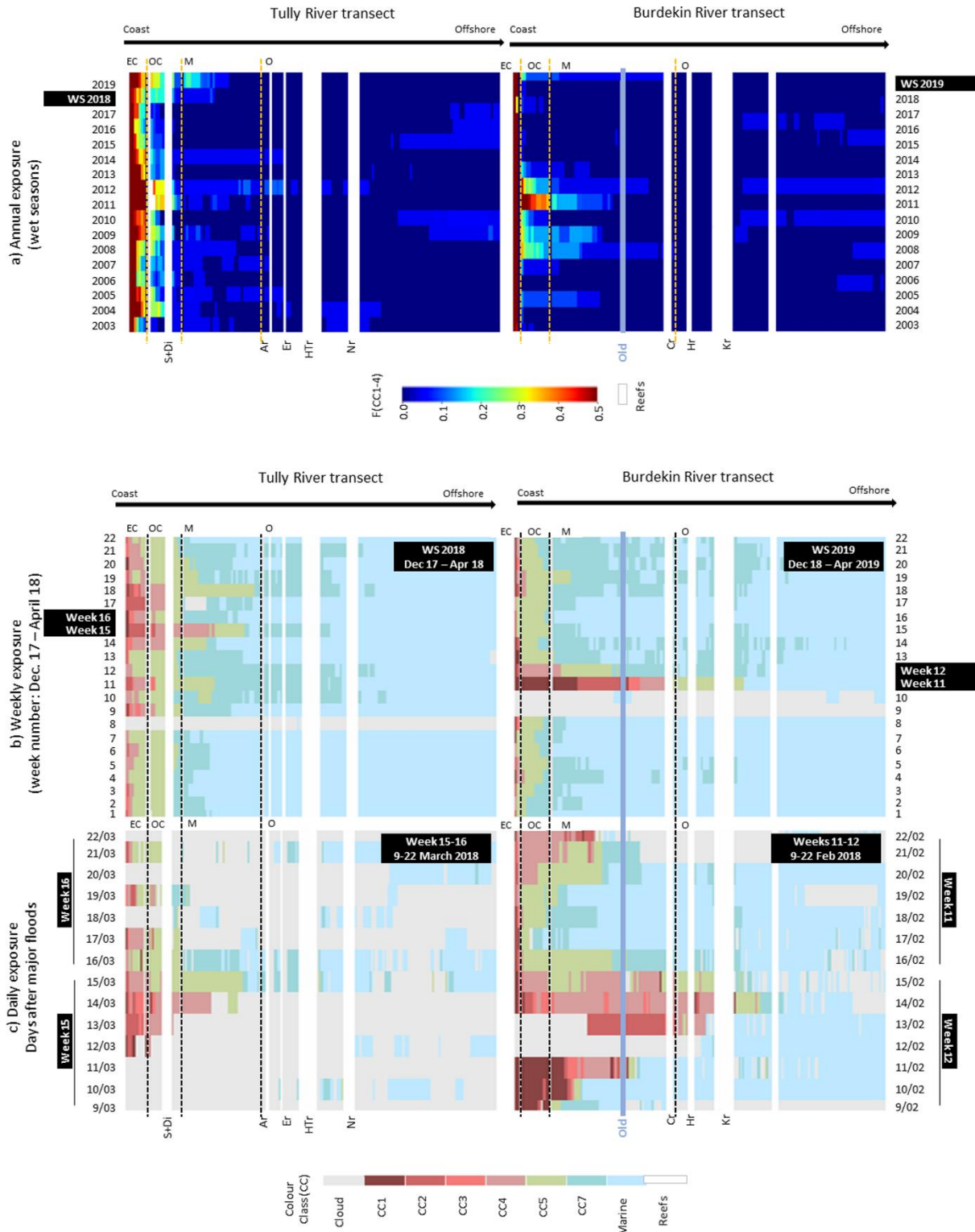
Figure 5.3. Flood frequency and exposure maps for the Tully River (left panel) and Burdekin (right panel) with particular focus on the exposure for the 2018 (Tully) and 2019 (Burdekin) flood events. The EC, OC, M and O refer to the different sections of the GBR shelf including enclosed coastal (EC) and open coastal (OC) from the inner shelf and the Mid-shelf (M) and outer shelf (O). The F(CC1-4) refers to the frequency of Colour Classes (CC) 1-4 (representative of the 'primary' water type), while the other acronyms refer to the various reefs intersected by the transect. These include for the Tully transect: Si+Di = Stingaree Reef and Dunk Island, Er = Ellison Reef, Ar = Adelaide Reef, HTr = Hall Thompson Reef, Nr = Nathan Reef; for the Burdekin transect: Old = Old Reef, Or = Ord Reef, Cr = Charity Reef, Hr = Hope Reef, Kr = Kangaroo Reef.

5.3.2 Mixing of SPM with depth

The SPM concentrations across the Burdekin River estuarine mixing zone for the 11th, 12th, 15th, 20th and 21st February 2019 show patterns consistent with previous sampling years, with the bulk (> 80%) of the SPM falling out by the ~5 to 10 PSU salinity zone. However, the collection of depth samples in the Burdekin flood plume in 2018/19 provided some interesting and somewhat unexpected results. In the past, water quality samples from GBR flood plumes have almost exclusively been collected from the sea surface (with a few exceptions listed previously including Taylor, 1996, 1997; Wu et al. 2006; Wolanski et al. 2008; Bainbridge et al. 2012). Our results demonstrate a decoupling of the SPM-salinity relationship in the depth samples at some sites and over the evolution of the flood plume; this contrasts the general contention that SPM is more concentrated at the lower salinities in the plume. For example, samples collected on the 11th February at the Burdekin mouth site (BUR-13) follow the expected pattern where SPM concentrations of 420 mg.L^{-1} at salinity of 0.1 PSU were recorded for the surface sample whereas and the sample collected from 6 m depth had a much lower SPM concentration of 26 mg.L^{-1} at 33.7 PSU. However, the samples taken on the 20th February at the same location were quite different. The SPM concentration at the surface was 9.2 mg.L^{-1} at 27.2 PSU which was lower than the sample collected from 7 m depth which had a SPM concentration of 45 mg.L^{-1} at a higher salinity of 32.2 PSU. In other cases, SPM concentrations were similar between the surface and depth samples despite a shift towards higher salinities in the deeper water column. Importantly the reduced differentiation between surface and depth SPM samples was recorded at all sites including those most distant from the Burdekin mouth including at Orchard Rocks (off Magnetic Island: surface 2.0 mg.L^{-1}, depth 8.5 mg.L^{-1}), Havannah Island (surface 0.5 mg.L^{-1}, depth 1.3 mg.L^{-1}), midway out to Old Reef (surface 1.0 mg.L^{-1}, depth 2.8 mg.L^{-1}) and at Old Reef (surface 2.7 mg.L^{-1}, depth 1.2 mg.L^{-1}). The surface and depth (within 2 m from the seafloor) sample SPM measurements on the Tully River plume were also very similar (commonly between 1.5 and 7.5 mg.L^{-1}).

5.3.3 Light reduction in flood plumes

Our PAR data profiles from the flood plumes from both the Burdekin and Tully Rivers show light availability was markedly reduced during plume conditions compared to during ambient dry season conditions (Figure 5.4). The CTD casts indicated the euphotic depth (when PAR reaches 1% of the surface value considered to be the threshold of light requirements for benthic phototrophs) may be several metres shallower across large distances in a plume (lines on profiles in Figure 5.4) compared to ambient 'non plume' conditions. Unfortunately, the true surface light readings for these profiles are unavailable; options to best estimate the surface light for these profiles are being investigated. The addition of the surface light will provide more robust quantification on the change in euphotic depth between the ambient and event samples. Hence these plots are only a demonstration of our approach, although the raw data clearly show the substantial relative reduction in light between the ambient and event samples.
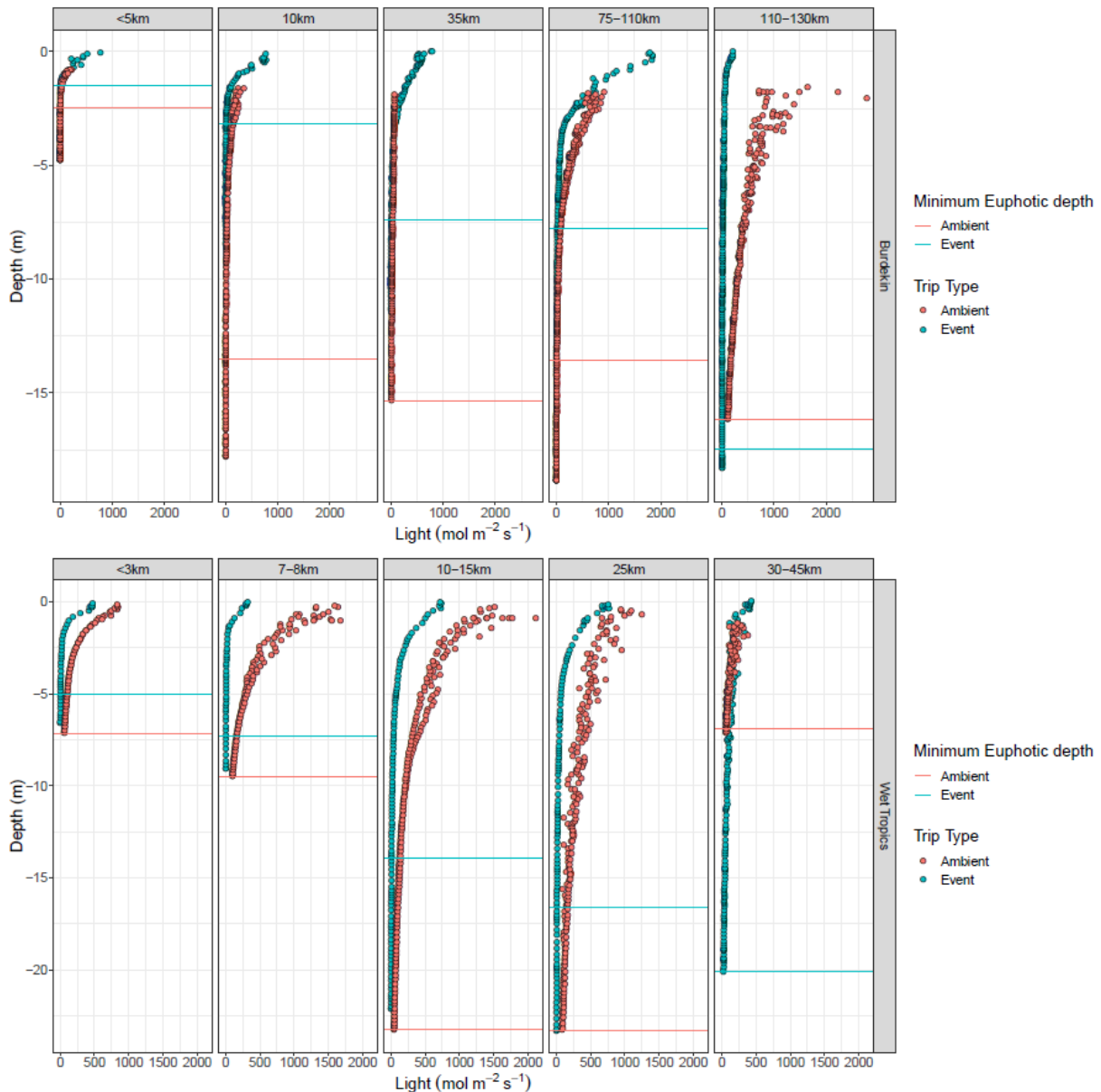
Figure 5.4. PAR-depth profile transects with distance offshore for the Burdekin River (top panels) and Tully River (bottom panels) plumes measured in the 2018/19 and 2017/18 seasons, respectively. Euphotic depth for ambient and event samples marked as lines on the plots. We note that discrepancies between the ambient and event euphotic depths for the 110-130 km Burdekin and 30-45 km Tully profiles (i.e. event euphotic depth is greater than the ambient depth) are due to the different sites (and hence different depths) measured in this sector (i.e. in both cases the ambient site is shallower and the euphotic depth reaches to the seafloor).

5.3.4 Old Reef transect results

The three sites sampled along a transect from the Burdekin River mouth to Old Reef on 15th Feb (Figure 5.5) also showed a salinity gradient in the water column from the surface to the deeper waters. Surface salinities of ~ 31 PSU and bottom depth salinities of ~ 34 PSU were observed in the cast profiles of the two sites closest to the Burdekin mouth (16 and 38 km; Figure 5.6A). However, both sites showed differences where the greatest transition in salinity values took place. The site 16 km off the mouth of the Burdekin showed a fairly sharp transition between 14 and 18 m depth while the site 38 km offshore showed a more gradual transition with the largest change between 7 and 14 m depth. Interestingly, the site at Old Reef (58 km

offshore) had a lens of lower salinity water (~ 30 PSU) in the upper ~ 50 cm of the water column but thereafter displayed a gradual increase in salinity from 32.8 to 33.6 PSU from 0.5 m below the surface to the bottom of the profile at 11.5 m (Figure 5.6A). All the salinity readings from the CTD casts point to at least some influence of freshwater, even in the deeper water column where salinity was ~34 to 34.5 PSU. The PAR profiles suggest very little light penetration through the water column below ~ 5 m depth (Figure 5.6B).
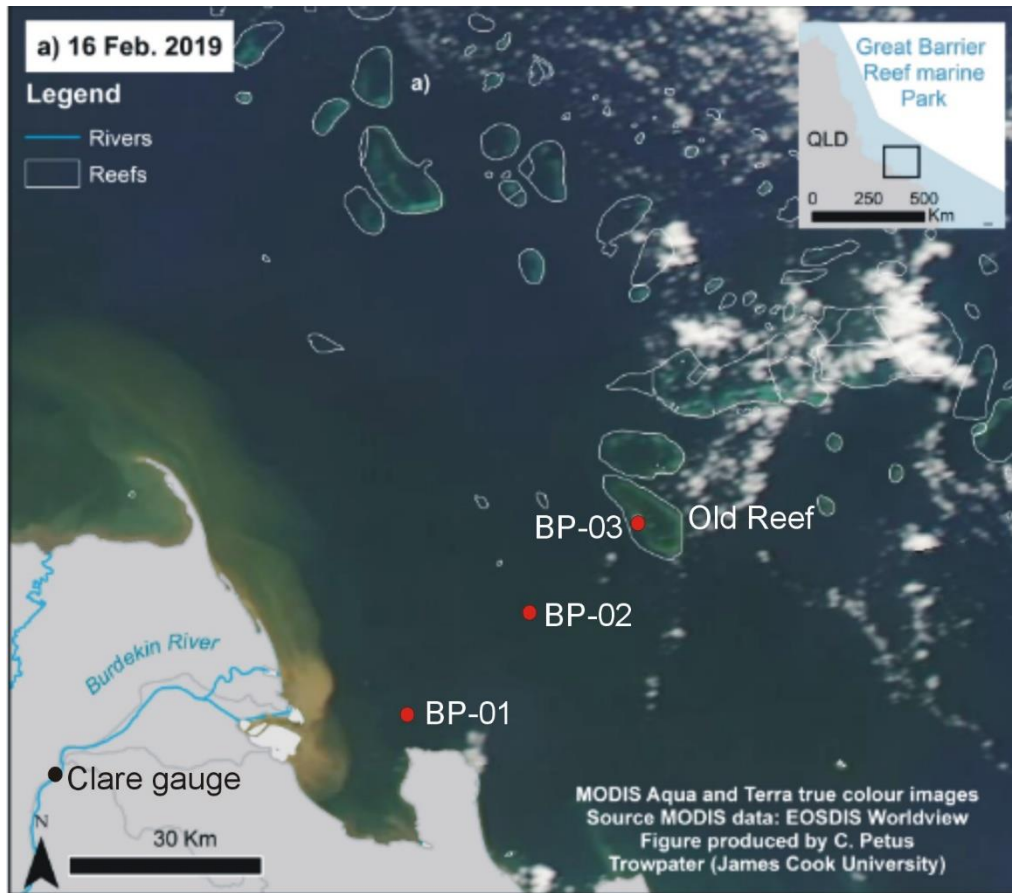
Figure 5.5. Locations of the three sampling sites offshore from the Burdekin River mouth out to Old Reef where surface and depth water quality samples were taken on the 15th Feb 2019.
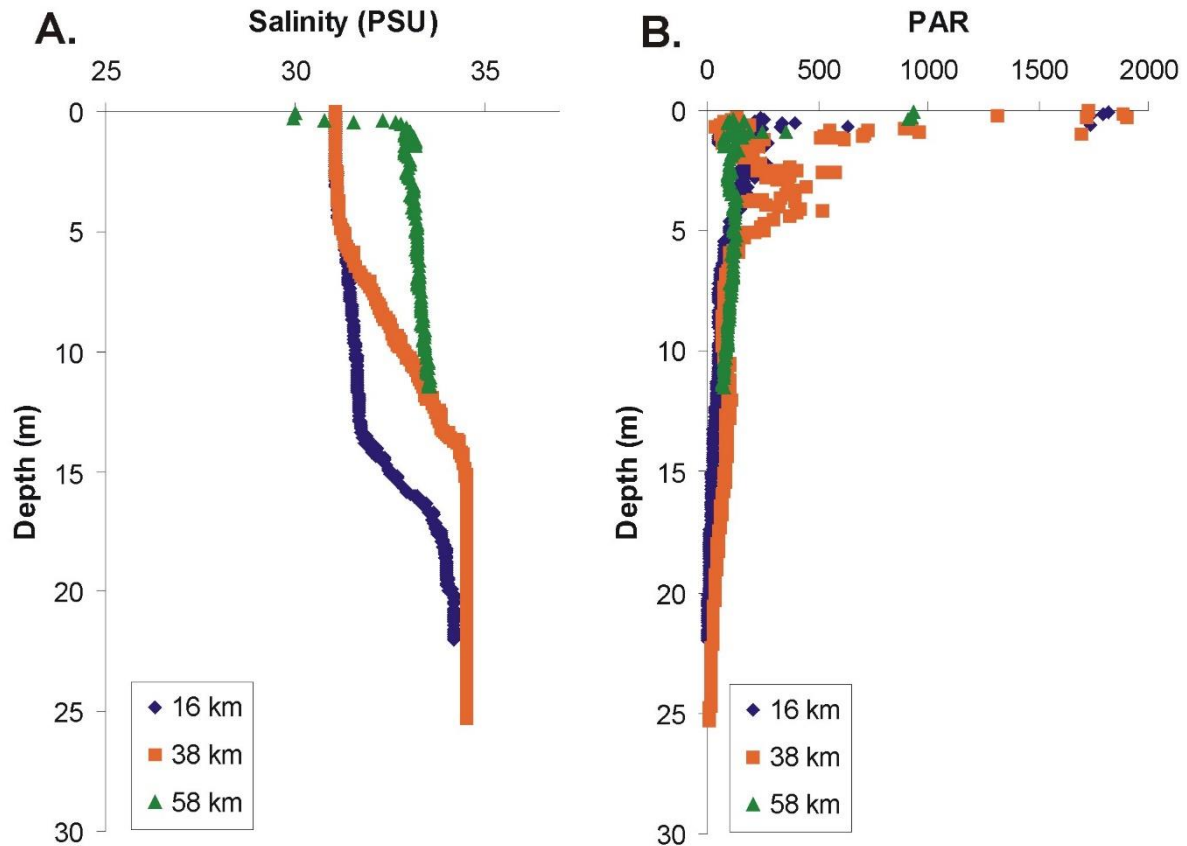
Figure 5.6. Seabird CTD cast salinity (A) and PAR (B) data from a transect of MMP sites sampled on the 15th February 2019 with increasing distance directly offshore from the Burdekin River mouth out to Old Reef on the mid-shelf of the GBR (given in km offshore). The Old Reef site is the cast taken 58 km offshore from the Burdekin mouth.

5.4 Discussion

5.4.1 Plume spatial extents

That flood plume movement in the GBR is predominantly controlled by wind speed and direction is well established from direct (aerial mapping) observations (e.g. Devin et al. 2001; Devlin and Brodie, 2005), satellite imagery (e.g. Devlin and Schaffelke 2009; Brodie et al. 2010) and hydrodynamic modelling (King et al. 2002; Xiao et al. 2019). During periods of low (or slight northerly) winds, river flood plumes typically extend further offshore, potentially reaching mid and outer shelf areas. Multiple lines of evidence (e.g. hydrodynamic modelling and satellite observations) on the recurrence interval of plume development over the mid-shelf show broad agreement, with regional variations largely a function of geographic variability in shelf width. Accordingly, flood plumes discharged by Wet Tropics rivers more regularly reach the mid and outer shelf zones as the continental shelf is much narrower in this region. Hydrodynamic modelling covering the period 1973-1998 suggests that the mid-shelf reefs closest to the mainland in the Wet Tropics are influenced by plumes nearly every year, while sites further offshore receive plume waters every 5-10s years (King et al. 2002). A coral core from Batt Reef on the mid-shelf offshore of the northern Wet Tropics records luminescent lines (i.e. proxy of river plumes) once every 1.2 years (Lough et al. 2002) in accord with the satellite

159

imagery analysis (once every 1.4 years: Figure 5.3). In addition, Devlin and Schaffelke (2009) presented aerial mapping and satellite images demonstrating that the Wet Tropics plumes impinged on the mid and outer shelf on 3 occasions in the 11 events examined between 1994 and 2008, although there analyses focused on the larger events.

In contrast, a frequency interval of 1 in 5 to 1 in 10-years for the Burdekin plume reaching the Old Reef mid-shelf area and a 1 in 3 to 1 in 5-year interval for the mid-shelf reefs further north of the Burdekin (e.g. Britomart and Rib Reefs) was calculated using the King et al. (2002) hydrodynamic model. The coral luminescent line record from Rib Reef suggested a plume influx once every 2.6 years (Lough et al. 2002), which is comparable to the once every 2.1 years calculated from the analysis of satellite imagery (Figure 5.3). The luminescent line record from Britomart Reef is perhaps problematic as it suggests Burdekin plume waters have extended to its location on average once every 12.5 years over the 20th Century (Lough et al. 2015). Importantly, the frequency with which the Burdekin plume has reached Britomart Reef has increased considerably in recent decades, associated with larger and more frequent Burdekin flows (Lough et al. 2015). The frequency interval for the Burdekin plume at Old Reef estimated by King et al. (2002) is also comparable to the once every 5.7 years on average derived from the satellite imagery (Figure 5.3).

While the frequency of plume waters from the Wet Tropics and Burdekin regions reaching the middle shelf (and outer shelf for the Wet Tropics) show broad agreement across different methods of investigation, our new analysis provides insights on the frequency of exposure for primary, secondary and tertiary waters at these locations. Indeed, the frequency of primary plume waters reaching the mid-shelf offshore from both the Burdekin and Wet Tropics regions is much longer than the frequency presented above for 'all plume waters' (Petus et al. 2014b). The water quality of the primary (or brownish) and secondary (or greenish) plume water types commonly exceed guideline values and have mean SPM concentrations of 18.3 (± 45.7) and 5.9 (± 8) mg.L^{-1}, respectively (Gruber et al. 2019). Indeed, during very large river flow events, it is possible that primary and secondary waters persist over parts of the mid-shelf for several weeks.

5.4.2 Plume salinity and SPM mixing and sediment budgets

Our data on SPM concentrations through the water column in plumes identify a far more variable and dynamic pattern than hitherto described, with concentrations ranging from being more concentrated at the surface, well-mixed throughout the water column, or concentrated in higher salinity waters at depth. Generally the Burdekin and Tully plumes become more consistently mixed through the water column with distance offshore, consistent with the international examples described in Geyer et al. (2004). This finding has important implications for our understanding of terrigenous sediment dispersal in the GBR, and on knowledge of the degree of direct sediment exposure at coral reef and seagrass meadow sites. Indeed, the findings provide new insights on how best to monitor SPM concentrations in flood plumes, whereby surface samples and satellite imagery analysis may not provide a holistic measure of (or even underestimate) the exposure and impact of SPM deeper in the water column.

Our new data allows us to revise the first-order calculations of the terrigenous sediment carried in river plumes developed in Larcombe and Woolfe (1999). In that study, it was assumed that plume SPM was solely concentrated in the upper 2 m of the water column. This assumption

was based on measurements made by Taylor (1996) on plumes discharged from the Barron River, and the mass of sediment calculated was compared with potential wind-driven sediment resuspension masses to estimate the relative contribution of both source components. Based on their calculations Larcombe and Woolfe (1999) calculated that the Barron Plume would only contain 9,000 tonnes of sediment (using SPM concentrations of 3-10 mg.L-1, a plume surface area of 450 km^2 and a depth of 2 m) and compared this to 50,000 tonnes of sediment generated by a Cleveland Bay resuspension event (using SPM concentration of 50 mg.L^{-1} over a surface area of 200 km^2 and a depth of 5 m). Our motivation for calculating these budgets is different as our objective was to provide a first-order approximation of the SPM dispersed in the plumes and the SPM mass that could potentially reach the mid-shelf during moderate to large discharge events from both the Burdekin and Tully Rivers.

Based on satellite images we calculated the area influenced by the Burdekin River plume in 2019 to be 7,700 km^2. Assuming an average depth of 20 m (our estimated average depth over the 7,700 km^2 area) and a SPM concentration of 3 mg.L^{-1} (conservative estimate based on mean concentrations measured in the distal plume waters > 50 km from river mouth) we calculate the plume sediment mass to be in the order of 460,000 tonnes. This mass is ~ 6% of the total sediment load (~7.1 million tonnes) estimated from the Burdekin River over the 2018/19 water year (Gruber et al. 2019) and is lower than the 10% of the load estimated to move beyond the Burdekin mouth by Lewis et al. (2014) and the ~ 20% calculated in the modelling of the 2007 plume (Delandmeter et al. 2015). This conservative first-order sediment budget does not take into account the Burdekin plume 'cumulative SPM' loading that is continuously delivered throughout the plume event duration, and would replenish the existing SPM that settled onto the seafloor. Further, the SPM concentrations used are conservative based on measurements in the plume (our mean for the middle and outer reaches of the Burdekin plume was in the order of 5 mg.L^{-1}); however, the lower concentration used was an attempt to only consider the terrigenous sediment delivered from the Burdekin River (i.e. to compare to the load measured at the end of river) and not the 'new organic' sediment (i.e. diatoms and the organic component of flocs) created in the plume waters. In any case, this approximation largely supports the sediment budgets produced by various modelling exercises (e.g. Delandmeter et al. 2015; Margvelashvili et al. 2018).

When the same approach is applied to only examine the period when the Burdekin plume moved out towards and over Old Reef on the middle shelf we calculate a mass in the order of 100,000 tonnes. This mass is likely much less than 5% of the load delivered by the Burdekin during this period of peak discharge, but could be considered a conservative estimation of the SPM delivered to the middle shelf in 2019. More sophisticated modelling will help provide a better quantification of the total terrigenous sediment mass reaching the middle shelf.

Interestingly, using a similar approach for the 2018 Tully plume (1,200 km^2 area by 20 m depth (average depth over the area) and SPM of 3 mg.L^{-1}) which impinged on the mid-shelf we calculated a terrigenous sediment mass of 72,000 tonnes. While this mass is much lower than the 2019 Burdekin plume, it represents a much higher proportion of the total sediment load exported from the Tully River in the 2017/18 water year (110,000 tonnes). This finding provides additional evidence to support the hypothesis that a much lower proportion of terrigenous sediment is deposited near the mouth of the Tully River compared to the Burdekin. We note that as for the Burdekin, this calculation only provides a first-order approximation and modelling would improve quantification of the sediment mass and potentially separate the contributions

of the neighbouring Wet Tropics rivers (e.g. in this case particularly the Herbert and Murray Rivers).

5.4.3 Light reduction in flood plumes

Our data show that compared to ambient conditions, euphotic depth is reduced by several metres at locations 10s to 100s of kilometres offshore from the river mouths during periods of flood plume incursion (Figures 5.4 & 5.6B). This has implications for benthic phototrophs such as corals and seagrass that have specific light requirements in which prolonged exposure to diminished light may reduce the depth/area of distribution (e.g. Petus et al. 2014a). Importantly, the reduction in euphotic depth shown in this study commonly coincides with SPM concentrations in the plume of < 5 mg.L^{-1} which have previously been described as 'low' and inferred to be ecologically benign (e.g. Orpin and Ridd, 2012). Indeed, under large flood conditions, some mid-shelf areas, and in particular autotrophs growing > 5 m depth, may experience suppressed light from the plumes for several weeks. These data suggest the influence of flood plumes – including those with 'low' SPM concentrations - requires reconsideration. Future work will examine the relative (to ambient conditions) reductions in euphotic depth under primary, secondary and tertiary plume colour class conditions (e.g. Petus et al. 2018).

5.4.4 Broader implications of the results

Until the recent work of Fabricius et al. (2014, 2016) and Margvelashvili et al. (2018), it was generally thought that SPM delivered in river plumes had little effect on the mid and outer shelf zones of the GBR. Indeed, there are few accounts of plumes reaching these areas prior to satellite imagery (see Devlin et al. 2001). Sedimentological investigations conclude that the mid-shelf of the GBR is sediment-starved and dominated by old remnant sediments rather than recent deposits (Belperio, 1983). Furthermore, sediment cores from mid and outer shelf reefs revealed little to no evidence of fine-grained terrigenous sediment accumulation (e.g. Davies and Hopley, 1983), although it must be noted that these cores were collected via the rotary coring method which allow very limited recovery of any fine grained terrigenous sediments which may (or may not) be present (see Ryan et al. 2018). While the mid-shelf of the GBR is clearly a zone of limited new terrigenous sediment accumulation, it is possible that the terrigenous sediment delivery and influence has to date been underestimated.

Our conservative first-order approximations of the mass of terrigenous sediment that may reach mid-shelf areas of the GBR suggest unsurprisingly that the Burdekin plume carries more sediment in large events because of its larger discharge (and coverage of a greater area) and its higher sediment loads. However, when the frequency of such events are considered, the mass of terrigenous sediment delivered to the mid-shelf offshore from the more frequently flooding Wet Tropics rivers may be similar to the Burdekin. Indeed, mid-shelf reef structures may represent preferential sediment accumulation areas for SPM carried in flood plumes due to their baffling effect and new investigations in these areas should employ coring techniques that are conducive to recovering fine-grained terrigenous sediments (e.g. Browne et al. 2012; Perry et al. 2012; Ryan et al. 2018). Only then will we have a more complete picture on the influence of terrigenous sediment on the middle shelf.

The most critical question to resolve (at least on a finer scale) is to quantify the influence of SPM deemed to derive from an anthropogenic source. Our first order sediment budget

approximations provide some guidance for future modelling approaches to help answer this question. For example, the loads of terrigenous sediment delivered from the Burdekin River have increased by 5 to 10 fold since European settlement (Kroon et al. 2012; Lewis et al. 2014). If we assume that this increase is in proportion to the amount of sediment transported beyond the initial deposition zone near the mouth of the river then our first approximation would be that 360,000 to 410,000 tonnes of the 460,000 tonnes (i.e. the sediment mass calculated for the 2019 flood plume) would be anthropogenic. Using back calculations (of the 360,000 to 410,000 tonnes range) from this initial approach (i.e. plume area and average depth), we produce an anthropogenic SPM concentration range of 2.3 to 2.7 mg.L^{-1}. In addition, the evidence of larger Burdekin flood events in the past 50 years compared to the ~350 year record (Lough et al. 2015) would not only coincide with higher sediment loadings but also result in a greater plume extent in the GBR (and hence increase the frequency of influence on the mid-shelf). We note that these are very preliminary estimates and the dynamics of SPM behaviour in the estuarine mixing zone are not fully understood (e.g. Geyer et al. 2004); for example, additional sediment concentrations in the water column from increased loadings would provide more opportunity for the collision of individual particles to form more flocs potentially leading to increased sediment deposition at the mouth. Because of these uncertainties we refrain from speculating on the potential effects of the anthropogenic sediment that travels further afield, other than point out that our data suggests that even a small increase in SPM concentrations (i.e. 2 to 3 mg.L^{-1}) will significantly reduce light availability for several metres in the water column with potentially large implications for coral reefs and seagrasses (e.g. Chartrand et al. 2016; Bainbridge et al. 2018).

5.5 Conclusions

This case study examined the dispersal of SPM within river plumes over the estuarine mixing zone under different environmental conditions. We show that the dispersal of SPM was more variable but generally mixed throughout the water column with increasing distance offshore. SPM concentrations previously considered 'low' in some studies (i.e. < 5 mg.L^{-1}) had a considerable influence on light attenuation in the water column. First order approximations of the mass of sediment transported further offshore from plumes suggest that while the Burdekin carries more sediment, the level of exposure on the middle shelf may be similar to the Wet Tropics plumes due to the difference in plume frequencies for these regions (i.e. more frequent in the Wet Tropics). Further sediment coring of mid-shelf reefs is required to better quantify the level of terrigenous sediment exposure in this section of the GBR. Our conservative first-order sediment budget approximations provide some insights however a more sophisticated modelling approach is required to better understand the potential impacts of newly delivered anthropogenic terrigenous sediment on the GBR middle shelf.

Acknowledgements

References

Álvarez-Romero, J.G., Devlin, M., da Silva, E.T., Petus, C., Ban, N.C., Pressey, R.L., Kool, J., Roberts, J.J., Cerdeira-Estrada, S., Wenger, A.S. and Brodie, J., 2013. A novel approach to model exposure of coastal-marine ecosystems to riverine flood plumes based on remote sensing techniques. *Journal of Environmental Management*, *119*, 194-207.

APHA (2005) Standard methods for the examination of water and wastewaters, 21st edn., American Public Health Association, American Water Works Association and Water Environment Federation, Washington, USA.

Bainbridge, Z.T., Wolanski, E., Álvarez-Romero, J.G., Lewis, S.E. and Brodie, J.E., 2012. Fine sediment and nutrient dynamics related to particle size and floc formation in a Burdekin River flood plume, Australia. *Marine pollution bulletin*, *65*, 236-248.

Bainbridge, Z. Lewis, S. Bartley, R. Fabricius, K. Collier, C. Waterhouse, J. Garzon-Garcia, A. Robson, B. Burton, J. Wenger, A. Brodie, J. 2018. Fine sediment and particulate organic matter: a review and case study on ridge-to-reef transport, fates, and impacts on marine ecosystems. *Marine Pollution Bulletin* 135, 1205-1220.

Belperio, A.P., 1983. Terrigenous sedimentation in the central Great Barrier Reef lagoon: A model from the Burdekin Region. BMR J. Geol. Geophys. 8, 179-190.

Brodie, J., Schroeder, T., Rohde, K., Faithful, J., Masters, B., Dekker, A., Brando, V. and Maughan, M., 2010. Dispersal of suspended sediments and nutrients in the Great Barrier Reef lagoon during river-discharge events: conclusions from satellite remote sensing and concurrent flood-plume sampling. *Marine and Freshwater Research*, *61*(6), pp.651-664.

Browne, N.K., Smithers, S.G. and Perry, C.T., 2012. Coral reefs of the turbid inner-shelf of the Great Barrier Reef, Australia: an environmental and geomorphic perspective on their occurrence, composition and growth. *Earth-Science Reviews*, *115*(1-2), pp.1-20.

Chartrand, K.M., Bryant, C.V., Carter, A.B., Ralph, P.J. and Rasheed, M.A., 2016. Light thresholds to prevent dredging impacts on the Great Barrier Reef seagrass, Zostera muelleri ssp. capricorni. *Frontiers in Marine Science*, *3*, p.106.

Dagg, M., Benner, R., Lohrenz, S. and Lawrence, D., 2004. Transformation of dissolved and particulate materials on continental shelves influenced by large rivers: plume processes. *Continental Shelf Research*, *24*, 833-858.

Davies, P.J. and Hopley, D., 1983. Growth fabrics and growth-rates of Holocene reefs in the Great Barrier-Reef. *BMR Journal of Australian Geology & Geophysics*, *8*(3), pp.237-251.

Delandmeter, P., Lewis, S.E., Lambrechts, J., Deleersnijder, E., Legat, V. and Wolanski, E., 2015. The transport and fate of riverine fine sediment exported to a semi-open system. *Estuarine, Coastal and Shelf Science*, *167*, 336-346.

Devlin, M.J. and Brodie, J., 2005. Terrestrial discharge into the Great Barrier Reef Lagoon: nutrient behavior in coastal waters. *Marine pollution bulletin*, *51*, 9-22.

Devlin, M. and Schaffelke, B., 2009. Spatial extent of riverine flood plumes and exposure of marine ecosystems in the Tully coastal region, Great Barrier Reef. *Marine and Freshwater Research*, *60*(11), pp.1109-1122.

Devlin, M., Waterhouse, J., Taylor, J. and Brodie, J., 2001. Flood plumes in the Great Barrier Reef: spatial and temporal patterns in composition and distribution. *GBRMPA research publication*, *68*.

Devlin, M.J., McKinna, L.W., Alvarez-Romero, J.G., Petus, C., Abott, B., Harkness, P. and Brodie, J., 2012. Mapping the pollutants in surface riverine flood plume waters in the Great Barrier Reef, Australia. *Marine pollution bulletin*, *65*, 224-235.

Devlin, M., Petus, C., Da Silva, E., Tracey, D., Wolff, N., Waterhouse, J. and Brodie, J., 2015. Water quality and river plume monitoring in the Great Barrier Reef: an overview of methods based on ocean colour satellite data. *Remote Sensing*, *7*, 12909-12941.

Geyer, W.R., Hill, P.S. and Kineke, G.C., 2004. The transport, transformation and dispersal of sediment by buoyant coastal flows. *Continental Shelf Research*, *24*(7-8), pp.927-949.

Gruber, R., Waterhouse, J., Logan, M., Petus, C., Howley, C., Lewis, S., Tracey, D., Langlois, L., Tonin, H., Skuza, M., Costello, P., Davidson, J., Gunn, K., Lefevre, C., Shanahan, M., Wright, M., Zagorskis, I., Kroon, F., Neilen, A., 2019, *Marine Monitoring Program: Annual Report for Inshore Water Quality Monitoring 2018-19. Report for the Great Barrier Reef Marine Park Authority*, Great Barrier Reef Marine Park Authority, Townsville.

Howley, C., Devlin, M. and Burford, M., 2018. Assessment of water quality from the Normanby River catchment to coastal flood plumes on the northern Great Barrier Reef, Australia. *Marine and Freshwater Research*, *69*, 859-873.

King, B. McAllister, F. Done, T. 2002. *Modelling the impact of the Burdekin, Herbert, Tully and Johnstone River plumes on the Central Great Barrier Reef*. CRC Reef Research Centre Technical Report No 44, CRC Reef Research Centre, Townsville.

Kroon, F.J., Kuhnert, P.M., Henderson, B.L., Wilkinson, S.N., Kinsey-Henderson, A., Brodie J.E., Turner R.D.R., 2012. River loads of suspended solids, nitrogen, phosphorus and herbicides delivered to the Great Barrier Reef lagoon. Mar. Pollut. Bull. 65, 167-181.

Larcombe, P. and Woolfe, K.J., 1999. Increased sediment supply to the Great Barrier Reef will not increase sediment accumulation at most coral reefs. *Coral reefs*, *18*(2), pp.163-169.

Larcombe, P. and Carter, R.M., 2004. Cyclone pumping, sediment partitioning and the development of the Great Barrier Reef shelf system: a review. *Quaternary Science Reviews*, *23*(1-2), pp.107-135.

Lewis, S. Brodie, J. Ledee, E. Alewijnse M. 2006. *The Spatial Extent of Delivery of Terrestrial Materials from the Burdekin Region in the Great Barrier Reef Lagoon*. ACTFR Report No. **06/02** for the Burdekin Dry Tropics NRM, Australian Centre for Tropical Freshwater Research, James Cook University, Townsville.

Lewis, S.E., Olley, J., Furuichi, T., Sharma, A. and Burton, J., 2014. Complex sediment deposition history on a wide continental shelf: Implications for the calculation of accumulation rates on the Great Barrier Reef. *Earth and Planetary Science Letters*, *393*, 146-158.

Lough, J., Barnes, D. and McAllister, F., 2002. Luminescent lines in corals from the Great Barrier Reef provide spatial and temporal records of reefs affected by land runoff. *Coral reefs*, *21*(4), pp.333-343.

Lough, J.M. Lewis, S.E. Cantin, N.E. 2015. Freshwater impacts in the central Great Barrier Reef: 1648-2011. *Coral Reefs* 34, 739-751.

Margvelashvili, N., Andrewartha, J., Baird, M., Herzfeld, M., Jones, E., Mongin, M., Rizwi, F., Robson, B.J., Skerratt, J., Wild-Allen, K. and Steven, A., 2018. Simulated fate of catchment-derived sediment on the Great Barrier Reef shelf. *Marine pollution bulletin*, *135*, 954-962.

Orpin, A.R., Ridd, P.V. and Stewart, L.K., 1999. Assessment of the relative importance of major sediment-transport mechanisms in the central Great Barrier Reef lagoon. *Australian Journal of Earth Sciences*, *46*(6), pp.883-896.

Orpin, A.R. and Ridd, P.V., 2012. Exposure of inshore corals to suspended sediments due to wave-resuspension and river plumes in the central Great Barrier Reef: a reappraisal. *Continental Shelf Research*, *47*, pp.55-67.

Perry, C.T., Smithers, S.G., Gulliver, P. and Browne, N.K., 2012. Evidence of very rapid reef accretion and reef growth under high turbidity and terrigenous sedimentation. *Geology*, *40*(8), pp.719-722.

Petus, C., Collier, C., Devlin, M., Rasheed, M. and McKenna, S., 2014a. Using MODIS data for understanding changes in seagrass meadow health: a case study in the Great Barrier Reef (Australia). *Marine environmental research*, *98*, 68-85.

Petus, C., da Silva, E.T., Devlin, M., Wenger, A.S. and Álvarez-Romero, J.G., 2014b. Using MODIS data for mapping of water types within river plumes in the Great Barrier Reef, Australia: Towards the production of river plume risk maps for reef and seagrass ecosystems. *Journal of environmental management*, *137*, 163-177.

Petus, C., Devlin, M., Thompson, A., McKenzie, L., Teixeira da Silva, E., Collier, C., Tracey, D. and Martin, K., 2016. Estimating the exposure of coral reefs and seagrass meadows to land-sourced contaminants in river flood plumes of the Great Barrier Reef: Validating a simple satellite risk framework with environmental data. *Remote Sensing*, *8*(3), p.210.

Petus, C., Devlin, M., da Silva, E.T., Lewis, S., Waterhouse, J., Wenger, A., Bainbridge, Z. and Tracey, D., 2018. Defining wet season water quality target concentrations for ecosystem conservation using empirical light attenuation models: A case study in the Great Barrier Reef (Australia). *Journal of environmental management*, *213*, pp.451-466.

Petus, C. Waterhouse, J. Lewis, S. Vacher, M. Tracey, D. Devlin, M. 2019. A flood of information: using Sentinel-3 water colour products to assure continuity in the monitoring of water quality trends in the Great Barrier Reef (Australia). *Journal of Environmental Management* 248, 109255.

Ryan, E.J. Smithers, S.G. Lewis, S.E. Clark, T.R. Zhao, J-x. Hua, Q. 2018. Fringing reef growth over a shallow last interglacial reef foundation at a mid-shelf high island: Holbourne Island, central Great Barrier Reef. *Marine Geology* 398, 137-150.

Schroeder, T., Devlin, M.J., Brando, V.E., Dekker, A.G., Brodie, J.E., Clementson, L.A. and McKinna, L., 2012. Inter-annual variability of wet season freshwater plume extent into the Great Barrier Reef lagoon based on satellite coastal ocean colour observations. *Marine pollution bulletin*, *65*, 210-223.

Soja-Woźniak, M., Baird, M., Schroeder, T., Qin, Y., Clementson, L., Baker, B., Boadle, D., Brando, V. and Steven, A.D., 2019. Particulate backscattering ratio as an indicator of changing particle composition in coastal waters: observations from Great Barrier Reef waters. *Journal of Geophysical Research: Oceans*.

Taylor, J., 1996. Sediment input to the Great Barrier Reef lagoon via river discharge: the Barron River. *Great Barrier Reef: Terrigenous Sediment Flux and Human Impacts.*

Taylor, J., 1997. Nutrient distribution in the Barron River and offshore during cyclone Sadie. In *Workshop series. Great Barrier Reef Marine Park Authority* (No. 22, pp. 17-26).

Thompson, A., Schroeder, T., Brando, V.E. and Schaffelke, B., 2014. Coral community responses to declining water quality: Whitsunday Islands, Great Barrier Reef, Australia. *Coral Reefs*, *33*, 923-938.

Wolanski, E. and Jones, M., 1981. Physical properties of Great Barrier Reef lagoon waters near Townsville. I. Effects of Burdekin River floods. *Marine and Freshwater Research*, *32*, 305-319.

Wolanski, E. and Van, S.D., 1983. Mixing of Burdekin river flood waters in the Great Barrier Reef. *Marine and Freshwater Research*, *34*, 49-63.

Wolanski, E., Fabricius, K.E., Cooper, T.F. and Humphrey, C., 2008. Wet season fine sediment dynamics on the inner shelf of the Great Barrier Reef. *Estuarine, Coastal and Shelf Science*, *77*(4), pp.755-762.

Woolfe, K.J., and Larcombe, P. 1998. Terrigenous sediment accumulation as a regional control on the distribution of reef carbonates. In Camoin, G.F. and Davies, P.J. (Eds), *Reefs and carbonate platforms in the Pacific and Indian Oceans* (Vol. 25, pp. 295-310). Blackwell Science Publications.

Wu, J., Ametistova, L., Heron, M., Lemckert, C.J. and Kalangi, P., 2006. Finite dispersal of a separative nepheloid plume by an internal hydraulic jump in a tropical mountainous river estuary. *Journal of Geophysical Research: Oceans*, *111*(C11).

Xiao, Y., Wang, X.H., Ritchie, E.A., Rizwi, F. and Qiao, L., 2019. The development and evolution of the Burdekin River estuary freshwater plume during Cyclone Debbie (2017). *Estuarine, Coastal and Shelf Science*, *224*, 187-196.

CHAPTER 6

The shift in the chemical composition of particulate organic matter and microbial community from catchment to reef

Chengrong Chen[1], Mohammad Bahadori[1], Mehran Rezaei Rashti[1], Thomas Stevens[2] and Stephen Lewis[2]

[1] Australian Rivers Institute Griffith University
[2] Catchment to Reef Research Group, TropWATER, James Cook University

Summary

This study aimed to explore the shift in the chemical composition and bioavailability of particulate organic matter from terrestrial to marine environment using isotopic ($\delta^{15}N$, $\delta^{13}C$) and ^{13}C nuclear magnetic resonance (^{13}C-NMR) spectroscopy approaches. The change in the microbial community and composition was also examined using DNA sequencing to provide more insights into the origin and fate of sediments and associated organic matter during their transportation from soil to freshwater and eventually into the GBR lagoon. The key results included:

a) Soils, freshwater plume sediments and marine sediments showed distinct patterns of ^{13}C NMR spectra. ^{13}C NMR spectra showed that soil samples from different land uses were more enriched in labile fractions (e.g., carbohydrates), while marine sediments were more enriched in the recalcitrant organic carbon fractions (e.g., aliphatic compounds). The ^{13}C NMR signatures of freshwater plume samples from three rivers (the Johnstone, Tully and Burdekin) were quite similar to soil samples, indicating their terrestrial origin.

b) Soil organic matter had different isotopic signatures ($\delta^{13}C$ and $\delta^{15}N$) compared to marine sediments. Freshwater plume sediments collected from the Burdekin River were more enriched in $\delta^{13}C$ compared to those collected from the Johnstone and Tully Rivers. The variation in the $\delta^{13}C$ values of plume sediments originating from the Dry and Wet Tropics regions are due to the dominant vegetation types in these catchments. The C_3 plants (*e.g.,* forest and bananas) are dominant in the Johnstone and Tully catchments while the majority of the Burdekin catchment is grassland (C_4 plants).

c) Microbial community and composition significantly changed along the sediment transportation pathway from soil to freshwater and marine environment. Proteobacteria, Actinobacteria and Acidobacteria were predominant groups of bacteria in soil and freshwater plume sediments. In the marine environment, Protobacteria and Bacteroidetes were dominantly associated with seawater plume and trap sediments.

The change in the microbial community composition was due to the shift in environmental factors (e.g., pH and salinity) and chemical composition of organic matter from soil to freshwater to the marine environment.

d) Bacteria to fungi gene copy number ratio increased along the salinity gradient from the end of Burdekin River (freshwater) to primary and secondary plume sediments. For the Tully River, the bacteria/fungi ratio dramatically increased from primary plume to secondary plume.

e) The results of this study have significant implications for scientists, managers and policy makers and provide a better understanding of the origin and fate of terrestrially derived organic matter in the GBR lagoon which is critical for developing targeted management to improve water quality in the GBR.

6.1 Introduction

Sediments and associated organic components are transported to the ocean through the rivers and eventually buried in the marine environment. Through this pathway, chemical and biological interactions occur such as organic matter (OM) decomposition, organic nutrient mineralisation and transformation, aquatic plant and microbial uptake and immobilisation. Rivers comprise a small proportion of the catchment area, however all the catchment runoff must pass through the streams to open oceans. The terrestrial-derived organic carbon (OC) and nutrients (e.g., N) find their way into streams through both channel interception and surface (or subsurface) runoff.

The terrestrial-derived OC and nutrients associated with sediments pass through several transition zones (hot spots) such as soils-freshwater-seawater before discharging into the marine environment of the GBR lagoon. The hydrological, ecological and biogeochemical processes are strongly coupled through these hot spots, and together act like successive filters in which a significant fraction of the nutrients are retained and transported from catchment to reef (Billen et al. 1991). Any changes in the primary form of nutrients and sediments along this transition can strongly affect the water quality within an ecosystem and thus may change the whole ecosystem structure (Richardson and Qian 1999).

A variety of biotic and abiotic interactions impact different chemical forms of OC and nutrients within a stream. For example, primary production of different organisms such as fungi, algae and bacteria immobilise and take nutrients out of the water column. These nutrients are subsequently returned to the stream by plant materials, particulate OM and through the various chemical and biological processes such as decomposition and mineralisation. The main abiotic processes within a stream include adsorption onto sediments (Bencala et al. 1984), leaching from organic materials, formation of particulates from dissolved materials, and deposition of particles (Mulholland 1981). Dynamical structure of an aquatic ecosystem is dependent on environmental factors such as geographical position, precipitation and temperature. Any change in dynamical structure of an ecosystem can affect the absolute amount and chemical composition of OC and nutrients reaching to the GBR lagoon by influencing physical forces, or the balance among organisms living in that ecosystem.

Because river networks link terrestrial landscapes to oceans, perturbations to river ecosystems can have large consequences for biogeochemical cycling at local, regional, and global scales. It can also change the ratio in which C, N and P, in both dissolved and particulate OM, are being transferred from terrestrial ecosystems to the ocean (Ensign and Doyle 2006). Any change in the absolute amount of C, nutrients and also the chemical forms of each element reaching the GBR lagoon can influence the rates of photosynthetic and heterotrophic productivity and lead to fundamental changes to the aquatic food web (Vollenweider, Rinaldi, and Montanari 1992).

To take all the above-mentioned factors into account, it is necessary to investigate the biogeochemical processes that OC and nutrients undergo during their transportation from soil and along the river from upstream catchments to the GBR lagoon. This approach improves our understanding of the key biogeochemical processes in different ecosystems as well as the transition hot spots from catchment to reef. Such a conceptual model would also help us to find out about how OC and nutrients behave through transition zones from terrestrial to marine ecosystems.

Aims of this study were to:

a) investigate the changes in the chemical composition and labile fraction of organic matter associated with soil and sediments during transportation from soil to freshwater and marine environment using ^{13}C nuclear magnetic resonance (^{13}C-NMR) spectroscopy and isotopic signatures (δ^{13}C and δ^{15}N).

b) examine the shift in the microbial community composition and the ratio of bacteria to fungi along the salinity gradient from freshwater to marine environment using Quantitative Real-Time Polymerase Chain Reaction (qPCR)

6.2 Methodology

Soil and sediment sampling and preparation

In this study, soil samples were collected from the topsoil and subsoil of land uses that potentially contribute sediments and particulate N to the river during rainfall events and then transported downstream. Four potential land use sources (grazing, sugarcane, forest and banana) were identified and sampled in the Johnstone and Burdekin catchments. For collecting a representative group of soil samples from the Johnstone catchment, several sampling points were selected throughout the catchment. Grazing and forest soil samples were exclusively collected from the upper catchment, while banana soil samples were collected from the lower catchment. Sugarcane soil samples were collected from both the upper and lower Johnstone catchment. Sampling locations for different sources were selected using maps prepared by ArcGIS (10.0) (Bahadori et al. 2018). Burdekin soil samples were collected from grazed Bowen sub-catchment.

Soil samples were air dried, gently crushed using a pestle and mortar and then passed through a 63 μm sieve. Before that, the collected samples were passed through 4 mm and then 2 mm sieves and all physically visible fragments such as root and litters were removed from samples (Collins, Walling, and Leeks 1997). Plume samples were centrifuged upon their arrival at the

laboratory to recover as much sediment as possible from the buckets, and then were freeze dried prior to chemical analyses. There was no need for passing suspended sediments through a sieve as they were already less than 63 µm in size. Subsamples were also collected and stored at -80 °C until DNA extraction.

Stable isotopes and geochemical analysis

In accordance with the procedure for measuring the stable isotope $\delta^{15}N$, all soil and sediments were pelletized in tin capsules. For $\delta^{13}C$, first inorganic carbonates were removed by shaking the small aliquot (2–5 g of each sample) with 2 ml of 10% hydrochloric acid (HCl) and allowing the suspension to stand overnight. More HCl was added to the samples until no further effervescence occurred. The sample was finely ground in a mortar and pestle after being dried at 60°C for 48 h. The samples were then pelletized in silver capsules and weighed for analysis with a Sercon Hydra 20-22 Europa EA-GSL isotope-ratio mass spectrometer. Stable isotope ratios are reported in standard delta (δ) notation per mil (‰) as: $\delta X = [(Rsample/Rstandard)-1] \times 1000$, where X is ^{13}C or ^{15}N and $R = ^{13}C/^{12}C$ or $^{15}N/^{14}N$, respectively.

Hydrofluoric acid pre-treatment of soil and sediment samples and carbon-13 solid state NMR spectroscopy

Pre-treatment of soil and sediment samples with HF before solid-state ^{13}C CPMAS NMR analysis removes substantial amounts of Fe^{2+} and Mn^{2+} in soil and concentrates the organic matter content of the whole sample, improving the signal/noise ratio. In this study, all soil and sediment samples for NMR analysis were pre-treated with 5% HF. Solid-state ^{13}C CPMAS NMR spectra of the HF treated soils were obtained at a frequency of 100.6 MHz on a 300 MHz Varian VNMRS spectrometer (Varian Inc.,CA). Samples were packed in a silicon nitride rotor (optical density=7mm) and spun at 5 kHz at the magic angle. Single contact times of 2 ms were applied, with an acquisition time of 14 ms, and a recycle delay of 1.5 s. Approximately 20,000 transients were collected for all samples and a Lorentzian line broadening function of 150 Hz was applied to all spectra. Chemical shift values were referenced externally to hexamethylbenzene at 132.1 ppm, which is equivalent to tetramethylsilance at 0 ppm. The solid-state ^{13}C CPMAS NMR spectra were divided into the seven common chemical shift regions: aliphatic C (0-45 ppm), methoxyl C (45-60 ppm), carbohydrate C (60-90 ppm), di-o-alkyl (90-110 ppm), aryl C (110-145 ppm), O aryl C (145-160 ppm) and carboxyl C (160-180 ppm) and the relative intensity for each region was determined by integration using Varian NMR 3.1A software package (Chen, Xu, and Mathers 2004).

DNA extraction and sequencing

The total genomic DNA was extracted from 0.3-0.5 g of frozen soil using MoBio Powersoil DNA isolation kit following the manufacturer`s instruction. 10-fold dilution of DNA template was used for downstream PCR analysis to reduce PCR inhibitors such as humic acid.

The V4 domain of bacterial 16S rRNA genes was amplified by PCR using the universal primer pair 515F (5´-NNNNNNNNNGTGTGCCAGCMGCCGCGGTAA-3´) and 806R (5´-GGACTACHVGGGTWTCTAAT-3´). PCR was conducted in a total volume of 30 mL containing 15 mL of Phusion® High-Fidelity PCR Master Mix (NEB, Ipswich, MA, USA), 0.2 mM of forward and reverse primers, and ~10 ng DNA template; each PCR run included a negative control. Thermal cycling conditions were as follows: initial denaturation at 94 °C for 3 min, 35 cycles of

denaturation at 94 °C for 45 s, annealing at 50 °C for 1 min, and extension at 72 °C for 1.5 min, and a final extension at 72 °C for 10 min. The amplified products were checked by gel electrophoresis and samples containing main fragments of 400e450 bp were chosen for further analysis. Sequencing libraries were generated using the NEB Next® Ultra™ DNA Library Prep Kit for Illumina (NEB) following the manufacturer's recommendations, and index codes were added. The library was sequenced on an Illumina HiSeq platform at Novogene Bioinformatics Technology Co., Ltd. (Beijing, China), and 250-bp paired-end reads were generated. For the fungal community, an approximately 300–350 bp region of the Internal Transcribed Spacer 2 (ITS2) region was amplified with forward primer gITS7 (Ihrmark et al. 2012) and reverse primer ITS4 (Gardes and Bruns 1993). Finally, all PCR products were combined in equimolar amounts and run on an Illumina HiSeq platform at Novogene Bioinformatics Technology Co., Ltd. (Beijing, China).

6.3 Results and discussion

A) Use of 13C NMR spectroscopy to examine the shift in the chemical composition of organic matter from catchment to reef

The OC, nitrogen and metals are subject to different processes such as mineralisation, transformation and mobilisation through biogeochemical cycles. The organic fraction attached to mineral particles (soil and sediment) is composed of different pools which are different in stability and resistance to decomposition over time. The active fraction is the most unstable part and can be easily decomposed via microbial activities in a short time. The passive fraction is the most stable part of organic matter which can resist microbial decomposition for longer periods, and the slow pool which lies between these two categories and has moderate susceptibility to microbial activities (Brady 1984). This becomes important as OM is composed of many different compounds at different proportions such as lignin, carbohydrates, polyphenols and amino acids which have different resistance to microbial decomposition. Some fractions of organic matter are more likely to be totally degraded due to microbial activities, and consequently change the quantity as well as the composition of OM in the marine environment (Brady 1984).

The soluble component of OM is predominantly labile organic fractions (carbohydrate, di-O-alkyl and methoxy groups) (Figure 6.1). This readily available proportion of dissolved organic C is easily washed off the land to the adjacent river systems and provides energy for microbial communities to decompose OM and release available nutrients.
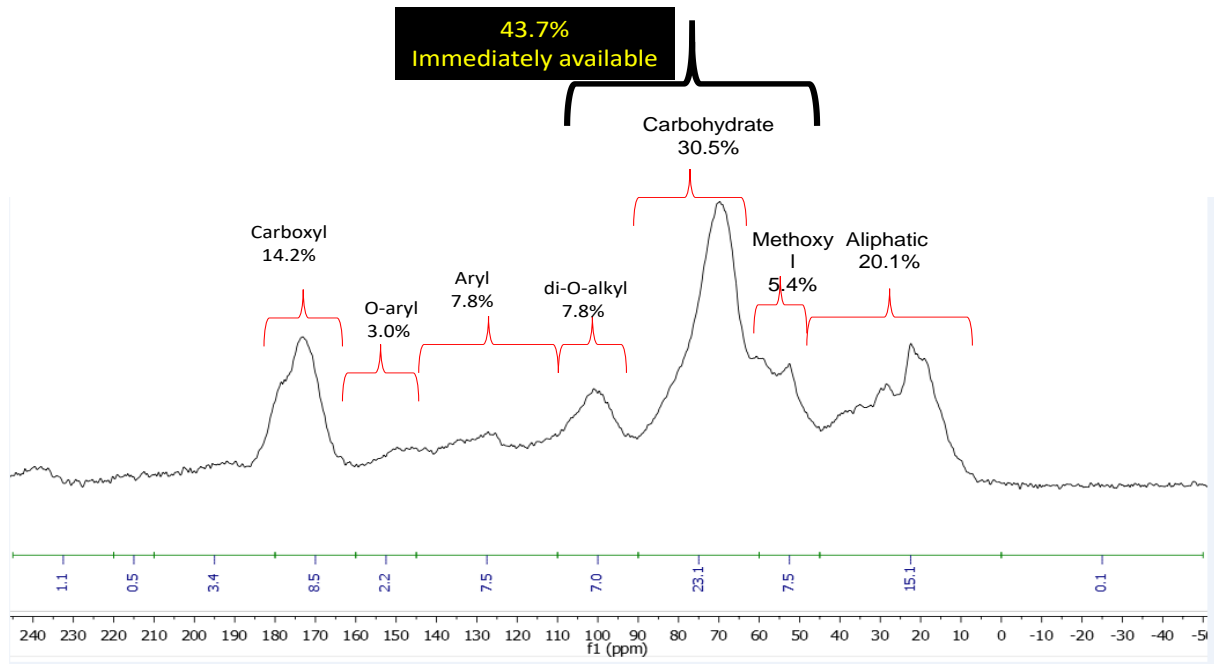
Figure 6.1. Chemical composition of <u>dissolved organic matter</u> extracted from forest litter materials as revealed by ^{13}C CPMAS NMR.

The OC and nutrient input from the decomposition of leaf organic matter from different land uses is a major part of particulate nutrient export from land to the adjacent river systems and eventually into the GBR lagoon. Sugarcane had a higher proportion (48% carbohydrates) in their leaf than other plants, followed by grass species (46% carbohydrates) and then forest and banana (40-38% carbohydrates) (Figure 6.2 and Table 6.1).
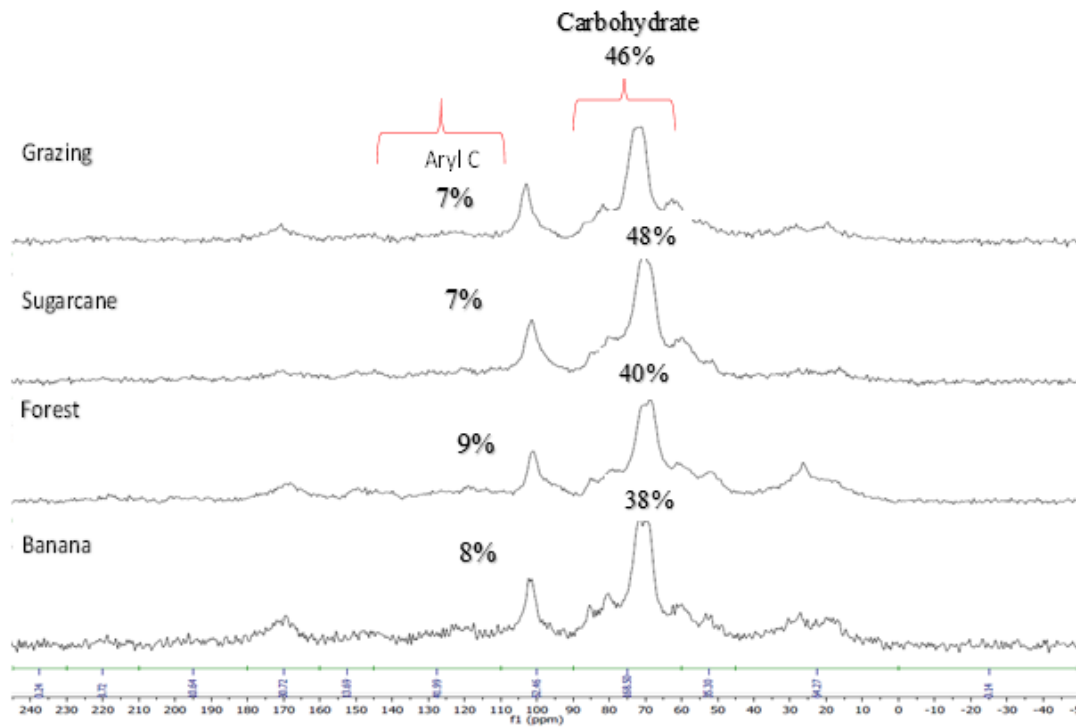
Figure 6.2. Chemical composition of leaf organic matter of different vegetation types (grass, sugarcane, forest and banana) as revealed by 13C NMR CP MASS.

Table 6.1. Proportion (%) of different carbon functional groups in leaf organic matter of different vegetation types (grass, sugarcane, forest and banana) as revealed by ^{13}C NMR CPMAS.

Vegetation type	carbonyl C	Carboxyl C	O-aryl C	aryl C	di-O-alkyl C	carbohyd C	methoxyl C	aliphatic C
Sugarcane	1.49	6.51	2.44	7.40	14.17	48.08	9.18	10.73
Forest	1.85	7.50	3.92	8.53	13.21	40.07	8.96	15.05
Banana	2.11	11.36	2.52	7.63	11.47	37.73	9.16	18.01
Grazing	1.61	7.89	2.46	6.86	13.44	46.37	9.03	12.33

On the other hand, grass and grazing leaves had less aryl C group (less labile, 7% aryl C) compared with forest and banana (9-8%). These results showed that grass and sugarcane leaf litter would be more easily decomposed compared to other species. Moreover, grassland and sugarcane soils had a greater carbohydrate fraction compared to the other land uses (Figure 6.3), which is consistent to the trend in 13C NMR spectra for leaf samples among different species (Figures 6.1, 6.2 and 6.3).

	carboxyl	Oaryl	aryl	di-O-alkyl	carbohyd	methoxyl	aliphatic
Chemical shift (ppm)	180 .. 160	160 .. 145	145 .. 110	110 .. 90	90 .. 60	60 .. 45	45 .. 0
Sugarcane	9.9	4.8	24.4	10.1	26.0	6.9	17.9
grazing	9.6	3.6	17.6	9.8	27.9	8.8	22.7
forest	9.6	4.6	21.6	10.3	24.5	7.5	21.8
banana	9.4	4.8	22.7	10.4	24.8	7.6	20.3
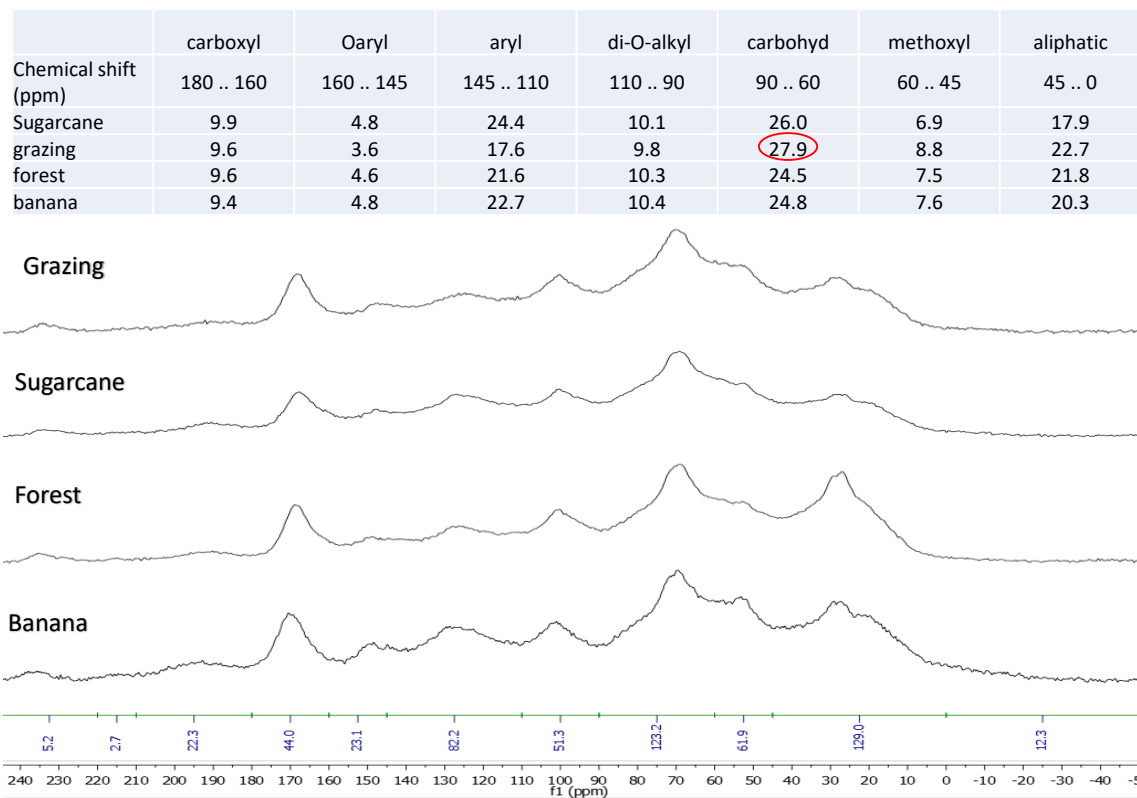
Figure 6.3. Chemical composition of soil organic matter in different land uses (grass, sugarcane, forest and banana) as revealed by ^{13}C CPMAS NMR.

The ^{13}C NMR spectral pattern for freshwater and marine plume sediments varied with the locations where sediment samples were collected, particularly in key recalcitrant organic fractions (e.g., alkyl, aryl C fractions), which can be used as potential ^{13}C NMR fingerprints to determine the origin and fate of particulate organic nutrients in the GBR (Golding, Smernik, and Birch 2004).

The ^{13}C NMR spectra of the plume samples collected from the three rivers (Johnstone, Tully, Burdekin) are shown in Figure 6.4 and Table 6.2. Results showed that there are different patterns in OC functional groups among the three rivers. The plume from the Johnstone River had the highest proportion (46%) of labile organic fraction (carbohydrate, di-O-alkyl and methoxyl), followed by the Tully River (40%) and the Burdekin River had the lowest proportion (35%) (Table 6.2). The plume samples from the Burdekin River had a higher proportion of recalcitrant C fractions (e.g., aliphatic, aryl C) than those from the Johnstone and Tully rivers. Therefore, the A/O-A ratio was much greater for the plume samples collected from the Burdekin River (0.79) than those from the Johnstone and Tully rivers (0.46-0.55), indicating the organic matter in the Burdekin plume samples were decomposed to a greater extent (i.e. with a higher proportion of the recalcitrant organic fraction remaining) compared with those from Johnstone and Tully rivers (Chen, Xu, and Mathers 2004) (Table 6.2). Different patterns of ^{13}C-NMR spectra among the plume samples collected from different rivers provide an excellent opportunity of comparing the bioavailability and chemical signatures of OM discharged from the Wet Tropics (Johnstone and Tully Rivers) and Dry Tropics (Burdekin River) regions (Golding, Smernik, and Birch 2004).
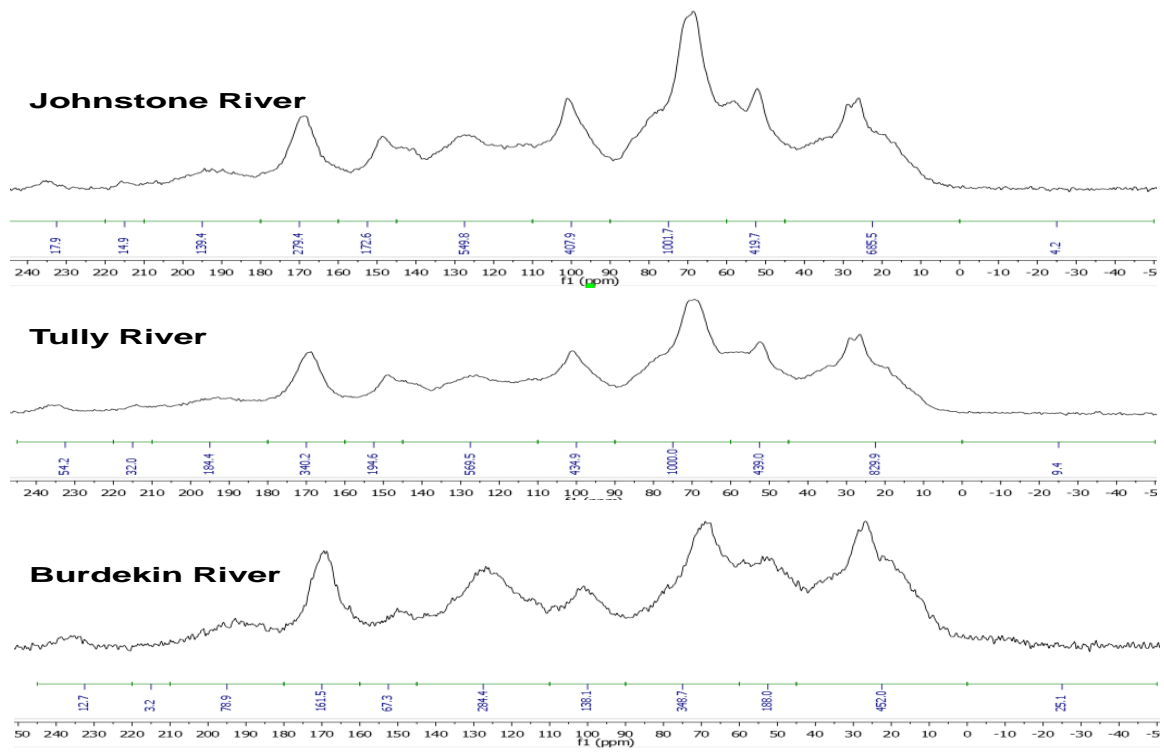
Figure 6.4. Chemical composition of organic matter in plume sediments collected from the Johnstone, Tully and Burdekin Rivers as revealed by ^{13}C CPMAS NMR.

Table 6.2. Composition of C functional groups (%) in riverine plume samples collected from the Johnstone, Tully and Burdekin Rivers as characterized by ^{13}C cross-polarization magic-angle-spinning nuclear magnetic resonance (^{13}C CPMAS NMR) spectroscopy.

	Carboxyl	O-aryl	Aryl	di-O-alkyl	Carbohydrate	Methoxyl	Aliphatic	Labile fractions	A/O-A ratio	*n*
Johnstone	8.67±0.26	4.3±0.56	19.86±3.81	10.35±0.37	26.71±0.78	8.84±1.72	21.17±3.55	45.91±0.56	0.46±0.07	2
Tully	11.21±0.18	4.62±0.27	22.79±0.55	9.06±0.49	23.90±1.15	6.76±0.66	21.65±1.62	39.72±0.98	0.55±0.05	2
Burdekin	9.04±2.13	5.22±0.89	23.69±2.22	6.89±0.45	21.34±0.84	6.47±1.21	27.35±2.51	34.70±1.55	0.79±0.04	4

Labile fractions = sum of carbohydrate, di-O-alkyl and methoxyl C; n = number of samples; A/-A ratio = the ratio of alkyl C region intensity (0–45 ppm) to O-alkyl C region intensity (45 –110 ppm) as an index of the extent of decomposition.

The ^{13}C-NMR spectra of the trap sediments collected from the marine environment are shown in Figure 6.5. Results showed that there are different patterns in OC functional groups among the marine sediments collected at different sediment trap sites. The marine sediments collected from Middle Reef had the highest proportion (24%) of carbohydrate, followed by Geoffrey Bay (21%) and with lowest proportion at Orchard Rocks (18%) (i.e. an inshore to offshore gradient). The trap sediments collected from Cleveland Bay had a higher proportion of recalcitrant C fractions (e.g., aliphatic) compared to the other sites. The aromatic carbon (e.g., aryl C) was much greater for trap sediments located at Orchard Rocks (26%) than those from Cleveland Bay, Geoffrey Bay and Middle Reef. These results indicated that the organics in the marine environment vary depending on the location along the shoreline of the GBR catchments.

Chemical shift (ppm)	Carboxyl 180 .. 160	O-aryl 160 .. 145	Aryl 145 .. 110	di-O-alkyl 110 .. 90	Carbohydrate 90 .. 60	Methoxyl 60 .. 45	Aliphatic 45 .. 0
Cleveland	9.9	3.5	19.0	6.1	19.0	8.6	33.9
Geoffrey bay	11.7	3.6	18.4	5.6	21.0	7.6	32.1
Magnetic Island- orchid rock	10.2	3.9	26.2	6.0	18.1	5.9	29.7
Middle reef	11.5	2.8	16.1	7.1	24.4	9.0	29.0
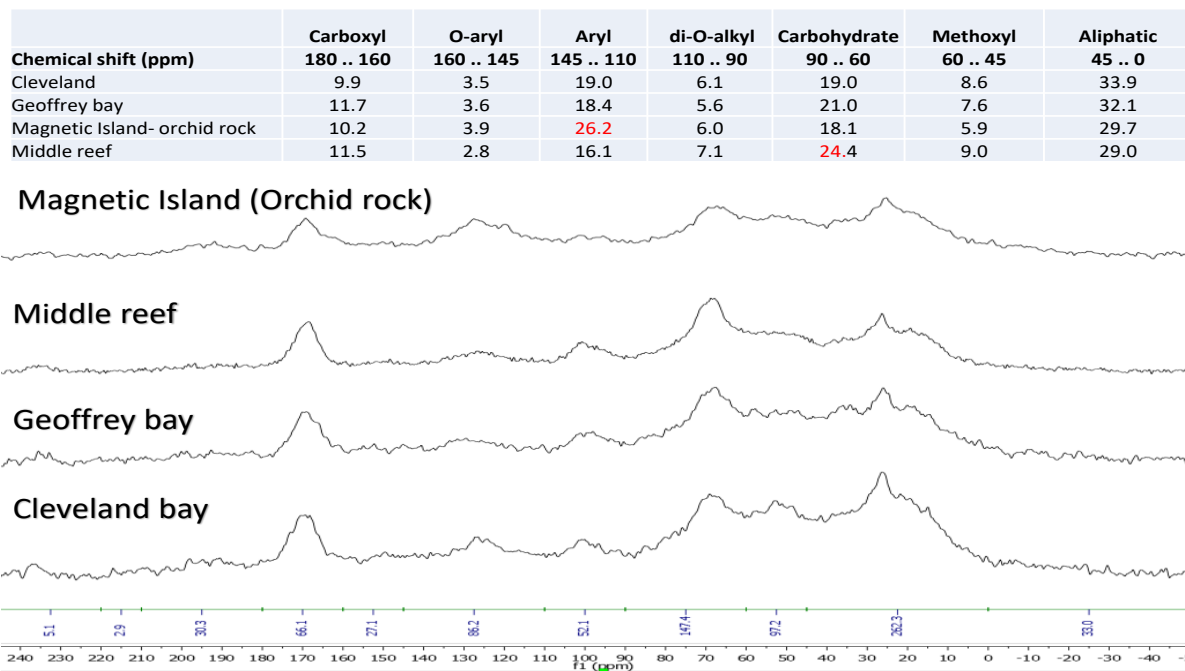
Figure 6.5. Chemical composition of organic matter in marine sediments collected from different sediment traps (Orchard Rocks, Middle Reef, Geoffrey Bay, Cleveland Bay) as revealed by ^{13}C-NMR.

B) Exploring isotopic (δ^{13}C and δ^{15}N) and chemical (^{13}C-NMR spectra) signatures to determine the origin and fate of organic matter in the GBR

In order to develop sound strategies to manage particulate OM discharge and its subsequent detrimental impacts on the GBR lagoon, it is critical to gain a better understanding of what biogeochemical processes the sediments and their associated particulate OM undergo during their transportation from catchment to reef (Bainbridge et al. 2016; Baldock et al. 2004). In addition, the chemical and biological nature of the organic components of soil and sediments (freshwater and marine) in the GBR area are largely unknown, although it is critical for understanding their influence on the reef.

The ^{13}C-NMR functional groups in soil, plume sediment and marine sediment (sediment trap) samples are presented in Figure 6.6. The PCA was used to demonstrate the distribution of ^{13}C-NMR functional groups in OM component of soil and sediments. The samples taken from the Wet Tropics region (Tully and Johnstone plume sediments) were different from the

Burdekin River plume sediments. Burdekin sediments were more enriched in aliphatic, O-aryl and aryl compounds, while the Johnstone plume samples were mainly composed of di-O-alkyl and carbohydrate. Carboxyl was the dominant OC functional group in the plume sediments collected from the Tully River mouth. The PCA analysis also demonstrated that soil samples from different land uses are distinguished from the sediments collected from the marine environment (Figure 6.6). Terrestrial samples mainly contain aryl, O-aryl, carbohydrate and di-O-alkyl. Marine sediments collected from sediment traps mainly were composed of aliphatic and carboxyl compounds (Golding, Smernik, and Birch 2004).

The ^{13}C NMR spectra revealed that plume samples from the Wet Tropics region (Johnstone and Tully) and Burdekin River are more similar to soil samples rather than marine sediments (Figure 6.6). Thus, taken together, plume sediments dominantly carry the signature of terrestrial plant-derived OM. Of these three main rivers, the Johnstone had the highest carbohydrate and di-O-alkyl content. Soil samples and marine samples were clearly separated from each other, with sediment traps being more enriched in aliphatic and recalcitrant compounds compared to soil samples (Golding, Smernik, and Birch 2004).
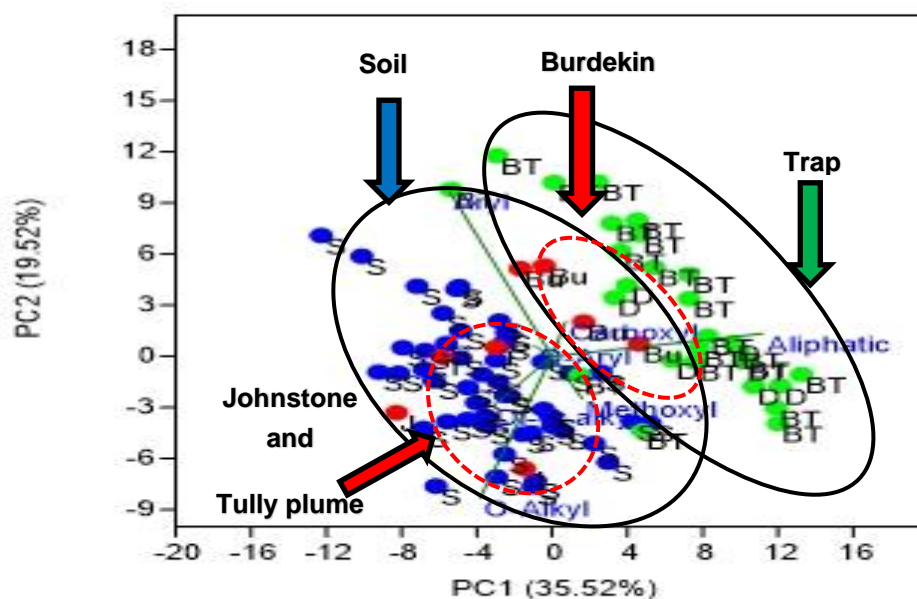
Figure 6.6. The principal component analysis for distinguishing the soil, plume and trap sediments according to the chemical composition of the organic fraction as revealed by ^{13}C-NMR. The blue points(S): topsoil and subsoil collected from grazing, forest and banana land uses; red points are plume sediments collected from Johnstone (J), Tully (T) and Burdekin (Bu) Rivers; green points are sediment traps collected off the Tully catchment coastline (Dunk island sediment trap (D)) and off the coast of Burdekin catchment (BT) including sediment trap samples from Orchard Rocks, Cleveland Bay and Middle Reef marine sites.

During the transportation of sediments to the GBR lagoon through the river streams, organic compounds can be depleted due to chemical and biological processes, so that sediments and associated OM acquire new chemical signatures that may no longer reflect their terrestrial origin. It is because of photochemical and biological degradation of organic compounds along

the transportation pathway from catchment-to-reef through which the bioavailability of nutrients significantly change by transforming from organic to inorganic forms (Thayer 2002). Furthermore phytoplankton are also locally responsible for synthesizing a part of organic matter in the marine environment in addition to the terrestrial derived organic matter that are delivered to the coast from rivers (Zhang et al. 2015; Meyers 1994; Watanabe and Kuwae 2015; Baldock et al. 2004).

The stable isotope signatures (δ^{13}C, δ^{15}N) for soil, plume sediment and marine sediment (sediment trap) samples are presented in Figure 6.7. The PCA was used to demonstrate the distribution of different samples as function of their stable isotope signatures. The samples taken from the Wet Tropics region (Tully and Johnstone plume sediments) were different from the Burdekin River plume sediments. Burdekin sediments were more enriched in δ^{13}C, while Johnstone and Tully plume samples were characterised by higher ^{15}N.
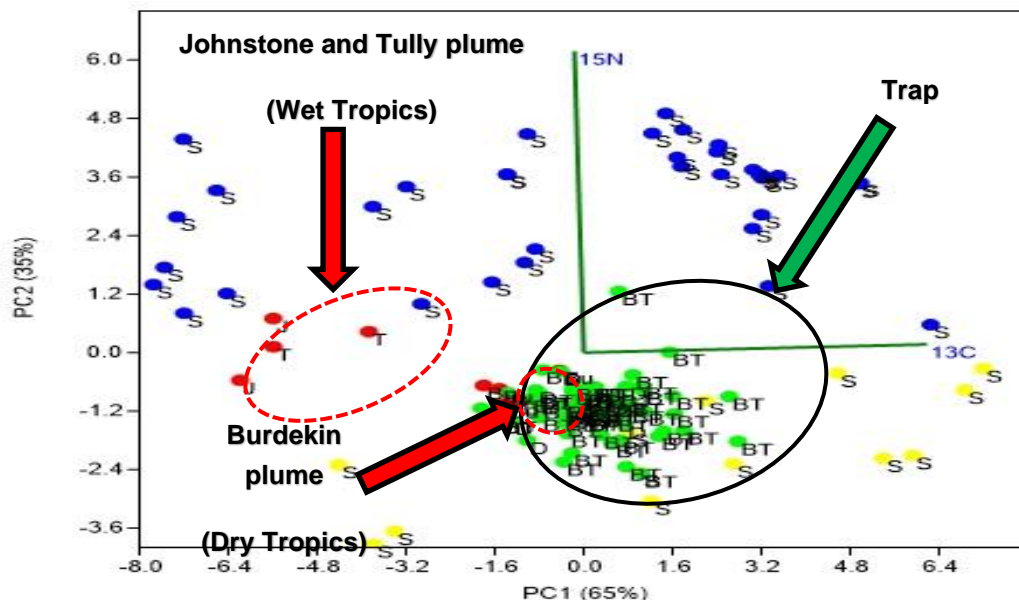
Figure 6.7. The principal component analysis for distinguishing the soil, plume and trap sediments according to their isotopic signatures. S: topsoil and subsoil collected from grazing, forest and banana land uses of Johnstone (blue points) and Burdekin (yellow points); red points are plume sediments collected from the Johnstone (J), Tully (T) and Burdekin (Bu) Rivers; green points are sediment traps collected off the Tully catchment coastline (Dunk island sediment trap (D)) and off the coast of Burdekin catchment (BT) including sediment trap samples from Orchard Rocks, Cleveland Bay and Middle Reef marine sites.

The variation in the δ^{13}C values of plume sediments originating from the Dry and Wet Tropics are due to the variation in the vegetation types. The majority of the Johnstone catchment area (52%) are trees (forest) and follow the Calvin-Benson cycle (C$_3$) photosynthetic pathway with a mean δ^{13}C of −28‰ (Boutton 1991; Fry 2006). On the other hand, grassland is the dominant vegetation type in the Burdekin catchment. Grass species in warmer climates, mainly follow the Hatch-Slack cycle (C$_4$) pathway with a mean δ^{13}C of −13‰ (Coleman 2012; Werth and Kuzyakov 2010). Generally, δ^{15}N fractionation is much more complex than δ^{13}C due to multiple N sources and different potential internal transformations which can affect N isotopic values

in derived OM from different plant materials. The majority of N in the terrestrial environment has δ^{15}N values between −10‰ and +10‰ depending on land use and N input (Evans 2007; Finlay and Kendall 2007).

Plume samples from the Wet Tropics region including the Johnstone and Tully rivers are more similar to soil samples rather than marine sediments. However, the δ^{13}C and δ^{15}N signatures of Burdekin plume sediments are more similar to marine sediments. It is due to the nature of terrestrial-derived OM in the Burdekin catchment which are enriched in δ^{13}C compared to that originating from the Johnstone and Tully catchments (Figure 6.7).

C) Microbial community (bacteria and fungi) associated with flocs (plume samples) in the GBR area

A wide range of habitats are occupied by different microorganisms such as bacteria and fungi which are a key driver of microbial processes and have significant effects on many other forms of life in terrestrial and marine ecosystems (Fuhrman et al. 1989). They can have an active role in pollutant decomposition and nutrient cycling in both marine and terrestrial environments (Amaral-Zettler et al. 2010). Despite their importance, microbial processes in the marine environment (e.g., GBR) are poorly understood. Any changes to the microorganisms living environment can substantially change their ability to modulate biological processes. In fact, the efficiency of microbial activities change in environments in response to changes in nutrient concentration, pH, electrical conductivity, temperature and oxygen concentration (Stat et al. 2009).

The results on community composition of dominant bacterial and fungal phyla for the soil, plume sediments and trap sediments are presented in Figures 6.8 and 6.9, respectively. For the bacterial community, the collected samples showed a different pattern during their transportation from catchment to reef. Proteobacteria, Actinobacteria and Acidobacteria were the predominant groups of bacteria in soils. In the marine environment, Protobacteria and Bacteroidetes were dominantly associated with the trap sediments. Regarding the fungal community composition, there were distinct patterns between the terrestrial and aquatic environments. Ascomycota was dominant group of fungi in plume and trap sediments. Mortierellaomycota was the second dominant group of fungi after Ascomycota in the soil samples. These different patterns of microbial community composition are related to the bioavailability of OM in various environments and the variations in the environmental factors (pH, salinity, hydrology etc.) in different habitats along the transportation pathway from catchment to reef (Angly et al. 2016).
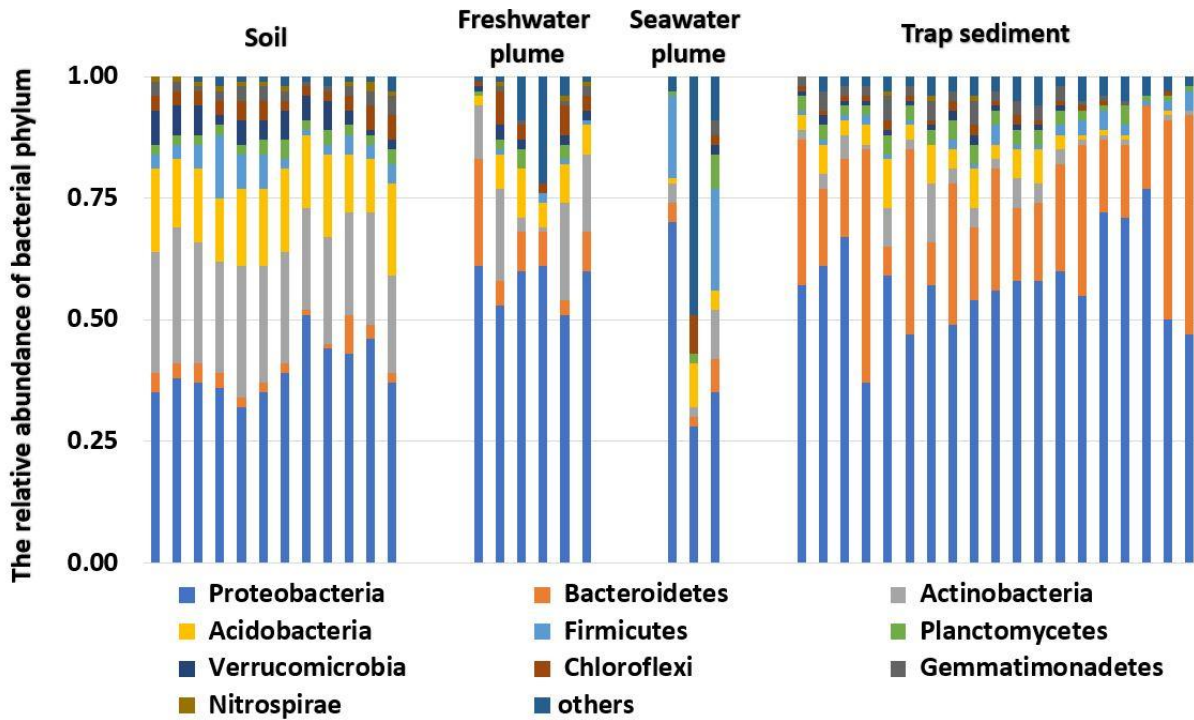
Figure 6.8. Percent community composition of dominant bacterial phyla in soil, plume sediments and trap sediments. Proteobacteria, Actinobacteria and Acidobacteria were predominant groups of bacteria in soils. In the marine environment, Protobacteria and Bacteroidetes were dominantly associated with sediments.
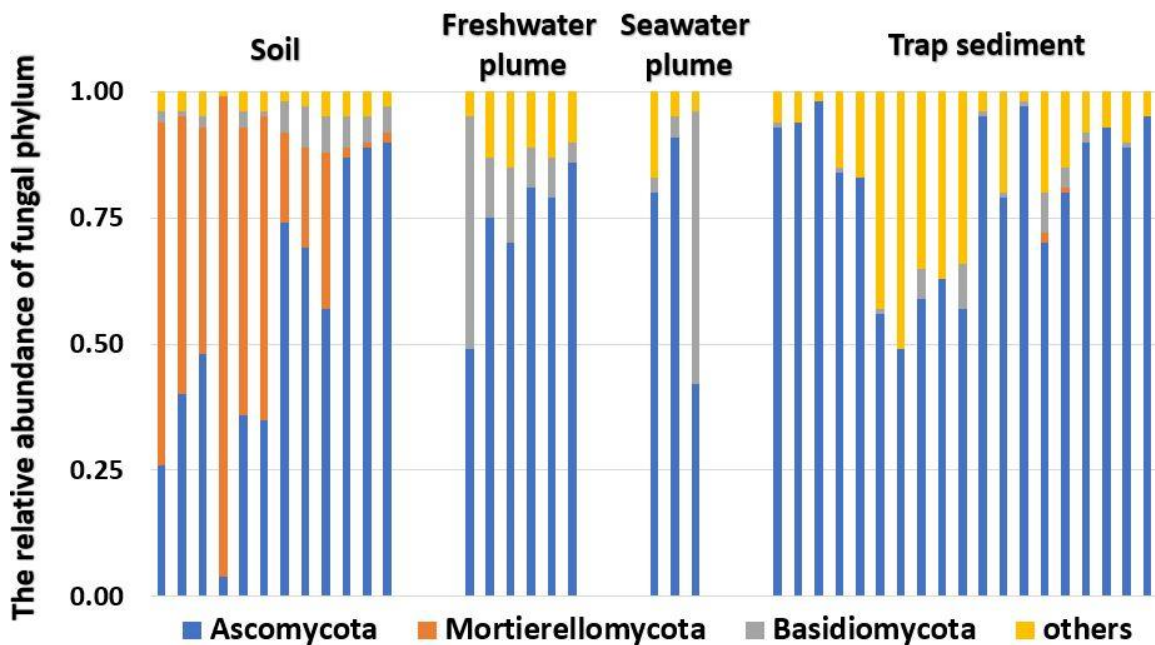
Figure 6.9. Percent community composition of dominant fungi phyla in soil, plume sediments and trap sediments. Ascomycota and Basidiomycota were dominant groups of fungi in plume and trap sediments. Ascomycota and Mortierellaomycota were the dominant groups of fungi in soils.

In addition to the microbial community composition, we also explored the change in bacteria/fungi gene copy number ratio along the salinity gradient from freshwater to the primary and secondary plumes. The fungi/bacteria ratio is the ratio of copy numbers measured with the "all *Fungi*" and "all *Bacteria*" using qPCR analysis. The bacteria/fungi ratio was also examined over time at the Orchard Rocks sediment trap site.

We found that the bacteria to fungi gene copy number ratio increased along the Burdekin River transect, in the sediments from the end of river (Freshwater) to the primary and secondary plume water types (Figure 6.10). For Tully River, the bacteria/fungi ratio dramatically increased from the primary plume to the secondary plume water types (Figure 6.11). Bacteria and fungi, as the main microbial decomposer communities in both terrestrial and marine ecosystems, are distinct in their metabolic requirements and OM decomposition capabilities. Their ecological functions also vary with environmental factors, and OM quality which varies widely in aquatic ecosystems (Fabian et al. 2017).
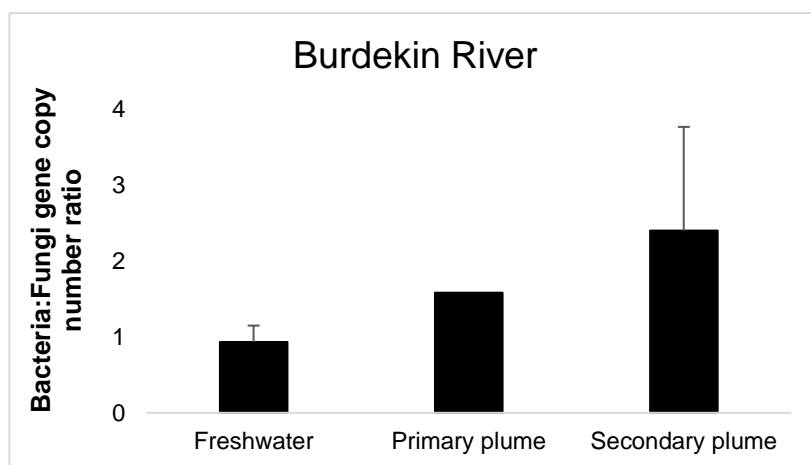
Figure 6.10. Bacteria to fungi gene copy number ratio for the suspended sediments from Burdekin River transect, from End of River (Freshwater) to primary and secondary plume water types.
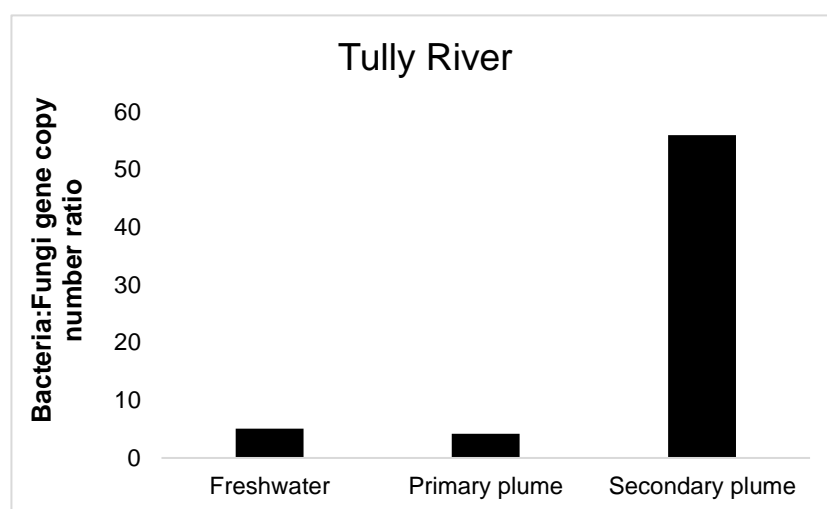
Figure 6.11. Bacteria to fungi gene copy number ratio for the suspended sediments from the Tully River transect, from End of River (Freshwater) to primary and secondary plume water types.

Fungi are known as primary degraders of particulate, predominately terrestrial-derived OC and bacteria act as rapid recyclers of simply structured nutrient-rich OM compounds. Therefore, the change in the relative abundance of fungi and bacteria along the salinity gradient from freshwater to marine environments is, partially, due to the shift in the chemical composition and bioavailability of particulate OM (Fabian et al. 2017). For example, the particulate forms of terrestrial-derived OC in freshwater have higher labile fractions and carbohydrate (see section C of this report) compared to marine environment and therefore are considered quite critical in shaping microbial community and composition (Fabian et al. 2017).

Figure 6.12 demonstrates the change in the bacteria to fungi gene copy number ratios in trap sediments collected from the Orchard Rocks site over time (from January 2017 to May 2018). The lowest bacteria to fungi ratio was recorded in trap sediments collected during the January to April 2017 deployment. The bacteria to fungi ratio was highest during the October to December 2017 deployment. Such a variation in the microbial communities and composition reflects the impact of riverine inputs along with the variation in the environmental factors at the Orchard Rocks sampling site throughout the year.
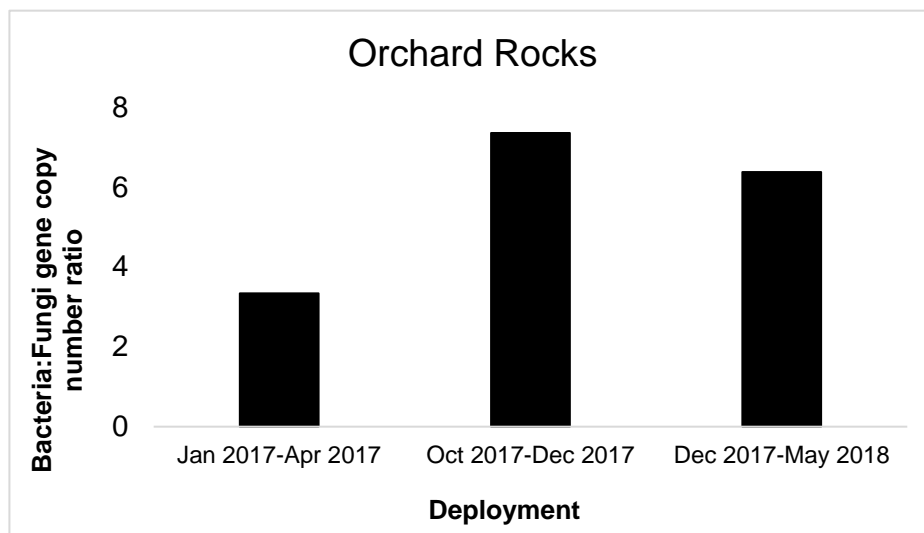
Figure 6.12. The changes in the bacteria to fungi gene copy number ratio over time (from January 2017 to May 2018) for the Orchard Rocks sediment trap.

The trap sediments collected from Orchard Rocks showed different abundance of bacteria and fungi ratios during significant flood plume events in the wet season compared to the sediments collected during dry season (with almost no significant flood plume events). Such variation in the abundance and composition of microorganisms offshore from the GBR catchments was due to the terrestrial-derived OM input as well as other chemical and physical influences of riverine inputs into the ecosystem of the GBR lagoon.

6.4 Conclusions, implications for management and future works

Many of the biological reactions and biogeochemical processes that occur in the riverine environment and plume (e.g., algal bloom) are related directly or indirectly to the nutrients delivered to the coastal area by the rivers. Particulate organic matter associated with the mineral fraction is an important source of nutrients delivered to the coastal area through rivers. The particulate organic matter is degraded and transformed into mineral nutrients (e.g., dissolved inorganic nitrogen) which are highly bioavailable and cause higher algal growth in the marine ecosystem. Results of this study demonstrated that a substantial fraction of the terrestrial-derived labile organic carbon degraded along the transportation pathway from soil to freshwater and to marine ecosystems. The labile fractions of organic matter (e.g., carbohydrates) was the major chemical classes identified in soil and river sediments, while the sedimentary organic matter in the marine environment was more recalcitrant (e.g., more aliphatic compounds). Therefore, greater effort is required to reduce the particulate organic matter delivered to the GBR through rivers using an expanded scope of tailored and innovative solutions. There is a need for investment in practice change programs, the use of regulatory tools and other policy mechanisms to reduce the sediment load and associated particulate organic matter delivered to the marine environment through rivers.

List of publications derived from this project

1. Mohammad Bahadori, Chengrong Chen, Stephen Lewis, Sue Boyd, Mehran Rezaei Rashtia, Maryam Esfandbod, Alexandra Garzon-Garcia, Lukas Van Zwieten and Yakov Kuzyakov, 2021. *Soil organic matter formation is controlled by the chemistry and bioavailability of organic carbon inputs across different land uses*. Science of the Total Environment. doi.org/10.1016/j.scitotenv.2021.145307

2. Mohammad Bahadori, Chengrong Chen, Stephen Lewis, Mehran Rezaei Rashti, Freeman Cook, Andrew Parnell, Maryam Esfandbod, and Thomas Stevens. 2020. *Tracing the sources of sediment and associated particulate nitrogen from different land uses in the Johnstone River catchment, Wet Tropics, north-eastern Australia.* Marine Pollution Bulletin. Volume 157, August 2020, 111344. https://doi.org/10.1016/j.marpolbul.2020.111344

3. Mohammad Bahadori, Chengrong Chen, Stephen Lewis, Mehran Rezaei Rashti, Freeman Cook, Andrew Parnell, Maryam Esfandbod, and Sue Boyd. 2019. *'A novel approach of combining isotopic and geochemical signatures to differentiate the sources of sediments and particulate nutrients from different land uses',* Science of The Total Environment, 655: 129-40. doi.org/10.1016/j.scitotenv.2018.11.084

References

Amaral-Zettler, Linda, Luis Felipe Artigas, John Baross, Loka Bharathi, Antje Boetius, Dorairajasingam Chandramohan, Gerhard Herndl, Kazuhiro Kogure, Phillip Neal, and Carlos Pedrós-Alió. 2010. 'A global census of marine microbes', Life in the world's oceans: diversity, distribution and abundance. Oxford: Blackwell Publishing Ltd: 223-45.

Angly, Florent E, Candice Heath, Thomas C Morgan, Hemerson Tonin, Virginia Rich, Britta Schaffelke, David G Bourne, and Gene W Tyson. 2016. 'Marine microbial communities of the Great Barrier Reef lagoon are influenced by riverine floodwaters and seasonal weather events', PeerJ, 4: e1511.

Bahadori, Mohammad, Chengrong Chen, Stephen Lewis, Mehran Rezaei Rashti, Freeman Cook, Andrew Parnell, Maryam Esfandbod, and Sue Boyd. 2018. 'A novel approach of combining isotopic and geochemical signatures to differentiate the sources of sediments and particulate nutrients from different land uses', Science of The Total Environment.

Bainbridge, Zoe, Stephen Lewis, Scott Smithers, Scott Wilkinson, Grant Douglas, Stephen Hillier, and Jon Brodie. 2016. 'Clay mineral source tracing and characterisation of Burdekin River (NE Australia) and flood plume fine sediment', Journal of soils and sediments, 16: 687-706.

Baldock, JA, CA Masiello, Y Gelinas, and JI Hedges. 2004. 'Cycling and composition of organic matter in terrestrial and marine ecosystems', Marine Chemistry, 92: 39-64.

Bencala, Kenneth E, Vance C Kennedy, Gary W Zellweger, Alan P Jackman, and Ronald J Avanzino. 1984. 'Interactions of solutes and streambed sediment: 1. An experimental analysis of cation and anion transport in a mountain stream', Water Resources Research, 20: 1797-803.

Billen, Gilles, Christiane Lancelot, M Meybeck, RFC Mantoura, Jean Marie Martin, and Roland Wollast. 1991. "N, P and Si retention along the aquatic continuum from land to ocean." In Ocean Margin Processes in Global Change, 1, 19-44. John Wiley & Sons.

Boutton, Thomas W. 1991. 'Stable carbon isotope ratios of natural materials: II. Atmospheric, terrestrial, marine, and freshwater environments', Carbon isotope techniques, 1: 173.

Brady, Nyle C. 1984. The nature and properties of soils (Macmillan publishing company).

Chen, CR, ZH Xu, and NJ Mathers. 2004. 'Soil carbon pools in adjacent natural and plantation forests of subtropical Australia', Soil Science Society of America Journal, 68: 282-91.

Coleman, David C. 2012. Carbon isotope techniques (Academic Press).

Collins, AL, DE Walling, and GJL Leeks. 1997. 'Sediment sources in the Upper Severn catchment: a fingerprinting approach', Hydrology and Earth System Sciences Discussions, 1: 509-21.

Ensign, Scott H, and Martin W Doyle. 2006. 'Nutrient spiraling in streams and river networks', Journal of Geophysical Research: Biogeosciences, 111.

Evans, R Dave. 2007. 'Soil nitrogen isotope composition', Stable isotopes in ecology and environmental science, 2: 83-98.

Fabian, Jenny, Sanja Zlatanovic, Michael Mutz, and Katrin Premke. 2017. 'Fungal–bacterial dynamics and their contribution to terrigenous carbon turnover in relation to organic matter quality', The ISME journal, 11: 415-25.

Finlay, Jacques C, and CAROL Kendall. 2007. 'Stable isotope tracing of temporal and spatial variability in organic matter sources to freshwater ecosystems', Stable isotopes in ecology and environmental science, 2: 283-333.

Fry, Brian. 2006. Stable isotope ecology (Springer).

Fuhrman, Jed A, Thomas D Sleeter, Craig A Carlson, and Lita M Proctor. 1989. 'Dominance of bacterial biomass in the Sargasso Sea and its ecological implications', Marine Ecology-Progress Series, 57: 207-17.

Gardes, Monique, and Thomas D Bruns. 1993. 'ITS primers with enhanced specificity for basidiomycetes-application to the identification of mycorrhizae and rusts', Molecular ecology, 2: 113-18.

Golding, CJ, RJ Smernik, and GF Birch. 2004. 'Characterisation of sedimentary organic matter from three south-eastern Australian estuaries using solid-state 13C-NMR techniques', Marine and Freshwater Research, 55: 285-93.

Ihrmark, Katarina, Inga Bödeker, Karelyn Cruz-Martinez, Hanna Friberg, Ariana Kubartova, Jessica Schenck, Ylva Strid, Jan Stenlid, Mikael Brandström-Durling, and Karina E Clemmensen. 2012. 'New primers to amplify the fungal ITS2 region–evaluation by 454-sequencing of artificial and natural communities', FEMS microbiology ecology, 82: 666-77.

Meyers, Philip A. 1994. 'Preservation of elemental and isotopic source identification of sedimentary organic matter', Chemical geology, 114: 289-302.

Mulholland, Patrick J. 1981. 'Formation of particulate organic carbon in water from a southeastern swamp-stream', Limnology and Oceanography, 26: 790-95.

Richardson, Curtis J, and Song S Qian. 1999. 'Long-term phosphorus assimilative capacity in freshwater wetlands: a new paradigm for sustaining ecosystem structure and function', Environmental science & technology, 33: 1545-51.

Stat, Michael, WKW Loh, TC LaJeunesse, O Hoegh-Guldberg, and DA Carter. 2009. 'Stability of coral–endosymbiont associations during and after a thermal stress event in the southern Great Barrier Reef', Coral Reefs, 28: 709-13.

Thayer, John S. 2002. 'Review: Biological methylation of less-studied elements', Applied Organometallic Chemistry, 16: 677-91.

Vollenweider, RA, A Rinaldi, and G Montanari. 1992. 'Eutrophication, structure and dynamics of a marine coastal system: results of ten-year monitoring the Emilia-Romagna coast (Northwest Adriatic Sea)', Science of the total environment: 63-106.

Watanabe, Kenta, and Tomohiro Kuwae. 2015. 'How organic carbon derived from multiple sources contributes to carbon sequestration processes in a shallow coastal system?', Global change biology, 21: 2612-23.

Werth, Martin, and Yakov Kuzyakov. 2010. '13 C fractionation at the root–microorganisms–soil interface: a review and outlook for partitioning studies', Soil Biology and Biochemistry, 42: 1372-84.

Zhang, Yan, Xueqiang Lu, Honglei Liu, Qiongqiong Liu, and Dan Yu. 2015. 'Identifying the sources of organic matter in marine and riverine sediments of Bohai Bay and its catchment using carbon and nitrogen stable isotopes', Chinese journal of oceanology and limnology, 33: 204-09.

CHAPTER 7

The bioavailability of nitrogen associated with sediment in riverine plumes entering coastal environments of the Great Barrier Reef

Alexandra Garzon-Garcia[*1,2], Joanne M. Burton[1,2], Stephen Lewis[3], Zoe Bainbridge[3], Rob De Hayr[1], Philip Moody[1], Jon Brodie[4]

[1] Department of Environment and Science, Brisbane
[2] Australian Rivers Institute, Nathan Campus, Griffith University, Nathan, Brisbane
[3] Catchment to Reef Research Group, TropWATER, James Cook University, Townsville
[4] ARC Centre of Excellence for Coral Reef Studies, James Cook University, Townsville

Abstract

Land use change has caused an increase in sediment and associated particulate nutrient loads in rivers draining to the Great Barrier Reef (GBR). Recent research in GBR catchments has indicated that particulate nutrients in sediment are bioavailable to both freshwater and marine phytoplankton but, the relative contribution of this source to fuel algal blooms in the GBR is unknown. This study quantified the bioavailable nitrogen (i.e. Dissolved Inorganic Nitrogen) contribution associated with particulate nutrients carried within riverine sediment plumes to GBR marine environments. Water samples were taken at different positions in three riverine sediment plumes from the Burdekin River, a Dry Tropics grazing dominated catchment, and one plume from the Tully River, a Wet Tropics mixed land use catchment of cropping (sugar cane and bananas) and grazing. Samples were extracted in the field and incubated in the lab to quantify dissolved inorganic nitrogen (DIN) generation rates and estimate DIN generation loads from riverine plume events. The estimated potential DIN generation load in the three riverine plumes from the grazing catchment was considerable (equivalent to approximately 9 - 30% of the end-of-catchment DIN load in 4 to 5 days of plume travel time). Particulate inorganic nitrogen (PIN) conversion to DIN (i.e. ammonium desorption) was an important process in short timeframes accounting for between 25% and 100% of the generated DIN load. The remaining DIN was contributed by microbial mineralisation of the organic nitrogen (PON+DON). The importance of mineralisation of the organic fraction increased with the time the sediment was in suspension. Mineralisation was still increasing linearly at the end of the incubation experiments (7 days). This indicates that the sediment and associated particulate nitrogen have the potential to continue to generate

DIN once deposited on the marine floor and/or resuspended. DIN generation was insignificant in the mixed land use catchment plume and in the Burdekin 2019 plume where immobilisation of DIN in bacteria biomass occurred. Multivariate analysis indicated that the source of the organic matter in the plumes and the availability of DIN relative to the available organic matter for mineralisation are important determinants of mineralisation/immobilisation in marine sediment plumes. This research demonstrates that riverine plumes have the potential to be a significant source of bioavailable nitrogen to the GBR and its coastal ecosystems and that organic matter is a key driver of this process. Understanding this contribution will enhance risk assessment of anthropogenic sediment delivery to and impacts on the Reef. The link between the source of organic matter and DIN generation in sediment plumes is critical to inform rehabilitation and management strategies to reduce the impact of sediment in the marine environment.

7.1 Introduction

Riverine sediments are recognised as important suppliers of nutrients to coastal environments (Bianchi and Bauer, 2011; Mayer et al. 1998). This function of rivers in fuelling marine productivity is an important one and when nutrient supplies are greatly reduced by damming of rivers or alternatively, when supplies are greatly increased upon catchment development, serious impacts to the marine environment can be observed. Well-known examples include the history of fisheries and planktonic population declines after the damming of the Nile River (Azov, 1991; Mayer et al. 1998; Stanley and Warne, 1993) and the formation of marine 'dead zones' such in the Gulf of Mexico and Florida Keys as a result of increased nutrient supply (Rabalais et al. 2010, 2002; Van Meter et al. 2018). The importance of regeneration from particulate nutrients in overall nutrient requirements of coastal environments has seldomly been quantified (Dagg et al. 2004). In the Northern Gulf of Mexico, the Mississippi riverine plumes did not seem important in sustaining primary production from particulates due to the co-existing high DIN loads (Lohrenz et al. 1997), but there has been substantial nutrient regeneration from particulates measured in the system (Dagg et al. 2004). In the Amazon shelf, biotic regeneration from particulates sustains >50% of nitrogen (N) requirements for primary production (Demaster and Pope, 1996). Clearly understanding nutrient supply processes and how these have changed over time is critical to understand and manage coastal environments.

Riverine plumes across the estuarine mixing zone are highly dynamic places of transformation for sediments and nutrients (Bainbridge et al. 2012; Dagg et al. 2004) and influence biogeochemical cycles of the water column and sediments of coastal systems (Bianchi and Bauer, 2011). This is due to the input of elevated concentrations of biologically important elements (bioavailable N, P and Si) as well as plumes having a complex physico-chemical structure, which leads to biogeochemical transformations and fast turnover rates of organic matter. Plume dynamics and associated biogeochemical processes vary over several time scales associated with inter-annual differences in climate; seasonal differences in variables like rainfall intensity, frequency, amount and location; and daily variables like wind speed/direction, tides and currents (Dagg et al. 2004). These variables determine the spatial and temporal extent of riverine plumes and coupled with land use considerations, their water quality characteristics. There is considerable variability in the phasing of these signals, which causes non-linear relations between plume transformations and freshwater discharge (Dagg et al. 2004).

There are some commonalities to the riverine plume environment including reduced turbulence, which facilitates the settling of suspended materials; and mixing with ocean waters, which reduces riverine coloured dissolved organic matter (CDOM), also enhancing light penetration. These characteristics have important effects on the transformation processes within riverine plumes including aggregation, flocculation and desorption associated with large changes in ionic strength; enhanced primary productivity and cascading effects through the food web including the microbial loop; and the release of organically bound nutrients through photo-chemical and microbial transformations, which in turn further stimulate phytoplankton production (Dagg et al. 2004). All these complexities explain highly variable rates and proportions of various processes between riverine plumes.

Coastal waters of the Great Barrier Reef (GBR) receive terrestrially sourced organic matter and nutrients during pulsed, short duration, high intensity riverine flood events associated with tropical cyclones and monsoonal rainfall (Furnas and Mitchell, 2001). Riverine plumes bring nutrient-rich waters which include particulate nutrients in association with suspended particulate matter to inshore and some mid-shelf reefs for periods of days to weeks (Devlin et al. 2001). An excess of bioavailable nutrients and sediment post-European settlement has been associated with a range of damaging effects to the GBR including an increase in the frequency of Crown-of-Thorns starfish (COTS) outbreaks (Brodie et al. 2005; Fabricius et al. 2010); loss of seagrass and coral through reduced photic depth (Fabricius et al. 2016, 2014); an increased susceptibility to coral bleaching (Wooldridge, 2009); reef degradation and reduced coral biodiversity (DeVantier et al. 2006; Fabricius, 2005); an increase in macroalgae and consequent competition with coral (De'ath and Fabricius, 2010); and possible links to coral disease (Haapkyla et al. 2011). The excess of bioavailable nutrients [targeted as dissolved inorganic nitrogen (DIN) and phosphate) has been mostly attributed to the use of fertilisers in agriculture, mainly from the catchments of the Wet Tropics or smaller coastal catchments where higher rainfall allows for this type of agriculture (predominantly sugarcane and banana) (Bartley et al. 2017). Nonetheless, it has been recognised that internal biological recycling in the GBR is by far, the largest source of bioavailable N and P over seasonal to annual time scales and that particulate nutrients may provide an important source of bioavailable nutrients to the Reef (Brodie et al. 2015; Furnas et al. 2011).

Recent research has indicated that particulate nutrients associated with fine sediment are bioavailable to marine phytoplankton of the Great Barrier Reef (GBR) (Franklin et al. 2018; Garzon-Garcia et al. 2018). The magnitude of this bioavailability depends not only on the sediment load, but on sediment characteristics associated with its parent soil. These characteristics vary with soil type, land use and erosion process (e.g., surface versus subsurface erosion) (Garzon-Garcia et al. 2018). Particulate nutrients become bioavailable either by desorption or remineralisation of organic matter (Dagg et al. 2004; Mayer et al. 1998). The bioavailability of particulate nutrients to phytoplankton from remineralisation is mediated by microorganisms (e.g., bacteria and fungi), which transform organic nutrients into inorganic forms that are directly available and preferentially used by phytoplankton [e.g., dissolved inorganic nitrogen (DIN)]. Bacteria are not always the most important remineralisers of N in plume systems, with organisms >1µm (microzooplankton and mesozooplankton) making a large contribution (Gardner et al. 1994) due to high grazing rates in plume waters (Dagg et al. 2004). Bioavailability from desorption is mediated by physico-chemical processes including the sediment cation exchange capacity and the concentrations of cations in seawater (Mackin

and Aller, 1984; Rosenfeld, 1979). However, the contribution to bioavailable N from eroded sediments entering the coastal environments of the GBR in riverine plumes has not previously been quantified. Understanding this contribution will enhance risk assessment of anthropogenic sediment and associated particulate nutrients to the GBR. It will also improve our understanding of the complex dynamics of large floc formation (muddy marine snow) in riverine sediment plumes (Bainbridge et al. 2012) and of longer term biogeochemical processes that drive nutrient dynamics in the GBR (Furnas et al. 2011).

In this study, we sampled riverine plumes from a Wet Tropics catchment containing extensive fertilised cropping lands and a Dry Tropics catchment dominated by cattle grazing entering coastal environments of the GBR to quantify potential DIN generation from remineralisation of organic matter and desorption of ammonium-N. In the GBR, N is considered the limiting nutrient for phytoplankton growth (Furnas et al. 2011, 2005). DIN is of major importance because it is immediately available to phytoplankton. We demonstrate that nutrients associated with terrestrially sourced sediment have the potential to generate significant loads of DIN during riverine plume transport and that this sediment will continue to be bioavailable after settling. We also postulate the main drivers of this bioavailability.

7.2 Methods

7.2.1 Riverine flood plume study and sampling sites

Four riverine flood plumes were sampled between 2017 and 2019: three generated from the predominantly grazed (>90%) Burdekin River catchment in the Dry Tropics and one from the Tully River catchment in the Wet Tropics, which is dominated by rainforest (~74%) and sugarcane cropping (~10%). The first sampled Burdekin River flood plume (BBB 2017) was generated by an event triggered by Tropical Cyclone (TC) Debbie (late March – early April 2017). The Burdekin River end-of-river (EoR) gauging site at Home Hill (Inkerman Bridge) peaked at a moderate flood level on the 30th of March 2017 and discharged 2.1 million ML in the 3-week period. This event was almost exclusively derived from the Bowen-Broken-Bogie subcatchments (below the Burdekin Falls Dam), which are the dominant contributors to sediment loads at the EoR (Bainbridge et al. 2014). The riverine plume was sampled along a salinity gradient of the estuarine mixing zone to the plume boundary 1 day after the peak of the event at EoR (Figure 7.1a).

The second sampled Burdekin River flood plume was almost exclusively sourced from the upper Burdekin River (Upper B 2018) (late February – early March 2018) which resulted in minor flood levels in the downstream river reaches to the Burdekin Falls Dam. This flow event was the largest in the catchment area above the dam since 2012, although it peaked just below the minor flood level at the EoR gauging site on the 5th of March 2018 and discharged 2.4 million ML in the 3-week period. The riverine plume was sampled 1 day after the EoR event peak in the estuarine mixing zone and at the plume boundary. An additional sample was collected 7 days after the peak flow near Orchard Rocks (off Magnetic Island), ~ 100 km north of the river mouth (Figure 7.1a).

The third sampled Burdekin River flood plume (Mixed B 2019), generated by a monsoon trough, peaked at the moderate flood level on the 8th of February 2019 and discharged 14.5

million ML in the 3-week period between 30 January and 19 February 2019 (Gruber et al. 2020). This event had approximately a 1 in 5-year frequency and was the largest discharged by the river in 8 years. During this event, moderate to major flooding occurred in the Upper Burdekin, Cape River and Bowen-Broken-Bogie sub-catchments. The riverine plume was sampled in the estuarine mixing zone 3 days after the peak of the event at EoR. Additional sites were sampled in the secondary plume at Orchard Rocks (off Magnetic Island) and Havannah Island (Palm Island Group) 4 days after the EoR flood peak and at Old Reef (mid shelf) on the 15th of February, 7 days following EoR flood peak (Figure 7.1a).

The sampled Tully River flood plume (Tully 2018) was generated by two moderate level EoR flow events (late January – early February 2018) and discharged approximately 0.3 million ML in a 2-week period. The riverine plume was sampled in the estuarine mixing zone and secondary waters were sampled 5 days after, including at Ellison Reef on the 14th of February (Figure 7.1b).

Water samples collected at different positions in the plumes targeted the water mass associated with the peak of the flow event and the subsequent development of different water types in the plume as described by Petus et al. (2019) and Bainbridge et al. (in review). In summary, different water types would associate with different plume water characteristics including location, suspended particulate matter (SPM) concentration, organic content, sediment particle size, degree of mixing with marine water (salinity), colour, and time after event peak. Sampling locations can be observed in Figure 7.1 and a summary of sample number and type can be observed in Table 7.1.

Figure 7.1. Riverine plume coastal water sampling site locations for the Burdekin River EoR site (all plumes, in yellow), BBB 2017 plume (dark blue), the Upper B 2019 plume (green) and the Mixed B 2019 plume (light blue) (a) and the Tully 2018 plume (b).

Table 7.1. Plume sample date, water type, salinity and number analysed for PIN (particulate inorganic N and mineralisable N.

Plume	Date range	Water type	Salinity (PSU)	No. of samples PIN	No. of samples mineralisable N
BBB 2017	30/03/2017	EoR	0	2	2
	31/03/2017	Turbid primary	0.1-6	2	2
	31/03/2017	Primary	12-23	3	3
	31/03/2017	Secondary	26	1	1
Upper B 2018	03/03/2018 - 06/03/2018	EoR	0	5	5
	6/03/2018	Turbid primary	4	1	1
	6/03/2018	Primary	23	0	1
	13/03/2018	Secondary	31-33	0	2
Tully 2018	9/02/2018	EoR	0	0	1
	9/02/2018	Primary	5-22	0	2
	14/02/2018	Secondary	31-33	0	2
	14/02/2018	Tertiary	33	0	1
Mixed B 2019	03/02/2019 - 18/02/2019	EoR	0	11	11
	11/02/2019	Turbid primary	9	2	2
	12/02/2019 - 15/02/2019	Secondary	21-34	0	5

7.2.2 Quantification of potential DIN generation from riverine flood plumes

Here we quantify two processes which generate DIN, the most bioavailable form of N in estuarine and marine plumes. They are the desorption of particulate inorganic nitrogen (PIN) (i.e. ammonium); and net organic N potential mineralisation (i.e. the mineralisation of PON + DON). These processes were quantified on samples obtained for each of the four riverine plumes (BBB 2017, Upper B 2018, Mixed B 2019 and Tully 2018).

Particulate inorganic nitrogen desorption (estuary)

To estimate PIN desorption from sediment (i.e. ammonium desorption), a 2 M KCl or 0.5M K_2SO_4 ammonium-N extraction was carried out on the water samples to quantify the adsorbed ammonium-N present on the sediment. The method was changed from 2M KCl to 0.5M K_2SO_4 for the second year (i.e. from 2018) of sampling, because the latter method allows for direct quantification of the soluble organic fractions on samples treated with K_2SO_4 reducing the required analysis time. This makes it a more practical method when working on both sediment suspensions and sediment samples. Results from both methods are not significantly different as per a comparison carried out for 58 soils (Adjusted R^2 = 0.98, p<0.0001) and 44 sediments (<10 um) (Adjusted R^2 =0.98, p<0.0001) from the Johnstone and Bowen River catchments (A. Garzon-Garcia, unpublished data). Extractions carried out on all the BBB 2017 plume samples indicated all the PIN was desorbed in the <11.5 PSU area of the plume, hence analysed samples to estimate PIN desorption included EoR samples and samples taken at low salinity sections of the plume (0-9 PSU) for the Upper B 2018 plume and the Mixed B 2019 plume. Due to difficult weather conditions to sample, it was not possible to obtain water samples to quantify PIN at the EoR or low salinity section for the Tully plume at the time the plume was sampled. Samples were taken instead at the nearby Johnstone River catchment that was impacted by the same rainfall event and has similar land use characteristics (at the end of its two subcatchments, the North Johnstone and the South Johnstone Rivers).

The extractions were carried out in the field by adding 29.8 g of KCl or 17.4 g of K_2SO_4 to 200 mL of plume water, shaking the bottle for 10 seconds and allowing the extract to sit for at least 10 minutes under chilled conditions in the dark. The sample was then filtered to <0.45 µm and frozen to quantify NH_4-N in the laboratory. The (PIN) adsorbed ammonium-N was calculated by subtracting the total NH_4-N measured in the extracted sample from a corresponding filtered subsample.

Net organic nitrogen potential mineralisation

Net organic N potential mineralisation (i.e. PON + DON conversion to DIN – referred to here as mineralised DIN) was estimated using incubations. Water samples from various plume water types were incubated in 300 mL air-tight plastic bottles, for 7 days at 25°C under aerobic dark conditions to carry out destructive sampling at 0, 1, 3 and 7 days. Some outer (secondary water type) plume samples from the Tully 2018 and Upper B 2018 plume were incubated for 21 days with additional destructive sampling at 14 and 21 days. Mineralised DIN was calculated at 1, 3 and 7 days (PMN1, PMN3 and PMN7) by subtracting the DIN (NH_4-N + NOx-N) measured at the start of the incubation from the DIN measured at each incubation timeframe. Other additional parameters were quantified during the incubation including suspended particulate matter (SPM), TOC, total Kjeldahl N (TKN), TN (TN = TKN + NOx-N), total Kjeldahl phosphorus (TKP) and phosphate phosphorus (PO_4-P) as well as dissolved organic carbon (DOC), dissolved Kjeldahl N (DKN) and dissolved Kjeldahl phosphorus (DKP) after filtering through a 0.45 ☐m polyethyl sulfone filter.

A blank (DI water) was included for each plume incubation set and destructively sampled at 0, 1, 3 and 7 days.

7.2.3 Carbon and nitrogen isotopes on plume suspended sediment

A water subsample from each incubation time (0, 1, 3, 7 days) for the low salinity sectors of the BBB 2017 flood plume (2 x EoC, 0 PSU and 6.6 PSU) was vacuum filtered over a 1.2 µm fibre glass filter to recover all SPM present. Recovered sediment samples were pelletized for TN and $\delta^{15}N$ analysis. For TOC and $\delta^{13}C$ analysis, samples were treated repeatedly with 10% HCl solution to remove carbonates until there was no visual evidence of effervescence. Following the HCl treatment, the samples were oven dried at 60° C for 48 hours, pelletized, and weighed prior to analysis. Samples were combusted in a Thermo Scientific Flash 2000 elemental analyser with sample gases delivered to a Thermo Scientific Delta V Advantage isotope-ratio mass spectrometer at the Chemistry Centre, Department of Environment and Science, Brisbane.

$\delta^{13}C$ and $\delta^{15}N$ values are reported in per mil (‰) relative to the Pee Dee Belemnite (PDB) standard and relative to air N_2, respectively.

7.2.4 Data analysis and assumptions

Net organic nitrogen potential mineralisation rates

Net organic N potential mineralisation rates ('Mineralised DIN rates') were obtained for each plume sample (from plume mineralisation incubations) by iteratively fitting a linear first order decay model with one pool or an exponential first order decay model with two pools (a labile

and a recalcitrant pool), which ever had a better fit to the DIN concentrations along the incubations (Kalbitz et al. 2003; McDowell et al. 2006; Qualls and Haines, 1992). The models were fitted using the 'growthrates' package in R (Petzoldt, 2018).

$$(1)\; DIN_t = DIN_o + ON_o \times k_m \times t$$
$$(2)\; DIN_t = DIN_o + a \times ON_o \times [1 - e^{-k_m \times t}]$$

Where t = time (days), *a* is the organic N in the labile fraction, k_m is the net DIN generation rate (day^{-1}), DIN_t is the DIN present at any time (mg l^{-1}), DIN_0 is the DIN present at the start of the incubation (mg l^{-1}) and ON_0 is the organic N (PON + DON) at the start of the incubation (mg l^{-1}).

End-of-catchment event loads

The Lynne-Hollick method (Ladson et al. 2013) was used to determine the start and end of each high-flow event at the Burdekin end-of-catchment gauged site and separate base flow from high flow using hourly flows and the historical daily flow datasets for the corresponding gauging station. River discharge data (hourly-interpolated flow, m^3 s^{-1} and historical daily flow) at the Burdekin River EoR gauged site (Clare 120006B) were extracted from the Department of Natural Resources and Mines, Surface Water Database (DNRM 2012).

Event SPM and DIN loads were calculated using the Loads Tool component of the software Water Quality Analyser 2.1.1.6 (eWater Coop, 2015) using sampled SPM and DIN concentrations across the hydrograph. The average load (linear interpolation of concentration) method was used. Average Load (linear interpolation of concentration) is the most accurate and reliable method, provided events are adequately sampled, or at least with reasonably representative sampling including the peak concentration (Joo et al. 2012).

Riverine sediment plume potential DIN generation loads

The Burdekin River plumes were divided into four sectors to calculate potential DIN generation loads according to estimated sediment travel times and water types (Figure 7.2):

1. a freshwater sector (Burdekin River at Inkerman to 0.1 PSU), with an estimated travel time of 1 hr;

2. a turbid primary sector (0.1 PSU to 11.5 PSU), with an estimated travel time of 4-7 hours;

3. a primary to secondary sector (>11.5 PSU to Orchard Rocks), with an estimated travel time of 3-5 days and;

4. a primary to secondary sector (>11.5 PSU to the Palm Island Group), with an estimated travel time of 4-8 days. While the plumes were not sampled between Orchard Rocks and Palm Island, this was still considered a sector for DIN generation as the plumes reached all the way to Palm Island.
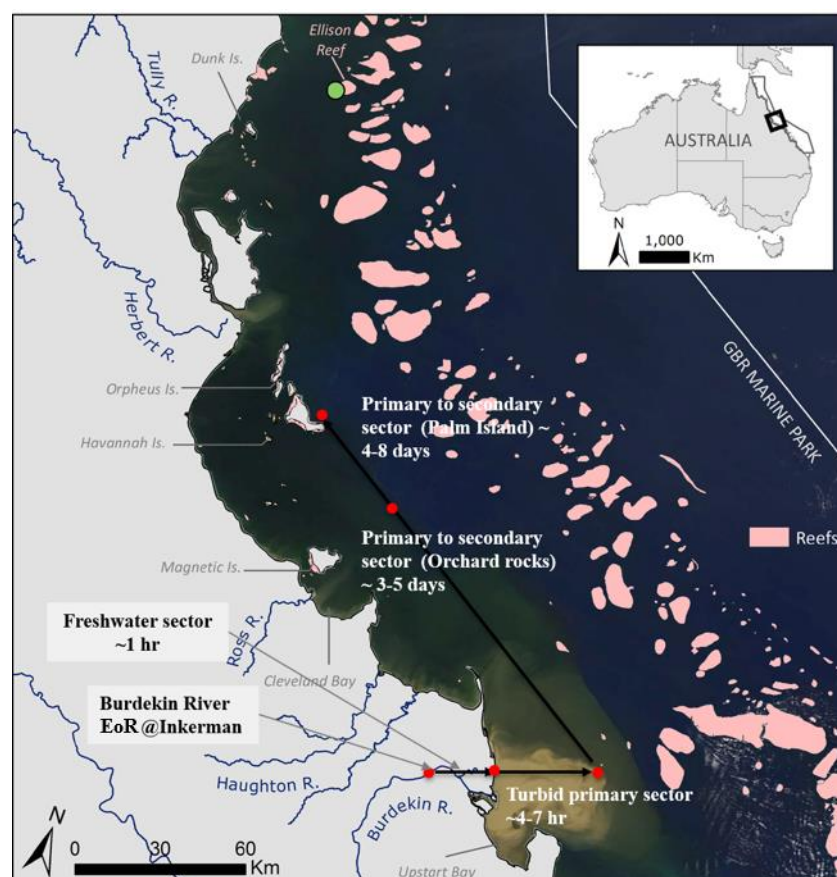
Figure 7.2. Burdekin River plume sectors (represented as black lines) to calculate DIN generation loads according to estimated travel time and water type, overlaid on a MODIS satellite (Aqua true colour) image captured on 12th February 2019 following peak Burdekin River discharge (modified from Bainbridge et al. in press). Reefs shown as pink polygons.

Potential DIN generation loads were calculated from the addition of DIN loads generated by PIN desorption and mineralised DIN loads from organic N.

To estimate DIN loads generated from PIN desorption, average PIN concentrations (adsorbed ammonium-N) measured at EoR (Inkerman) were normalised by the corresponding SPM concentration to estimate the mass of PIN per kg of sediment to be desorbed. It was assumed that all PIN was desorbed in the turbid primary sector as explained earlier (*see PIN desorption section*). The DIN load generated by PIN desorption was calculated by multiplying the PIN per kg of sediment by the total event sediment load at EoR under the assumption that all event sediment would eventually be carried out into or beyond this sector. The EoR load is dominated by fines with clay minerals comprising ~>60% of the bulk mineralogy (Bainbridge, unpublished data). The freshwater sector of the Burdekin River is characterised by a sand bottom below Inkerman, which is additional evidence that fine sediment does not tend to deposit in this sector.

Mineralised DIN loads were calculated for the plume events that presented net DIN production during laboratory incubation experiments only (BBB 2017 and Upper B 2018). Mineralised DIN loads for each plume sector were calculated as follows: Firstly, the mineralised DIN generated as a function of sediment travel time was modelled for each plume

sector using the linear first order decay mineralised DIN equation (1) with the estimated 'mineralised DIN rates' and DIN and organic N concentrations measured at the start of the plume sector; secondly, the mineralised DIN was normalized by the average SPM concentration measured at the start of the corresponding plume sector (mg mineralised DIN /kg sediment in suspension); lastly, the high-flow event sediment load estimated to be in suspension for each sector was multiplied by the normalized mineralised DIN to obtain a mineralised DIN load for each plume sector.

An approximate estimate of the load remaining in suspension for each sector was calculated using percentual changes in sediment concentrations for different positions in the plume. The SPM concentration at Inkerman that corresponded to the water mass sampled at 0 PSU, was estimated by interpolation from SPM concentrations sampled at different times at Inkerman using the estimated travel time of the water mass between the two positions (~10 hr).

The average plume travel times at the peak of the event for each of the two high-flow events that mineralised DIN were obtained from the eReefs model ("eReefs Marine Water Quality Dashboard," n.d.) by calculating the time between the fastest rates of conservative tracer increase between different positions in the plumes using the 3 hour interval model. Estimated plume travel times were validated by comparing them with times between the event peak at EoR and observed peaks in the turbidity logger at Orchard Rocks and Havannah Island.

Multivariate analysis

A multivariate analysis was carried out using all the data collected from the Burdekin plumes between 2017 and 2019 to determine if it is possible to predict mineralised DIN from other water quality parameters measured in the water sample. The multivariate analysis was carried out for parameters reported in concentration (mg/L) and also for these parameters normalised by SPM and reported as mg/kg. The multivariate analysis method was an all-subsets step-up regression using the Leaps package in R (Lumley, 2017) to determine which combination of water quality parameters measured on a water sample best estimated mineralised DIN at different days. This type of regression tests all the possible combinations of parameters and reports on the best subsets for each size (number of explanatory variables used in the regression). The multiple linear model with a significant regression for all parameters ($p<0.05$) and the best adjusted R^2 was selected, considering the latter measure is an unbiased estimator of the model fit and allows comparison of R^2 between regressions with different numbers of variables. The selection also considered that the number of water quality parameters in the equation was reasonable (preferably less than 3) and that the combination of parameters and the type of relationship with mineralised DIN (positive or negative) made sense in terms of the biogeochemical processes that may be driving it. The predictive R^2, a measure that estimates how well the model predicts responses for new observations, was calculated for the selected models. This measure is calculated by systematically removing each observation from the data set, estimating the regression equation, and determining how well the model predicts the removed observation.

The water quality parameters used in the multivariate analysis were: SPM, particulate organic carbon (POC), particulate nitrogen (PN), dissolved organic carbon (DOC), dissolved organic nitrogen (DON), DIN, phosphate (PO_4^{-2}-P), DOC:DON, DIN:PO_4^{-2}-P, DOC:DIN and PIN (adsorbed NH_4^+-N), TOC (%) content in the sediment and TN (%) content in the sediment.

7.2.5 Analytical methods

Analytical methods used for water samples were as follows (APHA/AWWA/WPCF, 2012): TOC and DOC determined using an automated carbon analyser by combustion at 680° C over a platinum catalyst in accordance with method 5310 D (uncertainty = ±8%); TKN, TKP, DKN and DKP determined according to methods 4500-Norg D and 4500-P B (using a catalysed acidic block digestion with colorimetric segmented flow analyser finish) (uncertainty = ± 12%); NH_4-N, NO_x-N and PO_4-P determined colorimetrically by a segmented flow analyser according to methods 4500-NH3, 4500-NO3 and 4500-P (uncertainty = ± 8%).

7.3 Results

7.3.1 Marine plume characteristics

Riverine plume description

The spatial extent of the plumes was predominantly driven by river discharge volume and wind speed and direction as has been documented before (Devlin et al. 2001; Devlin and Brodie, 2005). The most common scenario is when elevated river discharge coincides with south-easterly winds which drive the riverine plumes northwards while remaining close to the coast. This was the case for the Upper B 2018 plume. Light northerly winds during the peak of the BBB 2017 plume drove the estuarine mixing zone directly offshore (Figure 7.1) before an easterly-south easterly change towards the latter part of the flow event resulted in the plume shifting northwards and at least to Cleveland Bay (Orchard Rocks) according to the eReefs hydrodynamic model river tracer ("eReefs Marine Water Quality Dashboard," n.d.). The Upper B 2018 plume extended well northwards into the Palm Island Group 5 days after peak discharge at the EoC. This plume was largely confined to the inner shelf of the GBR and did not impinge on the mid shelf (Lewis et al. 2018).

When calmer conditions coincide with moderate to large river discharge, the riverine plumes tend to push further offshore and may affect the mid shelf (and possibly outer shelf) of the GBR. This was the case for the Mixed B 2019 plume where the riverine plume moved directly offshore during its peak flow. Sampled sites in this plume 3 days after peak Burdekin River flow still showed considerable riverine influence (salinity <10 PSU) at the surface within 30 km of the River mouth (Bainbridge et al. n.d.; Gruber et al. 2020). The plume had extended to the mid-shelf area of the GBR by 5 days after peak discharge at EoR and to the outer shelf by the 6th day (Gruber et al. 2020).

The Tully 2018 riverine plume was mainly confined to the inner shelf of the GBR with some influence on the mid shelf (Lewis et al. 2019).

Water quality

Water quality characteristics varied between plumes and positions within the plume water types (Figure 7.3). In the samples from the freshwater (EoR) and turbid primary plume sectors, the BBB 2017 plume had the highest SPM and organic carbon and nitrogen concentrations of all plumes (particulate and dissolved), followed by the Upper B 2018, Mixed B 2019 and Tully 2018. SPM concentrations were very low (<20 mg l^{-1}) in the freshwater sector of the Tully 2018 plume. DIN concentrations tended to be higher in the Upper B 2018 plume followed by the

Tully 2018 and the BBB 2017 plume (Figure 7.3). Nitrogen oxides (NO_x-N) were the dominant DIN forms under riverine influence with an increase in the ammonium-N contribution to DIN with increasing marine influence (Supplementary material). There is a trend for SPM, organic C and N, DIN and PO_4-P concentrations to decline along the estuarine mixing gradient in the plumes (Figure 7.3).

The concentrations of the total organics in the plume did not necessarily reflect the concentrations of the SPM. The content of organics in the particles (as indicated by volatile TSS) was higher for the Tully 2018, followed by the Upper B 2018 and lastly the BBB 2017 plume. This organic content increased steadily along the plumes.

The Mixed B 2019 plume had the lowest SPM, DIN, DOC, DON, PON and POC concentrations of all Burdekin plumes (Figure 7.3). In addition, the content of TOC (%) and TN (%) in the sediment was slightly higher as well as the DIN, DON and DOC concentrations per unit of sediment mass (Supplementary material).
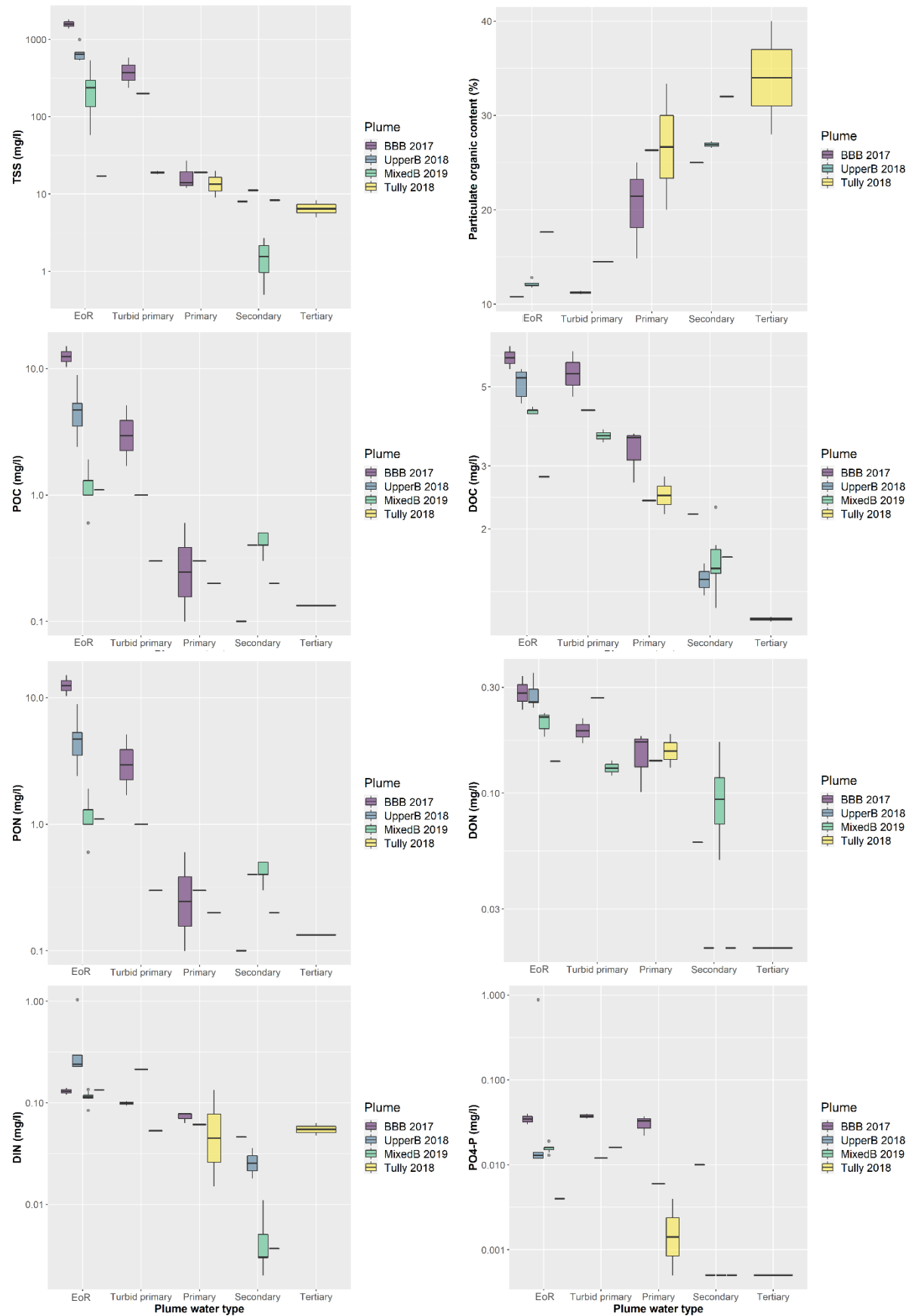
Figure 7.3. Water quality parameter concentrations measured for sampled marine sediment plumes at different positions along a water type gradient [end-of-catchment: EoR, turbid primary (no data for Tully 2018), primary (no data for Mixed B 2019), secondary, and tertiary (only data for Tully 2018)].

7.3.2 Potential DIN generation from marine flood plumes

Particulate inorganic N concentrations

PIN (adsorbed ammonium-N) concentrations tended to be higher in the BBB 2017 plume, followed by the Upper B 2018 plume (Figure 7.4a). The adsorbed ammonium concentrations were the lowest in the Mixed B 2019 plume event, but the adsorbed ammonium content per unit mass of sediment was the largest in this plume (Figure 7.4b). Adsorbed ammonium was not detectable in the Johnstone river EoR sample.
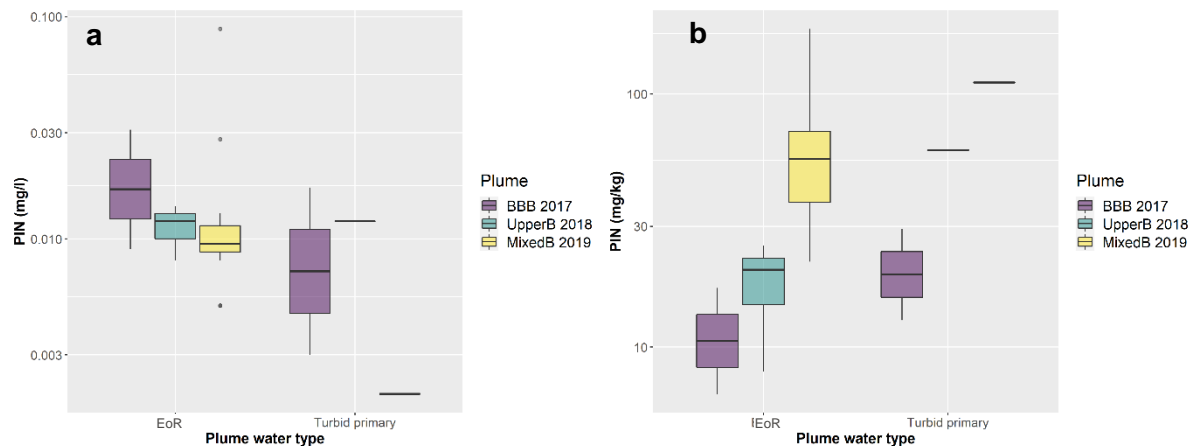
Figure 7.4. Particulate inorganic N (adsorbed ammonium-N) concentrations (a) and mass per kg of sediment (mg/kg) (b) for sampled marine sediment plumes at different positions in the plume [end-of-catchment: EoR (no data for Tully 2018), turbid primary (no data for Tully 2018)].

Potential mineralised DIN from organic N

The potential mineralised DIN associated with organic N mineralisation in the marine environment was significant in two plumes sourced from different areas of the Burdekin River catchment (BBB 2017 and Upper B 2018). This is evident in the net increase of DIN during the incubation experiments (Figure 7.5). In contrast, incubation experiments resulted in no net mineralised DIN (N immobilisation) from the mineralisation of organic matter for the samples associated with the Tully 2018 and the Mixed B 2019 plumes.   There was an initial consumption of DIN in the Upper B 2018 plume incubations (1 day) which did not occur in the BBB 2017 plume that had lower initial DIN concentrations. Dissolved organic C and N tended to decrease during the incubation experiments for all plume samples.

A linear first order decay model with one pool was the best model describing net mineralised DIN in lab incubation experiments for most plume samples (Supplementary material). Potential mineralised DIN rates had the tendency to increase along the plume salinity gradient, with faster rates at sites sampled in more well mixed waters with increasing marine influence. The BBB plume had significantly larger potential mineralised DIN rates than the Upper B plume (Figure 7.5). Importantly, DIN was still increasing linearly at the end of both incubation experiments (Figure 7.5). For the Upper B plume, mineralised DIN rates drastically decreased one week after the plume event (secondary waters) (Figure 7.5).
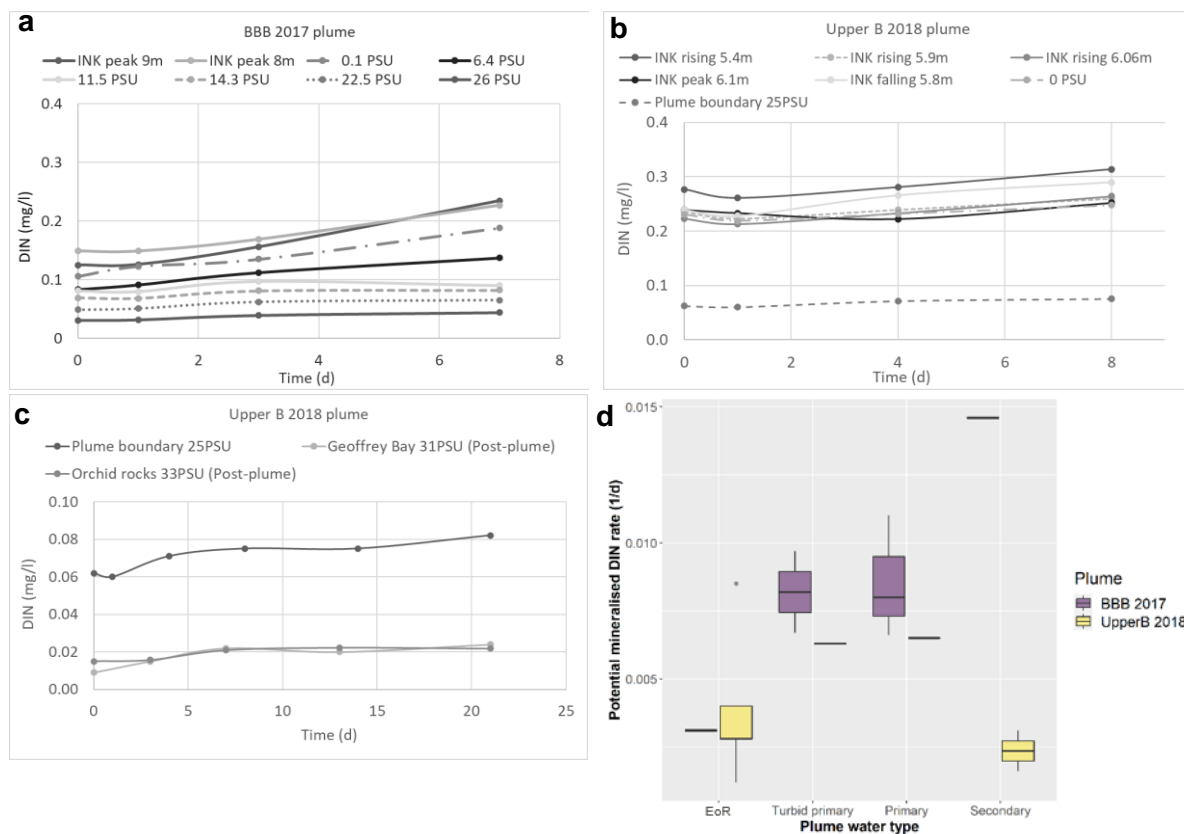
Figure 7.5. DIN concentrations during mineralisation incubation experiments in marine sediment plume samples taken at different positions along the plume for the BBB 2017 plume (a), Upper B 2018 plume (b), (c) and corresponding estimated potential mineralised DIN rates (d) using a linear first order decay model.

Sediment carbon and nitrogen isotopic composition

There were significant differences in the isotopic composition of SPM in incubated samples from different positions in the BBB 2017 riverine plume (Figure 7.6). There tended to be enrichment in δ^{13}C between freshwater and turbid primary plume sectors which indicates a new source of carbon and a depletion in δ^{15}N which suggests the new source of biomass would be overriding the usually enriching effect on δ^{15}N from sediment mineralisation along the plume.
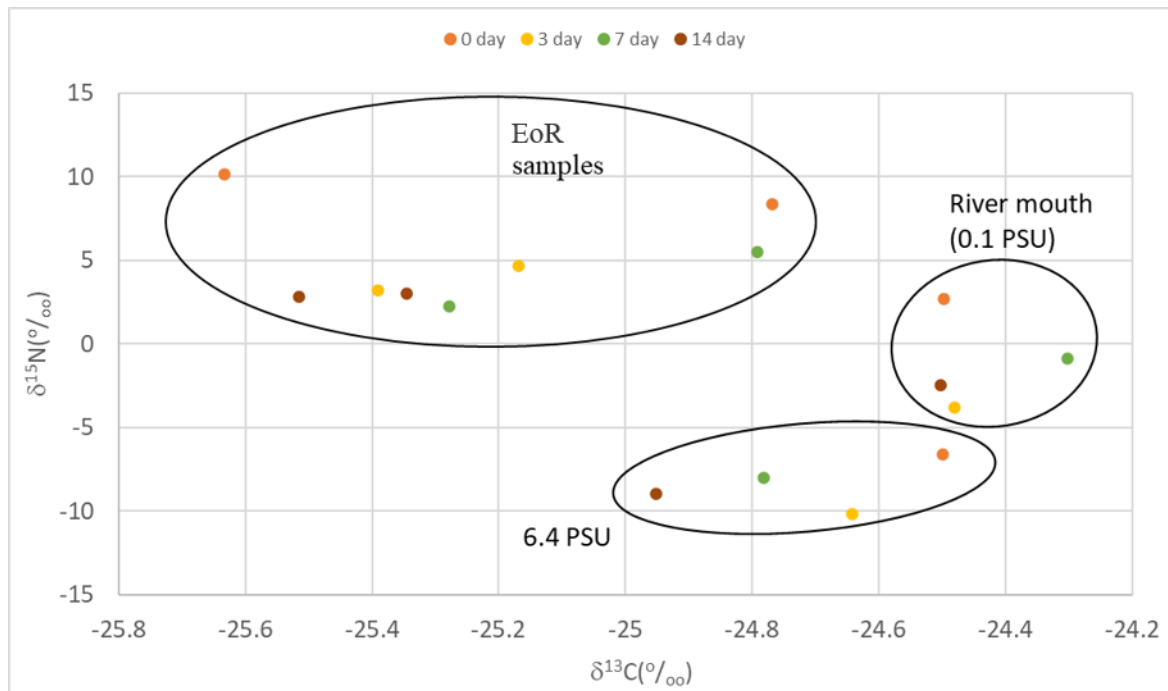
Figure 7.6. Carbon and nitrogen isotopic concentrations of SPM obtained from riverine plume samples of the BBB 2017 plume at different positions along a salinity gradient and incubated for different timeframes (0, 3, 7 and 14 days) in the lab to quantify organic N mineralisation.

Load estimates

The duration, total flow, peak flow, and other characteristics for each of the Burdekin high-flow events that presented net DIN generation in the lab for all plume samples can be observed in Table 7.2. The BBB 2017 high-flow event peaked at 12,000 m^3 s^{-1} (end-of-catchment), almost three times the peak of the Upper B 2018 high-flow event (4,400 m^3 s^{-1}) but carried a slightly lower total volume of water (Table 7.2). The Mixed B 2019 high-flow event was the largest in peak flow and water volume (Table 7.2). All high-flow events had similar durations (~20 days). The BBB 2017 high-flow event exported a larger SPM load to the EoR (1.6 Mt) than the Upper B 2018 event (1.3 Mt), but the DIN load exported from the Upper B 2018 event was > 2 fold larger (Table 7.2). Again, the Mixed B 2019 high-flow event exported the largest SPM and DIN load to the EoC.

It was estimated that a SPM concentration of 990 mg L^{-1} at Inkerman (EoC) would correspond to the 580 mg L^{-1} measured at the start of the turbid primary sector for the BBB 2017 plume. The change in concentrations between the end-of-catchment and start of the turbid primary sector accounted for an estimate of 41% of the sediment settling in the freshwater sector of the plume (Table 7.2). The change in SPM concentrations between the start of the turbid primary sector and the start of the primary to secondary sector (a drop from 580 mg L^{-1} to 27 mg L^{-1}) would account for 55% of the sediment settling in the turbid primary sector (Table 7.2). This leaves an estimated 5% of the sediment load in suspension in the primary to secondary sector of the BBB 2017 plume (Table 7.2).

Similarly, it was estimated that a SPM concentration of 542 mg L^{-1} at Inkerman (end-of-catchment) would correspond to the 200 mg L^{-1} measured at the start of the turbid primary sector for the Upper B 2018 plume. The change in concentrations between the end-of-catchment and start of the turbid primary sector accounted for an estimate of 63% of the

sediment settling in the freshwater sector of the plume (Table 7.2). The change in SPM concentrations between the turbid primary sector and the start of the primary to secondary sector (a drop from 200 mg L^{-1} to 19 mg L^{-1}) would account for an estimated 27% of the sediment load settling in the turbid primary sector and 10% of the sediment load remaining in suspension in the primary to secondary sector of the Upper B 2018 plume (Table 7.2).

The estimated maximum plume travel speed (for the peak of the event water mass) from the eReefs model (Steven et al. 2019) were 0.24 m s^{-1} for the BBB 2017 plume and 0.45 m s^{-1} for the Upper B 2018 plume. The corresponding estimated travel times for each plume sector can be observed in Table 7.2.

The total potential load of DIN estimated to be generated in the 2017, 2018 and 2019 Burdekin plumes was 79, 60 and 271 tonnes, respectively, which is equivalent to 28%, 9% and 17% of the EoR DIN loads (280, 690 and 1580 tonnes of DIN, respectively) (Table 7.2). These loads were generated in 4 to 5 days of average sediment travel time during the whole duration of the plume event. The estimated cumulative mineralised DIN load in each of the plume sectors and PIN desorbed in the primary turbid sector can be observed in Figure 7.7. In the hypothetical case that the plumes had travelled to (and beyond) Palm Island, which occurred in the Upper B 2018 plume, the DIN generation load would increase to 36% of the EoR DIN load for the BBB 2017 plume event (Table 7.2).

Particulate inorganic nitrogen (PIN) conversion to DIN (i.e. ammonium desorption) was an important process accounting for 25%, 43% and 100% of the total generated DIN load for the 2017, 2018 and 2019 plumes, respectively. The remaining was contributed by the mineralised DIN from microbial processing of the organic nitrogen (PON+DON). PIN was the only source of DIN in the Mixed B 2019 plume generating 10 to 14 times that in the 2017 and 2018 plumes (Table 7.2), but this only accounted for 17% of the EoR DIN load (1580 tonnes of DIN) for that high-flow event.

Table 7.2. Plume characteristics, model parameters and output to estimate potential DIN generation from Burdekin riverine sediment plumes sampled in 2017, 2018 and 2019.

		Freshwater			Turbid primary			Primary to secondary (to Orchard Rocks)		Subtotal (to Orchard)			Primary to secondary (to Palm Island)		Total (to Palm Island)	
		BBB	Upper B	Mixed B	BBB	Upper B	Mixed B	BBB	Upper B	BBB	Upper B	Mixed B	BBB	Upper B	BBB	Upper B
Plume characteristics	Total flow (x 10^6 m3)									2100	2400	14500			2100	2400
	Peak flow (m3/s)									12000	4400	17700			12000	4400
	SPM event load (tonnes)									1600000	1300000	5900000			1600000	1300000
	Annual PN load (tonnes)									7300	2400	10000			7300	2400
	DIN event load at EoC (tonnes)									280	690	1580			280	690
Parameters	Initial SPM in sector (mg/l)	739	521	534	580	200	19	27	19				27	19		
	Adsorbed NH_4-N (mg/kg)	13	20	46												
	Mineralisation rate k (1/d)	0.0031	0.0037	n/a	0.0077	0.0063	n/a	0.0113	0.0065				0.0113	0.0065		
	PON+DON_{0d} (mg/l)	4.2	1.09	n/a	1.63	0.47	0.18	0.26	0.19				0.26	0.19		
	DIN_{0d} (mg/l)	0.125	0.283	0.114	0.106	0.231	0.053	0.081	0.062				0.081	0.062		
	Fraction of sediment settled	0.41	0.63	0.63	0.55	0.27	n/a	0.05	0.1				0.05	0.1		
	Travel time	1 hr	1 hr	n/a	7 hr	4 hr	n/a	5 d	3 d				8 d	4 d		
Model outputs	DIN load mineralised (tonnes)	1.1	0.4	0	6	1	n/a	52	25	59	26	n/a	73	33	80	34
	DIN load desorbed (tonnes)				20	26	271			20	26	271			20	25.7
	DIN load generated (tonnes)	1.1	0.4	0	26	27	271	52	25	**79**	**52**	**271**	73	33	**100**	**60**
	% of EoC DIN load	0.4	0.1	0	9	4	17	19	4	**28**	**7**	**17**	26	5	**36**	**9**
	Cumulative DIN load (tonnes)	1.1	0.4	0	27	27	271	79	52				100	60		
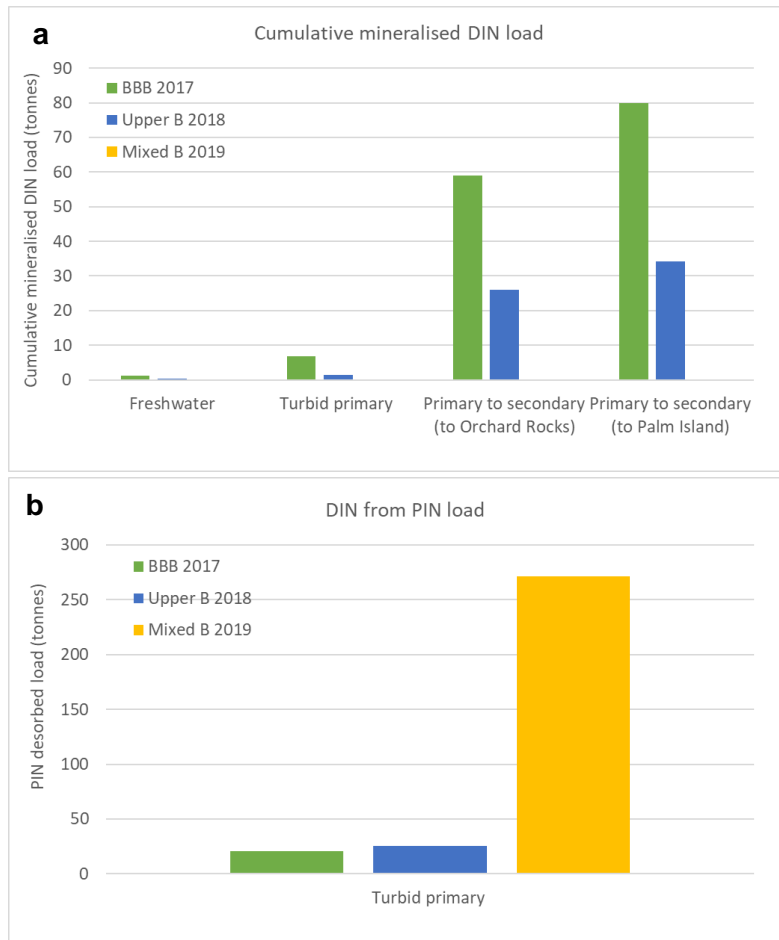
Figure 7.7. Cumulative modelled mineralised DIN load at different plume sectors (a) and PIN desorbed load in the turbid primary sector (b) for the BBB 2017, Upper B 2018 and Mixed B 2019 Burdekin river sediment plume events.

7.3.3 Multivariate analysis

The multivariate analysis indicated that the mineralised DIN at different positions in the plume (negative when immobilisation occurs) could be predicted from parameters including the content of organic C and N in the sediment, sample DIN concentration, the ratio of sample DOC to DIN (for the shorter 1-3 day timeframes) and the ratio of DOC to DON (for the longer 7 day timeframe) (Table 7.3). PO_4^{-2}-P was also a parameter which significantly predicted mineralised DIN. The identified parameters had different values depending on the plume sampled as can be observed in the Marine plume characteristics section.

Table 7.3. Multiple linear equation parameters and fit to estimated mineralised DIN at 1, 3 and 7 days (PMN1, PMN3, PMN7) in riverine sediment plumes using water quality parameters measured in the water sample.

Predicted variable	Parameter 1	Parameter 2	Parameter 3	b	adjusted r^2	predictive r^2
PMN1 (mg/kg)	-127.66 TOC (%) ***	-86.084 TN (%)	-5.152 DOC/DIN **	275.168*	0.93	0.45
PMN3 (mg/kg)	3375.92 PO4-P	-3604.32 DIN	-12.905 DOC/DIN ***	858.497*	0.66	0.36
PMN7 (mg/kg)	-105.618 TOC (%)***	-8.867 DOC/DIN **	25.872 DOC/DON .	-340.781	0.84	0.84

(***) p<0.001, (**) p<0.01, (*) p<0.05

The units of parameters are mg L^{-1} unless stated otherwise

7.4 Discussion

7.4.1 Significance of DIN generation from riverine flood plumes

In this study, we quantified the generation of DIN (NO_3^--N + NH_4^+-N), encompassing the most bioavailable nitrogen forms, from sediments in riverine plumes entering coastal environments of the GBR. The DIN generating processes quantified, were the desorption of PIN to DIN and mineralised DIN from particulate and dissolved organic N. For the first time, we found that potential DIN generation from riverine plumes are likely a considerable source of DIN to the GBR coastal environments both during plume conditions and possibly for an undefined period thereafter. Although DIN generation was considerable in some plumes, this was not a consistent pattern. Only two of the four sampled plumes (BBB 2017, Upper B 2018) had the potential to mineralise DIN from organic N, and only three (all but the Johnstone 2018 plume) had the potential to generate DIN from PIN desorption in low salinity environments. The potential of riverine flood plumes to generate DIN in the coastal environment can be predicted using EoR sample potential to generate DIN. In all cases, riverine plumes that generated DIN in samples obtained at the EoR also generated DIN in samples obtained at the offshore coastal positions in the plume. Therefore, there is potential to use EoR riverine plume samples to assess the riverine plume contribution of DIN to GBR coastal environments.

DIN generation processes contributed a considerable proportion relative to the corresponding EoR DIN load, during a short timeframe within the dynamic plume environment (i.e. up to ~40%). In the Amazon river plumes, biological degradation can remineralise a significant fraction (10-30%) of riverine dissolved organic matter (DOM) on time scales (days-weeks) relevant to plume processes (Benner et al. 1995). The BBB 2017, Upper B 2018 and Mixed B 2019 plumes generated an estimated 79, 60 and 271 tonnes of DIN in 4 to 5 days of travel time. This DIN load is in addition to the 280, 690 and 1580 tonnes of DIN exported from the EoR monitoring site over the measured flows in 2017, 2018 and 2019, respectively. A considerable proportion of this Burdekin EoR DIN load may in turn have been generated from soil erosion processes including sediment processing during stream transport as indicated by a recent mixed empirical and modelling study for the Bowen River catchment (one of the top sediment generating catchments of the Burdekin River) (Garzon-Garcia et al. in preparation). But is this generated DIN load from riverine plumes significant to the Reef? The Burdekin River catchment exports an annual average load of 1,382 tonnes of DIN (SD = 863, 9-year data set)

(Bartley et al. 2017). This is comparable to the annual average of 1,216 tonnes of DIN exported by three of the monitored rivers in the Wet Tropics (Barron, Johnstone and Tully) in which fertilised agriculture is the main source (Bartley et al. 2017). It is worth mentioning though, that these Wet Tropics rivers contain a much smaller catchment area (4,750 km^2) compared to the Burdekin River catchment, which is 27 times larger. Therefore, it is clear that the DIN yield from these Wet Tropic catchments is 22 times larger (~216 kg km^{-2}) (Bartley et al. 2017). But, the likelihood of exposure of Reef habitats to high DIN concentrations and loads relates to the length of time of exposure and not necessarily to the catchment yield (Waterhouse et al. 2017). EoR DIN concentrations from our sampled plumes were comparable between the Burdekin river plumes and the Tully River plume sampled, but were much higher for secondary plume waters of the BBB 2017 and Upper B 2018 plumes relative to plumes that did not mineralise DIN (almost one order of magnitude). This may relate to the mineralisation of DIN from sediment and/or a reduced use of DIN by algae due to higher turbidity within these Burdekin plumes. Nonetheless, Tully 2018 tertiary plume waters had higher DIN than plume secondary water types, which may indicate a delayed DIN generation process. A decrease in the relationship between nutrients and salinity along river/ocean mixing gradients have been attributed to biological uptake in various large river plumes and an increase in several cases has been attributed to inputs from sources like desorption, remineralisation of organic matter or entrainment from below the plume (Alongi and McKinnon, 2005; Dagg et al. 2004). The Tully plume is more representative of the Wet Tropics catchments having lower SPM and higher DIN concentrations, which would explain differences in the biogeochemical cycling magnitude and timeframes observed in the plumes.

Some limitations of this study include the standardised experimental conditions of laboratory generated remineralisation rates, which are not directly comparable to those generated *in-situ* within the plume environment and cannot account for other factors like turbulence or photochemical reactions. However, the incubation experiments enable the removal of the effect of algae in floc dynamics and of conservative mixing in the plume, allowing the quantification of gross mineralised DIN. The difficulty in quantifying conservative mixing in riverine plumes has been recognised (Dagg et al. 2004). The value of this type of experiment is that it provides additional information on the cycling rates of N in the plume, which cannot be obtained from direct DIN measurements in the plume water. Direct DIN measurements along the plumes indicated a trend for reduction in DIN concentrations. The calculated DIN loads generated from sediment provide an order of magnitude estimate of these processes and should be considered as such.

7.4.2 The importance of PIN desorption

Adsorbed ammonium-N is attached to the negatively charged sediment particles originated from soil erosion. The potential for sediment to adsorb ammonium-N (PIN) depends on sediment type and characteristics as it is related to the cation exchange capacity of the sediment, which is a function of organic matter content, humic content and clay mineralogy (Boatman and Murray, 1982; Zhang et al. 2016). Most of the PIN will desorb from sediment (desorption of ammonium-N) in short timeframes (hours) when riverine sediment enters estuaries where there is higher ionic strength in the water as salinity increases, which allows for the replacement of the NH_4-N^+ by other cations (e.g. Na^+, K^+, Ca^{2+}, Mg^{2+}) (Boatman and Murray, 1982; Mackin and Aller, 1984).

PIN desorption was an important contributor to DIN generation in riverine flood plumes from the Burdekin River. This was localised to a specific area of the plume with lower salinities, but with a cation concentration enough to exchange with all the adsorbed ammonium present (as indicated by some initial preliminary measurements in the <11 PSU area of the plume). The objective of this study was not to examine the dynamics of PIN desorption/sorption processes, which have high complexity (Boatman and Murray, 1982; Zhang et al. 2016), but to obtain an indication of the magnitude of this potential source of DIN to coastal environments of the GBR. Indeed, the direct effect of this source of DIN from riverine sediment plumes would be localised at lower salinities, but may have an important secondary effect in generating DIN at later plume stages by fuelling primary production around the plume, which will in turn continue to generate DIN when secondary succession processes occur (Alongi and McKinnon, 2005).

7.4.3 The dynamics of DIN generation from the mineralisation of organic nitrogen

The potential mineralised DIN from organic nitrogen was verified in some of the sampled riverine flood plumes, but this was not the case in all sampled plumes. When it occurred, potential mineralised DIN increased linearly with no signs of slowing down after approximately 7 days (a typical longer plume travel time in the Burdekin River). After this time, it is likely that most of the sediment would have been deposited in the marine environment. This indicates that riverine sediment has the potential to continue to generate DIN once deposited on the marine floor and/or resuspended. It also indicates that predominantly labile sources of organic matter were mineralised in the timeframes associated with plume travel. Previous research in the GBR has demonstrated that 74 to 92% of deposited PN (Alongi et al. 2007) and 75 +/- 6% of the resuspended PN (Lønborg et al. 2018) are mineralised to DIN, and an average of 50% of the total N input to the sediment is lost through denitrification (Alongi et al. 2007). Most of the organic matter would be remineralised on broad continental shelves, like the GBR (Brunskill, 2010).

Changes in organic N mineralisation rates between plumes (i.e. catchment source), position in the plume and time after the peak of the plume event may likely be explained by a shift in the quality of the organic N (organic matter) in the plume as indicated by the multivariate analysis. This finding is supported by previous research which has found respiration rates (a proxy for remineralisation rates) are spatially and temporally variable in riverine plumes, indicating the heterogenous nature of organic matter sources and biological processes (Dagg et al. 2004). Larger DIN generation rates indicate a higher bioavailability of the organic N in the plume. Riverine (terrestrial) sources of organic matter have been found to be the main source of bacterial production in some riverine plumes with shifts in this source contribution between seasons where phytoplankton become the main source in the summer months of temperate riverine plumes. In this research, we found that mineralised DIN rates were highest in secondary plume water types associated with higher salinities. Research in the Mississippi River has found higher rates in the mid-salinity plume surface waters where the highest concentrations of plankton production and DOM occurred (Benner and Opsahl, 2001), which was not the case in plumes sampled in this research. It was argued that in high salinity waters of the Mississippi River plumes, phytoplankton production is greatly reduced by nutrient limitation and therefore bacterial DIN generation is also reduced (Cotner and Gardner, 1993). In the case of the Burdekin plumes that generated DIN, there were no signs of this type of limitation to the DIN generation process occurring. The increased rates at the higher salinities

observed in this study indicate an increased importance of a more labile organic matter source in the plume, which is likely plankton derived organic matter as in the Mississippi mid-salinity section of the plume. The higher decomposition rates of phytoplankton derived organic matter relative to terrestrially derived sources in estuaries, has been widely recognised (Bauer et al. 2013; Kandasamy and Nath, 2016). Although the source of organic matter to remineralisation was not assessed directly as part of this research (neither between terrestrial or marine nor between particulate and dissolved), there is evidence to indicate that at higher salinities the contribution of plankton derived organic matter became more important. This evidence includes the significantly higher remineralisation rates in the clearer sector of the plumes, the increase in the $\delta^{13}C$ of suspended organic matter in the outer sections of the BBB 2017 plume (Savoye et al. 2012) and the gradual increase in the relative presence of bacteria to fungi from freshwater to secondary plume waters (Chen et al. see Chapter 6 on Shifts in the chemical composition of particulate organic matter and microbial community from catchment to Reef). More research is needed to understand what the relative contribution is to mineralised DIN from riverine (terrestrial) sources of organic matter and plume generated organic matter (plankton) in riverine plumes of the GBR, as well as between POM and DOM.

Reductions in the mineralisation rates of organic N occurring one week after the peak of the Upper B 2018 plume (secondary waters) indicate that the bioavailability of the organic matter for microbial remineralisation was reduced. Bacterial production in riverine plumes has been found to be higher than in river waters and adjacent ambient marine waters (Dagg et al. 2004). A strong spatial relationship between bacterial production and primary production has also been found in many riverine plumes suggesting a strong coupling between both types of metabolism in riverine plumes (Dagg et al. 2004), which makes riverine plumes a temporal and spatial hotspot for organic matter processing and the generation of bioavailable nutrients.

The role of redox conditions on the bioavailability of organic N in the plumes also deserves further attention. Although some studies have shown faster organic matter decay rates under oxic conditions, some studies have shown no effect of redox conditions (Bianchi and Bauer, 2011). Incubation experiment conditions in our study were optimised to sustain an oxic environment during the experiment (large enough bottle headspace and continuous shaking). This may not be the case in the plume environment, though there is no clear evidence of the presence of anoxia in the sampled plumes. There was an increase in ammonium-N relative to NO_x-N at higher salinities both in the plume water samples and at the end of the incubation experiments. This seems to indicate faster N remineralisation rates than nitrification at higher salinities. However, this does not seem to be related to a lower availability of oxygen in the plume at higher salinities where the organic carbon loads are lower because it would be expected that oxic conditions would be more limiting to microbial processes at lower salinities where loads are higher. The lower NO_x-N levels at higher salinities may be explained by changes in the microbial community and/or faster NO_x-N uptake.

Lønborg et al. (2017) found PN and DON degradation rates of 0.29 d^{-1} ± 0.04 (average +/- SE) and 0.16 d ±0.07 $^{-1}$ respectively, from water column samples obtained at three sites of the GBR during the late dry, wet and early dry seasons. These rates are an order of magnitude higher than the highest rates estimated for the riverine plumes that mineralised N in this study and were also obtained using incubation experiments at similar temperatures (22-24℃). Differences in DOM bioavailability were related to plankton biomass and activity and DOM contained the majority of the bioavailable N in the system (60 ± 10%) although it also contained

a higher recalcitrant proportion than POM (Lønborg et al. 2018). Lønborg's rates reflect longer term conditions present in the GBR in which autochthonous production has a larger influence. Our study, on the other hand, reflects temporary conditions found during increased terrestrial influence of riverine sediment plumes, when terrestrial sediment and vegetation litter have an important influence. The relatively lower degradation rates in riverine plumes would be explained by terrestrial material being less bioavailable than marine derived material (Bauer et al. 2013; Lønborg et al. 2018). Irrespective of the differences in timeframes and drivers of bioavailability considered in both studies, our study also suggests that future work in the GBR should focus on total nutrient bioavailability and not only inorganic nutrient concentrations, in this case towards assessing the impact from end-of-catchment and riverine plume contributions.

7.4.4 Drivers of organic N mineralisation in riverine plumes

Net N immobilisation occurs when the metabolic N requirements of bacteria mineralising available organic carbon sources for energy exceed the N released from these sources. Consequently, any mineral N at the microsites of bacterial activity is absorbed by the microbes, resulting in a net removal (immobilisation) of mineral N from the surrounding water and/or the mineralisation process. Samples from the Tully 2018 and Mixed B 2019 plumes appear to have exhibited such behaviour, which was also the case for several gully remediation sites monitored in the Burdekin catchment during the same wet season (Garzon-Garcia et al. 2019). This indicates that the 2018/19 wet season events in the Burdekin may have had special characteristics that caused immobilisation instead of mineralisation.

Water quality differences between riverine plumes from the Burdekin River and the multivariate analysis results indicate that the source of the organic matter (quality to remineralisation) and the availability of DIN relative to the available organic matter for mineralisation were important determinants of immobilisation or remineralisation of N in the riverine plumes sampled. This confirms some of our previous findings, which indicate organic carbon as a key driver of particulate nitrogen bioavailability (Garzon-Garcia et al. 2018; Garzon-Garcia et al. 2018). A great fraction of the organic matter in large riverine plumes is soil-derived, diagenetically altered and relatively resistant to microbial degradation (Dagg et al. 2004; Keil et al. 1997; Meybeck, 1982). Decaying vascular plant material, which is considered generally refractory unless microbial activity converts it to more labile forms, is especially important in some estuarine systems (Bianchi and Bauer, 2011). Carbon has been found to limit heterotrophic processes in riverine plumes of the Amazon River (Benner et al. 1995) and previous research has also highlighted the importance of available DIN in the riverine plume in determining how important DIN generation from sediment is in driving primary production from riverine plumes (Dagg et al. 2004). Nonetheless, even in riverine plumes with relatively higher DIN concentrations, regeneration processes from particulate N appear to be of importance (Dagg et al. 2004). Catchment conditions before the high-flow event producing riverine plumes, including antecedent soil moisture conditions, and the distribution, frequency and intensity of rainfall may have also had an important role in determining organic matter characteristics and DIN availability in riverine sediment plumes, which would also explain immobilisation in samples from the Burdekin 2018/19 wet season (Birch, 1964). Further research is needed on the relative importance to riverine plume mineralisation of different organic matter sources (e.g. vegetation litter type) and its associated catchment processes (e.g. leaching versus erosion).

The trend for a decrease in DON along the salinity gradient indicates a large contribution of terrestrial sources to DON in plume water and potentially some production along the plume. The decreasing trend may be partly explained by mineralisation of DON to generate DIN, as confirmed in mineralisation experiments, as well as conservative mixing. The fact that the DOC to DON ratio became an important explanatory variable of mineralisation for longer timeframes (~7 days), indicates that DON increases its importance as a source of DIN as DIN is depleted in the plume. It is recognised that the extent of DON contribution from riverine plumes to marine primary production is uncertain and that a portion of the riverine DON pool is likely refractory, though there is no evidence that indicates riverine DOM accumulates in the ocean (Bainbridge et al. 2018; Dagg et al. 2004). It has been suggested though, that given the important proportion of dissolved organic matter in riverine plumes and the rapid settling of particulates, DOM may be important in the cycling of C, N and P in riverine plumes. More research is needed to understand the relative importance of particulate and dissolved organic N to DIN generation from riverine plumes of the GBR.

7.5 Conclusions and implications for management

This research has demonstrated that riverine flood plumes have the potential to contribute significant loads of bioavailable N to GBR coastal environments and that deposited sediment from these plumes has the potential to continue to generate bioavailable N *in-situ* or during subsequent resuspension. Cascading effects associated with plume biogeochemistry, including primary production fuelled by these plumes, may have longer term effects on the GBR and have wider spatial scale effects than the riverine plume itself. The risk to the GBR from this source of bioavailable nutrients needs further assessment, but it is likely that it would be of larger importance to inshore reefs impinged by riverine plumes from grazing catchments with high quantities of soil erosion like the Burdekin River and the Fitzroy River. The impact on the GBR from riverine plume DIN generation depends on the type of organic matter in the plume and DIN availability to mineralisation, which in turn are likely dependent on the POM type/source and other catchment processes including vegetation type, litter availability and antecedent catchment conditions. Understanding the sources of the sediment with a larger risk of generating DIN in the marine environment and the link between the organic matter (e.g. vegetation type) and DIN generation in sediment plumes is critical to inform catchment rehabilitation and vegetation management strategies to reduce the impact of sediment and its associated bioavailable nutrients to the GBR and its coastal ecosystems.

Acknowledgements

References

Alongi, D.M., McKinnon, A.D., 2005. The cycling and fate of terrestrially-derived sediments and nutrients in the coastal zone of the Great Barrier Reef shelf, in: Marine Pollution Bulletin. pp. 239–252. https://doi.org/10.1016/j.marpolbul.2004.10.033

Alongi, D.M., Trott, L.A., Pfitzner, J., 2007. Deposition, mineralization, and storage of carbon and nitrogen in sediments of the far northern and northern Great Barrier Reef shelf. Cont. Shelf Res. 27, 2595–2622. https://doi.org/10.1016/j.csr.2007.07.002

APHA/AWWA/WPCF, 2012. Standard Methods for the Examination of Water and Wastewater, 21st and 22nd edition.

Azov, Y., 1991. Eastern Mediterranean-a marine desert? Mar. Pollut. Bull. 23, 225–232. https://doi.org/10.1016/0025-326X(91)90679-M

Bainbridge, Z., Lewis, S., Bartley, R., Fabricius, K., Collier, C., Waterhouse, J., Garzon-Garcia, A., Robson, B., Burton, J., Wenger, A., Brodie, J., 2018. Fine sediment and particulate organic matter: A review and case study on ridge-to-reef transport, transformations, fates, and impacts on marine ecosystems. Mar. Pollut. Bull. 135, 1205–1220. https://doi.org/10.1016/j.marpolbul.2018.08.002

Bainbridge, Z., Lewis, S., Stevens, T., Petus, C., Lazarus, E., Gorman, J., Smithers, S., n.d. Measuring sediment grain size across the catchment to reef continuum: Improved methods and environmental insights. Mar. Pollut. Bull.

Bainbridge, Z.T., Lewis, S.E., Smithers, S.G., Kuhnert, P.M., Henderson, B.L., Brodie, J.E., 2014. Fine-suspended sediment and water budgets for a large, seasonally dry tropical catchment: Burdekin River catchment, Queensland, Australia. Water Resour. Res. 50, 9067–9087. https://doi.org/10.1002/2013wr014386

Bainbridge, Z.T., Wolanski, E., Alvarez-Romero, J.G., Lewis, S.E., Brodie, J.E., 2012. Fine sediment and nutrient dynamics related to particle size and floc formation in a Burdekin River flood plume, Australia. Mar. Pollut. Bull. 65, 236–248. https://doi.org/10.1016/j.marpolbul.2012.01.043

Bartley, R., Waters, D., Turner, R., Kroon, F., Wilkinson, S., Garzon-Garcia, A., Kuhnert, P., Lewis, S., Smith, R., Bainbridge, Z., Olley, J., Brooks, A., Burton, J., Brodie, J., Waterhouse, J., 2017. Sources of sediment, nutrients, pesticides and other pollutants to the Great Barrier Reef, in: Scientific Consensus Statement 2017: A Synthesis of the Science of Land-Based Water Quality Impacts on the Great Barrier Reef. State of Queensland, Queensland.

Bauer, J.E., Cai, W.J., Raymond, P.A., Bianchi, T.S., Hopkinson, C.S., Regnier, P.A.G., 2013. The changing carbon cycle of the coastal ocean. Nature 504, 61–70. https://doi.org/10.1038/nature12857

Benner, R., Opsahl, S., 2001. Molecular indicators of the sources and transformations of dissolved organic matter in the Mississippi river plume. Org. Geochem. 32, 597–611. https://doi.org/10.1016/S0146-6380(00)00197-2

Benner, R., Opsahl, S., Chin-Leo, G., Richey, J.E., Forsberg, B.R., 1995. Bacterial carbon metabolism in the Amazon River system. Limnol. Oceanogr. 40, 1262–1270. https://doi.org/10.4319/lo.1995.40.7.1262

Bianchi, T.S., Bauer, J.E., 2011. Particulate Organic Carbon Cycling and Transformation. Treatise Estuar. Coast. Sci. Vol 5 Biogeochem. 69–117.

Birch, H.F., 1964. Mineralisation of plant nitrogen following alternate wet and dry conditions. Plant Soil 20. https://doi.org/10.1007/BF01378096

Boatman, C.D., Murray, J.W., 1982. Modeling exchangeable NH4+ adsorption in marine sediments - Process and controls of adsorption. Limnol. Oceanogr. 27, 99–110.

Brodie, J., Burford, M., Davis, A., da Silva, E., Devlin, M., Furnas, M., 2015. The relative risks to water quality from particulate nitrogen discharged from rivers to the Great Barrier Reef in comparison to other forms of nitrogen.

Brodie, J., Fabricius, K., De'ath, G., Okaji, K., 2005. Are increased nutrient inputs responsible for more outbreaks of crown-of-thorns starfish? An appraisal of the evidence. Mar. Pollut. Bull. 51, 266–278. https://doi.org/10.1016/j.marpolbul.2004.10.035

Brunskill, G.J., 2010. An overview of tropical margins, in: Atkinson, L., Quinones, R., Talaue-McManus, L. (Eds.), Carbon and Nutrient Fluxes in Continental Margins: A Global Synthesis. Springer, pp. 423–426.

Cotner, J.B., Gardner, W.S., 1993. Heterotrophic bacterial mediation of ammonium and dissolved free amino acid fluxes in the Mississippi River plume. Mar. Ecol. Prog. Ser. 93, 75–87. https://doi.org/10.3354/meps093075

Dagg, M., Benner, R., Lohrenz, S., Lawrence, D., 2004. Transformation of dissolved and particulate materials on continental shelves influenced by large rivers: Plume processes. Cont. Shelf Res. 24, 833–858. https://doi.org/10.1016/j.csr.2004.02.003

De'ath, G., Fabricius, K., 2010. Water quality as a regional driver of coral biodiversity and macroalgae on the Great Barrier Reef. Ecol. Appl. 20, 840–850. https://doi.org/10.1890/08-2023.1

Demaster, D.J., Pope, R.H., 1996. Nutrient dynamics in Amazon shelf waters: Results from AMASSEDS. Cont. Shelf Res. 16, 263–289. https://doi.org/10.1016/0278-4343(95)00008-O

DeVantier, L.M., De'ath, G., Turak, E., Done, T.J., Fabricius, K.E., 2006. Species richness and community structure of reef-building corals on the nearshore Great Barrier Reef. Coral Reefs 25, 329–340. https://doi.org/10.1007/s00338-006-0115-8

Devlin, M., Waterhouse, J., Taylor, J., Brodie, J.E., 2001. Flood plumes in the Great Barrier Reef: spatial and temporal patterns in composition and distribution. GBRMPA Res. Publ. No. 68.

Devlin, M.J., Brodie, J., 2005. Terrestrial discharge into the Great Barrier Reef Lagoon: Nutrient behavior in coastal waters, in: Marine Pollution Bulletin. pp. 9–22. https://doi.org/10.1016/j.marpolbul.2004.10.037

eReefs Marine Water Quality Dashboard [WWW Document], n.d. URL http://www.bom.gov.au/marinewaterquality/ (accessed 11.30.20).

eWater Coop, 2015. Water Quality Analyser v2.1.1.6.

Fabricius, K.E., 2005. Effects of terrestrial runoff on the ecology of corals and coral reefs: review and synthesis. Mar. Pollut. Bull. 50, 125–146. https://doi.org/10.1016/j.marpolbul.2004.11.028

Fabricius, K.E., Logan, M., Weeks, S., Brodie, J., 2014. The effects of river run-off on water clarity across the central Great Barrier Reef. Mar. Pollut. Bull. 84, 191–200. https://doi.org/10.1016/j.marpolbul.2014.05.012

Fabricius, K.E., Logan, M., Weeks, S.J., Lewis, S.E., Brodie, J., 2016. Changes in water clarity in response to river discharges on the Great Barrier Reef continental shelf: 2002-2013. Estuar. Coast. Shelf Sci. 173, A1–A15. https://doi.org/10.1016/j.ecss.2016.03.001

Fabricius, K.E., Okaji, K., De'ath, G., 2010. Three lines of evidence to link outbreaks of the crown-of-thorns seastar Acanthaster planci to the release of larval food limitation. Coral Reefs 29, 593–605. https://doi.org/10.1007/s00338-010-0628-z

Franklin, H.M., Garzon-Garcia, A., Joanne., B., Moody, P.W., De Hayr, R.W., Burford, M.A., 2018. A novel bioassay to assess phytoplankton responses to soil-derived particulate nutrients. Sci. Total Environ. 636, 1470–1479.

Furnas, M., Alongi, D., McKinnon, D., Trott, L., Skuza, M., 2011. Regional-scale nitrogen and phosphorus budgets for the northern (14 degrees S) and central (17 degrees S) Great Barrier Reef shelf ecosystem. Cont. Shelf Res. 31, 1967–1990. https://doi.org/10.1016/j.csr.2011.09.007

Furnas, M., Mitchell, A., Skuza, M., Brodie, J., 2005. In the other 90%: phytoplankton responses to enhanced nutrient availability in the Great Barrier Reef Lagoon. Mar. Pollut. Bull. 51, 253–265. https://doi.org/10.1016/j.marpolbul.2004.11.010

Furnas, M.J., Mitchell, A.W., 2001. Runoff of terrestrial sediment and nutrients into the Great Barrier Reef World Heritage Area, in: Wolanski, E. (Ed.), Oceanographic Processes of Coral Reefs: Physical and Biological Links in the Great Barrier Reef. CRC Press, Boca Raton, pp. 37–51.

Gardner, W.S., Cotner, J.B., Eadie, B.J., Cavaletto, J.F., Benner, R., Chin-Leo, G., 1994. Mineralization of organic material and bacterial dynamics in Mississippi River plume water. Estuaries 17, 816–828. https://doi.org/10.2307/1352750

Garzon-Garcia, A, Bunn, S.E., Olley, J.M., Oudyn, F., 2018. Labile carbon limits in-stream mineralization in a subtropical headwater catchment affected by gully and channel erosion. J. Soils Sediments 18, 648–659. https://doi.org/DOI 10.1007/s11368-017-1832-z

Garzon-Garcia, A., Burton, J., Ellis, R., Askildsen, M., Moody, P., DeHayr, R., n.d. The bioavailability of particulate nitrogen in sediment: catchment sources and processes. Prep.

Garzon-Garcia, Alexandra, Burton, J., Franklin, H.M., Moody, P.W., De Hayr, R.W., Burford, M.A., 2018. Indicators of phytoplankton response to particulate nutrient bioavailability in fresh and marine waters of the Great Barrier Reef. Sci. Total Environ. 636, 1416–1427.

Garzon-Garcia, A., Burton, J., Prance, M., Moody, P., DeHayr, R., 2019. Towards the standardisation of bioavailable particulate nitrogen in sediment methods. Department of Environment and Science, Brisbane.

Gruber, R., Waterhouse, J., Logan, M., Petus, C., Howley, C., Lewis, S., Tracey, D., Langlois, L., Tonin, H., Skuza, M., Costello, P., Davidson, J., Gunn, K., Lefevre, C., Moran, D., Robson, B., Shanahan, M., Zagorskis, I., Shellberg, J., Neilen, A., 2020. Marine Monitoring Program: Annual Report for Inshore Water Quality Monitoring 2018-19. Townsville, Australia.

Haapkyla, J., Unsworth, R.K.F., Flavell, M., Bourne, D.G., Schaffelke, B., Willis, B.L., 2011. Seasonal Rainfall and Runoff Promote Coral Disease on an Inshore Reef. PLoS One 6. https://doi.org/10.1371/journal.pone.0016893

Joo, M., Raymond, M.A.A., McNeil, V.H., Huggins, R., Turner, R.D.R., Choy, S., 2012. Estimates of sediment and nutrient loads in 10 major catchments draining to the Great Barrier Reef during 2006-2009. Mar. Pollut. Bull. 65, 150–166. https://doi.org/10.1016/j.marpolbul.2012.01.002

Kalbitz, K., Schmerwitz, D., Schwesig, D., Matzner, E., 2003. Biodegradation of soil-derived dissolved organic matter as related to its properties. Geoderma 113, 273–291. https://doi.org/10.1016/S0016-7061(02)00365-8

Kandasamy, S., Nath, B.N., 2016. Perspectives on the terrestrial organic matter transport and burial along the land-deep sea continuum: Caveats in our understanding of biogeochemical processes and future needs. Front. Mar. Sci. https://doi.org/10.3389/fmars.2016.00259

Keil, R.G., Mayer, L.M., Quay, P.D., Richey, J.E., Hedges, J.I., 1997. Loss of organic matter from riverine particles in deltas. Geochim. Cosmochim. Acta 61, 1507–1511. https://doi.org/10.1016/S0016-7037(97)00044-6

Ladson, A.R., Brown, R., Neal, B., Nathan, R., 2013. A standard approach to baseflow separation using the Lyne and Hollick filter. Aust. J. Water Resour. 17, 25–34. https://doi.org/10.7158/W12-028.2013.17.1

Lewis, S., Bainbridge, Z., Stevens, T., Garzon-Garcia, A., Chen, C., Burton, J., Bahadori, M., Rezaei Rashti, M., Smithers, S., Olley, J.M., Moody, P.W., Dehayr, R., 2019. Progress report on 2018/19 NESP What's really damaging the Reef? - results and activities. Townsville, Australia.

Lewis, S., Bainbridge, Z., Stevens, T., Gorman, J., Smithers, S., Chen, C., Olley, J., Bahadori, M., Burton, J., Garzon-Garcia, A., Moody, P., Dehayr, R., 2018. Sediment tracing from the catchment to the reef: preliminary results from 2018 flood plume case studies, logger and sediment trap time series and an overview of project progress. Report to the National Envirohmental Science Programme. Cairns.

Lohrenz, S.E., Lang, G.A., Chenl, X., 1997. Variations in primary production of northern Gulf of Mexico continental shelf waters linked to nutrient inputs from the Mississippi River.

Lønborg, C., Álvarez–Salgado, X.A., Duggan, S., Carreira, C., 2018. Organic matter bioavailability in tropical coastal waters: The Great Barrier Reef. Limnol. Oceanogr. 63, 1015–1035. https://doi.org/10.1002/lno.10717

Lumley, T., 2017. leaps: Regression Subset Selection. R package.

Mackin, J.E., Aller, R.C., 1984. Ammonium adsorption in marine-sediments. Limnol. Oceanogr. 29, 250–257.

Mayer, L.M., Keil, R.G., Macko, S.A., Joye, S.B., Ruttenberg, K.C., Aller, R.C., 1998. Importance of suspended particulates in riverine delivery of bioavailable nitrogen to coastal zones. Global Biogeochem. Cycles 12, 573–579. https://doi.org/10.1029/98GB02267

McDowell, W.H., Zsolnay, A., Aitkenhead-Peterson, J.A., Gregorich, E.G., Jones, D.L., Jodemann, D., Kalbitz, K., Marschner, B., Schwesig, D., 2006. A comparison of methods to determine the biodegradable dissolved organic carbon from different terrestrial sources. Soil Biol. Biochem. 38, 1933–1942. https://doi.org/10.1016/j.soilbio.2005.12.018

Meybeck, M., 1982. Carbon, nitrogen, and phosphorus transport by world rivers. Am. J. Sci. 282, 401–450. https://doi.org/10.2475/ajs.282.4.401

Petus, C., Waterhouse, J., Lewis, S., Vacher, M., Tracey, D., Devlin, M., 2019. A flood of information: Using Sentinel-3 water colour products to assure continuity in the monitoring of water quality trends in the Great Barrier Reef (Australia). J. Environ. Manage. 248. https://doi.org/10.1016/j.jenvman.2019.07.026

Petzoldt, T., 2018. growthrates: Estimation of growthrates. R package.

Qualls, R.G., Haines, B.L., 1992. Biodegradability of dissolved organic matter in forest throughfall, soil solution and stream water. Soil Sci. Soc. Am. J. 56, 578–586.

Rabalais, N.N., Diaz, R.J., Levin, L.A., Turner, R.E., Gilbert, D., Zhang, J., 2010. Dynamics and distribution of natural and human-caused hypoxia. Biogeosciences 7, 585–619.

Rabalais, N.N., Turner, R.E., Scavia, D., 2002. Beyond science into policy: Gulf of Mexico hypoxia and the Mississippi River. Bioscience 52, 129–142. https://doi.org/10.1641/0006-3568(2002)052[0129:BSIPGO]2.0.CO;2

Rosenfeld, J.K., 1979. Ammonium adsorption in nearshore anoxic sediments. Limnol. Oceanogr. 24, 356–364.

Savoye, N., David, V., Morisseau, F., Etcheber, H., Abril, G., Billy, I., Charlier, K., Oggian, G., Derriennic, H., Sautour, B., 2012. Origin and composition of particulate organic matter in a macrotidal turbid estuary: The Gironde Estuary, France. Estuar. Coast. Shelf Sci. 108, 16–28. https://doi.org/10.1016/j.ecss.2011.12.005

Stanley, D.J., Warne, A.G., 1993. Nile delta: Recent geological evolution and human impact. Science (80-.). 260, 628–634. https://doi.org/10.1126/science.260.5108.628

Steven, A.D.L., Baird, M.E., Brinkman, R., Car, N.J., Cox, S.J., Herzfeld, M., Hodge, J., Jones, E., King, E., Margvelashvili, N., Robillot, C., Robson, B., Schroeder, T., Skerratt, J., Tickell, S., Tuteja, N., Wild-Allen, K., Yu, J., 2019. eReefs: An operational information system for managing the Great Barrier Reef. J. Oper. Oceanogr. 12, S12–S28. https://doi.org/10.1080/1755876X.2019.1650589

Van Meter, K.J., Van Cappellen, P., Basu, N.B., 2018. Legacy nitrogen may prevent achievement of water quality goals in the Gulf of Mexico. Science. 360, 427–430. https://doi.org/10.1126/science.aar4462

Waterhouse, J., Mann, R., Sutcliffe, T., Waters, D., Adame, F., 2017. The risk from anthropogenic pollutants to the Great Barrier Reef coastal and marine ecosystems, in: Scientific Consensus Statement 2017: A Synthesis of the Science of Land-Based Water Quality Impacts on the Great Barrier Reef. State of Queensland, Brisbane, Australia, p. 196.

Wooldridge, S.A., 2009. Water quality and coral bleaching thresholds: Formalising the linkage for the inshore reefs of the Great Barrier Reef, Australia. Mar. Pollut. Bull. 58, 745–751. https://doi.org/10.1016/j.marpolbul.2008.12.013

Zhang, L., Wang, S.R., Jiao, L.X., Li, Y.P., Yang, J.C., Zhang, R., Feng, S., Wang, J., 2016. Effects of organic matter content and composition on ammonium adsorption in lake sediments. Environ. Sci. Pollut. Res. 23, 6179–6187. https://doi.org/10.1007/s11356-015-5820-9

CHAPTER 8

Geochemistry and provenance of sediment plume samples collected from the Burdekin region of the Great Barrier Reef lagoon, Australia

Zoe Bainbridge[1], Jon Olley[2], Stephen Lewis[1] and Thomas Stevens[1]

[1]Catchment to Reef Research Group, TropWATER, James Cook University, Townsville
[2]Australian Rivers Institute, Griffith University, Nathan, Brisbane

Abstract

The novel application of the SediPump® sampling device to capture sufficient sediment mass from low concentration flood plume waters has enabled catchment source tracing of GBR flood plume sediment for the first time. Focused on the single largest exporter of sediment to the GBR, the Burdekin River, three wet season discharge events were sampled from 2017 to 2019 to characterise and trace flood plume suspended sediments using geochemistry, fallout radionuclides and clay mineralogy. Sampling targeted the end-of-river (EoR) flow hydrograph to capture contributing catchment sources, and flood plume samples from both the adjacent turbid primary waters and offshore secondary waters up to 160 km from the EoR. Analysis of EoR and plume sediment major element geochemistry indicates standard geochemical sediment tracing approaches cannot be applied to a large river catchment such as this, or across the catchment-marine continuum, where particle fractionation has occurred both within the catchment and across the salinity gradient from the river mouth. Further, the secondary plume sediments have also been affected by the addition of marine-sourced carbonate and biogenic silica. We show elemental ratios of the rare earth elements (REE) and thorium (Th) can be used as stable tracers across this continuum, and importantly, used to trace Burdekin plume terrigenous sediment transported >100 kms from the river mouth back to its EoR REE/Th signal, which was unique for each of the three discharge events. These ratios were also used to trace this sediment to a major sub-catchment source. Additional fallout radionuclide ^{137}Cs and ^{210}Pb$_{ex}$ analysis of a sub-set of Burdekin EoR and plume samples also reveal sediment being transported in these GBR flood plumes are almost exclusively derived from sub-surface erosion processes.

8.1 Introduction

The Great Barrier Reef World Heritage Area (GBRWHA) extends along the Queensland coast for 2000 km. The coast adjoining the GBRWHA has a diverse range of wet and dry tropical catchments covering an area of 423,000 km^2. The Burdekin River catchment (133,000 km^2) drains into the central region of the Great Barrier Reef lagoon and has been identified as the largest contributor of sediment to the GBRWHA using catchment scale modelling (e.g. Kroon

et al. 2012). Hence the catchment is a priority for erosion mitigation measures (Waterhouse et al. 2012). Focused research within the Burdekin catchment over the past decade have constructed catchment-scale sediment budgets and identified the higher sediment contributing sub-catchments (Bainbridge et al. 2014, 2016; Bartley et al. 2015; Lewis et al. 2013; Furuichi et al. 2016), as well as ascertained the dominant erosion processes at a sub-catchment scale (Wilkinson et al. 2013; 2015). However, further characterisation of the sediment exported from the Burdekin into the central GBR lagoon, and its source within the Burdekin is still required to further refine key source areas and prioritise management efforts (see Bartley et al. 2014). Here sediment tracing techniques are used to determine the provenance of sediments present in Burdekin flood plumes delivered to the inshore Great Barrier Reef lagoon, and to determine the dominant contributing erosion processes.

To determine the provenance, we compare the geochemical characteristics of suspended sediments collected from Burdekin flood plumes in 2017, 2018, and 2019, with suspended sediment samples collected from the major tributary catchments. The geochemical characteristics of sediments are strongly influenced by those of the soils and ultimately the rock-types from which they are derived (Caitcheon et al. 2006). Different underlying parent rock materials often results in spatial sources with distinct geochemical compositions (Olley et al. 2001; Douglas et al. 2003). Sediments eroded from soils derived from a particular rock type often maintain these distinct geochemical properties during sediment generation and transport processes (Caitcheon et al. 2006; Hughes et al. 2009). Sediment geochemistry has been widely used to identify the spatial sources of sediments in Australia and around the World (Collins et al. 1996; Collins et al. 1998; Olley and Caitcheon, 2000; Hardy et al. 2010; Weltje and Brommer, 2010).

The fallout radionuclides ^{137}Cs and ^{210}Pb$_{ex}$ have been widely used to determine the relative contributions of surface soil and channel erosion (gully and stream banks) to stream sediments (Wallbrink et al. 1994, 1998; Walling and Woodward, 1992; Olley et al. 1993; Everett et al. 2008; Hancock et al. 2014). ^{137}Cs is a product of atmospheric nuclear weapons testing that occurred during the 1950-60s. Caesium has a half-life of 30 years and deposition of ^{137}Cs largely ceased in Australia by 1970. Initially the distribution of this nuclide in the soil decreased exponentially with depth, with the maximum concentration at the surface. However, due to processes of diffusion the maximum concentration is now generally found just below the surface in undisturbed soils. The bulk of the activity of this nuclide is retained within the top 100 mm of the soil profile (Wallbrink et al. 1998). In subsoils recently exposed by erosion, ^{137}Cs is virtually absent (Wallbrink and Murray 1993, Hancock et al. 2014).

Fallout ^{210}Pb$_{ex}$ is a naturally occurring radionuclide, formed through the radioactive decay of ^{222}Rn gas. The parent of ^{222}Rn is ^{226}Ra, part of the ^{238}U decay series. These radionuclides are present in all soils. Some ^{222}Rn gas escapes from the soil into the atmosphere where it decays to ^{210}Pb. This ^{210}Pb is then deposited on the soil surface, primarily by rain. ^{210}Pb$_{ex}$ is calculated as the activity concentration of ^{210}Pb minus that of ^{226}Ra. The maximum concentrations of fallout ^{210}Pb$_{ex}$ (known as 'unsupported' or 'excess') in soils are found at the surface. Concentrations then generally decrease over depth to detection limits at about 100 mm depth (Wallbrink et al. 1998). ^{210}Pb has a half-life of 22.3 years and deposition across a region is more or less constant.

As fallout radionuclides are concentrated in the surface soil, sediments derived from sheet and rill erosion will have the highest concentrations, while sediment eroded from gully walls or channel banks have little or no fallout nuclides present. Sediments eroded from areas such as scalds or gully floors, which have previously lost all of the material labelled with ^{137}Cs may contain ^{210}Pb$_{ex}$, because it is continuously being deposited. Sediments labelled with ^{210}Pb$_{ex}$ but not having ^{137}Cs present may therefore have been derived from erosion of gully floors or scalds (Wallbrink et al. 1998). Also once a sediment particle is transported into the fluvial system it can accumulate additional fallout ^{210}Pb by direct deposition. As storage and transport time in the river system increases, the sediments would attain higher ^{210}Pb$_{ex}$ activities (Wallbrink et al. 2002). This additional ^{210}Pb$_{ex}$ can be used to estimate the storage and transit time of the sediment (Wallbrink et al. 2002).

Here we measure, for the first time, activity concentrations of ^{137}Cs and ^{210}Pb$_{ex}$ in Burdekin flood plume sediment delivered to the inshore Great Barrier Reef lagoon and compare them with concentrations in catchment source sediments.

Chapter 2 has characterised the 2017 to 2019 Burdekin end of river and flood plume suspended sediment samples of this study for mineral grain size and the transformation to organic-rich flocs that occur once this sediment is transported within the marine environment. Sediment exported from this catchment is dominated by fine sediment (<20 µm fraction = 88 ±4%), highlighting the particle fractionation of sediment that has occurred during transport through this large river catchment. For four of the major sub-catchments of the Burdekin this includes passing through a large reservoir, the Burdekin Falls Dam, and the preferential trapping of coarser-sized particles (Lewis et al. 2013). Previous clay mineral analysis of limited plume sampling by Bainbridge et al. (2016) also identified potential sediment fractionation processes occurring and the associated challenges. These transport processes often change the properties of sediment that are being used to trace the source of the material, and form a major challenge in sediment tracing research that is investigated in this study.

8.2 Methods

8.2.1 Burdekin River flood plume events

This study focuses on three Burdekin River flood plumes generated by minor to large end-of-river discharge events that occurred in March 2017, March 2018 and February 2019 (Figure 8.1). A moderate flood level for the Burdekin River (Inkerman Bridge) was reached on the 30th March 2017, following Tropical Cyclone Debbie's crossing of the Queensland coastline and associated heavy rainfall and rapid river rises. Over a six-day period the Burdekin discharged 1.6 million ML and 1.5 million tonnes of suspended sediment (Waterhouse et al. 2018). This discharge was almost exclusively sourced from the Bowen-Broken-Bogie River sub-catchments below the Burdekin Falls Dam (BFD) with a minor input from the Suttor River catchment. The resultant flood plume moved in an easterly/south-easterly direction coinciding with northerly winds (Figure 8.1a).

Heavy rainfall occurred in the upper Burdekin River catchment in late February/early March 2018, which triggered minor flood levels in the downstream river reaches that flow into the BFD. While the end-of-river water level peaked just below the Inkerman Bridge minor flood level on the 5th March, the flow event was the largest in the catchment area above the BFD

since 2012. Four million ML was discharged during the three weeks from the 28th February. Satellite imagery showed the early plume extent was largely confined to Upstart Bay, and began to extend northwards into Bowling Green Bay on the 6th March (Figure 8.1b). By the 10th March the plume had extended northwards past Magnetic Island and into the Palm Island Group. Subsequent imagery showed the plume continued to influence this northern region until at least the 29th March (last clear image), including the NESP sediment trap site at Havannah Island.

In February 2019 a prolonged and 'large flood event' discharged 14.5 million ML in the three-weeks from 30th January (Gruber et al. 2020). This was the largest Burdekin discharge event since the extreme flows of 2010/11. Over this time, moderate to major flooding occurred in the Upper Burdekin, Cape and Bowen-Broken-Bogie sub-catchments of the Burdekin. The resulting flood plume moved in a northerly direction following the coastline (Figure 8.1c), until weather conditions changed and the plume moved easterly offshore on the 12th February. Satellite imagery documented the passing of these turbid plume waters over the mid-shelf at Old Reef on 13th February (Figure 8.1c; refer also to Figure 2.12, Chapter 2).

8.2.2 Plume sediment sampling and sample preparation

Flood plume suspended sediment samples (hereafter referred to as plume sediment) were collected following Burdekin end-of-river flood peak during the March 2017, March 2018 and February 2019 discharge events. Plume sampling targeted inshore turbid primary waters within Upstart Bay and offshore secondary waters during each event (where conditions allowed) to best characterise plume sediment being transported within the GBR lagoon. Near real-time MODIS satellite imagery was used to track plume movement and extent to guide sampling, with locations shown in Figures 8.1 a to c. Due to poor weather conditions the 2017 plume sampling focused only on the turbid primary plume within Upstart Bay. The 2018 and 2019 sampling targeted Burdekin plume secondary waters as they passed over the NESP sediment trap and environmental logger sites at Orchard Rocks off Magnetic Island and further north at Havannah Island (Palm Island Group). The 2019 sampling also targeted Burdekin plume waters that reached the mid-shelf at Old Reef (refer to Chapter 2), following a shift in plume direction due to changing weather conditions.

The SediPump® high-volume filtration system (Stevens, 2019) was used to capture sufficient suspended particulate matter (SPM) for sediment tracing analysis from low concentration (i.e. <5 mg L^{-1}) surface plume waters (top 0.5 m of water column) (Bainbridge et al. In review, Chapter 2). SediPump® sampling of the plume water at depth (i.e.1-2 m above local benthic depth) was also conducted at the NESP logger sites at Orchard Rocks (Magnetic Island) and Havannah Island in 2018 and 2019, and at Old Reef. The SediPump® allows large volumes of water (> 6 KL) to be filtered over 2.5 to 3 hours of operation through a 1 μm string filter to recover ~ 0.4 to 5.0 g of material. The string filters were placed in a 10 L container with site water and, on return to the laboratory, cut to release the SPM. The samples were transferred into dialysis tubing to remove salts through continuous rinsing in RO water (Bainbridge et al. In review) and the <10 μm fraction was then recovered via the settling method for geochemistry and radionuclide analysis. Salinity at the time of sampling was measured at each location.
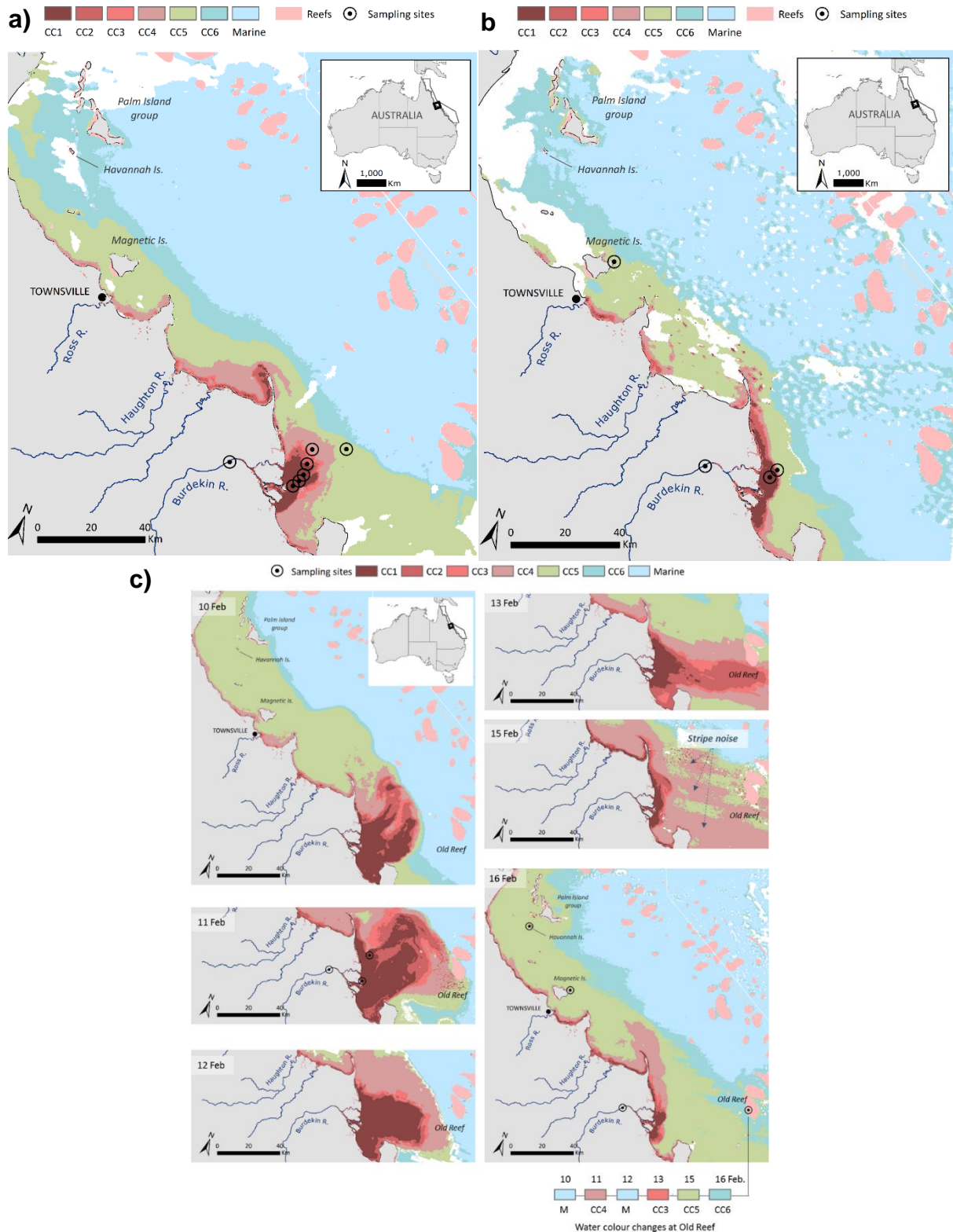
Figure 8.1. Burdekin River 2017, 2018 and 2019 flood plume sampling locations and associated water type mapped using corresponding MODIS satellite imagery (refer to Chapter 2) for each day the flood plume was sampled. For further detail on water type mapping refer to Chapter 2. Map series (a) 31st March 2017; (b), 6th March 2018 with primary plume samples collected on this date and northern sites (collected on the 13th March) also shown and (c) February 2019 time series (10-16th) highlighting the plume movements; the primary turbid plume sites were sampled and shown on the 11th February image, and the northern (sampled on the 13th) and Old Reef (sampled on the 15th) sites shown on the 16th February image. Source: Bainbridge et al. In review.

8.2.3 River sediment sampling and sample preparation

During each event (March 2017, March 2018 and February 2019) river suspended sediment samples (freshwater) were collected from the Burdekin River at the Inkerman Bridge. This sample location (Figure 8.2) is taken as the End of River (EoR) sampling site. Surface water 'grab' samples (top 0.5 m of water column) were collected throughout the streamflow hydrograph and represent the material being delivered to the river mouth. Hereafter these samples will be referred to as EoR sediment.

Samples were also collected to characterize each of the major contributing sub-catchments. River water samples were collected from existing streamflow gauge locations draining the five major sub-catchments of the Burdekin River (Upper Burdekin, Cape, Belyando, Suttor and Bowen rivers) and the ungauged Bogie River during streamflow events over five consecutive wet seasons (2005/06 - 2009/10). Further detail on sampling and site locations are provided in Bainbridge et al. (2014). Additional samples for the Bogie River (2) and Upper Burdekin River (2) were collected in the 2018/19 wet season. The <10 μm sediment fraction was recovered from collected water samples (1-5 L per sample) via the settling method for mineralogy and geochemistry analysis (Bainbridge et al. 2016).
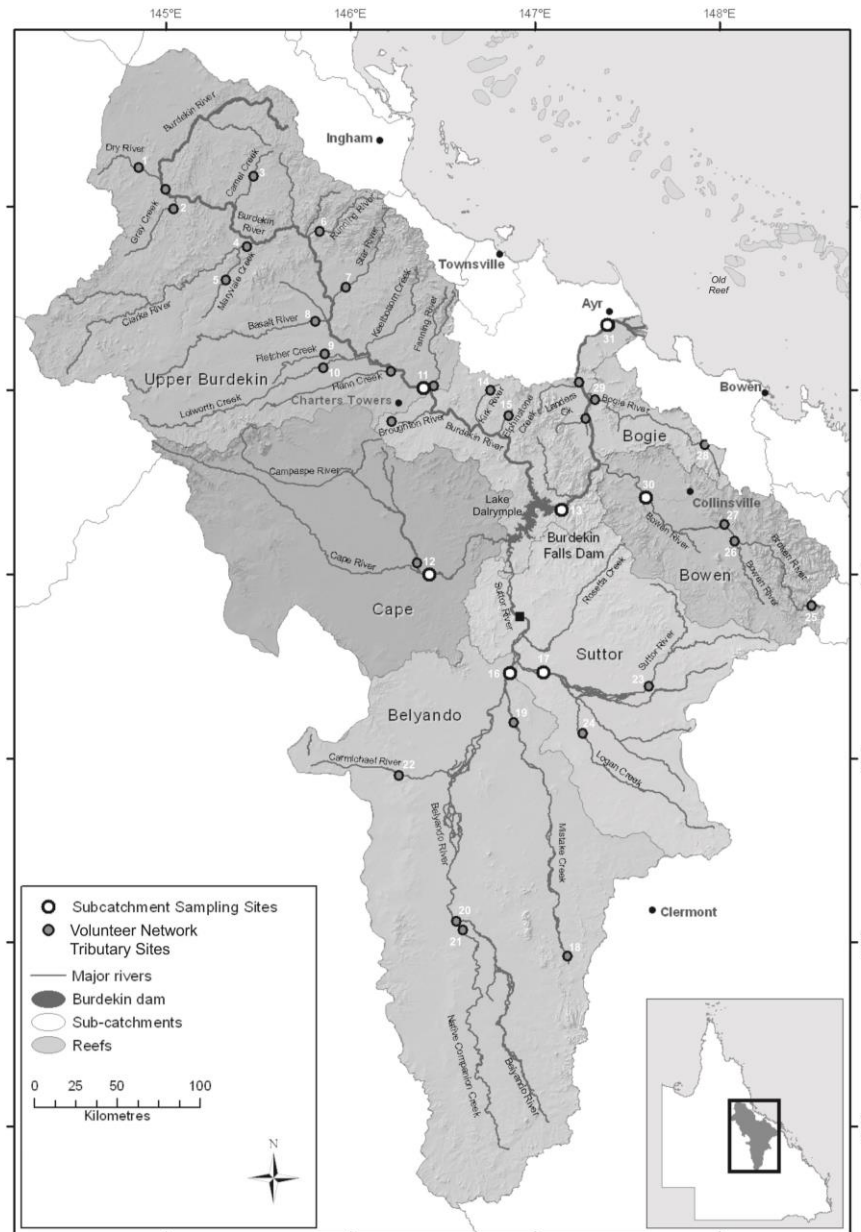
Figure 8.2. Map of the Burdekin River catchment indicating the five major sub-catchment areas, Burdekin Falls Dam and end-of-river sample site locations (white circles) and ungauged tributary network sample sites (grey circles). Source: Bainbridge et al. 2014.

8.2.4 Geochemical Analysis

The samples were analysed at the Queensland Government Department of Environment and Science (DES) Chemistry Centre, with lithium metaborate fusion and Inductively Coupled Plasma-Mass Spectrometry (ICP-MS) for the major element concentrations and Inductively Coupled Plasma-Optical Emission Spectrometry (ICP-OES) for the trace elements concentrations. The major element data was converted to weight percent oxides and summed. The summed weights were then corrected to 100% (i.e. exclude the loss on ignition). The same correction factors were applied to the trace element data.

8.2.5 Fallout Radionuclide Analysis

End member characterisation

To characterise ^{137}Cs and ^{210}Pb$_{ex}$ activity concentrations of both surface soils across the Burdekin River Basin and in subsurface sources (gully and channel banks) we have used the data from Wilkinson et al. 2015. In that study samples from prior studies in GBRL catchments were used to estimate the variability of radionuclide concentrations in sub-surface soil. These samples comprised 80 samples from gullies, channel banks and in-channel benches in the Normanby catchment (Olley et al. 2013), and 10 samples from sub-soil scalds, gullies, and channel banks in the Burdekin basin (Wilkinson et al. 2015). These samples were collected to represent the full depth of the exposed soil profile.

For surface soil sources Wilkinson et al. (2015) sampled 120 sites stratified based on the spatial pattern in soil erosion rates and rainfall. Vertosol were excluded from sampling, because this dark cracking clay soil type is prone to self-mulching where the soil profile is disturbed by cycles of wetting and drying causing radionuclides to become mixed through the soil profile. Consequently, soil eroded from both surface and sub-surface components of vertosol soil profiles have negligible radionuclide concentrations. Wilkinson et al. (2015) asserted that excluding the vertosol areas was unlikely to affect the results, with vertosol soils generally occurring in low-gradient areas, and primarily within the south western sub-catchments (Suttor and Belyando) of the Burdekin, that are minor contributors to EoR sediment export (Lewis et al. 2013; Bainbridge et al. 2014; Furuichi et al. 2014).

The data reported in Wilkinson et al. (2015) is for the clay and fine silt fraction (<10 µm) of the soils and sediments. Correction was made for variations in organic matter and interstitial water content by reporting radionuclide activity concentrations in terms of the weight of the mineral fraction, after ashing samples in a muffle furnace. Correction has also been made to the data for the difference in sampling times between the current study and that of Wilkinson et al. (2015).

Plume and EoR sediment samples

Fourteen of the plume and EoR samples recovered for the <10 µm particle size fraction had sufficient mass for analysis by high-resolution gamma-ray spectrometry (>1g). Samples ranged in weight from 1.2g to 13g and were counted for a minimum of three days on a high resolution germanium gamma detector. Activity concentrations for ^{210}Pb, ^{226}Ra and ^{137}Cs were determined following the procedures of Leslie (2009). The spectrometry analysis was undertaken at Griffith University. The ^{210}Pb$_{ex}$ activity concentrations were calculated as the difference between the ^{210}Pb and ^{226}Ra activity concentrations of each sample. Measurement uncertainty is represented as one standard error on the mean, incorporating analytical detection limits for each FRN.

8.2.6 Clay Mineralogy Analysis

Clay mineralogy was determined for 22 plume and EoR samples, recovered for the <10 µm fraction. Oriented clay smears were analysed at the James Hutton Institute, Scotland, following Hillier (2003) to estimate the relative weight percentages of the clay mineral groups kaolin, illite and 'expandables'. The expandable clay group includes smectites (e.g. montmorillonite) as well as other mixed-layer clay minerals with a smectitic (expandable) component, all of which

have a high capacity to 'shrink-swell' through water and cation exchange. This classification emphasises that the expandable clays are not necessarily pure smectites and may vary in composition from place to place. Kaolin is used in preference to kaolinite since the kaolin group mineral halloysite is likely present in some sources and we have not attempted to distinguish between kaolinite and halloysite in this investigation.

8.3 Results and Discussion

8.3.1 Major element chemistry

Concentrations of major elements in suspended sediment samples collected from the six major sub-catchments (Upper Burdekin, Cape, Belyando, Suttor and Bowen-Bogie rivers) are shown together with the EoR and flood plume samples for the 2017, 2018 and 2019 events in Figures 8.3, 8.4 and 8.5, respectively. Elements are plotted against Al_2O_3 (wt%).

First, the Kruskal–Wallis H-test and linear discriminant analysis were used to assess the degree to which the six major sub-catchments could be distinguished using just the major element chemistry. For the Kruskal–Wallis H-test major elements having a test statistic of $p > 0.05$ were excluded from further consideration, as previously applied by Collins et al. (1998; 2010). SiO_2 was the only element excluded on this basis. Linear discriminant analysis was then applied to the remaining major elements to identify the optimum combination which distinguished between the sources. The percentage of samples correctly classified by each individual geochemical property was assessed. Next, starting with the individual element that provided the highest proportion of correctly classified samples, major elements were added in turn and the proportion of source samples correctly classified calculated. Parameters were added such that with each addition the number of samples correctly classified was maximised. The highest correct classification achieved was 89%, with 67 of 75 samples classified back to their correct sources. This required all major elements except SiO_2 and CaO (Table 8.1). This analysis shows that using just the major elements the six major tributaries can be mostly distinguished from one another.

Table 8.1. Samples classification based on the linear combination of major elements best differentiating between the six sub-catchments and the percentage of samples from each catchment correctly classified.

Actual Group	Predicted Group						Correctly Classified
	Upper Burdekin	Cape	Belyando	Suttor	Bowen	Bogie	
Upper Burdekin	20	0	1	0	3	0	83%
Cape	0	7	0	0	1	0	88%
Belyando	1	0	9	0	0	0	90%
Suttor	0	0	0	11	0	2	85%
Bowen	0	0	0	0	11	0	100%
Bogie	0	0	0	0	0	9	100%
Overall Correct Classification							89%

A major challenge in tracing the movement of sediment is the effects of particle fractionation during transport on the properties of the sediment. In general, the average size of particles decreases, while the degree of sorting and the average roundness increases with distance travelled. These changes result from a combination of selective transport and particle abrasion (Krumbein and Sloss 1963; Moss et al. 1973; Walling et al. 2000; Laceby et al. 2017). These processes often change the properties that are being used to trace the source of the material. To assess whether our EoR and Plume sediment samples have been affected by particle sorting we first compare major element concentration in these samples with those from sample collected from each of the major sub-catchments (Figure 8.3-8.5). Any changes in major element concentrations will also affect the concentrations of the minor and trace elements.

The March 2017 floodwaters were almost exclusively sourced from the Bowen-Bogie River sub-catchments below the Burdekin Falls Dam (BFD). It would therefore be expected that the EoR and Plume sediment samples would also be derived from these sub-catchments, and that the major element concentrations of these samples would fall within the range of samples collected from the Bowen-Bogie sub-catchments. This is largely the case for the EoR samples (Figure 8.3) which group tightly, indicating a well-mixed source. However, the plume samples collected from Upstart Bay do not meet this expectation. This would normally be interpreted as indicating that the plume sediments are derived from a different source to the EoR or Bowen-Bogie samples. Particularly given that sediments collected from the Bowen and Bogie sub-catchments could be 100% ascribed back to their source catchment using just the major element concentrations (Table 8.1). However, changes in SiO_2 and Al_2O_3 are correlated (see arrow on the plot) and follow the expected concentration changes resulting from an enrichment in mineral clays, and a loss of quartz and feldspars. This suggests that changes in the major element concentrations between the Bowen-Bogie source samples, the EoR samples and the Plume samples are the result of particle fractionation during transport. An increase in the proportion of finer smectite/expandable clays from the EoR to plume sediment samples at the expense of larger illite particles (Figure 8.6) also supports this finding.
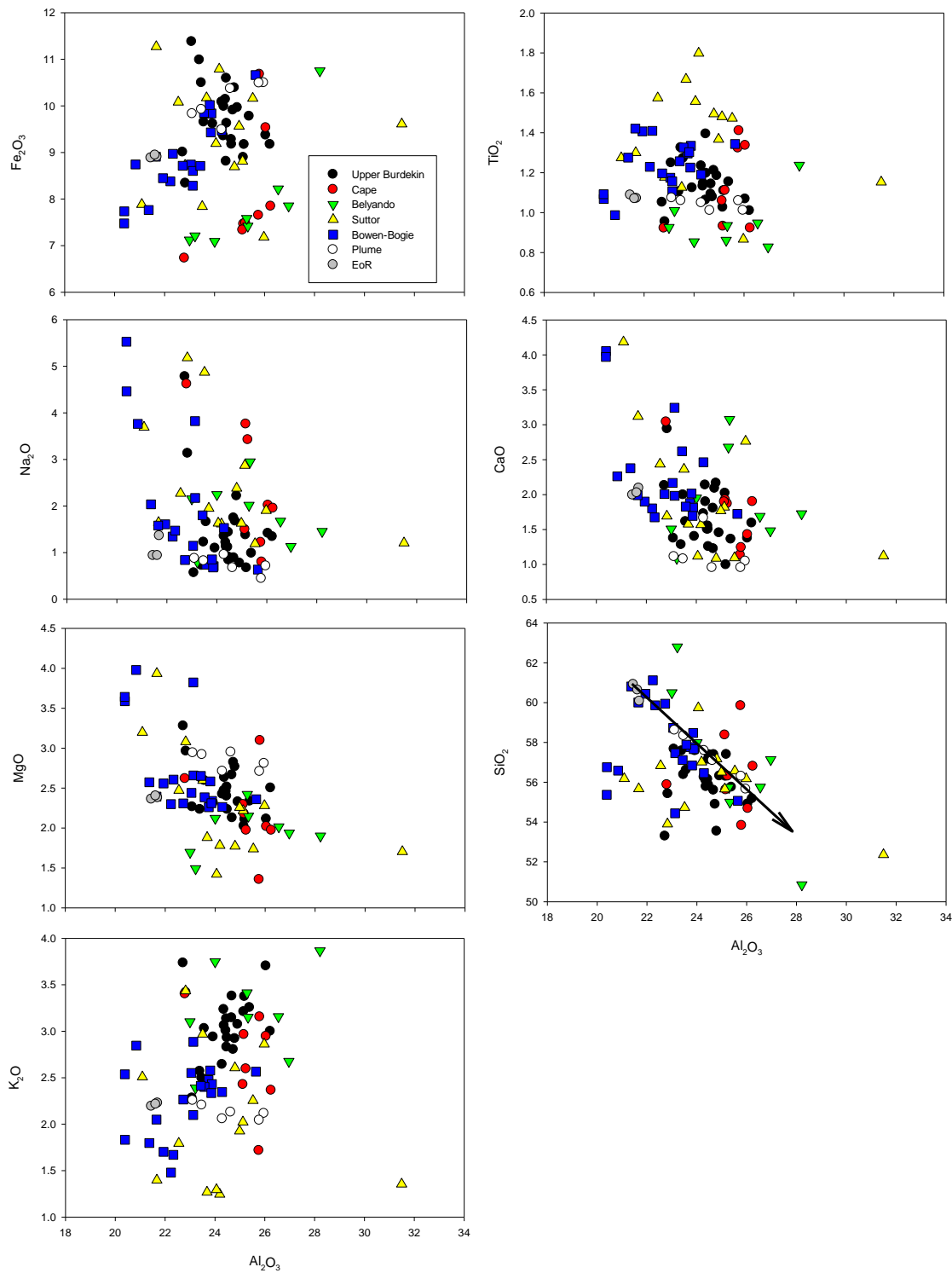
Figure 8.3. Concentrations of major elements in suspended sediment samples collected from the six major sub-catchments (Upper Burdekin, Cape, Belyando, Suttor and Bowen-Bogie rivers) shown together with the EoR and flood plume samples for the 2017 event. Element concentrations are weight percent oxides and are plotted against Al_2O_3 (wt%). The arrow on the SiO_2 to Al_2O_3 indicates the expected changes in concentrations as a result of enrichment in mineral clays.

Figure 8.4. Concentrations of major elements in suspended sediment samples collected from the six major sub-catchments (Upper Burdekin, Cape, Belyando, Suttor and Bowen-Bogie rivers) shown together with the EoR and flood plume samples for the 2018 event. Element concentrations are weight percent oxides and are plotted against Al2O3 (wt%).
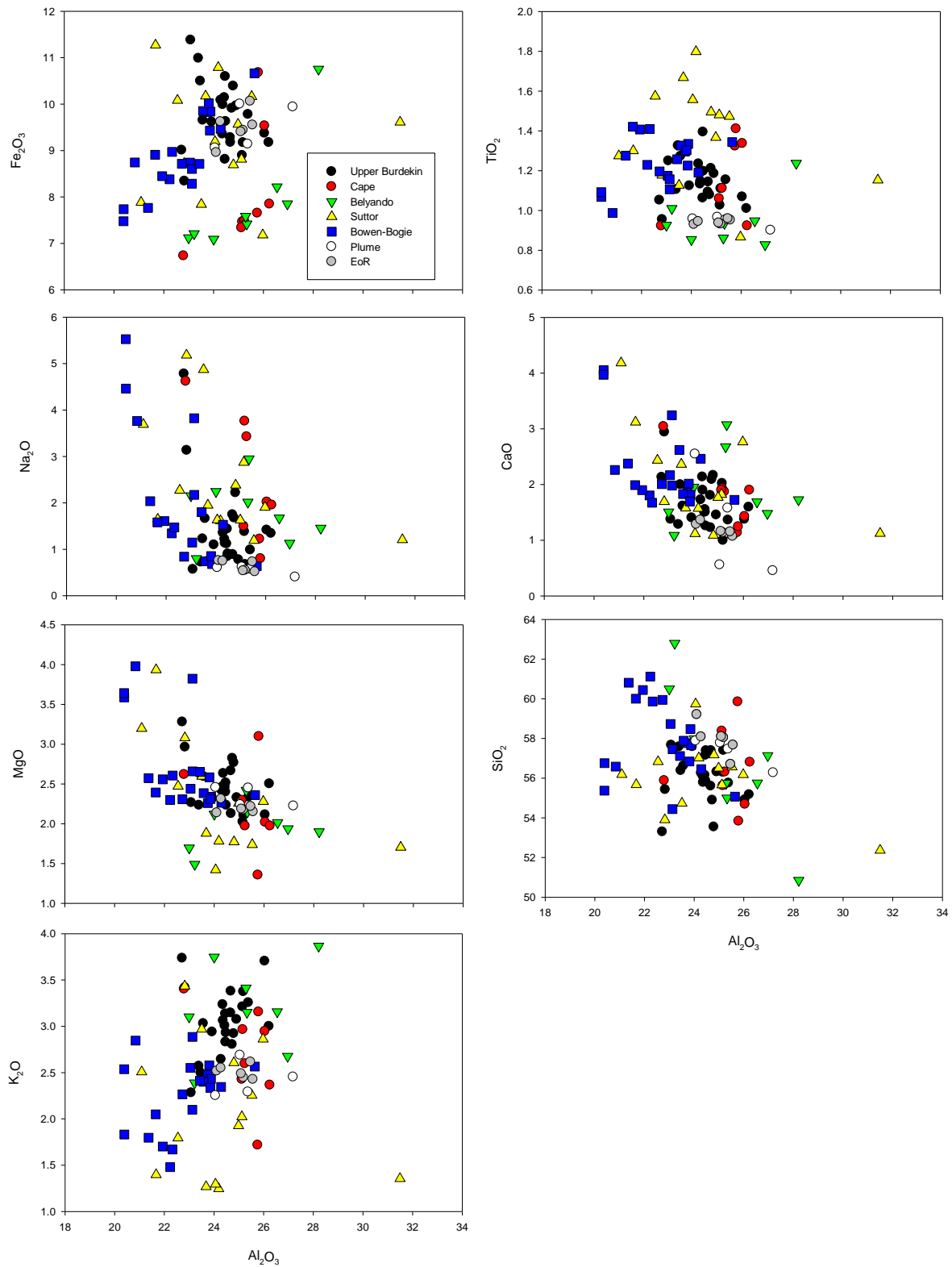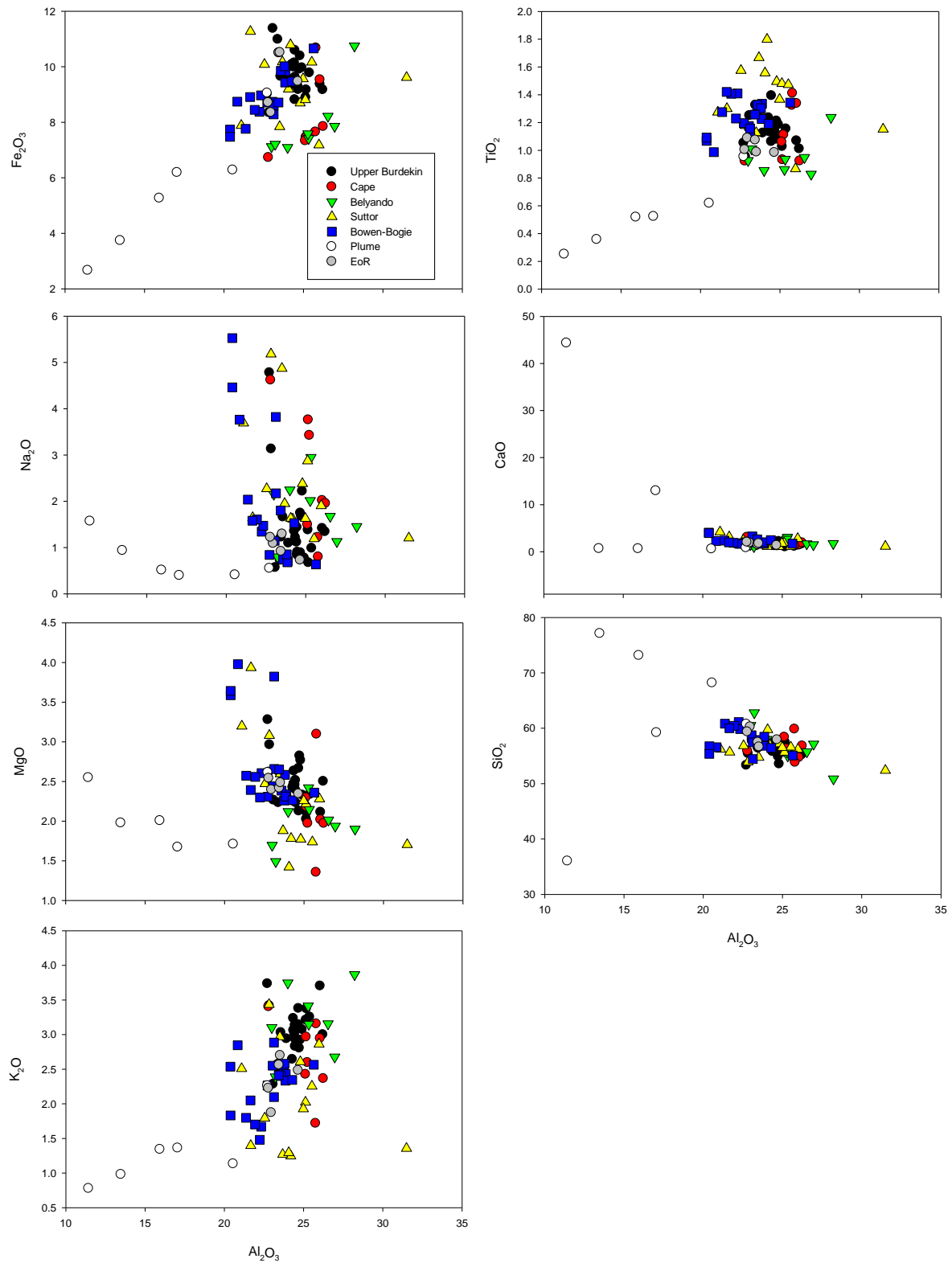
Figure 8.5. Concentrations of major elements in suspended sediment samples collected from the six major sub-catchments (Upper Burdekin, Cape, Belyando, Suttor and Bowen-Bogie rivers) shown together with the EoR and flood plume samples for the 2019 event. Element concentrations are weight percent oxides and are plotted against Al₂O₃ (wt%).
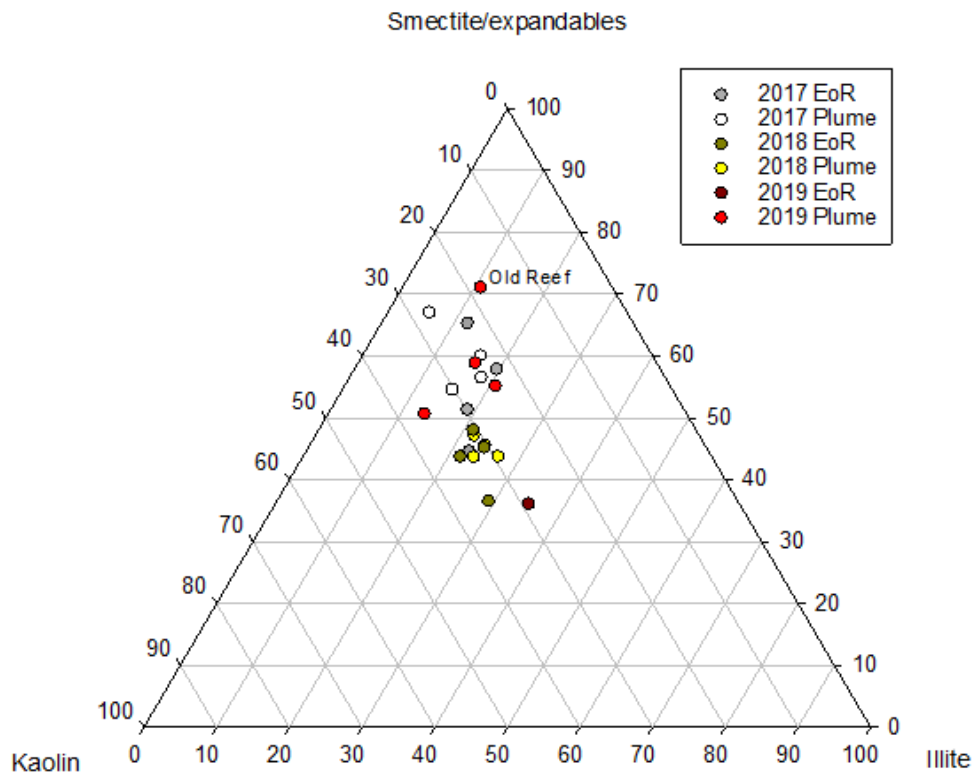
Figure 8.6. Ternary plot showing the proportion illite, kaolin and Smectite/expandable clays for Burdekin EoR and Plume sediment samples collected from the 2017, 2018 and 2019 events.

The March 2018 flood waters were derived from heavy rainfall in the upper Burdekin River catchment in late February/early March 2018. It would therefore be expected that this area would also be the dominant source of the 2018 EoR and Plume sediments. However, while Fe_2O_3, MgO and CaO concentrations are consistent between this source and EoR and plume samples (Figure 8.4), the other major element concentrations are not, and they inconsistently fall within other source sub-catchment ranges. While not clearly indicating particle fractionation, as was evident with the 2017 data, it does indicate that something is amiss.

The major element concentrations from the February 2019 event flood plume sediment samples largely (five out of six) fall outside the source sub-catchment concentration ranges (Figure 8.5). Most of the variation (91.2%) in the plume sediment major element concentrations data is explained by two principal components. Principal component 1 which explains 57.4% of the variance is primarily related to the marine carbonate associated elements (CaO and MgO) and the silt/clay associated elements (those strongly correlated with Al_2O_3). Principle component 2 is primarily related to the marine carbonate associated elements, and SiO_2 and P_2O_5 which are primarily associated with biogenic silica (diatoms are present in the samples, refer to Chapter 2). The relationship between these three primary components (Al_2O_3-CaO-SiO_2) in the plume sediment is presented as a ternary plot (Figure 8.7). In this figure the marine carbonate component would plot close to 100% CaO, the biogenic silica close to 100% SiO_2 and the terrestrial derived river silt-clays along the Al_2O_3-SiO_2 axis. The figure clearly illustrates the addition of both carbonate and biogenic silica to the 2019 plume samples. The 2019 clay mineralogy data also show an increase in the finer smectite/expandable clays at the expense of larger illite particles (and kaolin to a lesser extent) in all plume samples compared to the EoR sediment (Figure 8.6). The major element and clay mineralogy data presented above

clearly indicate that the plume sediment samples have been affected to varying degrees by both particle fractionation and the addition of marine-sourced carbonate and biogenic silica. This being the case the standard geochemical sediment tracing approach using element concentrations in a mixing model (eg. Collins et al. 1996; Collins et al. 1998; Olley and Caitcheon, 2000; Hardy et al. 2010; Weltje and Brommer, 2010) will not work.
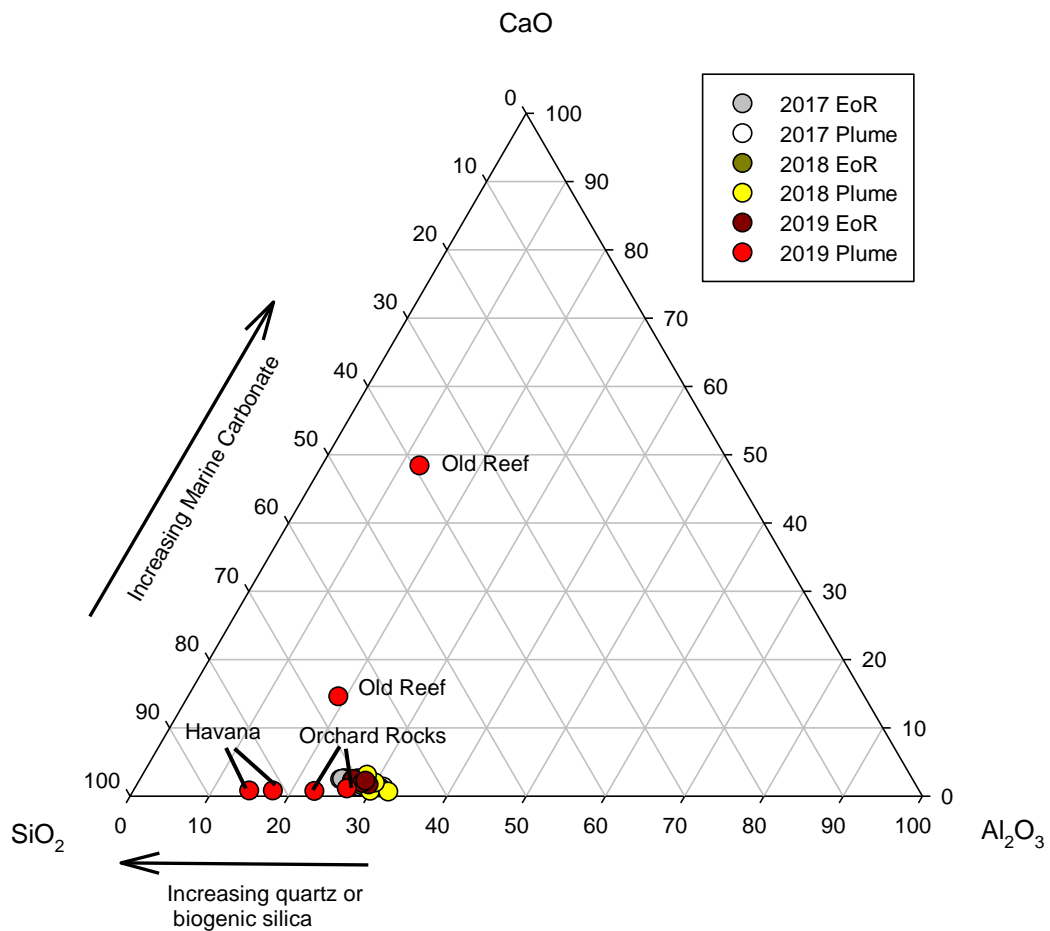

Figure 8.7. Al$_2$O$_3$-CaO-SiO$_2$ ternary plot of EoR and flood plume sediment samples collected from the 2017, 2018 and 2019 events.

8.3.2 Rare Earth elements, yttrium, scandium, and thorium

The rare earth elements (REE) plus yttrium (Y), scandium (Sc) and thorium (Th) have been widely used in tracing studies (McCulloch et al. 2003; Douglas et al. 2006; Smith et al. 2008; Takesue et al. 2009) because they strongly partition into the mineral particulate phase, they behave coherently during weathering, erosion, and fluvial transportation, and they are highly resistance to chemical mobilization. In the GBR lagoon they will also be primarily derived from the terrestrial environment (Wyndham et al. 2004) and therefore provide a means of tracing the terrestrial component of the flood plume sediments. While concentrations of these elements will also be affected by particle fractionation, it is likely, because of their chemical stability, that element ratios will be stable across both the catchment and marine environments.

The element ratios, because the marine derived component contain little or none of these elements, should also be unaffected by the addition of marine carbonate or biogenic silica.

In the plume and EoR sediments changes in the Al_2O_3 wt% concentrations are associated with changes in the proportion of clays, either through the preferential loss of other components, such as quartz and feldspar (i.e. 2017 event), or the gains of components such as marine carbonate and biogenic silica (i.e. 2019 event). In Figure 8.8 selected REE/Th ratios for EoR and flood plume sediment samples collected during the 2017 and 2018 flood events are plotted against Al_2O_3 (wt%). The solid lines and dashed lines represent the mean ratios for the 2017 and 2018 EoR samples, respectively. On the right-hand side the sub-catchment sediment sample ratios are shown for comparison. While only six of the REE/Th ratios are shown, all of the REE elements plus Sc and Y from each of the 2017 and 2018 events showed similar constant element ratios against Al_2O_3, with the individual ratios being different for the 2017 and 2018 events. These selected REE/Th ratios for the 2019 flood event are plotted in Figure 8.9, with the solid line representing the mean ratio of the EoR samples. The individual elemental ratios fall in between the 2017 and 2018 events.

The REE/Th, Sc/Th and Y/Th ratios from the 2017 and 2018 plume sediments are consistent with those from their respective EoR samples. This is despite the significant changes in major element concentrations and mineralogy identified above. This indicates that these ratios are unaffected by the transport associated particle fractionation. Further, the consistency of the ratios between the EoR and plume sediments in each year indicates a common source, and the difference in ratios between years indicates the sediments from the 2017 and 2018 events were derived from different source areas within the catchment.

The ratios from the plume and EoR sediments were compared with those from the samples collected from each of the sub-catchment sources using the following equation:

$$GOF = 1 - \sum_{i=1}^{n} \left| \frac{(R_i - R_{is})}{R_i} \right| / n$$

(Equation 1)

Where n is the number of elements included; R_i is the thorium ratio in the plume or EoR sample for the geochemical property (i); R_{is} is the same ratio in the sub-catchment source sample. The goodness of fit (GOF) indicates how closely on average the ratios match, with a GOF=1 indicating a perfect match for all ratios. For the 2017 event all of the EoR and Plume samples most closely matched source sediment samples from the Bowen-Bogie sub-catchments with a 94-95% GOF.
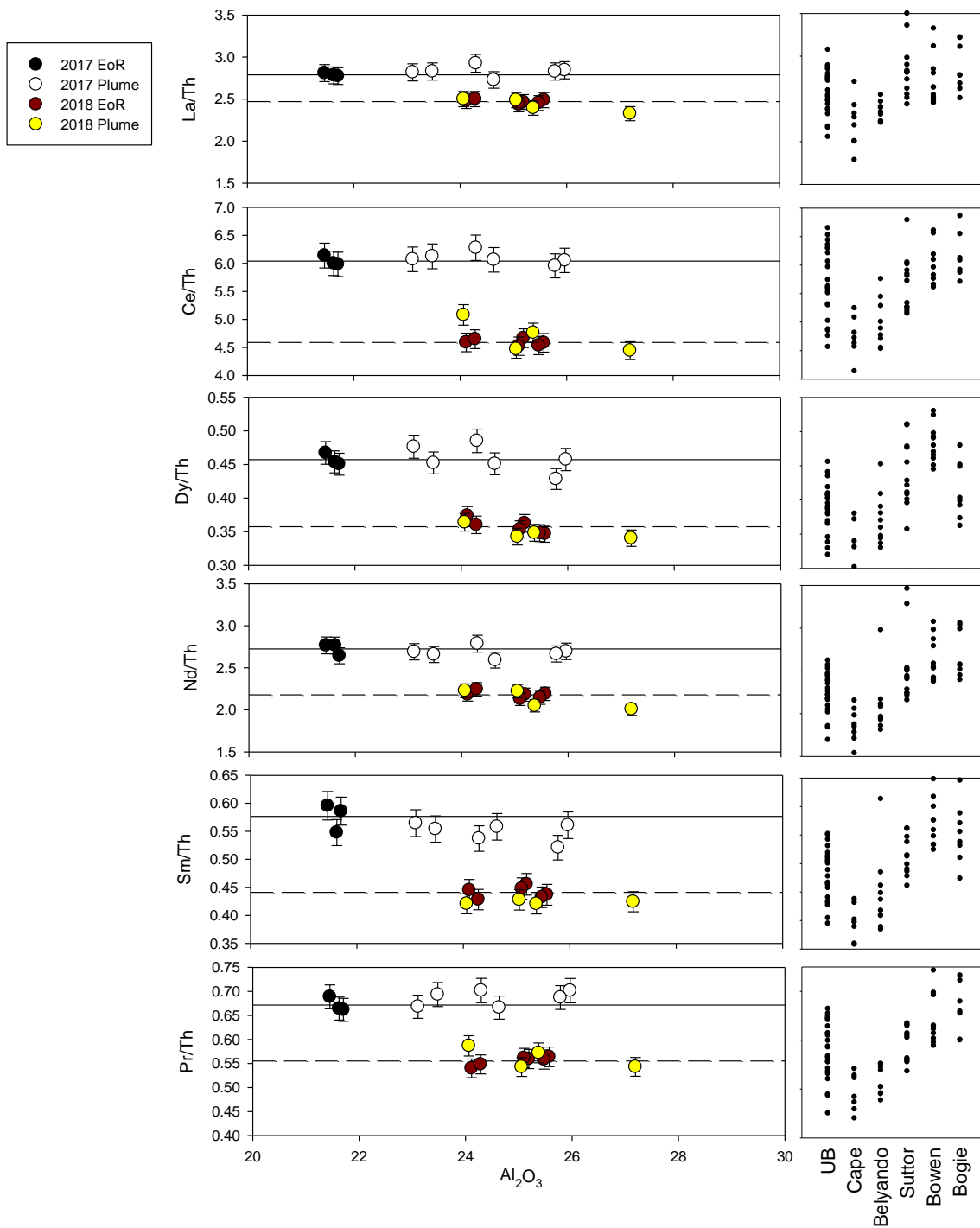
Figure 8.8. Plots of selected REE/Th ratios vs Al₂O₃ (wt%) for EoR and flood plume sediment samples collected during the 2017 and 2018 flood events. The solid lines and dashed lines represent the mean ratios for the 2017 and 2018 EoR samples, respectively. On the right-hand side the sub-catchment sediment sample ratios are shown for comparison. Error bars are equivalent to one standard error and were estimated from repeat sample analyses.

Figure 8.9. Plots of selected REE/Th ratios vs Al2O3 (wt%) for EoR and flood plume sediment samples collected during the 2019 flood event. The solid lines represent the mean ratios for the EoR samples. On the right-hand side the sub-catchment sediment sample ratios are shown for comparison. Error bars are equivalent to one standard error and were estimated from repeat sample analyses.
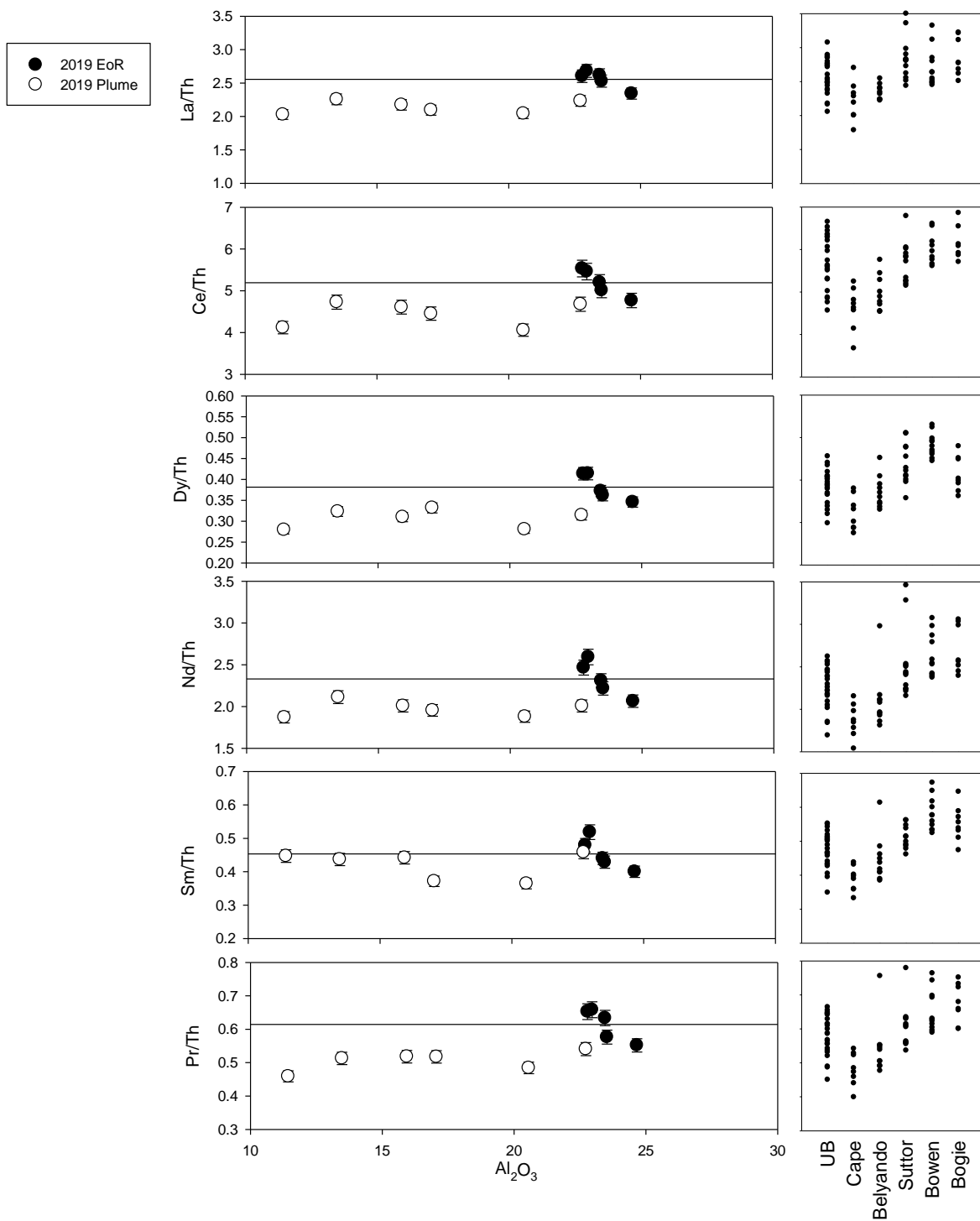
Two of the first three EoR samples for the 2018 event most closely matched source sediments from the Cape River sub-catchment with GOFs = 94%. For all of the other EoR and plume samples the best matches were to samples from the Upper Burdekin sub-catchment with GOFs between 91 and 94%.

For the 2019 event EoR samples, the first one most closely matched the Suttor sub-catchment (GOF = 93%), the others most closely matched source sediments from the Cape River (1 out of 4 samples GOF = 97%) and Upper Burdekin (3 out of 4 GOFs between 91-93%). Four of the plume samples matched most closely to the Upper Burdekin sub-catchment (GOFs between 91 and 94%), and two to the Cape (78% and 94%). The lowest maximum GOF (78%) was for the plume sample with the lowest Al_2O_3 concentration. This sample consisted of ~50% flocculated organic matter (Chapter 2).

8.3.3 Fallout Radionuclides

Activity concentrations of $^{210}Pb_{ex}$ and ^{137}Cs in EoR and Burdekin plume sediments are shown in Figure 8.10 together with the decay corrected hillslope surface soil and subsoil source samples from Wilkinson et al. (2015). Also included are the activity concentrations in EoR samples collected by Wilkinson et al. (2015). The vertical and horizontal dashed lines respectively indicate the range of ^{137}Cs and $^{210}Pb_{ex}$ activity concentration in subsoil sources. The error bars are equivalent to one standard error on the mean and are derived from the analytical uncertainties. The ^{137}Cs activity concentrations for the EoR and Burdekin plume sediments are also reported in Table 8.2. The plume sediment samples were collected within the Upstart Bay primary plume and further offshore in northern secondary waters sampled at Orchard Rocks, Magnetic Island. All of the EoR and Burdekin plume sediments samples ^{137}Cs activity concentrations are consistent with the concentration range of the sub-surface source samples (<2.7 Bq kg^{-1}) at one standard error.
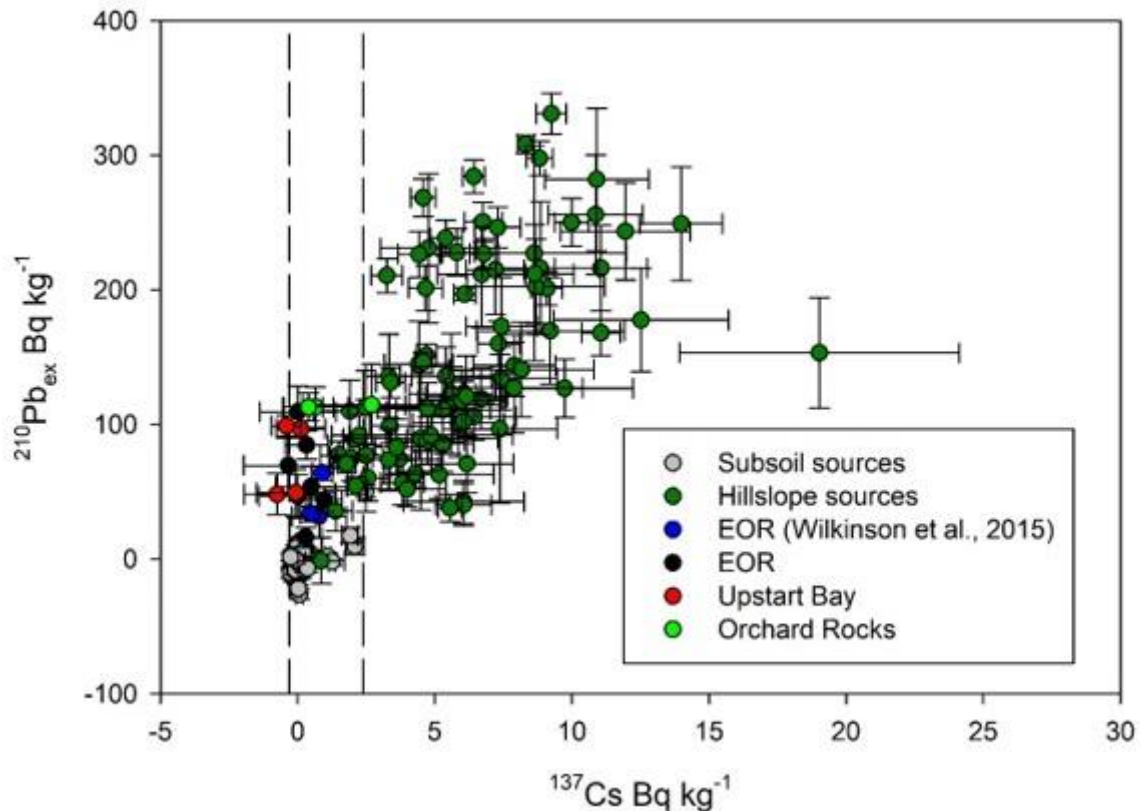
Figure 8.10. Activity concentrations of $^{210}Pb_{ex}$ and ^{137}Cs in EoR and Burdekin plume sediments (2017-2019) together with the decay corrected hillslope surface soil and subsoil source samples from Wilkinson et al. (2015). Also included are the activity concentrations in EoR samples collected by Wilkinson et al. (2015). The vertical and horizontal dashed lines respectively indicate the range of ^{137}Cs and $^{210}Pb_{ex}$ activity concentration in subsoil sources. Plume sediment samples were collected within the Upstart Bay primary plume and further offshore in secondary waters at Orchard Rocks, Magnetic Island. The error bars are equivalent to one standard error on the mean and are derived from the analytical uncertainties.

We have made the assumption that individual EoR and Plume samples represent a discrete mix of surface soil and sub-surface derived material such that the surface soil derived proportion is x, and 1-x the proportion derived from sub-soil erosion, with $0 \leq x \leq 1$. Such that

$$Ax + B(1-x) = C, \qquad\qquad\qquad \text{(Equation 2)}$$

where A is the ^{137}Cs activity concentration in the surface soil, B is that of the sub-surface sources and C is the resultant concentration. We have used the values of 6.1±0.6 Bq Kg^{-1}, and 0.2±0.1 Bq Kg^{-1} for A and B respectively (after Wilkinson el al. 2015) to estimate the proportion of surface soil contributing to each sample (Table 8.2). The average contribution across all samples is 5±3%. This figure is consistent with previous estimates of surface soil contributing 6±1% to sediment sampled from the downstream Burdekin River (Wilkinson et al. 2015).

Table 8.2. Individual EoR and plume sediment sample locations, measured concentrations of 137Cs (Bq kg-1) including associated analytic uncertainties (one standard error on the mean), and the estimated percent contribution of surface soil to each sample.

Wet season event	Sample type	Sample location	^{137}Cs		Surface soil contribution	
			Bq kg^{-1}	*se*	%	*se*
2017	EoR	Burdekin@Inkerman	1.0	0.7	14	12
	EoR	Burdekin@Inkerman	0.3	0.6	2	10
	Plume	Upstart Bay	-0.7	1.2	0	5
	Plume	Upstart Bay	-0.1	1.4	0	19
	Plume	Upstart Bay	0.1	0.9	0	13
2018	EoR	Burdekin@Inkerman	-0.3	1.6	0	19
	EoR	Burdekin@Inkerman	0.0	1.4	0	20
	EoR	Burdekin@Inkerman	0.3	0.8	2	14
	Plume	Upstart Bay	-0.4	0.5	0	1
	Plume	Orchard Rocks-Surface	0.7	1.2	8	20
	Plume	Orchard Rocks-Depth 15m	2.7	2.5	42	43
2019	EoR	Burdekin@Inkerman	0.5	1.3	5	22
	EoR	Burdekin@Inkerman	0.0	1.4	0	20
	Plume	Orchard Rocks	0.4	0.9	3	15

Activity concentrations of ^{210}Pb$_{ex}$ in the end of river samples collected in this study range from 110±20 to 16±7 Bq kg^{-1}. The maximum concentration observed in the subsoil samples is 55 Bq kg^{-1}. At least two of the EoR samples exceed this value at two standard error, and all of them exceed the mean value for the subsoil sources of -1 Bq kg^{-1} ^{210}Pb$_{ex}$. Given that the ^{137}Cs data indicate that the sediments are predominantly derived from subsoil sources this additional ^{210}Pb$_{ex}$ can have arisen in three possible ways:

i) the sediments are derived from areas such as scalds or gully floors, which have previously lost all of the material labelled with ^{137}Cs but subsequently been exposed to ^{210}Pb$_{ex}$ fallout.

ii) the sediments are derived from channel and gully walls that have been in transit within the catchment for a period of time long enough to accumulate the additional ^{210}Pb$_{ex}$ (i.e. eroded and temporarily stored within a gully floor or exposed river bed prior to wet season discharge and remobilisation downstream).

iii) Or a combination of both of the above.

At this stage we can't distinguish between these possibilities.

The plume sample ^{210}Pb$_{ex}$ concentrations all fall within the range of those of the EoR samples indicating that sediment transport was rapid (0 years). However if we use the lowest EoR ^{210}Pb$_{ex}$ of 16±7 Bq kg^{-1} and the maximum plume sediment activity concentration of 115±30 Bq kg^{-1} at Orchard Rocks, together with the water depth at Orchard Rocks (15m), and the average sediment concentration of ~12 mg L^{-1} (based on three samples), and the area ^{210}Pb$_{ex}$ fallout rate of 38 Bq m^{-2} yr^{-1} (Turekian et al. 1977), we can estimate a maximum transit/residence time. The assumption here is that the sediments (and associated organic matter) in the water column scavenge the fallout ^{210}Pb$_{ex}$. At 12 mg L^{-1} there would be ~200g of sediment in the 15m x 1m^2 water

column. At a fallout rate of 38 Bq m^{-2} yr^{-1} the sediment activity concentration would increase by ~200 Bq kg^{-1} in 12 months. This calculation, while simplistic, shows that the ~100 Bq kg^{-1} difference in ^{210}Pb$_{ex}$ activity concentration between the Orchard Rocks sample and the EoR sample could have arisen in less than 6 months. This demonstration provides an example of how ^{210}Pb$_{ex}$ activity concentrations can be used to calculate the residence time of terrigenous sediment across the catchment to reef. In this case the transport is rapid and supports our observations (satellite imagery and eReefs model) of a travel time of 3-5 days from EoR to Orchard Rocks (Chapter 7).

8.3.4 Additional Bowen sub-catchment soil source tracing

Additional sediment and associated particulate nutrient source tracing research is in preparation under collaborative Project RP128G, within the Bowen sub-catchment (Garzon-Garcia et al. In prep). Instream composite samplers (i.e. rocket samplers) installed at the Bowen River - Myuna gauge site captured sediment during the 2017 and 2019 discharge events. Chromosol sub-surface soils were found to contribute the larger proportion of sediment to this downstream Bowen River site, during both of these events. Due to the varying nutrient concentrations of different soil types within this catchment (refer to Garzon-Garcia et al. 2018), surface dermosols were found to be the highest contributor of bioavailable nutrients in the 2017 event, as well as both surface vertosols and subsurface chromosols in both 2017 and 2019 events (Garzon-Garcia et al. In prep).

8.4 Conclusions

This chapter clearly demonstrates that terrestrial derived-material eroded from subsoil sources in the Burdekin catchment is being transported in flood plume secondary water types greater than 100 km's from the river mouth, and to the mid-shelf during larger discharge years. Whilst particle fractionation is occurring during sediment transport, the relationship between the rare earth elements and thorium (REE/Th ratios) is robust and clearly enables terrigenous sediment to be traced across the catchment to reef continuum.

ACKNOWLEDGEMENTS

REFERENCES

Bainbridge, ZT., Lewis, SE., Smithers, SG., Kuhnert, PM., Henderson, BL., Brodie, JE., 2014. Fine-suspended sediment and water budgets for a large, seasonally dry tropical catchment: Burdekin River catchment, Queensland, Australia. Water Resources Research 50, 9067-87.

Bainbridge, Z. Lewis, S. Smithers, S. Wilkinson, S. Douglas, G. Hillier, S. Brodie, J. 2016. Clay mineral source tracing and characterisation of Burdekin River (NE Australia) and flood plume fine sediment. Journal of Soils and Sediments 16, 687-706.

Bainbridge, Z., Lewis, S., Stevens, T., Petus, C., Lazarus, E., Gorman, J., Smithers, S. In review. Measuring sediment grain size across the catchment to reef continuum: Improved methods and environmental insights. Marine Pollution Bulletin.

Bartley R, Bainbridge Z, Lewis S, Kroon F, Wilkinson S, Brodie J and Silburn D 2014. Relating sediment impacts on coral reefs to watershed sources, processes and management: a review. Science of the Total Environment, 468-469. 1138-1153, DOI:10.1016/j.scitotenv.2013.09.030.

Caitcheon, G., Douglas, G., Palmer, G. 2006. Sediment source tracing in the Lake Burragorang catchment. CSIRO Land and Water Science Report 47/07 to the Sydney Catchment Authority.

Collins, A., Walling, D., Leeks, G. 1996. Composite fingerprinting of the spatial source of fluvial suspended sediment: a case study of the Exe and Severn River basins, United Kingdom. Géomorphologie: relief, processus, environnement 2, 41-53.

Collins, A., Walling, D., Leeks, G. 1998. Use of composite fingerprints to determine the provenance of the contemporary suspended sediment load transported by rivers. Earth surface processes and landforms 23 (1), 31-52.

Collins, A., Walling, D., Webb, L., King, P. 2010. Apportioning catchment scale sediment sources using a modified composite fingerprinting technique incorporating property weightings and prior information. Geoderma, 155(3-4), pp.249-261.

Douglas, G.B., Palmer, M.J., Caitcheon, G. 2003. The provenance of sediments in Moreton Bay, Australia: A synthesis of major, trace element and Sr-Nd-Pb isotopic geochemistry, modelling and landscape analysis. Hydrological Processes 494, 145-152.

Douglas, G.B., Ford, P.W., Palmer, M., Noble, R.M., Packett, R. 2006. Fitzroy River Basin, Queensland, Australia. II. Identification of sources of estuary bottom sediments. Environmental Chemistry 3, 377-385.

Everett, S., Tims, S., Hancock, G., Bartley, R., Fifield, L. 2008. Comparison of Pu and 137Cs as tracers of soil and sediment transport in a terrestrial environment. Journal of Environmental Radioactivity 99, 383-393.

Furuichi, T., Olley, J., Wilkinson, S., Lewis, S., Bainbridge, Z., Burton, J. 2016. Paired geochemical tracing and load monitoring analysis for identifying sediment sources in a large catchment draining into the Great Barrier Reef Lagoon. Geomorphology 266, 41-52.

Garzon-Garcia, A., Burton, J., Ellis, R., Askildsen, M., Bainbridge, Z., Lewis, S., DeHayr, R., Moody, P. In preparation. The bioavailability of particulate nitrogen in sediment: catchment sources and processes.

Hancock, G.J., Wilkinson, S.N., Hawdon, A.A., Keen, R.J. 2014. Use of fallout tracers 7Be, 210Pb and 137Cs to distinguish the form of sub-surface soil erosion delivering sediment to rivers in large catchments. Hydrological Processes, 28(12), 3855-3874.

Hardy, F., Bariteau, L., Lorrain, S., Theriault, I., Gagnon, G., Messier, D. and Rougerie, J. 2010. Geochemical tracing and spatial evolution of the sediment bed load of the Romaine River, Quebec, Canada. Catena 81, 66-76.

Hillier, S. 2003. Quantitative analysis of clay and other minerals in sandstones by X-ray powder diffraction (XRPD). Int Assoc Sedimentol Spec Publ 34:213-251

Hughes AO, Olley JM, Croke JC, McKergow LA. 2009. Sediment source changes over the last 250 years in a dry-tropical catchment, central Queensland, Australia. Geomorphology, 104: 262-275. http://dx.doi.org/10.1016/j.geomorph.2008.09.003.

Krumbein, W.C. & Sloss, L.L. 1963. Stratigraphy and Sedimentation (2nd Ed). W.G. Freeman & Co.

Kroon, F.J., Kuhnert, P.M., Henderson, B.L., Wilkinson, S.N., Kinsey-Henderson, A., Abbott, B., Brodie, J.E. and Turner, R.D.R., 2012. River loads of suspended solids, nitrogen, phosphorus and herbicides delivered to the Great Barrier Reef lagoon. Marine Pollution Bulletin, 65(4-9): 167-181, 10.1016/j.marpolbul.2011.10.018.

Laceby, J., Evrard, O., Smith, H., Blake, W., Olley, J., Minella, J., Owens, P. 2017. The challenges and opportunities of addressing particle size effects in sediment source fingerprinting: a review. Earth-Science Reviews 169, 85-103.

Lewis, S., Bainbridge, Z., Kuhnert, P., Sherman, B., Henderson, B., Dougall, C., Cooper, M., Brodie, J.E. 2013. Calculating sediment trapping efficiencies for reservoirs in tropical settings: a case study from the Burdekin Falls Dam, NE Australia. Water Resour Res 49:1017-1029. doi: 10.1002/wrcr.20117.

McCulloch, M. Pailles, C. Moody, P. Martin, C.E. 2003. Tracing the source of sediment and phosphorus into the Great Barrier Reef lagoon. Earth and Planetary Science Letters 210, 249-258.

Moss, A.J. 1963. The physical nature of the common sandy and pebbly deposits. Part II. American Journal of Science 261, 297-343.

Olley, J. and Caitcheon, G., 2000. Major element chemistry of sediments from the Darling–Barwon river and its tributaries: implications for sediment and phosphorus sources. Hydrological Processes, 14(7), pp.1159-1175.

Olley, J., Murray, A., Mackenzie, D., Edwards, K. 1993. Identifying sediment sources in a gullied catchment using natural and anthropogenic radioactivity. Water Resources Research, 29(4), pp.1037-1043.

Olley, J., Brooks, A., Spencer, J., Pietsch, T., Borombovits, D. 2013a. Subsoil erosion dominates the supply of fine sediment to rivers draining into Princess Charlotte Bay, Australia. JEnvRadioactivity, 124: 121-129. http://dx.doi.org/10.1016/j.jenvrad.2013.04.010.

Olley, J., Burton, J., Smolders, K., Pantus, F. and Pietsch, T., 2013b. The application of fallout radionuclides to determine the dominant erosion process in water supply catchments of subtropical South-east Queensland, Australia. Hydrological Processes, 27(6), pp.885-895.

Smith, J., Douglas, G., Radke, L., Palmer, M., Brooke, B. 2008. Fitzroy River Basin, Queensland, Australia. III. Identification of sediment sources in the coastal zone. Environmental Chemistry 5(3), 31-242.

Stevens, T. 2019. International Patent Application PCT/AU2019/051436 Improved Sampler and Method.

Takesue, R.K., Bothner, M.H., Reynolds, R.L. 2009. Sources of land-derived runoff to a coral reef-fringed embayment identified using geochemical tracers in nearshore sediment traps. Estuarine, Coastal and Shelf Science 85, 459-471.

Turekian, K.. Nozaki, Y. & Benninger, L. 1977. Geochemistry of atmospheric radon and radon products. Ann. Rev. Earth 52, 81-99.

Wallbrink, P.J. and Murray, A.S. 1993. Use of fallout radionuclides as indicators of erosion processes. Hydrological processes 7(3), 297-304.

Wallbrink, P., Olley, J., Murray, A. 1994. Measuring soil movement using Cs137: implications of reference site variability. IAHS Publications-Series of Proceedings and Reports-Intern Assoc Hydrological Sciences, 224, pp.95-102.

Wallbrink, P. Olley, J.M., Hancock, G 2002. Estimating residence times of fine sediment in river channels using fallout ^{210}Pb. IAHS Publication No. 276, 425-432.

Wallbrink, P., Murray, A., Olley, J. Olive, L. 1998. Determining sources and transit times of suspended sediment in the Murrumbidgee River, New South Wales, Australia, using fallout 137Cs and 210Pb. Water Resources Research 34, 879-887.

Walling, D.E. and Woodward, J.C., 1992. Use of radiometric fingerprints to derive information on suspended sediment sources. Erosion and sediment transport monitoring programmes in river basins, 210, pp.153-164.

Walling, D., Owens, P., Waterfall, B., Leeks, G., Wass, P. 2000. The particle size characteristics of fluvial suspended sediment in the Humber and Tweed catchments, UK. The Science of the Total Environment 252, 205-222.

Waterhouse, J., Brodie, J., Lewis, S., Mitchell, A., 2012. Quantifying the sources of pollutants in the Great Barrier Reef catchments and the relative risk to reef ecosystems. Mar. Pollut. Bull. 65, 394–406.

Weltje, G. and Brommer, M.. 2011. Sediment-budget modelling of multi-sourced basin fills: application to recent deposits of the western Adriatic mud wedge (Italy). Basin Research 23(3) 291-308.

Wilkinson, S., Hancock, G., Bartley, R., Hawdon, A., Keen R. 2013. Using sediment tracing to assess processes and spatial patterns of erosion in grazed rangelands, Burdekin River basin, Australia. Agr Ecosyst Environ 180:90-102.

Wilkinson, S.N., Olley, J.M., Furuichi, T., Burton, J., Kinsey-Henderson, A.E. 2015. Sediment source tracing with stratified sampling and weightings based on spatial gradients in soil erosion Journal of soils and sediments 15 (10), 2038-2051.

Wyndham, T., McCulloch, M., Fallon, S. and Alibert, C. 2004. High-resolution coral records of rare earth elements in coastal seawater: biogeochemical cycling and a new environmental proxy. Geochimica et Cosmochimica Acta, 68(9), 2067-2080.